museum für
naturkunde
berlin

Freie Universität Berlin

Global trends in nutrient dynamics during the Ediacaran-Cambrian period as revealed by nitrogen and carbon isotope trends

Dissertation in kumulativer Form
zur Erlangung des Doktorgrades der Naturwissenschaften
im Fachbereich Geowissenschaften an der Freien Universität Berlin

von

Antonia Gamper

im August 2014

Erstgutachter:

PD Dr. Ulrich Struck

Zweitgutachter:

Prof. Dr. Christoph Heubeck

Tag der Disputation:

1. Dezember 2014

ERKLÄRUNG

Hiermit erkläre ich, dass die vorliegende Arbeit selbstständig und ausschließlich unter der Verwendung der angegebenen Hilfsmittel und Quellen von mir verfasst wurde. Wörtlich oder inhaltlich übernommene Stellen habe ich als solche gekennzeichnet. Ich habe diese Arbeit in keinem früheren Promotionsvorhaben eingereicht.

Berlin, August 2014

DANKSAGUNG

Mein Dank gilt Ulrich Struck und Christoph Heubeck, die mich durch meine Studien- und Promotionszeit geführt haben und mich mit ihrem fachlichen Wissen, ihrer Geduld, sowie Rat und Tat zu jeder Zeit betreuten. Vielen Dank an Frank Ohnemüller und Marina Spanka für die gemeinsame Zeit an der Universität, die vielen besonderen Exkursionen und die fachlichen und freundschaftlichen Gespräche seit dem ersten Semester. Ein großes Dankeschön an meine Familie, die mit mir emotionale Höhen und Tiefen gemeistert hat, mir mit Verständnis zur Seite stand und dadurch einen wesentlichen Anteil an dieser Arbeit trägt. Vielen lieben Dank!

ZUSAMMENFASSUNG

Der Übergang vom Ediakarium (635 - 542 Ma) in das Kambrium (542 - 485 Ma) stellt eine entscheidende Epoche in der Evolutionsgeschichte dar. Geprägt durch tektonische Umbrüche und Veränderungen des Klimas und der Ozeanchemie, dokumentiert dieser Zeitabschnitt die Entfaltung der Metazoen und ist deswegen als „Kambrische Radiation“ bekannt. Gesteinseinheiten dieser Zeit weisen charakteristische Kohlenstoff- und Stickstoffisotopenanomalien auf, welche die Vermutung nahe legen, dass ein tiefgreifender biogeochemischer Wandel in den Ozeanen in großem Maße an den evolutionären Geschehnissen beteiligt war. Hierbei scheint die Anreicherung von Sauerstoff den Kohlen- und Stickstoffkreislauf wesentlich mit Hinsicht auf die Verfügbarkeit von reduzierten und oxidierten Nährstoffen (z.B. NH_4^+, NO_3^-) für die Primärproduktion im marinen Ökosystem modifiziert zu haben. Zudem ist es bislang ungeklärt, inwiefern die biogeochemischen Signaturen globale Umweltveränderungen repräsentieren und mit den evolutionären Ereignissen in Verbindung standen.

Im Rahmen dieser Fragen widmet sich diese Arbeit der integrierten Analyse von karbonatisch gebundenem Kohlenstoff ($\delta^{13}C_{carb}$), organisch gebundenem Kohlenstoff ($\delta^{13}C_{org}$) und Stickstoff ($\delta^{15}N$) mit dem Ziel, biogeochemische Kreisläufe in Zeiten evolutionärer Innovationen anhand von stratigraphischen Abfolgen auf zwei Mikrokontinenten näher zu beschreiben. Die Isotopenanalysen erfolgten an Gesteinsabfolgen der südchinesischen Yangtze Plattform (Gaojiashan Sektion), welche die Präkambrium-Kambrium Grenze umfassen, sowie an ediakarischen bis früh-kambrischen Gesteinen des Malyi Karatau Höhenzugs in Kasachstan (Kyrshabakty und Berkuty Sektionen). Die Isotopendaten weisen drei prominente, negative $\delta^{13}C_{carb}$ Exkursionen auf: (1) Die „Cap Carbonate Anomalie“ (~635 Ma), (2) die „Shuram-Wonoka Anomalie“ (Ende ~551 Ma) und (3) die „Präkambrium-Kambrium Anomalie“ (~542 Ma). Zusammen ermöglichen die Daten erstmals eine globale chemostratigraphische Korrelation zwischen kasachischen Gesteinshorizonten und vergleichbaren, zeitäquivalenten Sektionen aus Südchina und dem Oman. Ferner unterstützt dieses Ergebnis den global repräsentativen Charakter der Isotopensignaturen. Im Detail zeigen die Isotopenwerte, dass in Zeiten des frühen Ediakariums oxygene

N_2-Fixierung ($\delta^{15}N$ ~1‰) biologische Prozesse innerhalb des Stickstoffkreislaufes dominierte, vermutlich eng assoziiert mit der Änderung des CO_2-Partialdruckes als Folge der Marinoischen Eiszeit (Ende ~635 Ma). Ein Anstieg der $\delta^{15}N$ Werte auf 3.9‰ weist auf eine Erhöhung des marinen Nitratgehaltes hin, welche vermutlich die Evolution multizellulärer Eukaryoten begleitete. Beständig negative $\delta^{13}C_{carb}$ Daten bis zu -9‰ und variierende $\delta^{13}C_{org}$ Werte (von -33 bis zu -24‰) während des Shuram-Wonoka Intervalls deuten einen redox-stratifizierten Ozean an. Dies wird durch fluktuierende $\delta^{15}N$ Werte (1.6 - 3.7‰) bestärkt, welche Schwankungen zwischen der N_2-Fixierungsrate und interagierenden Nitrifikations- und Denitrifikationsprozessen in Abhängigkeit von vertikal wechselnden Redoxbedingungen anzeigen. Eine allmählich sauerstoffreichere Wasserbeschaffenheit und erhöhte Bioproduktivität während des oberen Ediakariums (Dengying Formation, 551 - 542 Ma) ist durch eine positive $\delta^{13}C_{carb}$ Exkursion und in einer schrittweisen Erhöhung der $\delta^{15}N$ Werte auf ~5‰ beschrieben. Die Isotopenwerte verdeutlichen eine Umstellung von Distickstoff (N_2) auf Nitrat (NO_3^-) als Hauptnährstoff für marine Organismen. Des Weiteren setzte ein erhöhter Nitratgehalt eine moderate Sauerstoffkonzentration im Meerwasser voraus, welche somit einen aeroben Stickstoffkreislauf anregte und die Entwicklung der ediakarischen Fauna (Gaojiashan Biota und *Cloudina*) auf (über-)regionalem Maßstab beeinflusst haben könnte. Das Präkambrium-Kambrium Grenzintervall (Kyrshabakty Sektion) zeigt negative $\delta^{13}C_{carb}$- und $\delta^{15}N$-Anomlien und bekräftigt somit ein „ozeanisch anoxisches Ereignis“ mit zeitweilig euxinischen Episoden. $\delta^{15}N$ Werte bis zu -2.3‰ des unteren Kambriums bestätigen vorhergehende Stickstoffanalysen aus Südchina und lassen eine verstärkte Beteiligung von anoxygenen Ammonium-assimilierenden (NH_4^+) phototrophen Organismen innerhalb des Ökosystems vermuten.

Insgesamt erwiesen sich die Kohlenstoff- und Stickstoffdaten als global-nutzbares chemostratigraphisches Instrument zur Beantwortung global ökologischer Fragestellungen an der Präkambrium-Kambrium Grenze. Die Forschungsergebnisse zeigen, dass Nitrat und demzufolge auch Sauerstoff während des Ediakariums bis zu einem globalen anoxischen Ereignis in weiten Teilen des Ozeans stabil vorhanden waren.

ABSTRACT

The Ediacaran (635 - 542 Ma) - Cambrian (542 - 485 Ma) interval marks a significant epoch in the evolution of the Earth's ecosphere. This key interval documents during a time of tectonic instabilities and fundamental atmospheric and oceanic compositional changes the prominent evolution of metazoans: The emergence of animals in the so-called "Cambrian radiation event". The stratigraphic record of this interval records characteristic carbon and nitrogen isotope fluctuations which suggest their close linkage to evolutionary innovations. It has been proposed that the transition to a fully oxygenated marine environment in the course of the Ediacaran and early Cambrian affected the carbon and nitrogen cycles by limiting the availability of reduced and oxidized nutrient species (e.g. NH_4^+, NO_3^-) for organisms. However, the global and simultaneous extent of the mentioned biogeochemical signatures and their control on evolutionary proceedings remains elusive.

Integrated studies of the three isotope systems carbonate carbon ($\delta^{13}C_{carb}$), organic carbon ($\delta^{13}C_{org}$) and nitrogen ($\delta^{15}N$) greatly assist in understanding biogeochemical cycling during a time of biological innovations at stratigraphic sections on two microcontinents. These span the Precambrian-Cambrian (Pc-C) boundary on the South China Yangtze craton (Gaojiashan section) and the Ediacaran to early Cambrian on the "Kazakh microcontinent" exposed in the Malyi Karatau Range of southern Kazakhstan (Kyrshabakty and Berkuty sections). Three prominent $\delta^{13}C_{carb}$ excursions representing the (1) "cap carbonate anomaly" (~635 Ma), (2) "Shuram-Wonoka anomaly" (end ~551 Ma) and (3) "Pc-C boundary anomaly" (~542 Ma) enable it for the first time to correlate Kazakh Pc-C strata geochemically to comparable intervals in South China and Oman, thus supporting arguments for the global applicability of isotope records from these regions. Isotope analyses suggest that the early Ediacaran nitrogen cycling was dominated by oxygenic N_2-fixation ($\delta^{15}N$ ~1‰) and intimately linked to changes in atmospheric pCO_2 in the aftermath of the global Marinoan glaciation (termination ~635 Ma). A subsequent rise of nitrate (NO_3^-) reflected in elevated $\delta^{15}N$ values most likely co-occurred with the evolution of multicellular eukaryotes. Persistent negative $\delta^{13}C_{carb}$ values to ~-9‰ and variable $\delta^{13}C_{org}$ data

(-33 to -24‰) during the middle Ediacaran Shuram-Wonoka event argue for a strongly stratified ocean. This is supported by intensely fluctuating $\delta^{15}N$ values (1.6 to 3.7‰), reflecting differences in the contribution between N_2-fixation and nitrification-denitrification processes which were likely dependent on the vertical movement of the redox boundary. A transition towards mildly oxygenated water conditions with an elevated bioproductivity during the latest Ediacaran (Dengying Formation, 551 - 542 Ma) is recorded by a positive $\delta^{13}C_{carb}$ anomaly, accompanied by a stepwise increase in $\delta^{15}N$ values to ~5‰. In this regard, NO_3^- subsequently outcompeted dinitrogen (N_2) as the key nutrient for marine organisms whereby the increasing stability of NO_3^- indicates sufficient oxygen concentration to allow aerobe nitrogen cycling on the shallow shelf; this may have affected the contemporaneous rapid evolution of late Ediacaran fauna (Gaojiashan biota and *Cloudina*) on at least supra-regional scale. The Pc-C boundary interval at the Kyrshabakty section is marked by negative $\delta^{13}C_{carb}$ and $\delta^{15}N$ anomalies, supporting widespread oceanic anoxia with intermittent episodes of euxinic conditions. $\delta^{15}N$ values to -2.3‰ during the lower Cambrian confirm previous analyses from South China and indicate a large contribution of anoxygenic ammonium assimilating (NH_4^+) phototrophs to the organic matter pool.

In conclusion, the Pc-C carbon and nitrogen isotopic records of South China and Kazakhstan reveal striking similarities in worldwide time-equivalent sections and thus are reliable chemostratigraphic markers. Data showed that seawater nitrate and hence oxygen became more widespread and stable through the Ediacaran until a global Pc-C oceanic anoxic event associated with the Cambrian ecosphere (r)evolution.

ABKÜRZUNGSVERZEICHNIS

α	fractionation factor
$\delta^{13}C_{carb}$	carbonate carbon isotope composition
$\delta^{13}C_{org}$	organic carbon isotope composition
$\delta^{15}N$	nitrogen isotope composition
$\delta^{18}O$	oxygen isotope composition
ε	isotope fractionation effect
ADM	Algal Dolomite Member (South China)
Ak Mb	Aksai Member (Kazakhstan)
AkT	Aktas Tillite (Kazakhstan)
AMG	Abu Mahara Group (Oman)
BK	Berkuty
Bk Mb	Berkuty Member (Kazakhstan)
C1	$\delta^{13}C_{carb}$ negative interval at cap carbonate level (Kyrshabakty section)
C2	$\delta^{13}C_{carb}$ negative interval at Shuram-Wonoka level (Kyrshabakty section)
C3	$\delta^{13}C_{carb}$ negative interval at Pc-C boundary level (Kyrshabakty section)
CAOB	Central Asian Orogenic Belt
C_{carb}	carbonate carbon
CCF	Cap carbonate Formation (Oman)
Ch Fm	Chulaktau Formation (Kazakhstan)
Cl	*Cloudina*
C_{org}	organic carbon
DBM	Daibu Member (South China)
DIC	dissolved inorganic carbon
DIN	dissolved inorganic nitrogen
DNRA	dissimilatory nitrate reduction
DOC	dissolved organic carbon
DON	dissolved organic nitrogen
EA-IRMS	Elemental Analyzer - Isotope Ratio Mass Spectrometry

FAD	first appearance datum
Fig.	Figure
Fm	formation (geological)
FOR	Forschergruppe
FQ	Fiq Formation (Oman)
Ga	billion years ago before present
Gj	Gaojiashan
GSB	green sulfur bacteria
GSSP	Global Boundary Stratotype Section and Point
H/C	hydrogen/carbon atomic ratio
Ha	Hadash Formation (Oman)
HREE	Heavy Rare Earth Elements
IAEA	International Atomic Energy Agency
ICP-MS	Inductively Coupled Plasma - Mass Spectrometry
ICP-OES	Inductively Coupled Plasma - Optical Emission Spectrometry
KY	Kyrshabakty
LBZ	Longbizui
LREE	Light Rare Earth Elements
M	molarity
Ma	million years ago before present
Mb	Member
MBF	Masirah Bay Formation (Oman)
Mgd	Marinoan-age glacial deposit
NE1	$\delta^{13}C_{carb}$ negative excursion 1 (Gaojiashan section)
NE2	$\delta^{13}C_{carb}$ negative excursion 2 (Gaojiashan section)
PAAS	post-Archean Australian Shale
Pc-C	Precambrian-Cambrian
pCO_2	partial pressure of CO_2
PE	$\delta^{13}C_{carb}$ positive excursion (Gaojiashan section)
POC	particulate organic carbon
PON	particulate organic nitrogen
PSB	purple sulfur bacteria

RSD	relative standard deviation
S2	Series 2
Sh Fm	Shabakty Formation (Kazakhstan)
SSF	small shelly fossil
St 2	Stage 2
St 3	Stage 3
SYT	Shyantou Formation (South China)
TN	total nitrogen
TOC	total organic carbon
VPDB	Vienna Pee Dee Belemnite
XF	Xiaofenghe
XRD	X-ray diffraction
YAS	Yu'anshan Formation (South China)
ZGM	Zhangyicun Member (South China)

INHALTSVERZEICHNIS

1. OBJECTIVES AND CONCEPT

1.1 Objectives

This thesis investigates the marine nitrogen and carbon biogeochemical cycling during the Precambrian (Ediacaran) and across the Precambrian-Cambrian boundary interval and examines its chemostratigraphic record on a global scale.

The pivotal transition from the Proterozoic to the Phanerozoic is characterized by a most significant radiation event of metazoan life in Earth history accompanied by large fluctuations in carbon isotope compositions of respective sediments (Shields-Zhou and Zhu, 2013; Smith and Harper, 2013). Isotope excursions are proposed to reflect intensely shifting oceanic redox conditions (Fike et al., 2006; Wang et al., 2012) which could have significantly affected the availability of bio-limiting nutrients for organisms in the ecosphere and the subsequent evolutionary events. Thus, this thesis examines the isotopic compositions of the bio-relevant elements nitrogen ($\delta^{15}N$), organic carbon ($\delta^{13}C_{org}$) and carbonate carbon ($\delta^{13}C_{carb}$) in sedimentary rocks spanning the Precambrian-Cambrian transition interval to gain insights into the paleoenvironmental conditions, ocean redox structure and past seawater chemistry. This research will focus particularly on the study of nitrogen isotopes which are known to provide information about the nutrient utilization of microorganisms in surface waters, as well as the water oxygenation and ocean ventilation state (e.g. Ader et al., 2014; Cremonese et al., 2014; Kikumoto et al., 2014). To date, no complete Ediacaran-Cambrian nitrogen isotope record outside of South China exists. Analyses will be supported by carbon isotopes specifying the rate of primary productivity and the intensity of the biological pump. To complement previous datasets (Cremonese et al., 2013; Ader et al., 2014; Cremonese et al., 2014; Kikumoto et al., 2014; Spangenberg et al., 2014) on regional and global scale, investigations are based on samples collected from two areas: The Yangtze platform of South China and the Karatau region of southern Kazakhstan. Field work was conducted in September 2011 (Kazakhstan) and in March-April 2012

(South China). In total, 16 sections were visited of which 14 were sampled for geochemical analyses. Additionally, a sample suite collected by Q. Scouflaire and B. Weber (Freie Universität Berlin) in 2009 was analyzed. All isotope analyses were performed at the laboratories of the Museum für Naturkunde Berlin.

This thesis is embedded in subproject 2 of the Forschergruppe 736 "*The Precambrian-Cambrian Ecosphere (R)evolution: Insights from Chinese Microcontinents*" which generated multi-proxy datasets across the Precambrian-Cambrian interval of South China and Kazakhstan and was funded by the German Research Foundation (DFG-FOR 736). Sample suites were in part also analyzed by Frank Ohnemueller and Simone Kasemann (Universität Bremen, subproject 7) for boron, strontium and partly lithium isotopes, by Simon Hohl and Harry Becker (Freie Universität Berlin, subproject 4) for Rare Earth Element analyses, by Christoph Heubeck (Freie Universität Berlin, subproject 1, now at Friedrich-Schiller Universität Jena) for sedimentary investigations and by Caroline Seidig and Michael Steiner (Freie Universität Berlin, subproject 3) for paleontological and biostratigraphic purposes.

1.2 Concept

This thesis comprises three single manuscripts (chapter 5, 6 and 7) in final preparation which will be published in peer-reviewed journals. Chapter 2 reviews the principal evolutionary and biogeochemical events across the Precambrian-Cambrian boundary, followed by a detailed review of the biogeochemistry in the marine nitrogen and carbon cycle in chapter 3. Chapter 4 introduces the geological and paleogeographic settings of the study areas. Chapter 5 discusses the chemostratigraphy at Gaojiashan section (manuscript 1) which is complemented by biogeochemical investigations at the same section presented in chapter 6 (manuscript 2). Chapter 7 discusses chemostratigraphic and biogeochemical results of Kyrshabakty and Berkuty sections (manuscript 3). Following the manuscripts (chapter 5 - 7), chapter 8 summarizes the main research results and evaluates them in a comprehensive context. Finally, chapter 9 offers an outlook for possible future studies.

Contributions by the co-authors to the manuscripts were as follows:

Chapter 5: Chemo- and biostratigraphy of the Gaojiashan section
(northern Yangtze Platform, South China): A new Pc-C boundary section

Antonia Gamper[a], Ulrich Struck[a], Frank Ohnemueller[b], Christoph Heubeck[c], Simon Hohl[c]

[a] Museum für Naturkunde Berlin, Leibniz-Institut für Evolutions- und Biodiversitätsforschung, Invalidenstraße 43, 10115 Berlin, Germany

[b] Fachbereich Geowissenschaften (FB 5) und MARUM - Zentrum für Marine Umweltwissenschaften, Universität Bremen, Leobener Str., 28359 Bremen, Germany

[c] Institut für Geologische Wissenschaften, Freie Universität Berlin, Malteserstraße 74-100, 12249 Berlin, Germany

The manuscript introduces the problematic discrepancies of purely lithostratigraphic correlation of late Ediacaran strata on the northern margin of the Neoproterozoic Yangtze platform (Shaanxi Province, South China) and suggests a new stratigraphic correlation based on carbon isotope chemostratigraphy. Chemostratigraphic correlations resulted from discussions between Antonia Gamper and Frank Ohnemueller. Paleoenvironment scenarios

were worked out by all authors. Fieldwork and sample collection was carried out by Quentin Scouflaire, Christoph Heubeck and Bernd Weber (Freie Universität Berlin) in 2009. Quentin Scouflaire drew an early version of the stratigraphic column which was subsequently modified by Antonia Gamper. Sample preparation for isotope analyses was conducted by Antonia Gamper and Frank Ohnemueller. Ulrich Struck introduced Antonia Gamper to analytical methods and supervised them. Carbonate carbon and oxygen isotope analyses were carried out by Ulrich Struck, total organic carbon (TOC) measurement by Antonia Gamper. Simon Hohl conducted Rare Earth Element (REE+Y) measurements. Antonia Gamper wrote the manuscript and composed figures and tables. Ulrich Struck, Christoph Heubeck and Frank Ohnemueller contributed to the manuscript through discussions and reviews.

Chapter 6: Carbon and nitrogen isotope biogeochemistry of the upper Dengying Formation in South China: Implications for the Late Ediacaran shallow-marine ecosphere and oceanic redox conditions

Antonia Gamper[a], Ulrich Struck[a], Simon Hohl[b], Hong-Fei Ling[c]

[a] Museum für Naturkunde Berlin, Leibniz-Institut für Evolutions- und Biodiversitätsforschung, Invalidenstraße 43, 10115 Berlin, Germany

[b] Institut für Geologische Wissenschaften, Freie Universität Berlin, Malteserstraße 74-100, 12249 Berlin, Germany

[c] State Key Laboratory for Mineral Deposits Research, Department of Earth Sciences, Nanjing University, Nanjing 210093, China

Chapter 6 presents organic carbon and nitrogen isotope data of the Gaojiashan section and discusses them in the light of biogeochemical cycling associated to the occurrence of late Ediacaran fauna assemblages. The paleoenvironmental model originated from discussions with Antonia Gamper and Ulrich Struck. Antonia Gamper performed isotopic measurements ($\delta^{13}C_{org}$, $\delta^{15}N$) of all samples which are the same reported in chapter 5, wrote the manuscript and drew figures and tables. Simon Hohl measured Rare Earth Element (REE+Y) abundance. Hong-Fei Ling provided access to sample locations and organized sample transport to Germany. Ulrich Struck assisted in structuring and writing the manuscript.

Co-authors contributed detailed reviews. Isotopic data of the Gaojiashan section (including $\delta^{13}C_{carb}$ data of chapter 5) were presented at the Fermor meeting of the Geological Society 2012 ("The Neoproterozoic Era") in London and at the Paläontologische Jahrestagung 2012 in Berlin (see for references Appendix A1).

Chapter 7: Ediacaran to Cambrian chemostratigraphy and biogeochemical cycling from carbon and nitrogen isotopes of the Kyrshabakty section (southern Kazakhstan)

Antonia Gamper[a], Ulrich Struck[a], Gappar Ergaliev[b]

[a] Museum für Naturkunde Berlin, Leibniz-Institut für Evolutions- und Biodiversitätsforschung, Invalidenstraße 43, 10115 Berlin, Germany

[b] Institute of Geological Sciences, Almaty 050010, Kazakhstan

The manuscript provides an extensive isotopic dataset ($\delta^{13}C_{carb}$, $\delta^{13}C_{org}$, $\delta^{15}N$) of a sedimentary sequence located on the Neoproterozoic-Cambrian Kazakh microcontinent, proposes global chemostratigraphic correlation based on three prominent Ediacaran to Cambrian negative $\delta^{13}C_{carb}$ anomalies and describes changes in biogeochemical cycling during each anomaly. Chemostratigraphic correlation was conducted by Antonia Gamper who wrote the manuscript and drafted figures and tables. Interpretation of the isotopic dataset grew during discussions between Antonia Gamper and Ulrich Struck. Samples were collected by Antonia Gamper and Frank Ohnemueller during a field trip to Kazakhstan of the Forschergruppe in 2011 except for 7 samples (marked with KR-11, chapter 7) which were provided by Dorothee Hippler (Technische Universität Berlin, subproject 5, FOR 736). Gappar Ergaliev guided the field trip in Kazakhstan and logistically organized sample transport to Germany. All isotope analyses of $\delta^{13}C_{org}$ and $\delta^{15}N$ as well as TOC measurements were performed by Antonia Gamper; $\delta^{13}C_{carb}$ and $\delta^{18}O$ analyses by Ulrich Struck who also provided manuscript reviews. First results have been presented at the Goldschmidt conference 2013 in Florence (see for reference Appendix A1). Detailed interpretations will be presented at the annual conference meeting of the

Geological Society of America in October 2014 in Vancouver (see for reference Appendix A1).

1.3 References

Ader, M., Sansjofre, P., Halverson, G. P., Busigny, V., Trindade, R. I. F., Kunzmann, M., and Nogueira, A. C. R., 2014, Ocean redox structure across the Late Neoproterozoic Oxygenation Event: A nitrogen isotope perspective: Earth and Planetary Science Letters, v. 396, no. 0, p. 1-13.

Cremonese, L., Shields-Zhou, G., Struck, U., Ling, H.-F., Och, L., Chen, X., and Li, D., 2013, Marine biogeochemical cycling during the early Cambrian constrained by a nitrogen and organic carbon isotope study of the Xiaotan section, South China: Precambrian Research, v. 225, no. 0, p. 148-165.

Cremonese, L., Shields-Zhou, G. A., Struck, U., Ling, H.-F., and Och, L. M., 2014, Nitrogen and organic carbon isotope stratigraphy of the Yangtze Platform during the Ediacaran–Cambrian transition in South China: Palaeogeography, Palaeoclimatology, Palaeoecology, v. 398, no. 0, p. 165-186.

Fike, D. A., Grotzinger, J. P., Pratt, L. M., and Summons, R. E., 2006, Oxidation of the Ediacaran Ocean: Nature, v. 444, no. 7120, p. 744-747.

Kikumoto, R., Tahata, M., Nishizawa, M., Sawaki, Y., Maruyama, S., Shu, D., Han, J., Komiya, T., Takai, K., and Ueno, Y., 2014, Nitrogen isotope chemostratigraphy of the Ediacaran and Early Cambrian platform sequence at Three Gorges, South China: Gondwana Research, v. 25, no. 3, p. 1057-1069.

Shields-Zhou, G., and Zhu, M., 2013, Biogeochemical changes across the Ediacaran–Cambrian transition in South China: Precambrian Research, v. 225, no. 0, p. 1-6.

Smith, M. P., and Harper, D. A. T., 2013, Causes of the Cambrian Explosion: Science, v. 341, no. 6152, p. 1355-1356.

Spangenberg, J. E., Bagnoud-Velásquez, M., Boggiani, P. C., and Gaucher, C., 2014, Redox variations and bioproductivity in the Ediacaran: Evidence from inorganic and organic geochemistry of the Corumbá Group, Brazil: Gondwana Research, http://dx.doi.org/10.1016/j.gr.2013.08.014.

Wang, W., Zhou, C., Yuan, X., Chen, Z., and Xiao, S., 2012, A pronounced negative $\delta^{13}C$ excursion in an Ediacaran succession of western Yangtze Platform: A possible equivalent to the Shuram event and its implication for chemostratigraphic correlation in South China: Gondwana Research, v. 22, no. 3–4, p. 1091-1101.

2. THE PRECAMBRIAN-CAMBRIAN ECOSPHERE (R)EVOLUTION

2.1 Introduction to the Precambrian-Cambrian Period

The Precambrian-Cambrian (Pc-C) interval represents the transition from the late Neoproterozoic Ediacaran (*ca.* 635 - 542 million years ago before present (Ma)) to the early Paleozoic Cambrian (*ca.* 542 - 485 Ma). The Pc-C period marks a significant time in Earth's history in which global tectonics led to the breakup of the Rodinia supercontinent, climatic conditions dramatically shifted from icehouse to greenhouse and the radiation of multicellular life culminated in the evolution of early animals (Kaufman et al., 1993; Hoffman et al., 1998; Fairchild and Kennedy, 2007; Shields, 2007; Shields-Zhou and Zhu, 2013; Smith and Harper, 2013). The beginning of the Ediacaran System is defined at the base of the cap carbonate strata of the Nuccaleena Formation in the Enorama Creek section of South Australia (Global Boundary Stratotype Section and Point (GSSP); Knoll et al., 2006). Cap carbonates were deposited in the direct aftermath of the late Cryogenian Marinoan glaciation, which ended ~635 Ma ago (Condon et al., 2005). Cap carbonate strata represent worldwide occurring characteristic lithological features of basal Ediacaran sections and therefore display an adequate lithostratigraphic correlation tool which defines the transition from the late Cryogenian icehouse era to a phase of global warming (Hoffmann et al., 2004). The Ediacaran period experienced profound changes in biogeochemical cycles linked to further (local) glaciation events (e.g. Gaskiers glaciation ~582 Ma; Bowring et al., 2003; Halverson et al., 2005; Baykonurian glaciation of possibly terminal Ediacaran-age; Chumakov, 2009; Chumakov, 2011) and the progressive oxygenation of the deep ocean associated with the rise of aquatic and atmospheric oxygen levels (Fike et al., 2006) culminating in a subsequent transition from anoxic-ferruginous to oxic "modern" deep-oceanic conditions in the early Cambrian (e.g. Och et al., 2013). Environmental perturbations are proposed to have played an integral role in evolutional innovations of Ediacaran organisms including the appearance of large spiny acritarchs followed by the soft-bodied, largely immobile Ediacaran biota with

earliest traces of (vertical) burrows and calcifying organisms towards the end of the Ediacaran (Weber et al., 2007; Zhu et al., 2007b; McFadden et al., 2008). However, the Ediacaran fauna disappeared (Shu et al., 2014) and was followed by the onset of colonization of the Earth's environment by metazoans (Steiner et al., 2007). The Pc-C boundary interval witnessed an important radiation event called the "Cambrian explosion" (Shu, 2008; Smith and Harper, 2013) in which a rapid diversification of animal groups took place and new trophic structures and complex food webs associated with major biogeochemical changes (e.g. oxygenation of surface waters, redox oscillations, advent of biomineralization and burrowing, predatory and camouflage strategies) in the ecosystem evolved (Brasier, 1992; Weber et al., 2007; Ishikawa et al., 2013). Therefore, the base of the Cambrian is defined by the first appearance datum (FAD) of the trace fossil *Treptichnus/Trichophycus pedum* (GSSP index fossil) in the Chapel Island Formation of the Fortune Head section, Newfoundland, Canada (Brasier et al., 1994). However, the biostratigraphy of Cambrian small shelly fossils (SSFs) recently came again into consideration because the occurrence of the trace fossil *Treptichnus/Trichophycus pedum* is widely absent in Cambrian sediments or occurs unconvincingly (Steiner et al., 2007). An U-Pb zircon age of 542.6 ± 0.3 Ma from the Ara Group in Oman which coincides with a prominent negative $\delta^{13}C_{carb}$ excursion represents the estimated age of the Pc-C boundary (Amthor et al., 2003).

Compositional changes of the Earth's atmosphere and oceans which accompany the evolutionary events are recorded by several global occurring isotope anomalies shown in Figure (Fig.) 1. Carbonate carbon isotope geochemistry is the most traditional isotopic proxy to interpret environmental changes; thus, three major carbonate carbon ($\delta^{13}C_{carb}$) anomalies characterize the Ediacaran to Cambrian time beginning with the lowermost Ediacaran "cap carbonate anomaly" (~635 Ma), followed by the "Shuram-Wonoka anomaly" (end ~551 Ma) and the "Pc-C boundary anomaly" (~542 Ma; e.g. Zhu et al., 2007b; Le Guerroué, 2010).

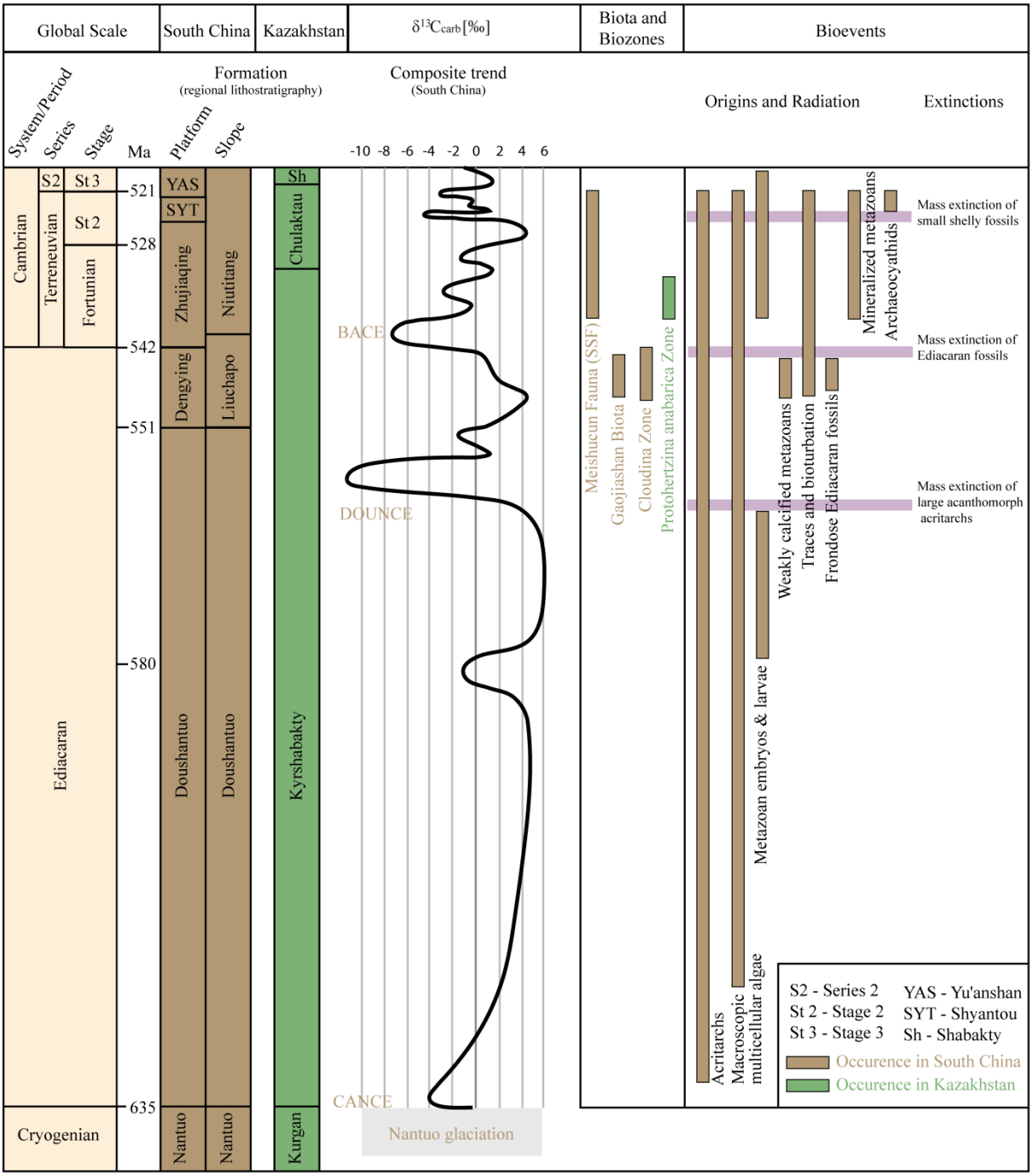

Figure 1: Integrated schematic stratigraphic record of the Ediacaran and lower Cambrian System showing the chronostratigraphic framework of South China and Kazakhstan with interpreted, time-equivalent occurrences of biota, biozones and bioevents. $\delta^{13}C_{carb}$ data represent a compilation of South China datasets after Zhu et al. (2007a). The CANCE, DOUNCE and BACE $\delta^{13}C_{carb}$ negative excursions represent the South China equivalents to the global "cap carbonate anomaly", "Shuram-Wonoka anomaly" and "Pc-C boundary anomaly", respectively. Figure 1 is compiled and modified after Zhu et al. (2007a); Zhu et al. (2007b); Shields-Zhou and Zhu (2013); Weber et al. (2013).

Reported isotope anomalies also serve for chemostratigraphic correlation because they are documented in time-equivalent strata on several Pc-C microcontinents and occur in, e.g., South China, Oman, Australia, Namibia, Brazil, Mongolia, Siberia, Kazakhstan and Canada (Brasier et al., 1994; Brasier et al., 1996; Calver, 2000; Amthor et al., 2003; Hoffmann et al., 2004; Halverson et al., 2005; Kasemann et al., 2005; Fike et al., 2006; Le Guerroué et al., 2006; McFadden et al., 2008; Boggiani et al., 2010; Kasemann et al., 2010; Pokrovsky et al., 2010; Sial et al., 2010; Meert et al., 2011; Sansjofre et al., 2011; Li et al., 2013; Lu et al., 2013; Macdonald et al., 2013; Cremonese et al., 2014). Mechanisms triggering the prominent isotope excursions as well as their primary origin are still a matter of debate (Bristow and Kennedy, 2008; Knauth and Kennedy, 2009; Derry, 2010). Nevertheless, a stepwise oxygenation of the Ediacaran ocean (Fike et al., 2006; McFadden et al., 2008) and a widespread oceanic anoxic event across the Pc-C boundary find wide acceptance and are suggested to have affected biogeochemical cycling and evolutional processes (Ishikawa et al., 2008; Wille et al., 2008).

Specific paleoenvironmental redox changes and biosignatures during the Pc-C interval are recorded by particular variations in nitrogen ($\delta^{15}N$) and organic carbon ($\delta^{13}C_{org}$) isotopes (Cremonese et al., 2013; Ishikawa et al., 2013; Cremonese et al., 2014; Kikumoto et al., 2014). Thereby, investigations of sedimentary $\delta^{15}N$ and $\delta^{13}C_{org}$ values provide information about the extent and magnitude of biogeochemical transformations during production and degradation of organic matter which result in different extents of isotopic fractionations and thus characteristic isotope values (Struck, 2012). Recently, a negative $\delta^{15}N$ excursion across the Pc-C boundary was suggested to represent a pronounced anoxic event (Cremonese et al., 2013; Cremonese et al., 2014) which largely affected the nutrient availability in terms of the stability of oxidized and reduced nitrogen species (e.g. nitrate and ammonium) and the microbial community involved; however, datasets collected to date lack global confirmation.

2.2 References

Amthor, J. E., Grotzinger, J. P., Schröder, S., Bowring, S. A., Ramezani, J., Martin, M. W., and Matter, A., 2003, Extinction of Cloudina and Namacalathus at the Precambrian-Cambrian boundary in Oman: Geology, v. 31, p. 431-434.

Boggiani, P. C., Gaucher, C., Sial, A. N., Babinski, M., Simon, C. M., Riccomini, C., Ferreira, V. P., and Fairchild, T. R., 2010, Chemostratigraphy of the Tamengo Formation (Corumbá Group, Brazil): A contribution to the calibration of the Ediacaran carbon-isotope curve: Precambrian Research, v. 182, no. 4, p. 382-401.

Bowring, S. A., Myrow, P., and Landing, E., 2003, Geochronological constraints on terminal Neoproterozoic events and the rise of Metazoan: Geophysical Research Abstracts, v. 5, p. 13219.

Brasier, M. D., 1992, Nutrient-enriched waters and the early skeletal fossil record: Journal of the Geological Society, v. 149, no. 4, p. 621-629.

Brasier, M. D., Rozanov, A. Y., Zhuravlev, A. Y., Corfield, R. M., and Derry, L. A., 1994, A carbon-isotope reference scale for the Lower Cambrian succession in Siberia - Report of IGCP project-303: Geological Magazine, v. 131, no. 6, p. 767-783.

Brasier, M. D., Shields, G., Kuleshov, V. N., and Zhegallo, E. A., 1996, Integrated chemo- and biostratigraphic calibration of early animal evolution: Neoproterozoic-early Cambrian of southwest Mongolia: Geological Magazine, v. 133, no. 4, p. 445-485.

Bristow, T. F., and Kennedy, M. J., 2008, Carbon isotope excursions and the oxidant budget of the Ediacaran atmosphere and ocean: Geology, v. 36, no. 11, p. 863-866.

Calver, C. R., 2000, Isotope stratigraphy of the Ediacarian (Neoproterozoic III) of the Adelaide Rift Complex, Australia, and the overprint of water column stratification: Precambrian Research, v. 100, no. 1–3, p. 121-150.

Chumakov, N. M., 2009, The Baykonurian Glaciohorizon of the Late Vendian: Stratigraphy and Geological Correlation, v. 17, no. 4, p. 373-381.

Chumakov, N. M., 2011, Glacial deposits of the Baykonur Formation, Kazakhstan and Kyrgyzstan: Geological Society, London, Memoirs, v. 36, no. 1, p. 303-307.

Condon, D., Zhu, M., Bowring, S., Wang, W., Yang, A., and Jin, Y., 2005, U-Pb Ages from the Neoproterozoic Doushantuo Formation, China: Science, v. 308, no. 5718, p. 95-98.

Cremonese, L., Shields-Zhou, G., Struck, U., Ling, H.-F., Och, L., Chen, X., and Li, D., 2013, Marine biogeochemical cycling during the early Cambrian constrained by a nitrogen and organic carbon isotope study of the Xiaotan section, South China: Precambrian Research, v. 225, no. 0, p. 148-165.

Cremonese, L., Shields-Zhou, G. A., Struck, U., Ling, H.-F., and Och, L. M., 2014, Nitrogen and organic carbon isotope stratigraphy of the Yangtze Platform during the Ediacaran–Cambrian transition in South China: Palaeogeography, Palaeoclimatology, Palaeoecology, v. 398, no. 0, p. 165-186.

Derry, L. A., 2010, A burial diagenesis origin for the Ediacaran Shuram–Wonoka carbon isotope anomaly: Earth and Planetary Science Letters, v. 294, no. 1–2, p. 152-162.

Fairchild, I. J., and Kennedy, M. J., 2007, Neoproterozoic glaciation in the earth system: Journal of the Geological Society, v. 164, p. 895-921.

Fike, D. A., Grotzinger, J. P., Pratt, L. M., and Summons, R. E., 2006, Oxidation of the Ediacaran Ocean: Nature, v. 444, no. 7120, p. 744-747.

Halverson, G. P., Hoffman, P. F., Schrag, D. P., Maloof, A. C., and Rice, A. H. N., 2005, Toward a Neoproterozoic composite carbon-isotope record: Geological Society of America Bulletin, v. 117, no. 9-10, p. 1181-1207.

Hoffman, P. F., Kaufman, A. J., Halverson, G. P., and Schrag, D. P., 1998, A Neoproterozoic snowball earth: Science, v. 281, no. 5381, p. 1342-1346.

Hoffmann, K. H., Condon, D. J., Bowring, S. A., and Crowley, J. L., 2004, U-Pb zircon date from the Neoproterozoic Ghaub Formation, Namibia: Constraints on Marinoan glaciation: Geology, v. 32, no. 9, p. 817-820.

Ishikawa, T., Ueno, Y., Komiya, T., Sawaki, Y., Han, J., Shu, D., Li, Y., Maruyama, S., and Yoshida, N., 2008, Carbon isotope chemostratigraphy of a Precambrian/Cambrian boundary section in the Three Gorge area, South China: Prominent global-scale isotope excursions just before the Cambrian Explosion: Gondwana Research, v. 14, no. 1–2, p. 193-208.

Ishikawa, T., Ueno, Y., Shu, D., Li, Y., Han, J., Guo, J., Yoshida, N., and Komiya, T., 2013, Irreversible change of the oceanic carbon cycle in the earliest Cambrian: High-resolution organic and inorganic carbon chemostratigraphy in the Three Gorges area, South China: Precambrian Research, v. 225, no. 0, p. 190-208.

Kasemann, S. A., Hawkesworth, C. J., Prave, A. R., Fallick, A. E., and Pearson, P. N., 2005, Boron and calcium isotope composition in Neoproterozoic carbonate rocks from Namibia: evidence for extreme environmental change: Earth and Planetary Science Letters, v. 231, no. 1-2, p. 73-86.

Kasemann, S. A., Prave, A. R., Fallick, A. E., Hawkesworth, C. J., and Hoffmann, K. H., 2010, Neoproterozoic ice ages, boron isotopes, and ocean acidification: Implications for a snowball Earth: Geology, v. 38, no. 9, p. 775-778.

Kaufman, A. J., Jacobsen, S. B., and Knoll, A. H., 1993, The Vendian record of Sr and C-isotopic variations in seawater: Implications for tectonics and paleoclimate: Earth and Planetary Science Letters, v. 120, no. 3-4, p. 409-430.

Kikumoto, R., Tahata, M., Nishizawa, M., Sawaki, Y., Maruyama, S., Shu, D., Han, J., Komiya, T., Takai, K., and Ueno, Y., 2014, Nitrogen isotope chemostratigraphy of the Ediacaran and Early Cambrian platform sequence at Three Gorges, South China: Gondwana Research, v. 25, no. 3, p. 1057-1069.

Knauth, L. P., and Kennedy, M. J., 2009, The late Precambrian greening of the Earth: Nature, v. 460, no. 7256, p. 728-732.

Knoll, A. H., Walter, M. R., Narbonne, G. M., and Christie-Blick, N., 2006, The Ediacaran Period: a new addition to the geologic time scale: Lethaia, v. 39, no. 1, p. 13-30.

Le Guerroué, E., Allen, P. A., and Cozzi, A., 2006, Chemostratigraphic and sedimentological framework of the largest negative carbon isotopic excursion in Earth history: The Neoproterozoic Shuram Formation (Nafun Group, Oman): Precambrian Research, v. 146, no. 1–2, p. 68-92.

Le Guerroué, E., 2010, Duration and synchroneity of the largest negative carbon isotope excursion on Earth: The Shuram/Wonoka anomaly: Comptes Rendus Geoscience, v. 342, no. 3, p. 204-214.

Li, D., Ling, H.-F., Shields-Zhou, G. A., Chen, X., Cremonese, L., Och, L., Thirlwall, M., and Manning, C. J., 2013, Carbon and strontium isotope evolution of seawater across the Ediacaran–Cambrian transition: Evidence from the Xiaotan section, NE Yunnan, South China: Precambrian Research, v. 225, no. 0, p. 128-147.

Lu, M., Zhu, M., Zhang, J., Shields-Zhou, G., Li, G., Zhao, F., Zhao, X., and Zhao, M., 2013, The DOUNCE event at the top of the Ediacaran Doushantuo Formation, South China: Broad stratigraphic occurrence and non-diagenetic origin: Precambrian Research, v. 225, no. 0, p. 86-109.

Macdonald, F. A., Strauss, J. V., Sperling, E. A., Halverson, G. P., Narbonne, G. M., Johnston, D. T., Kunzmann, M., Schrag, D. P., and Higgins, J. A., 2013, The stratigraphic relationship between the Shuram carbon isotope excursion, the oxygenation of Neoproterozoic oceans, and the first appearance of the Ediacara biota and bilaterian trace fossils in northwestern Canada: Chemical Geology, v. 362, no. 0, p. 250-272.

McFadden, K. A., Huang, J., Chu, X., Jiang, G., Kaufmann, A. J., Zhou, C., Yuan, X., and Xiao, S., 2008, Pulsed oxidation and biological evolution in the Ediacaran Doushantuo Formation: PNAS, v. 105, no. 9, p. 3197-3202.

Meert, J. G., Gibsher, A. S., Levashova, N. M., Grice, W. C., Kamenov, G. D., and Ryabinin, A. B., 2011, Glaciation and ~770 Ma Ediacara (?) Fossils from the Lesser Karatau Microcontinent, Kazakhstan: Gondwana Research, v. 19, p. 867-880.

Och, L. M., Shields-Zhou, G. A., Poulton, S. W., Manning, C., Thirlwall, M. F., Li, D., Chen, X., Ling, H., Osborn, T., and Cremonese, L., 2013, Redox changes in Early Cambrian black shales at Xiaotan section, Yunnan Province, South China: Precambrian Research, v. 225, no. 0, p. 166-189.

Pokrovsky, B. G., Chumakov, N. M., Melezhik, V. A., and Bujakaite, M. I., 2010, Geochemical properties of Neoproterozoic “cap dolomites” in the Patom paleobasin and problem of their genesis: Lithology and Mineral Resources, v. 45, no. 6, p. 577-592.

Sansjofre, P., Ader, M., Trindade, R. I. F., Elie, M., Lyons, J., Cartigny, P., and Nogueira, A. C. R., 2011, A carbon isotope challenge to the snowball Earth: Nature, v. 478, no. 7367, p. 93-96.

Shields-Zhou, G., and Zhu, M., 2013, Biogeochemical changes across the Ediacaran–Cambrian transition in South China: Precambrian Research, v. 225, no. 0, p. 1-6.

Shields, G. A., 2007, A normalised seawater strontium isotope curve: possible implications for Neoproterozoic-Cambrian weathering rates and the further oxygenation of the Earth: eEarth, v. 2, no. 2, p. 35-42.

Shu, D., 2008, Cambrian explosion: Birth of tree of animals: Gondwana Research, v. 14, no. 1–2, p. 219-240.

Shu, D., Isozaki, Y., Zhang, X., Han, J., and Maruyama, S., 2014, Birth and early evolution of metazoans: Gondwana Research, v. 25, no. 3, p. 884-895.

Sial, A. N., Gaucher, C., Filho, M. A. d. S., Ferreira, V. P., Pimentel, M. M., Lacerda, L. D., Filho, E. V. S., and Cezario, W., 2010, C-, Sr-isotope and Hg chemostratigraphy of Neoproterozoic cap carbonates of the Sergipano Belt, Northeastern Brazil: Precambrian Research, v. 182, no. 4, p. 351-372.

Smith, M. P., and Harper, D. A. T., 2013, Causes of the Cambrian Explosion: Science, v. 341, no. 6152, p. 1355-1356.

Steiner, M., Li, G., Qian, Y., Zhu, M., and Erdtmann, B.-D., 2007, Neoproterozoic to Early Cambrian small shelly fossil assemblages and a revised biostratigraphic correlation of the Yangtze Platform (China): Palaeogeography, Palaeoclimatology, Palaeoecology, v. 254, no. 1–2, p. 67-99.

Struck, U., 2012, On The Use of Stable Nitrogen Isotopes in Present and Past Anoxic Environments, *in* Altenbach, A. V., Bernhard, J. M., and Seckbach, J., eds., Anoxia, Volume 21, Springer Netherlands, p. 497-513.

Weber, B., Steiner, M., and Zhu, M.-Y., 2007, Precambrian–Cambrian trace fossils from the Yangtze Platform (South China) and the early evolution of bilaterian lifestyles: Palaeogeography, Palaeoclimatology, Palaeoecology, v. 254, no. 1-2, p. 328-349.

Weber, B., Steiner, M., Evseev, S., and Yergaliev, G., 2013, First report of a Meishucun-type early Cambrian (Stage 2) ichnofauna from the Malyi Karatau area (SE Kazakhstan): Palaeoichnological, palaeoecological and palaeogeographical implications: Palaeogeography Palaeoclimatology Palaeoecology, v. 392, p. 209-231.

Wille, M., Nagler, T. F., Lehmann, B., Schroder, S., and Kramers, J. D., 2008, Hydrogen sulphide release to surface waters at the Precambrian/Cambrian boundary: Nature, v. 453, no. 7196, p. 767-769.

Zhu, M., Strauss, H., and Shields, G. A., 2007a, From snowball earth to the Cambrian bioradiation: Calibration of Ediacaran–Cambrian earth history in South China: Palaeogeography, Palaeoclimatology, Palaeoecology, v. 254, no. 1–2, p. 1-6.

Zhu, M., Zhang, J., and Yang, A., 2007b, Integrated Ediacaran (Sinian) chronostratigraphy of South China: Palaeogeography, palaeoclimatology, Palaeoecology, v. 254, p. 7-61.

3. ISOTOPE BIOGEOCHEMISTRY OF THE MARINE NITROGEN AND CARBON CYCLE

The following section reviews biogeochemical nitrogen and carbon cycling and their associated isotope signatures. In contrast to nitrogen, carbon isotope geochemistry is a well-studied and widely applied geochemical proxy and is therefore only briefly introduced.

3.1 The modern marine nitrogen cycle

Nitrogen is a key component of marine biomass and essential for all living organisms. Therefore, the production of organic matter in the ocean is strongly dependent on the availability of nitrogen which forms together with carbon and phosphorus substantial nutrients for the living biosphere. The biogeochemistry of nitrogen is predominantly dependent on reduction-oxidation (redox) reactions mediated by microorganisms and is less affected by recycling through the geosphere over longer time periods (Falkowski, 1997; Canfield et al., 2010). During microbial metabolic activities, nitrogen transformation results in the gain or loss of electrons and thus the oxidation state of nitrogen varies from the most oxidized compound nitrate (+5) to the most reduced compound ammonium (-3). The most utilized nitrogen nutrients for primary producers are inorganic "fixed" species (dinitrogen, nitrate, and ammonium). In contrast, many protozoans and all metazoans are dependent on bioavailable forms of nitrogen and obtain nitrogen compounds by ingestion of particulate or dissolved organic nitrogen (PON, DON, respectively; Karl and Michaels, 2001). For an overview, Table 1 summarizes the most commonly used nitrogen transformation pathways by microorganisms in the ocean.

The Earth's atmosphere contains a large amount of nitrogen in the form of dinitrogen (presently ~3.98×10^{21} g; Busigny and Bebout, 2013). The exchange of gaseous nitrogen between the surface ocean and the atmosphere is constant resulting in a permanent nitrogen flux between the pools. The dominant form of nitrogen in the ocean is dissolved gaseous dinitrogen (N_2) accounting for ~95% of the total nitrogen inventory. However, N_2 has a strong triple bond which renders

this nitrogen species almost inert and thus highly limits its utility for organisms (Karl and Michaels, 2001). Nevertheless, some photoautotrophic primary producers are able to fix N_2 and are therefore referred to as diazotrophic organisms. During photosynthesis, these organisms use light as their energy source to fix carbon dioxide (CO_2) and N_2 for biosynthesis. Consequently, their occurrence is strictly bound to the photic zone in the ocean (Fig. 2; Table 1) and further limited by the availability of phosphorus, iron and molybdenum in some parts of the modern oceans (Sanudo-Wilhelmy et al., 2001; Zerkle et al., 2008; Zerkle et al., 2011; Zhang et al., 2014). The majority of oxygenic diazotrophs is among bacteria (cyanobacteria) and archaea which apply the high activation energy to break the triple bond of the N_2 molecule (Canfield et al., 2010). Thus, they provide newly bioavailable nitrogen to the biological cycle.

Table 1: The most significant biologically mediated processes transforming nitrogen in the marine nitrogen cycle modified after Gruber (2008).

Process	Organisms	Redoxenvironment	Trophic status	Biochemical role
N_2-fixation	Cyanobacteria, etc.	aerob	photoautotrophic	Source of N
N_2-fixation / NH_4^+ assimilation	Purple sulfur bacteria, etc.	anaerob	photoautotrophic	Source of N
NO_3^- assimilation	Phytoplankton	aerob	photoautotrophic	Source of N
NH_4^+ assimilation	Phytoplankton	aerob	photoautotrophic	Source of N
	Bacteria	aerob/anaerob	heterotrophic	Source of N
Nitrification:				
1) NH_4^+ oxidation	NH_4^+ oxidizers	aerob	chemoautotrophic	Source of energy
2) NO_2^- oxidation	NO_2^- oxidizers	aerob	chemoautotrophic	Source of energy
Ammonification	Bacteria/Zooplankton	aerob/anaerob	heterotrophic	Release of N
Denitrification	Bacteria	anaerob	heterotrophic	Electron acceptor
Anammox	Bacteria	anaerob	chemoautotrophic	Source of energy

Photosynthetic N_2-fixation can also operate in the anoxic part of the photic zone. This photosynthetic pathway mainly differs in terms of the electron donor used for CO_2 and N_2-fixation. While oxygenic phototrophs use water (H_2O), anoxygenic phototrophs (e.g. purple and green sulfur bacteria; Table 1) oxidize, for example, hydrogen sulfide (H_2S). However, the majority of these anoxygenic phototrophs utilize ammonium (NH_4^+) as the main nitrogen source. Yet, in recent oceans anoxygenic phototrophic N_2-fixation and NH_4^+ assimilation occur rarely as the

dominant processes providing bioavailable nitrogen because special environmental circumstances, such as the occurrence of H_2S-rich waters and the absence of oxygen in the photic zone, are required.

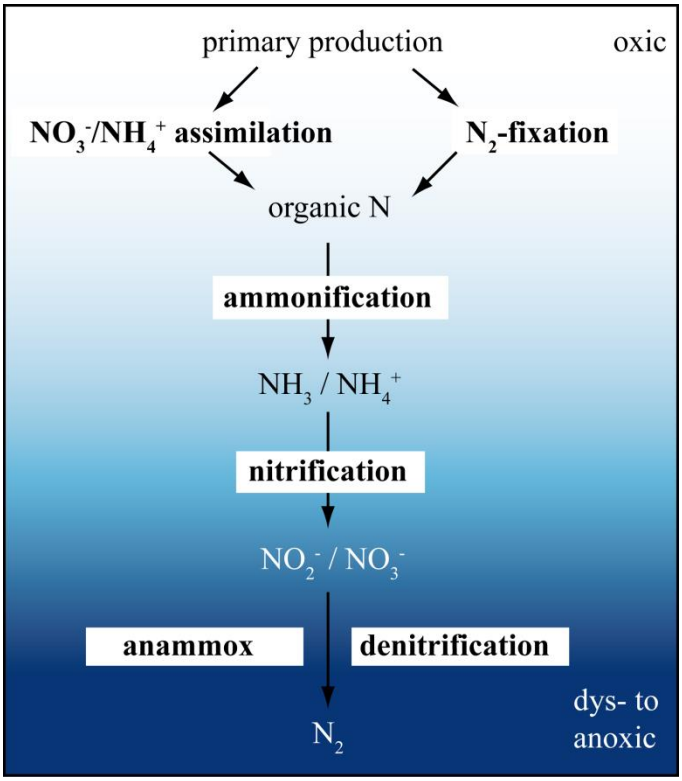

Figure 2: Sketch diagram of the modern marine nitrogen cycle illustrating the major biological nitrogen transformation pathways in the oxygenated ocean. Only the central nitrogen processes in the nitrogen cycle are shown.

Despite the overall presence of N_2 in the ocean, most autotrophic organisms cannot fix N_2 and are dependent on other inorganic nitrogen forms such as nitrate (NO_3^-), nitrite (NO_2^-) or NH_4^+. The most abundant nitrogen species used by both prokaryotic and eukaryotic primary producers in the oxic near-surface ocean is NO_3^- and its reduced form NH_4^+ (utilized via assimilatory nitrate reduction; Mulholland and Lomas, 2008). Bioavailable NH_4^+ is generated in the process called ammonification where microorganisms degrade organic matter in the water column (remineralization) and thereby return NH_4^+ to the environment (Fig. 2). Subsequently, several nitrifying bacteria (in general chemoautotrophic bacteria, but also some archaea; Table 1) oxidize NH_4^+, or ammonia (NH_3), respectively, via intermediate steps first to NO_2^- (ammonia oxidation) and in a second process to NO_3^- (nitrite oxidation) which then serves as the main nutrient for primary production (Fig. 2). During intermediate nitrification reactions,

nitrous oxide (N_2O) can escape to the atmosphere and thus displays an important source of this atmospheric greenhouse gas (Karl and Michaels, 2001). However, nitrification is strongly dependent on the presence of oxygen in the water and thus predominantly dominates the oxygenated part of the water column below the euphotic zone (Karl and Michaels, 2001). Yet it is rarely reported to occur within the euphotic zone (Casciotti and Buchwald, 2012). On the other hand, the distribution of nitrifying bacteria is dependent on the availability of NH_4^+. As a result, nitrification follows the supply of NH_4^+ from organic matter remineralization which in the oxic water column primarily operates below the euphotic zone and decreases with depth (Casciotti and Buchwald, 2012). Where oxygen availability is low or absent in the water column (e.g. oxygen minimum zones), at the sediment-water interface or within the sediment, NO_3^- is used by several organisms with different metabolic pathways. Hence, nitrate can either be used during the anaerobic oxidation of organic carbon and thus be transferred back to ammonium (dissimilatory nitrate reduction, DNRA) or reduced to gaseous N_2 via anammox (anaerobic ammonium oxidation) or denitrification (Fig. 2; Table 1; Canfield et al., 2010). Recently, the process of anammox has received increasing attention (Brunner et al., 2013). During that process, bacteria grow chemoautotrophically on the oxidation of NH_4^+ coupled to NO_2^- reduction, creating gaseous N_2. However, the dominant fate of NO_3^- in absence of oxygen is the reduction to N_2 gas, known as denitrification. Denitrifying bacteria include a variety of heterotrophic bacteria and archaea as well as some eukaryotes which use NO_3^- as an electron acceptor to degrade organic compounds. Thereby, organisms release gaseous N_2 as an end product which eventually returns to the atmosphere but also generate, albeit to a lesser degree, the greenhouse gas N_2O during intermediate steps. Consequently, the rate of denitrification is dependent on the availability of NO_3^- supplied by nitrification which in turn is limited by the availability of oxygen and NH_4^+. Therefore, denitrification is most effective across boundary areas of low oxygen and anoxic conditions where NH_4^+ concentration is high enough to sustain effective nitrification which then supplies sufficient nitrate for denitrification (Karl and Michaels, 2001). Altogether, denitrification acts as the main counterpart to N_2-fixation, removes bioavailable nitrogen and therefore closes the nitrogen cycle.

3.2 Nitrogen isotopes in the modern ocean

Nitrogen has two stable isotopes: ^{14}N and ^{15}N, from which ^{14}N is with 99.6% (by atoms) the more abundant isotope. During biochemical processes organisms fractionate between the two isotopes which results in measurable differences in the ratio of $^{15}N/^{14}N$ among the various nitrogen species in the ecosphere (Sigman et al., 2009). Fractionation results predominantly from kinetic isotope effects which mirror variances in reaction rates between the "heavy" ^{15}N and "light" ^{14}N isotopes in molecules containing the two isotopes of nitrogen which in turn is dependent on the bond strength and mobility of the nitrogen species (Montoya, 2008). N_2-fixation, NO_3^- assimilation, nitrification, denitrification and anammox are the known processes that affect the isotopic composition of dissolved inorganic nitrogen (DIN; e.g. Robinson et al., 2012). Therefore, nitrogen isotopes mirror both, the in- and output budget of fixed nitrogen (N_2-fixation, denitrification) and the internal nitrogen cycling (NO_3^- assimilation, nitrification). The nitrogen isotope ratio relative to a nitrogen standard is expressed in delta (δ) notation and given by:

$$\delta^{15}N\ (‰) = \left(\frac{\left(\frac{^{15}N}{^{14}N}\right) sample}{\left(\frac{^{15}N}{^{14}N}\right) standard} - 1 \right) * 1000$$

The standard is per definition atmospheric N_2 with $\delta^{15}N = 0‰$ (Sigman et al., 2009). The isotope fraction of a reaction can be expressed by a dimensionless fractionation factor α:

$$\alpha = \frac{^{14}k}{^{15}k}$$

with k displaying the rate constants of the light and heavy isotope (i.e. ^{14}N and ^{15}N) for molecules containing both isotopes (Montoya, 2008). Because most microbial biological reactions discriminate against the heavier isotope the fractionation factor is >1.

However, in stable isotope geochemistry, the most common factor used to describe the isotope discrimination is ε the kinetic isotope effect. ε is given in per mil (‰) and described by:

$$\varepsilon\ (‰) = (\alpha - 1) * 1000$$

For example, during nitrate assimilation phytoplankton discriminates against the heavier ^{15}N isotope with ε ~5‰ resulting in a ~5‰ decrease of the $\delta^{15}N$ of the respective product nitrogen. In general, the nitrogen source used to produce biomass imprints its isotope ratio on the organic matter which is eventually stored in the sediment. In turn, the $\delta^{15}N$ of the nitrogen source is influenced by previous processes in the water column that change the nitrogen inventory like remineralization and denitrification in subsurface waters, partial NO_3^- assimilation but as well alteration overprinting the "primary" nitrogen signature. Whenever one of the mentioned processes dominates, it results in a typical range of sedimentary $\delta^{15}N$ values for the respective nitrogen transformation (Table 2); although this does not imply the absence of further microbial processes. Thus, sedimentary nitrogen isotope ratios reflect the contribution of different biological processes, ocean circulation patterns and the effectiveness of the biological pump (Robinson et al., 2012).

Table 2: Characteristic approximate ranges of sedimentary bulk $\delta^{15}N$ values modified after Struck (2012). Isotope values are linked to the respective dominant microbial processes affecting the marine isotopic nitrogen cycle and their typical occurrence in the modern oceanic system. Note that only the predominant environments are listed.

Process	**Range of sedimentary $\delta^{15}N$**	**Typical marine environment**
Oxygenic N_2-fixation	-1 to +3‰	Oxic part of the photic zone, often overlying a stable redox-stratified water column
Anoxygenic N_2-fixation and NH_4^+ assimilation	<0‰	Anoxic to euxinic part of the photic zone in a highly redox-stratified water column
NO_3^- assimilation	3 to 8‰	Open marine, oxic surface water in a ventilated ocean
Denitrification	8 to 12‰	Within the sediment and at the sediment-water interface if overlain by dys- to anoxic waters

In the modern well-oxygenated, ventilated ocean nitrogen nutrients are typically irregular distributed with an excess where organic matter gets degraded and deficits where high bioproductivity prevails. Nitrate utilized by phytoplankton in surface waters predominantly originates from the deep-water nitrate pool with an initial $\delta^{15}N$ value of ~5‰ (Sigman et al., 2000) but can also be upwelled from a smaller nitrate pool in subsurface waters ($\delta^{15}N$ ~3‰; Fig. 3). Thereby, phytoplankton preferentially consumes the ^{14}N relative to ^{15}N which is reflected by sedimentary $\delta^{15}N$ values spanning from ~3 to 8‰ (Sigman et al., 2009; Struck, 2012). Isotope fractionation effects (ε) during NO_3^- assimilation are relatively low (prokaryotic strains ≤5‰, for eukaryotes ~5 to 8‰; Granger et al., 2010) or nearly negligible for NO_2^- and urea uptake (<1‰), whereas the assimilation of ammonium by phytoplankton causes higher isotope effects (≤20‰) but decreases with depth to 1‰ (Sigman et al., 2009). The remineralization of organic nitrogen to ammonium (ammonification) and via NO_2^- to NO_3^- (nitrification) also results in isotopic fractionation, yet little is known about these fractionation effects. In general, due to the heterogeneous nature of organic matter for degradation and their associated large variance in $\delta^{15}N$ the quantification of the isotope effect of internal nitrogen cycling in the ocean is difficult and unresolved. Whereas the nitrogen stable isotope effect for ammonia-oxidizing archaea and bacteria (laboratory culture studies) lies within the range from ε ~13 to 41‰, the fractionation during nitrite oxidation is to date unknown (Santoro and Casciotti, 2011; Casciotti and Buchwald, 2012). However, a complete consumption of the ammonium pool by assimilation in the surface ocean or by nitrification processes in subsurface waters result in buffering of their relatively high isotope effects with little impact on recent nitrogen isotope dynamics. In general, the net isotopic effect ε for remineralization is suggested to be <3‰ (Sigman et al., 2009). Denitrification occurs in both, the water column and the sediment where oxygen concentration is low (<5 μM). In contrast to sedimentary denitrification where isotopic fractionation is small (ε ~3‰), water column denitrification provokes a strong discrimination against the "heavier" ^{15}N isotope (ε ~20 to 30‰; Sigman et al., 2009; Kessler et al., 2014). Therefore, denitrification processes enrich the residual nitrate pool in ^{15}N leading to elevated $\delta^{15}N$ values in the deep-water nitrate reservoir. Because upwelled deep-water NO_3^- serves as the main nutrient

for phytoplankton in surface waters the $\delta^{15}N$ value of the respective biomass is slightly elevated compared to the organisms using N_2 as their main nitrogen source. In the sediment, elevated denitrification rates are mirrored by $\delta^{15}N$ values spanning from ~8 to 12‰ (Struck, 2012). Recently, studies on the nitrogen isotope effect of anammox in culture experiments showed that isotope effects of the conversion of ammonium to N_2 result in ε ~23 to 29‰ whereas the isotopic effects between nitrite and nitrate vary highly depending on e.g. the reversibility of enzymatic reaction steps involved (Brunner et al., 2013).

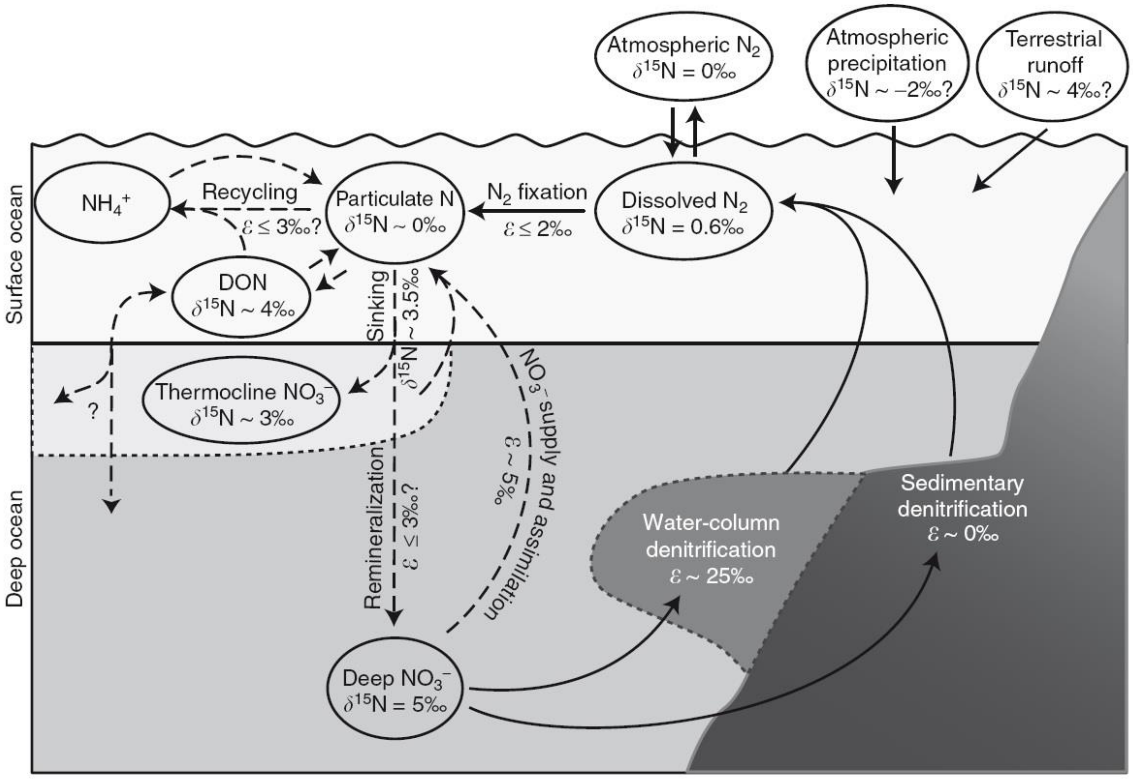

Figure 3: Processes affecting the dispersal of nitrogen isotopes in the ocean linked to their isotope fractionation effect ε and the $\delta^{15}N$ composition of the respective nitrogen pool after Sigman et al. (2009). In- and outputs are marked by solid arrows and described by marine N_2-fixation, terrestrial runoff and atmospheric precipitation (input) and denitrification (output). Dashed arrows represent internal cycling of nitrogen where particulate organic nitrogen of surface waters becomes degraded on its way sinking down the water column (remineralization) to either NH_4^+ which gets re-assimilated by microorganisms or via nitrification to NO_3^- creating a large deep-water nitrate pool. Upwelling of nitrate from deep-waters or from the thermocline displays the major source of nutrients for organisms in the surface ocean. Question marks imply uncertainties regarding nitrogen cycling processes and their isotopic effects.

If the availability of NO_3^- in the euphotic zone is limited, N_2-fixation by diazotrophic bacteria is promoted (Fu and Bell, 2003). Respective bacteria fix atmospheric N_2 with an initial $\delta^{15}N$ value of ~0‰ and little associated isotopic

fractionation (ε = 0 to ~3‰; Montoya et al., 2002; Bauersachs et al., 2009; Struck, 2012) resulting in low $\delta^{15}N$ values of ~0 to 3‰. Such cyanobacterial blooms are often documented from oceanic basins where oxic surface waters overly vertically redox-stratified water masses and deep-water anoxia like e.g. in the modern Baltic Sea (Struck et al., 2004; Ploug et al., 2010). In such basins, anoxic situations favor the release of phosphate from sediments which if upwelled results in changes of the N/P Redfield ratio (e.g. ≠16:1, with excess of P with regard to N) and thus stimulates diazotrophy (Sanudo-Wilhelmy et al., 2001). Typical lithologies deposited under these circumstances include organic-rich sediments such as sapropels (Struck et al., 2001).

Other exceptional settings are highly redox-stratified aquatic areas (predominantly stagnating basins) like the Black Sea (Eckert et al., 2013), the meromictic Lake Kaiike in Japan (Ohkouchi et al., 2005) or Lake Cadagno (Switzerland; Camacho et al., 2001) where permanent photic zone anoxia, euxinic bottom water conditions and excess availability of NH_4^+ evolved. In these settings, despite the occurrence of oxygenic phototrophs (Zerkle et al., 2008; Fulton et al., 2012), anoxygenic phototrophs (e.g. purple and green sulfur bacteria and purple nonsulfur bacteria; Camacho et al., 2001; Vila et al., 2002) which use NH_4^+ as the main nitrogen source (but also capable of N_2-fixation) contribute largely to the nitrogen cycle (Wahlund and Madigan, 1993; Beaumont et al., 2000; Ohkouchi et al., 2005). The excess of ammonium in anoxic waters is predominantly attributed to the limited rate of nitrification in overlying waters where NH_4^+ is consumed thus enriching the nutrient pool in the respective reduced nitrogen species. Once re-entered to the photic (anoxic) zone, NH_4^+ forms a major nutrient for primary productivity (Mulholland and Lomas, 2008; Higgins et al., 2012). Due to the large isotopic fractionation during NH_4^+ uptake (ε = ~10 to 20‰) their biomass is strongly depleted in ^{15}N leading to $\delta^{15}N$ values of -1 to -8‰ (Ohkouchi et al., 2005; Montoya, 2008; Sigman et al., 2009). Therefore, sedimentary records with $\delta^{15}N$ values <0‰ are interpreted to mirror elevated productivity by anoxygenic phototrophs (Beaumont et al., 2000; Zerkle et al., 2008; Higgins et al., 2012; Cremonese et al., 2013). Through geologic time, such negative $\delta^{15}N$ values, and the occurrence of geoporphyrins (the diagenetic

products of chlorophylls and bacteriochlorophylls) characteristic for (an-) oxygenic phototrophs have been reported from organic matter-rich sediments deposited under widespread oceanic anoxia, like from black shales of the Devonian Kellwasser Event (Suchi, 2005; Steinmann et al., 2013) and Punctata Event (Sliwinski et al., 2011) or the Cretaceous Oceanic Anoxic Event II (Pancost et al., 2004; Junium and Arthur, 2007; Higgins et al., 2012) but also from Archean kerogen-containing cherts (Beaumont and Robert, 1999).

Another highly productive ecosystem with specialized microbial biogeochemistry in the ocean is closely linked to coastal upwelling systems like e.g. the Benguela upwelling system (SW Africa) in the Atlantic and the Peru/Humboldt current system in the Pacific. There, wind-driven upwelling of nutrient-rich deep-water (including nitrate, phosphate, and silicate) stimulates enormous bioproductivity in surface waters. Advection of NO_3^- from deeper waters with highest NO_3^- concentration between 100 and 200 m depth leads to elevated photosynthetic activity and high "new" production (Wilkerson and Dugdale, 2008). Consequently, the eutrophic environment results in an effective biological pump which eventually leads to a rapid drawdown of CO_2 and therefore affects the partial pressure of CO_2 (pCO_2) and the pH of the ambient seawater (Capone and Hutchins, 2013). Characteristically, $\delta^{15}N$ compositions of sediments deposited in the coastal upwelling system off Peru, Ecuador and Namibia in general range from ~5 to ~9‰ thereby increasing towards the coast reflecting upwelling of high $\delta^{15}N$ NO_3^- (Meisel et al., 2011; Mollier-Vogel et al., 2012). However, NO_3^- upwelling is strongly dependent on e.g. the location of the upwelling system within the global oceanic conveyor belt and the degree of oceanic stratification. In settings where highly productive upwelling systems occur together with low-oxygen (e.g. oxygen minimum zones) or anoxic regions denitrification results in nearly complete NO_3^- consumption and a maximum of NH_4^+ as a result from the oxidation of organic material (Wilkerson and Dugdale, 2008). The complete drawdown of NO_3^- results in altered utilization ratio of nutrients and residual phosphorus can stimulate N_2-fixing blooms (Capone and Hutchins, 2013). Therefore, coastal upwelling systems are often associated with the deposition of phosphate-rich sediments (Piper et al., 1988) which is an important aspect while

considering nitrogen isotope compositions of ancient phosphate deposits like across the Pc-C boundary.

3.3 The evolution of the marine nitrogen cycle

A change in the nitrogen biogeochemical cycling culminating in the evolution of the modern marine nitrogen cycle is believed to have occurred between *ca.* 3.0 - 2.0 billion years ago before present (Ga; Beaumont and Robert, 1999). Nitrogen isotope analyses of Late Archean strata showed that aerobe nitrogen biogeochemical cycling with "modern" N_2-fixation and nitrification-denitrification interactions evolved at about ~2.7 to ~2.5 Ga in close association albeit slightly predating the Great Oxidation Event at 2.4 - 2.2 Ga (Bekker et al., 2004; Thomazo et al., 2011; Busigny et al., 2013). Thereby, rising atmospheric oxygen would have caused major changes in the marine nitrogen cycle with higher levels of seawater nitrate generating new ecological niches for denitrifying bacteria as well as archaea (Papineau et al., 2009). However, the Archean nitrogen cycle fundamentally differed from the "modern" cycle in terms of the availability of inorganic nitrogen species. Archean nitrogen cycling interacted in a largely anoxic ocean and thus $\delta^{15}N$ values from ~-6 to 0‰ document that N_2 and NH_4^+ must have been the dominant form of nitrogen for uptake by organisms (Beaumont and Robert, 1999; Thomazo et al., 2011; Busigny et al., 2013). After 2.0 Ga the establishment of a complete nitrogen cycle with denitrification-nitrification and the occurrence of seawater nitrate is documented by mostly positive $\delta^{15}N$ values ranging from 0 to 10‰ (Beaumont and Robert, 1999; Papineau et al., 2009). Recent analyses indicate that nitrate (and hence oxygen) was stable in the ocean since at least the middle Neoproterozoic as well as across the Late Neoproterozoic Oxygenation Event (Ader et al., 2014). Furthermore, $\delta^{15}N$ analyses of fluid inclusions from 3.5 to 3.0 Ga-old hydrothermal quartz revealed that the nitrogen isotope composition of the Archean atmosphere was comparable to today (Marty et al., 2013).

3.4 Preservation and alteration of the $\delta^{15}N$ signature in sediments

Nitrogen in sediments is preserved as either organic nitrogen or as fixed-ammonium substituting for potassium (K^+) in phyllosilicates (e.g. Schubert and Calvert, 2001). Despite the complexity of nitrogen cycling within the water column especially $\delta^{15}N$ signals from sediments deposited in continental margins and anoxic depositional settings have been demonstrated to reliably record surface nutrient utilization (Altabet and Francois, 1994; Higgins et al., 2010; Robinson et al., 2012). Furthermore, recent investigations minimize the effect of secondary alteration and argue for the fidelity of sedimentary $\delta^{15}N$ values as a recorder of past marine changes in the global nitrogen cycle (for a review see Robinson et al., 2012; Thomazo and Papineau, 2013).

Minor modifications of the isotopic composition of sedimentary organic nitrogen are predominantly caused by burial and early sedimentary diagenetic processes at the sediment-water interface particularly off of continental margins (Robinson et al., 2012). Heterotrophic degradation of organic matter during early diagenesis (in pore waters) causes an isotopic fractionation of less than 1‰ and is therefore nearly negligible. Other alteration reactions throughout the water column cause slightly higher isotopic variations albeit also relatively low (~2 to 3‰; Thomazo and Papineau, 2013). In this sense, respective alteration processes are dominantly controlled by water depth, sedimentation rate and oxygen exposure time of the sediment (Robinson et al., 2012). Thereby, $\delta^{15}N$ values in oceanic low organic nitrogen flux regions (slow accumulating sediments) are larger affected by alteration than isotopic values in high sediment accumulating regions, where $\delta^{15}N$ values of sediments are conform with those of the sinking organic matter (Altabet and Francois, 1994; Altabet et al., 1999; Mobius et al., 2010). Under oxic water conditions and low sedimentation rates sediments show predominantly slightly increased $\delta^{15}N$ values compared to the sinking organic matter (lower $\delta^{15}N$; Altabet and Francois, 1994; Freudenthal et al., 2001) which is attributed to the preferential loss of low $\delta^{15}N$ NH_4^+ into pore waters during deamination within the sediment (Gaye et al., 2009; Mobius et al., 2010). In contrast, $\delta^{15}N$ analyses of total nitrogen and chlorins (degradation products of chlorophyll) in sediments deposited in marine stratified environments with anoxic deep-waters

(Pleistocene and Holocene sapropels from the Eastern Mediterranean Sea) showed that the sedimentary $\delta^{15}N$ value reflects the isotopic composition of the nitrogen used by biomass without significant alteration (Sachs and Repeta, 1999; Higgins et al., 2010).

During burial diagenesis (including the onset of thermal maturation of organic matter) the $\delta^{15}N$ of organic nitrogen remains largely unaffected (Ader et al., 2006). In sedimentary rocks with high proportion of clay, the process of smectite-illite conversion during progressive burial diagenesis can absorb ammonium onto clay minerals whereby ammonium substitutes for potassium in the interlayer exchange sites of the illite (Schubert and Calvert, 2001). Additionally, ammonium can also be bound to micas of metamorphic rocks during burial diagenesis. Yet, the $\delta^{15}N$ value of the ammonium closely resembles the nitrogen isotope composition of the bulk sediment/rock and organic matter and differences only occur within ±2‰. This suggests that the ammonium derived from the degraded organic matter is bound to the clay minerals without major isotope fractionation (see Thomazo et al. (2011) and references therein).

As for burial diagenesis, during lower metamorphic grades (greenschist facies) the $\delta^{15}N$ value of organic matter retains its initial nitrogen isotope composition and nitrogen species (mainly ammonium) released during these processes experience minor isotopic fractionation (Ader et al., 2006; Boudou et al., 2008). Thermal devolatilization of ammonium-bearing clay minerals causes preferentially mobilization of ^{15}N-depleted fixed ammonium. If the mobilized ammonium migrates out of the rock during metamorphosis, the nitrogen content decreases while the $\delta^{15}N$ value of the residual sediment increases (Bebout and Fogel, 1992; Thomazo et al., 2011) with characteristic values dependent on the metamorphic facies (Table 3; e.g. Thomazo and Papineau, 2013).

Table 3: Post-depositional processes affecting the nitrogen isotope composition of sediments and sedimentary rocks and the estimated respective shift of the sedimentary $\delta^{15}N$ value. Data are compiled from reviews in Thomazo et al. (2011); Robinson et al. (2012); Thomazo and Papineau (2013).

Process	Shift of sedimentary $\delta^{15}N$
Heterotrophic degradation of organic matter	<1‰
Early diagenetic reactions in oxic or anoxic settings	Increase of ≤ 3‰
Thermal maturation, burial diagenesis	± 2‰
Metamorphosis (greenschist facies)	Increase of 1-2‰
Metamorphosis (amphibolite facies and higher)	Increase of 3-12‰

Therefore, while interpreting isotopic compositions of ancient rocks, thermal effects must be considered. However, if done so, the study of nitrogen isotope variations over geologic time has the potential to identify significant processes and changes in global biogeochemical cycling (Higgins et al., 2012).

3.5 The modern marine carbon cycle

Carbon is an important component of life and present in many different inorganic and organic forms on the Earth. In its inorganic phases (CO_2, methane (CH_4), and carbon monoxide (CO)), carbon has major greenhouse gas qualities which are known to influence the climate as well as the oceanic carbon cycle and vice versa (Carlson et al., 2001). Carbon in the ocean occurs as organic compounds and as dissolved inorganic carbon (DIC) including CO_2, bicarbonate (HCO_3^-), and carbonate (CO_2^{3-}). As CO_2 has good solubility in seawater it is an important factor controlling the ocean-atmosphere gas exchange. The ocean has a huge capacity to buffer atmospheric CO_2 changes closely interacting with changes in alkalinity and seawater pH (Carlson et al., 2001). Once passed over to the oceanic system carbon is either physically transported to deep waters (e.g. advection, diffusion, wind-driven and thermohaline circulation) or assimilated by organisms thus entering the "biological pump". Today, due to slow circulation rates in the deep oceans, the deep-water is commonly enriched in DIC species where they are stored for hundreds of years. Dissolved gaseous CO_2 is converted to organic matter by marine phytoplankton via photosynthesis which is limited to the euphotic zone (upper 100 - 150 m of the water column) and stored as either particulate organic carbon (POC) or dissolved organic carbon (DOC) in the ocean.

Afterwards, heterotrophic organisms use the produced organic carbon compounds to obtain energy and are in turn eventually remineralized back to DIC via respiration on their way sinking down the water column and re-introduced to the surface via upwelling thus closing the carbon cycle. However, calcareous skeletal material by some marine phytoplankton and animals is not remineralized during sinking and is only dissolved when it reaches the carbonate compensation depth. After all, only <1% of the exported organic matter from the surface waters is transported to the sediment due to elevated remineralization rate in the oxic water column. Taken together, the biological pump acts as an effective force to regulate the atmospheric CO_2 concentration which in turn mirrors its large dependence on the CO_2 concentration, although nutrient supply (e.g. nitrogen, phosphorus, silica) and plankton community structure play a major role as well (Carlson et al., 2001).

3.6 Carbon isotopes in the modern and ancient ocean

The ratio of the two stable carbon isotopes ^{12}C and ^{13}C is given relative to the Vienna PeeDee Belemnite standard in δ-notation by

$$\delta^{13}C\ (‰) = \left(\frac{\left(\frac{^{13}C}{^{12}C}\right) sample}{\left(\frac{^{13}C}{^{12}C}\right) standard} - 1 \right) * 1000$$

In the modern ocean isotopic ratios between carbonate carbon ($\delta^{13}C_{carb}$) and organic carbon ($\delta^{13}C_{org}$) vary in predictable, coupled ways. Isotopic fractionation, gas exchange (Air CO_2 $\delta^{13}C_{carb}$ ~-7‰; Turekian, 2001) and chemical reactions are best recorded in atmospheric CO_2 and surface-ocean DIC whereas the deep-water DIC is largely unaffected by those processes (Sundquist and Visser, 2011). In the modern ocean, marine limestone has an average $\delta^{13}C_{carb}$ value of ~0‰. Precipitation of carbonates involves little fractionation relative to the DIC; therefore, the $\delta^{13}C_{carb}$ of carbonates closely mirrors the DIC in the ocean (Saltzman and Thomas, 2012). $\delta^{13}C_{org}$ isotopes are a widely acknowledged proxy for the rate of bioproductivity in surface waters, the effectiveness of the biological

pump and the supply of inorganic carbon (Werne and Hollander, 2004). Attributed to the isotope effect and the carbon species used for assimilation, marine phytoplankton strongly discriminates against the heavier ^{13}C isotope resulting in organic matter with $\delta^{13}C_{org}$ values ranging in average from -28 to -18‰ depending on the environment (e.g. high-mid-low latitude), but mostly center around -25 to -20‰ in the modern ocean which is mirrored in sediments (Westerhausen et al., 1993; Turekian, 2001; Liu et al., 2007). In environments with elevated CH_4 fluxes like in the Black Sea (respective $\delta^{13}C_{carb}$ value of marine dissolved methane ~-48‰; Riedinger et al., 2010) methanotrophic bacteria and archaea utilize CH_4 as their sole carbon source which results in extreme ^{13}C-depleted organic matter with $\delta^{13}C_{org}$ values down to -120‰ (Chevalier et al., 2013). In contrast, isotope effects during heterotrophic carbon assimilation are nearly negligible and occur predominantly where very small molecules are absorbed. Thus, the respective $\delta^{13}C_{org}$ value represents that of the incorporated carbon source (Hayes, 1993).

During Earth's history, the $\delta^{13}C_{carb}$ value of the DIC has not been constant which is recorded by several carbon isotope excursions down to $\delta^{13}C_{carb}$ ~-10‰ (e.g. Precambrian-Cambrian boundary, Permian-Triassic boundary) and non-actualistic decoupled $\delta^{13}C_{carb}$ and $\delta^{13}C_{org}$ values during the Ediacaran which document large perturbations within the carbon cycle (McFadden et al., 2008; Korte and Kozur, 2010; Ishikawa et al., 2013). The $\delta^{13}C_{carb}$ of the DIC is known to be not only controlled by the CO_2 of the atmosphere but also by the circulation between the surface- and the deep-waters (Saltzman and Thomas, 2012) which may have affected respective anomalies. However, the potential alteration of primary isotope values is largely discussed especially for Precambrian rocks. Whereas Precambrian $\delta^{13}C_{carb}$ values are assumed to be prone to alteration (Knauth and Kennedy, 2009), $\delta^{13}C_{org}$ data nearly record primary organic matter values without significant alteration (Ader et al., 2009) and thus Precambrian $\delta^{13}C_{org}$ values around in average ~-30‰ show that primary producers were more enriched in ^{12}C compared to modern times.

Concluding, an essential difference between the carbon and nitrogen systems is attributed to the relative size of their respective atmospheric and oceanic reservoirs. Whereas the atmospheric nitrogen pool is comparatively large and thus buffers oceanic reservoir size changes, the atmospheric carbon inventory is relatively small and highly sensitive to e.g. climate variations. Thus, perturbations within the atmospheric carbon pool are directly reflected in the oceanic carbon composition and therefore in bioproductivity and vice versa.

3.7 References

Ader, M., Cartigny, P., Boudou, J.-P., Oh, J.-H., Petit, E., and Javoy, M., 2006, Nitrogen isotopic evolution of carbonaceous matter during metamorphism: Methodology and preliminary results: Chemical Geology, v. 232, no. 3–4, p. 152-169.

Ader, M., Macouin, M., Trindade, R. I. F., Hadrien, M. H., Yang, Z., Sun, Z., and Besse, J., 2009, A multilayered water column in the Ediacaran Yangtze platform? Insights from carbonate and organic matter paired $\delta^{13}C$: Earth and Planetary Science Letters, v. 288, no. 1-2, p. 213-227.

Ader, M., Sansjofre, P., Halverson, G. P., Busigny, V., Trindade, R. I. F., Kunzmann, M., and Nogueira, A. C. R., 2014, Ocean redox structure across the Late Neoproterozoic Oxygenation Event: A nitrogen isotope perspective: Earth and Planetary Science Letters, v. 396, no. 0, p. 1-13.

Altabet, M. A., and Francois, R., 1994, Sedimentary nitrogen isotopic ratio as a recorder for surface ocean nitrate utilization: Global Biogeochemical Cycles, v. 8, p. 103-116.

Altabet, M. A., Pilskaln, C., Thunell, R., Pride, C., Sigman, D., Chavez, F., and Francois, R., 1999, The nitrogen isotope biogeochemistry of sinking particles from the margin of the Eastern North Pacific: Deep Sea Research Part I: Oceanographic Research Papers, v. 46, no. 4, p. 655-679.

Bauersachs, T., Schouten, S., Compaore, J., Wollenzien, U., Stal, L. J., and Damste, J. S. S., 2009, Nitrogen isotopic fractionation associated with growth on dinitrogen gas and nitrate by cyanobacteria: Limnology and Oceanography, v. 54, no. 4, p. 1403-1411.

Beaumont, V., and Robert, F., 1999, Nitrogen isotope ratios of kerogens in Precambrian cherts: a record of the evolution of atmosphere chemistry?: Precambrian Research, v. 96, no. 1–2, p. 63-82.

Beaumont, V. I., Jahnke, L. L., and Des Marais, D. J., 2000, Nitrogen isotopic fractionation in the synthesis of photosynthetic pigments in Rhodobacter capsulatus and Anabaena cylindrica: Organic Geochemistry, v. 31, no. 11, p. 1075-1085.

Bebout, G. E., and Fogel, M. L., 1992, Nitrogen-isotope compositions of metasedimentary rocks in the catalina schist, california - implications for metamorphic devolatilization history: Geochimica et Cosmochimica Acta, v. 56, no. 7, p. 2839-2849.

Bekker, A., Holland, H. D., Wang, P. L., Rumble, D., Stein, H. J., Hannah, J. L., Coetzee, L. L., and Beukes, N. J., 2004, Dating the rise of atmospheric oxygen: Nature, v. 427, no. 6970, p. 117-120.

Boudou, J.-P., Schimmelmann, A., Ader, M., Mastalerz, M., Sebilo, M., and Gengembre, L., 2008, Organic nitrogen chemistry during low-grade metamorphism: Geochimica et Cosmochimica Acta, v. 72, no. 4, p. 1199-1221.

Brunner, B., Contreras, S., Lehmann, M. F., Matantseva, O., Rollog, M., Kalvelage, T., Klockgether, G., Lavik, G., Jetten, M. S. M., Kartal, B., and Kuypers, M. M. M., 2013, Nitrogen isotope effects induced by anammox bacteria: Proceedings of the National Academy of Sciences of the United States of America, v. 110, no. 47, p. 18994-18999.

Busigny, V., and Bebout, G. E., 2013, Nitrogen in the Silicate Earth: Speciation and Isotopic Behavior during Mineral-Fluid Interactions: Elements, v. 9, no. 5, p. 353-358.

Busigny, V., Lebeau, O., Ader, M., Krapež, B., and Bekker, A., 2013, Nitrogen cycle in the Late Archean ferruginous ocean: Chemical Geology, v. 362, no. 0, p. 115-130.

Camacho, A., Erez, J., Chicote, A., Florin, M., Squires, M. M., Lehmann, C., and Bachofen, R., 2001, Microbial microstratification, inorganic carbon photoassimilation and dark carbon fixation at the chemocline of the meromictic Lake Cadagno (Switzerland) and its relevance to the food web: Aquatic Sciences, v. 63, no. 1, p. 91-106.

Canfield, D. E., Glazer, A. N., and Falkowski, P. G., 2010, The Evolution and Future of Earth's Nitrogen Cycle: Science, v. 330, no. 6001, p. 192-196.

Capone, D. G., and Hutchins, D. A., 2013, Microbial biogeochemistry of coastal upwelling regimes in a changing ocean: Nature Geoscience, v. 6, no. 9, p. 711-717.

Carlson, C. A., Bates, N. R., Hansell, D. A., and Steinberg, D. K., 2001, Carbon Cycle, *in* Steele, J., Thorpe, S., and Turekian K., eds., A Derivative of Encyclopedia of Ocean Sciences (2nd Edition, 2010): Oxford, Academic Press, p. 495-504.

Casciotti, K. L., and Buchwald, C., 2012, Insights on the marine microbial nitrogen cycle from isotopic approaches to nitrification: Frontiers in Microbiology, v. 3, Article 356, p. 1-14.

Chevalier, N., Bouloubassi, I., Birgel, D., Taphanel, M. H., and López-García, P., 2013, Microbial methane turnover at Marmara Sea cold seeps: a combined 16S rRNA and lipid biomarker investigation: Geobiology, v. 11, no. 1, p. 55-71.

Cremonese, L., Shields-Zhou, G., Struck, U., Ling, H.-F., Och, L., Chen, X., and Li, D., 2013, Marine biogeochemical cycling during the early Cambrian constrained by a nitrogen and organic carbon isotope study of the Xiaotan section, South China: Precambrian Research, v. 225, no. 0, p. 148-165.

Eckert, S., Brumsack, H.-J., Severmann, S., Schnetger, B., März, C., and Fröllje, H., 2013, Establishment of euxinic conditions in the Holocene Black Sea: Geology, v. 41, no. 4, p. 431-434.

Falkowski, P. G., 1997, Evolution of the nitrogen cycle and its influence on the biological sequestration of CO_2 in the ocean: Nature, v. 387, no. 6630, p. 272-275.

Freudenthal, T., Wagner, T., Wenzhofer, F., Zabel, M., and Wefer, G., 2001, Early diagenesis of organic matter from sediments of the eastern subtropical Atlantic: Evidence from stable nitrogen and carbon isotopes: Geochimica et Cosmochimica Acta, v. 65, no. 11, p. 1795-1808.

Fu, F.-X., and Bell, P. R. F., 2003, Factors affecting N_2 fixation by the cyanobacterium Trichodesmium sp. GBRTRLI101: FEMS Microbiology Ecology, v. 45, no. 2, p. 203-209.

Fulton, J. M., Arthur, M. A., and Freeman, K. H., 2012, Black Sea nitrogen cycling and the preservation of phytoplankton $\delta^{15}N$ signals during the Holocene: Global Biogeochemical Cycles, v. 26, no. 2, p. GB2030.

Gaye, B., Wiesner, M. G., and Lahajnar, N., 2009, Nitrogen sources in the South China Sea, as discerned from stable nitrogen isotopic ratios in rivers, sinking particles, and sediments: Marine Chemistry, v. 114, no. 3–4, p. 72-85.

Granger, J., Sigman, D. M., Rohde, M. M., Maldonado, M. T., and Tortell, P. D., 2010, N and O isotope effects during nitrate assimilation by unicellular prokaryotic and eukaryotic plankton cultures: Geochimica et Cosmochimica Acta, v. 74, no. 3, p. 1030-1040.

Gruber, N., 2008, Chapter 1 - The Marine Nitrogen Cycle: Overview and Challenges, *in* Capone, D. G., Bronk, D. A., Mulholland, M. R., and Carpenter, E. J., eds., Nitrogen in the Marine Environment (2nd Edition): San Diego, Academic Press, p. 1-50.

Hayes, J. M., 1993, Factors controlling ^{13}C contents of sedimentary organic-compounds - principles and evidence: Marine Geology, v. 113, no. 1-2, p. 111-125.

Higgins, M. B., Robinson, R. S., Carter, S. J., and Pearson, A., 2010, Evidence from chlorin nitrogen isotopes for alternating nutrient regimes in the Eastern Mediterranean Sea: Earth and Planetary Science Letters, v. 290, no. 1–2, p. 102-107.

Higgins, M. B., Robinson, R. S., Husson, J. M., Carter, S. J., and Pearson, A., 2012, Dominant eukaryotic export production during ocean anoxic events reflects the importance of recycled NH_4^+: Proceedings of the National Academy of Sciences, v. 109, no. 7, p. 2269-2274.

Ishikawa, T., Ueno, Y., Shu, D., Li, Y., Han, J., Guo, J., Yoshida, N., and Komiya, T., 2013, Irreversible change of the oceanic carbon cycle in the earliest Cambrian: High-resolution organic and inorganic carbon chemostratigraphy in the Three Gorges area, South China: Precambrian Research, v. 225, no. 0, p. 190-208.

Junium, C. K., and Arthur, M. A., 2007, Nitrogen cycling during the Cretaceous, Cenomanian-Turonian Oceanic Anoxic Event II: Geochemistry Geophysics Geosystems, v. 8, no. 3, p. 1-18.

Karl, D. M., and Michaels, A. F., 2001, Nitrogen Cycle, *in* Steele, J., Thorpe, S., and Turekian K., eds., A Derivative of Encyclopedia of Ocean Sciences (2nd Edition, 2010): Oxford, Academic Press, p. 541-548.

Kessler, A. J., Bristow, L. A., Cardenas, M. B., Glud, R. N., Thamdrup, B., and Cook, P. L. M., 2014, The isotope effect of denitrification in permeable sediments: Geochimica et Cosmochimica Acta, v. 133, no. 0, p. 156-167.

Knauth, L. P., and Kennedy, M. J., 2009, The late Precambrian greening of the Earth: Nature, v. 460, no. 7256, p. 728-732.

Korte, C., and Kozur, H. W., 2010, Carbon-isotope stratigraphy across the Permian–Triassic boundary: A review: Journal of Asian Earth Sciences, v. 39, no. 4, p. 215-235.

Liu, K.-K., Kao, S.-J., Hu, H.-C., Chou, W.-C., Hung, G.-W., and Tseng, C.-M., 2007, Carbon isotopic composition of suspended and sinking particulate organic matter in the northern South China Sea-From production to deposition: Deep Sea Research Part II: Topical Studies in Oceanography, v. 54, no. 14–15, p. 1504-1527.

Marty, B., Zimmermann, L., Pujol, M., Burgess, R., and Philippot, P., 2013, Nitrogen Isotopic Composition and Density of the Archean Atmosphere: Science, v. 342, no. 6154, p. 101-104.

McFadden, K. A., Huang, J., Chu, X., Jiang, G., Kaufmann, A. J., Zhou, C., Yuan, X., and Xiao, S., 2008, Pulsed oxidation and biological evolution in the Ediacaran Doushantuo Formation: PNAS, v. 105, no. 9, p. 3197-3202.

Meisel, S., Struck, U., and Emeis, K. C., 2011, Nutrient dynamics and oceanographic features in the central Namibian upwelling region as reflected in $\delta^{15}N$-signals of suspended matter and surface sediments: Fossil Record, v. 14, no. 2, p. 153-169.

Mobius, J., Lahajnar, N., and Emeis, K. C., 2010, Diagenetic control of nitrogen isotope ratios in Holocene sapropels and recent sediments from the Eastern Mediterranean Sea: Biogeosciences, v. 7, no. 11, p. 3901-3914.

Mollier-Vogel, E., Ryabenko, E., Martinez, P., Wallace, D., Altabet, M. A., and Schneider, R., 2012, Nitrogen isotope gradients off Peru and Ecuador related to upwelling, productivity, nutrient uptake and oxygen deficiency: Deep Sea Research Part I: Oceanographic Research Papers, v. 70, no. 0, p. 14-25.

Montoya, J. P., Carpenter, E. J., and Capone, D. G., 2002, Nitrogen fixation and nitrogen isotope abundances in zooplankton of the oligotrophic North Atlantic: Limnology Oceanography, v. 47, no. 6, p. 1617-1628.

Montoya, J. P., 2008, Chapter 29 - Nitrogen Stable Isotopes in Marine Environments, *in* Capone, D. G., Bronk, D. A., Mulholland, M. R., and Carpenter, E. J., eds., Nitrogen in the Marine Environment (2nd Edition): San Diego, Academic Press, p. 1277-1302.

Mulholland, M. R., and Lomas, M. W., 2008, Chapter 7 - Nitrogen Uptake and Assimilation, *in* Capone, D. G., Bronk, D. A., Mulholland, M. R., and Carpenter, E. J., eds., Nitrogen in the Marine Environment (2nd Edition): San Diego, Academic Press, p. 303-384.

Ohkouchi, N., Nakajima, Y., Okada, H., Ogawa, N. O., Suga, H., Oguri, K., and Kitazato, H., 2005, Biogeochemical processes in the saline meromictic Lake Kaiike, Japan: implications from molecular isotopic evidences of photosynthetic pigments: Environmental Microbiology, v. 7, no. 7, p. 1009-1016.

Pancost, R. D., Crawford, N., Magness, S., Turner, A., Jenkyns, H. C., and Maxwell, J. R., 2004, Further evidence for the development of photic-zone euxinic conditions during Mesozoic oceanic anoxic events: Journal of the Geological Society, v. 161, p. 353-364.

Papineau, D., Purohit, R., Goldberg, T., Pi, D., Shields, G. A., Bhu, H., Steele, A., and Fogel, M. L., 2009, High primary productivity and nitrogen cycling after the Paleoproterozoic phosphogenic event in the Aravalli Supergroup, India: Precambrian Research, v. 171, no. 1–4, p. 37-56.

Piper, D. Z., Baedecker, P. A., Crock, J. G., Burnett, W. C., and Loebner, B. J., 1988, Rare earth elements in the phosphatic-enriched sediment of the Peru shelf: Marine Geology, v. 80, no. 3–4, p. 269-285.

Ploug, H., Musat, N., Adam, B., Moraru, C. L., Lavik, G., Vagner, T., Bergman, B., and Kuypers, M. M. M., 2010, Carbon and nitrogen fluxes associated with the cyanobacterium Aphanizomenon sp. in the Baltic Sea: ISME Journal, v. 4, no. 9, p. 1215-1223.

Riedinger, N., Brunner, B., Lin, Y. S., Voßmeyer, A., Ferdelman, T. G., and Jørgensen, B. B., 2010, Methane at the sediment–water transition in Black Sea sediments: Chemical Geology, v. 274, no. 1–2, p. 29-37.

Robinson, R. S., Kienast, M., Luiza Albuquerque, A., Altabet, M., Contreras, S., De Pol Holz, R., Dubois, N., Francois, R., Galbraith, E., Hsu, T.-C., Ivanochko, T., Jaccard, S., Kao, S.-J., Kiefer, T., Kienast, S., Lehmann, M., Martinez, P., McCarthy, M., Möbius, J., Pedersen, T., Quan, T. M., Ryabenko, E., Schmittner, A., Schneider, R., Schneider-Mor, A., Shigemitsu, M., Sinclair, D., Somes, C., Studer, A., Thunell, R., and Yang, J.-Y., 2012, A review of nitrogen isotopic alteration in marine sediments: Paleoceanography, v. 27, no. 4, p. PA4203.

Sachs, J. P., and Repeta, D. J., 1999, Oligotrophy and Nitrogen Fixation During Eastern Mediterranean Sapropel Events: Science, v. 286, no. 5449, p. 2485-2488.

Saltzman, M. R., and Thomas, E., 2012, Chapter 11 - Carbon Isotope Stratigraphy, *in* Gradstein, F. M., Ogg, J. G., Schmitz, M. D., and Ogg, G. M., eds., The Geologic Time Scale: Boston, Elsevier, p. 207-232.

Santoro, A. E., and Casciotti, K. L., 2011, Enrichment and characterization of ammonia-oxidizing archaea from the open ocean: phylogeny, physiology and stable isotope fractionation: ISME Journal, v. 5, no. 11, p. 1796-1808.

Sanudo-Wilhelmy, S. A., Kustka, A. B., Gobler, C. J., Hutchins, D. A., Yang, M., Lwiza, K., Burns, J., Capone, D. G., Raven, J. A., and Carpenter, E. J., 2001, Phosphorus limitation of nitrogen fixation by Trichodesmium in the central Atlantic Ocean: Nature, v. 411, no. 6833, p. 66-69.

Schubert, C. J., and Calvert, S. E., 2001, Nitrogen and carbon isotopic composition of marine and terrestrial organic matter in Arctic Ocean sediments: implications for nutrient utilization and organic matter composition: Deep Sea Research Part I: Oceanographic Research Papers, v. 48, no. 3, p. 789-810.

Sigman, D. M., Altabet, M. A., McCorkle, D. C., Francois, R., and Fischer, G., 2000, The $\delta^{15}N$ of nitrate in the Southern Ocean: Nitrogen cycling and circulation in the ocean interior: Journal of Geophysical Research: Oceans, v. 105, no. C8, p. 19599-19614.

Sigman, D. M., Karsh, K. L., and Casciotti, K. L., 2009, Nitrogen Isotopes in the Ocean, *in* Steele, J. H., ed., Encyclopedia of Ocean Sciences (2nd Edition): Oxford, Academic Press, p. 40-54.

Sliwinski, M. G., Whalen, M. T., Newberry, R. J., Payne, J. H., and Day, J. E., 2011, Stable isotope ($\delta^{13}C_{carb\ and\ org}$, $\delta^{15}N_{org}$) and trace element anomalies during the Late Devonian 'punctata Event' in the Western Canada Sedimentary Basin: Palaeogeography Palaeoclimatology Palaeoecology, v. 307, no. 1-4, p. 245-271.

Steinmann, Y., Struck, U., and Gamper, A., 2013, Late Devonian "Kellwasser-Event" A Global mass-extinction eqivalent to the Precambrian-Cambrian Boundary interval?: Mineralogical Magazine, v. 77, no. 5, p. 2260.

Struck, U., Emeis, K.-C., Voß, M., Krom, M. D., and Rau, G. H., 2001, Biological productivity during sapropel S5 formation in the Eastern Mediterranean Sea: Evidence from stable isotopes of nitrogen and carbon: Geochimica et Cosmochimica Acta, v. 65, no. 19, p. 3249-3266.

Struck, U., Pollehne, F., Bauerfeind, E., and v. Bodungen, B., 2004, Sources of nitrogen for the vertical particle flux in the Gotland Sea (Baltic Proper)-results from sediment trap studies: Journal of Marine Systems, v. 45, p. 91-101.

Struck, U., 2012, On The Use of Stable Nitrogen Isotopes in Present and Past Anoxic Environments, *in* Altenbach, A. V., Bernhard, J. M., and Seckbach, J., eds., Anoxia, Volume 21: Springer Netherlands, p. 497-513.

Suchi, E., 2005, Rekonstruktion der Evolution des marinen Nährstoffangebots im Verlauf des Jungpaläozoikums unter besonderer Berücksichtigung der Stickstoffisotopenzusammensetzung: Dissertation (unpublished), Westfälische Wilhelms-Universität Münster.

Sundquist, E. T., and Visser, K., 2011, 10 - The Geologic History of the Carbon Cycle, *in* Holland, H. D., and Turekian, K. K., eds., Geochemistry of Earth Surface Systems - From the Treatise on Geochemistry: Oxford, Elsevier, p. 341-388.

Thomazo, C., Ader, M., and Philippot, P., 2011, Extreme ^{15}N-enrichments in 2.72-Gyr-old sediments: evidence for a turning point in the nitrogen cycle: Geobiology, v. 9, no. 2, p. 107-120.

Thomazo, C., and Papineau, D., 2013, Biogeochemical Cycling of Nitrogen on the Early Earth: Elements, v. 9, no. 5, p. 345-351.

Turekian, K. K., 2001, Stable carbon isotope variations in the ocean, *in* Steele, J., Thorpe, S., and Turekian K., eds., A Derivative of Encyclopedia of Ocean Sciences (2nd Edition, 2010): Oxford, Academic Press, p. 566.

Vila, X., Guyoneaud, R., Cristina, X. P., Figueras, J. B., and Abella, C. A., 2002, Green sulfur bacteria from hypersaline Chiprana Lake (Monegros, Spain): habitat description and phylogenetic relationship of isolated strains: Photosynthesis Research, v. 71, no. 1-2, p. 165-172.

Wahlund, T. M., and Madigan, M. T., 1993, Nitrogen-fixation by the thermophilic green sulfur bacterium chlorobium-tepidum: Journal of Bacteriology, v. 175, no. 2, p. 474-478.

Werne, J. P., and Hollander, D. J., 2004, Balancing supply and demand: controls on carbon isotope fractionation in the Cariaco Basin (Venezuela) Younger Dryas to present: Marine Chemistry, v. 92, no. 1-4, p. 275-293.

Westerhausen, L., Poynter, J., Eglinton, G., Erlenkeuser, H., and Sarnthein, M., 1993, Marine and terrigenous origin of organic matter in modern sediments of the equatorial East Atlantic: the $\delta^{13}C$ and molecular record: Deep Sea Research Part I: Oceanographic Research Papers, v. 40, no. 5, p. 1087-1121.

Wilkerson, F., and Dugdale, R. C., 2008, Chapter 17 - Coastal Upwelling, *in* Capone, D. G., Bronk, D. A., Mulholland, M. R., and Carpenter, E. J., eds., Nitrogen in the Marine Environment (2nd Edition): San Diego, Academic Press, p. 771-807.

Zerkle, A. L., Junium, C. K., Canfield, D. E., and House, C. H., 2008, Production of ^{15}N-depleted biomass during cyanobacterial N_2-fixation at high Fe concentrations: Journal of Geophysical Research-Biogeosciences, v. 113, no. G03014.

Zerkle, A. L., Scheiderich, K., Maresca, J. A., Liermann, L. J., and Brantley, S. L., 2011, Molybdenum isotope fractionation by cyanobacterial assimilation during nitrate utilization and N_2 fixation: Geobiology, v. 9, no. 1, p. 94-106.

Zhang, X., Sigman, D. M., Morel, F. M. M., and Kraepiel, A. M. L., 2014, Nitrogen isotope fractionation by alternative nitrogenases and past ocean anoxia: Proceedings of the National Academy of Sciences of the United States of America, v. 111, no. 13, p. 4782-4787.

4. STUDY AREAS AND RESEARCH FOCUS

Investigations concentrate on two Precambrian-Cambrian microcontinental blocks: The Yangtze platform of the South China Block, and the Malyi Karatau Range of the Kazakh Block. Both microcontinents are believed to have been paleogeographically near each other during the late Neoproterozoic and early Cambrian (Levashova et al., 2011; Weber et al., 2013). According to paleomagnetic data, the South China Block was situated in low latitudes during the late Cryogenian - early Ediacaran (Fig. 4a) and moved towards near-equatorial latitudes in the early Cambrian (Fig. 4b; Steiner et al., 2007; Li et al., 2008; Li et al., 2013). In contrast to South China, the exact Ediacaran paleogeographic position of the Kazakh microcontinent is unknown; paleomagnetic data exist only for Neoproterozoic times (~770 Ma) and indicate a location at a paleolatitude of ~34° N or S near the South China Block (Levashova et al., 2011). For the early Cambrian Paleo-Kazakhstan, Weber et al. (2013) propose a position between 20°N and 20°S. Authors suggest that the Kazakh microcontinent was situated near the northwestern margin of Gondwana, east of South China and west of Siberia. This is supported by similarities in ichnofacies and in depositional regime of both regions. This scenario is also supported by preliminary paleomagnetic data of Pradhan et al. (2009), suggesting a paleolatitude of ~20° for the Malyi Karatau which is consistent with a peri-Siberian position in near-equatorial regions.

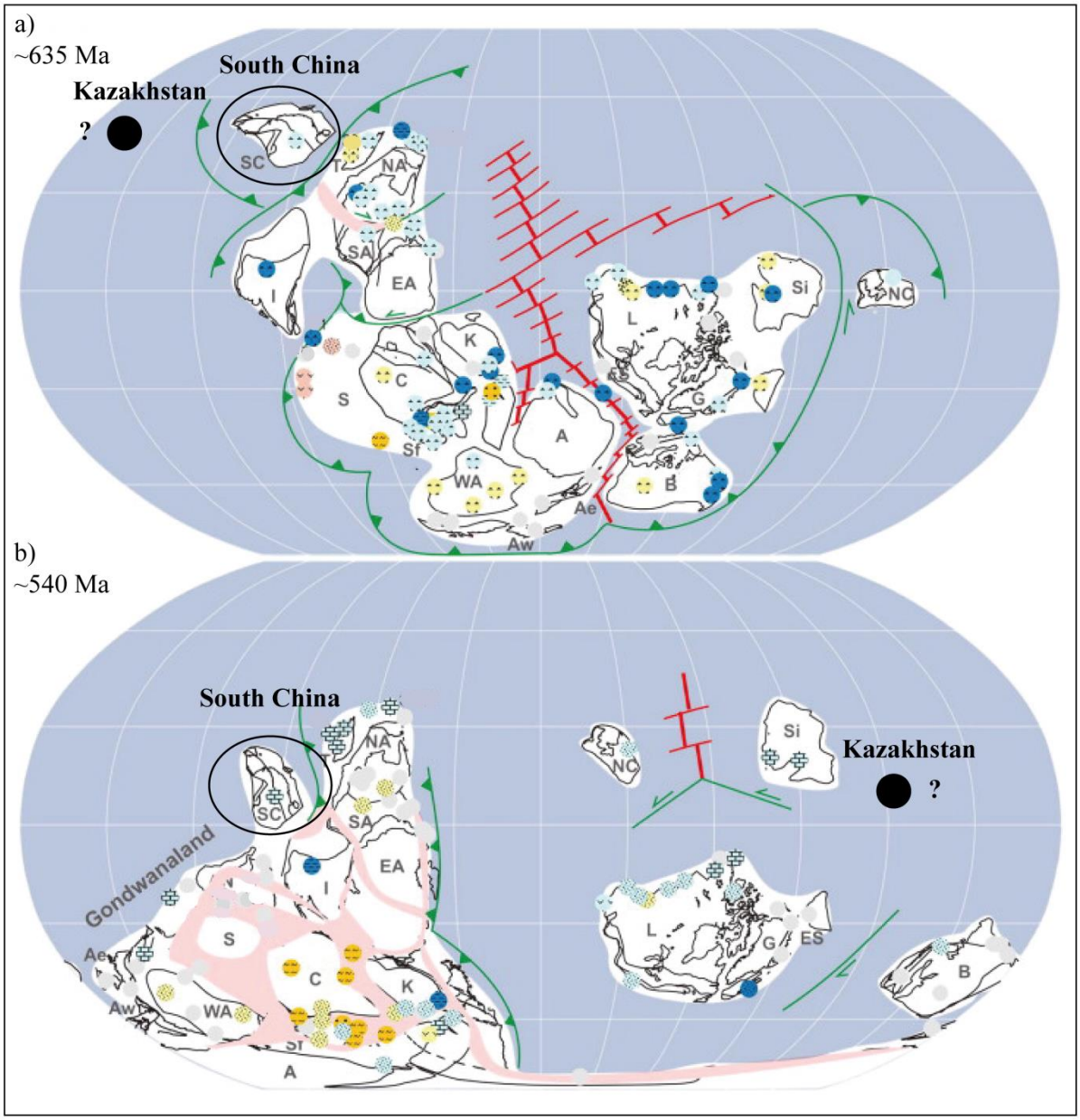

Figure 4: Paleogeographic reconstruction during (a) the lower Ediacaran (~635 Ma) and (b) the early Cambrian (~540 Ma) after Li et al. (2013). (a) During the early Ediacaran the South China Block (circle) is situated in lower latitudes. However, the position of the Kazakh Block (black circle) is hypothetical and suggested to be closely associated to the South China Block and Siberia (Weber et al., 2013). (b) In the early Cambrian paleomagnetic data indicate a position in near-equatorial regions for both Paleo-South China and Paleo-Kazakhstan. Paleobiogeographic analyses indicate a position for South China at the eastern realm of Gondwana during the early Cambrian (Steiner et al., 2007). According to paleomagnetic data of Pradhan et al. (2009) Kazakhstan was located close to Siberia. A: Amazonia, Ae: Avalonia (east), Aw: Avalonia (west), B: Baltica. C: Congo, EA: East Antarctica, ES: East Svalbard, G: Greenland, I: India, K: Kalahari, L: Laurentia, NA: Northern Australia, NC: North China, S: Sahara, SA: Southern Australia, SC: South China, Sf: Sao Francisco, Si: Siberia, T: Tarim, WA: West Africa.

4.1 South China

Several Pc-C geochemical and stratigraphical investigations concentrate on the Neoproterozoic to Cambrian Yangtze platform of South China where well-preserved thick marine sedimentary sequences of these ages crop out without major hiatuses (Zhu et al., 2007a). On the South China Block, Ediacaran strata developed on a passive margin and comprise the carbonate-siliciclastic Doushantuo Formation (~635 - 551 Ma) overlying glacial deposits of the Late Cryogenian Nantuo Formation (Zhu et al., 2007b; Jiang et al., 2011). The Doushantuo Formation in turn is overlain by the carbonate-dominated Dengying Formation (~551 - 541 Ma) of a shallow-shelf platform environment, and its deep-water-facies equivalent, the shaly and cherty Liuchapo Formation (Zhu et al., 2003). The onset of the Cambrian is marked by a widespread transgression and characterized by the deposition of a few cm-thick black shale or phosphatic nodules in deeper-water settings as well as carbonate-phosphatic strata in the northwestern part of the platform although both lithologies can also be absent (Steiner et al., 2007; Ishikawa et al., 2008). Compared to their global equivalents, Ediacaran and Cambrian strata on the Yangtze platform are well constrained in age: U-Pb zircon dating defines an age of ~635 Ma for an ash bed within the lower part of the basal Ediacaran cap carbonate (Condon et al., 2005), ~551 Ma for the uppermost Doushantuo Formation (Condon et al., 2005), and ~538 - 535 Ma for basal Cambrian units (Jenkins et al., 2002; Zhu et al., 2009).

The geologic and tectonic history of the area is complex. The Yangtze platform is part of the South China Block which formed during the Early Neoproterozoic collision of the Yangtze and the Cathaysia Blocks (Sibao-Jinning Orogeny ~1000 Ma or >900 Ma; Li et al., 2005; Zhu et al., 2007b). When the exact timing of the amalgamation occurred is still elusive but thought to either lie between 900 - 880 Ma or 860 - 830 Ma (Zhao and Cawood (2012), and references therein). In the course of the break-up of supercontinent Rodinia, South China became an isolated block with several rift basins resulting from the break-up (Zhu et al., 2007b). In the Cryogenian, interglacial-glacial successions were deposited during the final phase of the rift-drift transition (740 - 635 Ma) and subsequently overlain by Ediacaran strata, following a major global glaciation event (suspected

"snowball Earth" glaciations; Hoffman et al., 1998; Zhu et al., 2007b).The early Triassic collision of the Yangtze craton with the North China Block and the formation of the Cathaysian Block within the Yangtze craton (volcanic-arc setting) during the Silurian resulted in the evolution of two major structures which today build the frame of the Yangtze platform: the Qin-Lin fault to the north and the Cathaysia suture to the south (Vernhet and Reijmer, 2010). Despite the complex deformation history of South China, Neoproterozoic sedimentary successions remained largely unaffected by penetrative deformation but were only tilted or folded on a large scale.

The northern part of the Ediacaran Yangtze platform (Fig. 5a) forms a coastal to shallow-shelf environment with a slope facing south-east, thus merging into deep-water basinal facies (Vernhet et al., 2007; Jiang et al., 2011). In general, the bio-, litho-, and chemostratigraphy of the Ediacaran and early Cambrian of the Yangtze platform are best investigated in the Yangtze Gorges area (Hubei Province) where strata are mainly deposited in a shallow-platform environment (Zhu et al., 2007b). In contrast, strata cropping out at the northern rim of the Yangtze platform (southern Shaanxi Province) are correlated only by inconsistent (and in the literature in part contradictory) lithostratigraphy. Despite the presence of well-preserved sedimentary rocks (Guo et al., 2012) and an excellently documented Ediacaran fossil record (e.g. Hua et al., 2007; Weber et al., 2007; Meyer et al., 2012; Cai et al., 2014), Shaanxi Province remains geochemically poorly investigated. Therefore, we focus our isotopic investigation on the Gaojiashan section located in the Ningqiang area of southern Shaanxi Province (Fig. 5). To address the question of how late Ediacaran strata in the Ningqiang area are integrated in the chemo- and biostratigraphical framework of the Yangtze platform as well as on global scale, chapter 5 discusses regional lithostratigraphic uncertainties and proposes a new chemostratigraphic correlation based on $\delta^{13}C_{carb}$, $\delta^{18}O$ and TOC analyses. In addition, biogeochemical cycling in the late Ediacaran ecosphere is poorly known; especially, nitrogen isotope data are rare (Cremonese et al., 2014; Kikumoto et al., 2014). It remains unknown if isotopic trends from the shelf-to-slope environments can be confirmed from more proximal locations on the shallow shelf (Gaojiashan section) and to

what extent nitrogen (e.g. nitrate) experienced isotopic homogenization on the Yangtze platform.

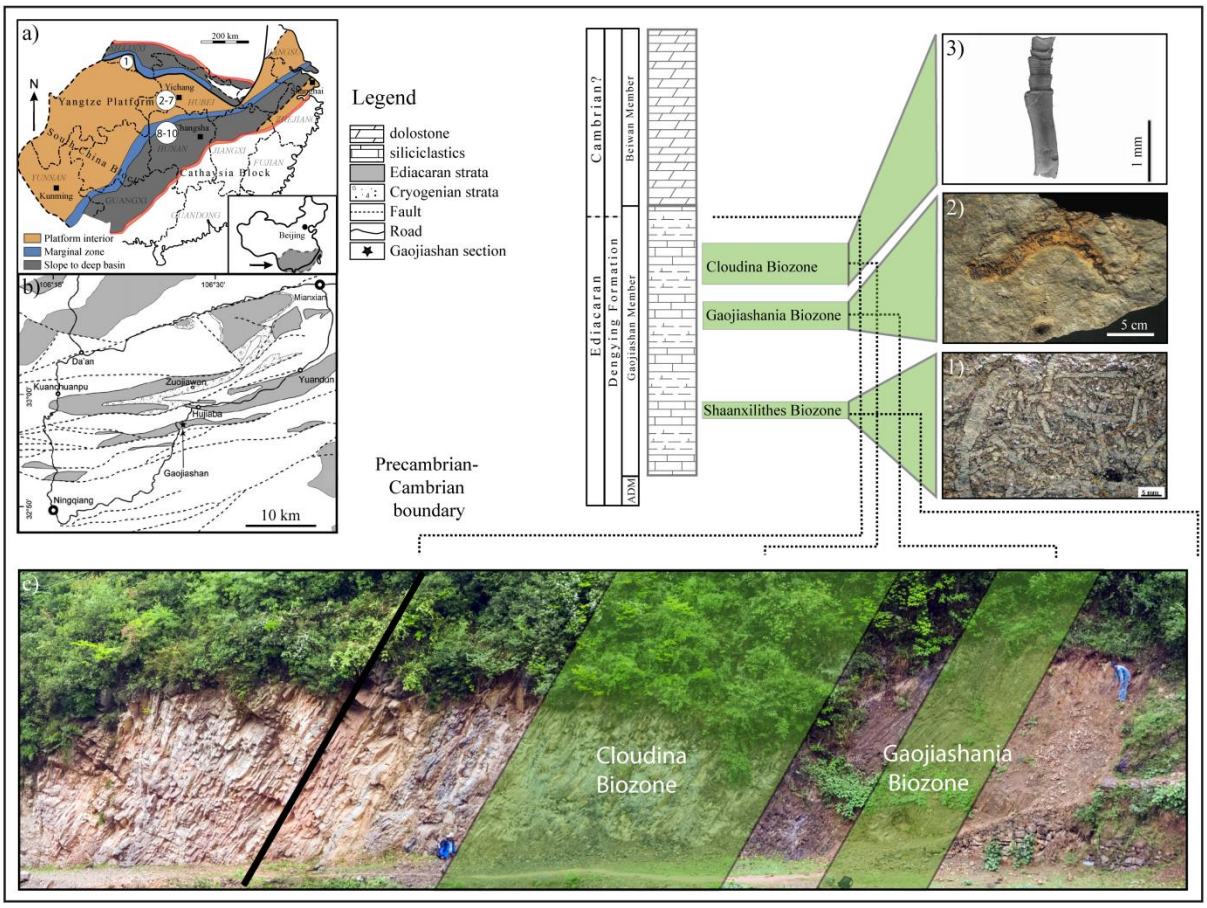

Figure 5: (a) Simplified geological map of the Yangtze platform modified after Guo et al. (2007) and Cremonese et al. (2013). Colors represent different paleogeographic settings. Numbers show approximate outcrop localities visited during field work in 2009 (section 1) and 2012 (sections 2 - 10). For outcrop coordinates see Appendix A3.1. (b) Regional geological map of the Ningqiang area in southern Shaanxi Province modified after Cai et al. (2013). The star symbol shows the location of the studied Gaojiashan section. (c) Panorama photograph of the outcrop at Gaojiashan section (source Q. Scouflaire) spanning the Pc-C boundary and its fossil record. Photomicrographs of 1) Shaanxilithes biota (source B. Weber), 2) Gaojiashania biota (source B. Weber), and 3) Cloudina biota (source Cai et al. (2014)) are linked to their stratigraphic occurrence in the outcrop. Outcrop-locations: 1 - Gaojiashan section, 2 - Xiaofenghe section, 3 - Jiulongwan section, 4 - Huajipo section, 5 - Sixi section, 6 - Jijiawan (Maoping) section, 7 - Hushan Wangji section, 8 - Longbizui section, 9 - Xixi section, 10 - Lijiatuo section.

In order to reconstruct biogeochemical cycling in the Pc-C shallow-water paleoecosphere on the Yangtze platform, chapter 6 links the isotopic dataset of bio-relevant elements nitrogen and organic carbon to the unique fossil record. During a field season in 2012, we studied 10 additional sections on the Yangtze platform (Fig. 5), from which two sections were selected for isotopic analyses (see chapter 9: Outlook and future work, and Appendix A3).

4.2 Kazakhstan

The second study area is located on the Pc-C Kazakh microcontinent, situated in south-central Kazakhstan. This investigation focuses on Pc-C strata of the Karatau Range (Fig. 6) which expands NW-SE over ~250 km across central Asia and forms a northwestern part of the Central Asian Tien Shan Mountains (Heubeck et al., 2013; Weber et al., 2013).

The Karatau Range is part of the Central Asian Orogenic Belt (CAOB; Meert et al., 2011) which represents the amalgamation of formerly independent tectonic blocks during the Paleozoic (Heubeck, 2001). However, the Precambrian geodynamic evolution and geological correlation of the several CAOB microcontinents is poorly known due to the lack of stratigraphic marker beds and insufficient paleomagnetic and geochronologic data for these times (Levashova et al., 2011). Geologic and paleomagnetic analyses by Levashova et al. (2011) propose that the CAOB microcontinents belonged to two larger domains (Kazakhstan and Mongol) which had originally been part of either South China or Tarim and remained closely associated since then. Nevertheless, lithostratigraphic similarities among CAOB microcontinents grow during the late Neoproterozoic-Cambrian where respective carbonate-clastic sequences overlie an Archean to Paleoproterozoic crystalline basement and are in turn covered by Devonian-Carboniferous folded terrigenous and calcareous strata (Eganov et al., 1986; Levashova et al., 2011). The tectonic framework and deformation history of the Karatau Range is poorly constrained (Levashova et al., 2011; Meert et al., 2011). Convergence and collision of the Kazakhstan microcontinent with the Europe (Baltica) craton and the Tarim, Alay and Turan microcontinents led to the Late Paleozoic fold-and-thrust belts of the Ural and Tien Shan Mountains (Alexeiev et al., 2009). Carboniferous to Triassic thrusting, folding and strike-slip tectonics affected the architecture of the Karatau Range and resulted in the NW-SE trending Main Karatau Fault (Fig. 6) which separates the Karatau Range into Malyi (Lesser) Karatau to the northeast and the Bolshoi (Greater) Karatau to the southwest.

The northwestern part of Bolshoi Karatau comprises largely (albeit regionally) greenschist or higher-grade metamorphosed and tectonic deformed rocks (Alexeiev et al., 2009), and thus, sections investigated there (Fig. 6) were not considered for isotopic analyses.

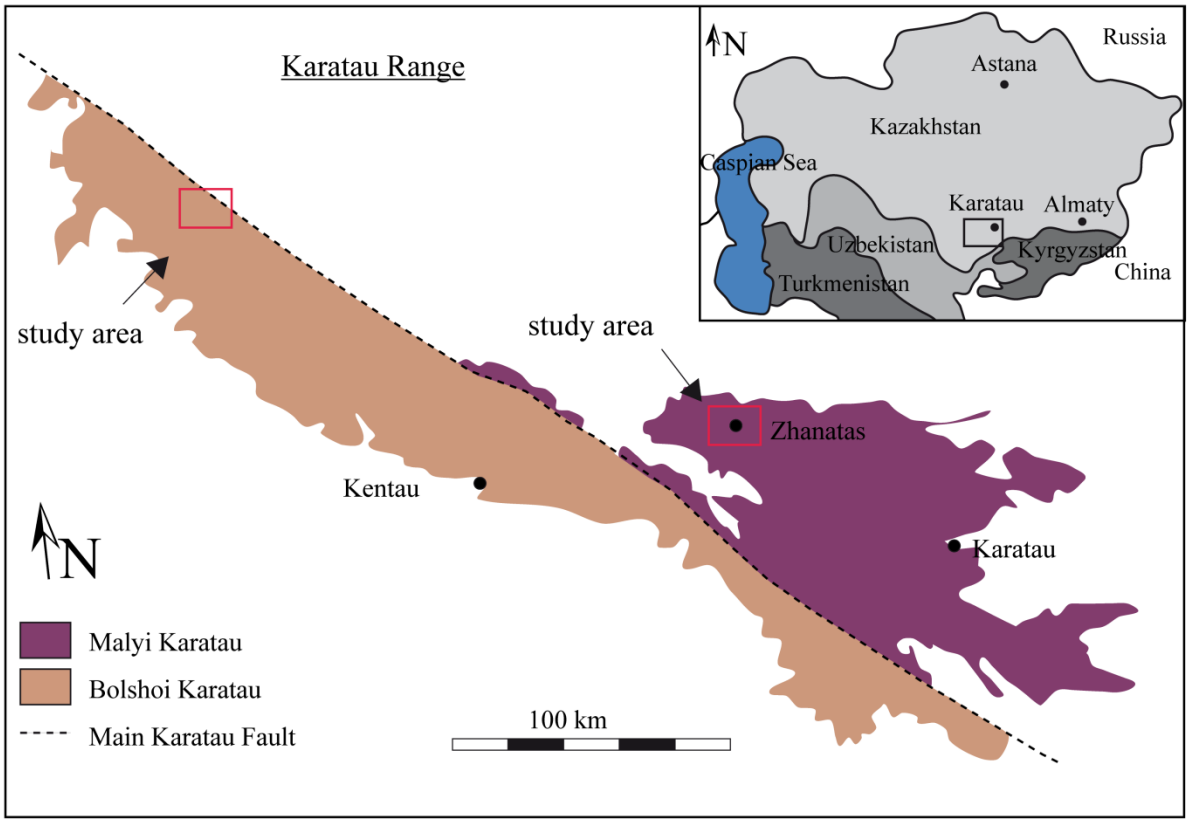

Figure 6: Sketch map of the Karatau Range after Alexeiev et al. (2009) with inset map showing the geographical framework. The Karatau Range is situated in south Kazakhstan and forms a northwestern branch of the Central Asian Tien Shan Mountains. The Mesozoic Karatau Fault separates the Karatau Range into the Bolshoi (Greater) Karatau and the Malyi (Lesser) Karatau. Both areas were investigated during field work in 2011. The study areas are marked by a red rectangle.

The Malyi Karatau area offers numerous and nearly unmetamorphosed sections spanning from the Neoproterozoic into the Triassic within a NE-vergent fold-and-thrust belt (Alexeiev et al., 2009) which is predominantly exposed on anticlinal flanks dipping 20° to 50° (Heubeck et al., 2013). Respective Neoproterozoic siliciclastic rocks are interpreted as being indicative of a continental rift setting and Early Paleozoic carbonates are deposited within an isolated seamount (Alexeiev et al., 2009) or an island arc (Weber et al., 2013). Cambrian strata in the Malyi Karatau area are known for its well-preserved Cambrian fossil assemblages (Weber et al., 2013) and have been largely studied over many

decades for their economically important phosphate deposits (Eganov et al., 1986). The stratigraphic subdivision and correlation, especially of the Ediacaran to early Cambrian strata, varies widely, attributable to the paucity of Ediacaran fossils, of geochemical studies and of radiometric age constraints (e.g. Meert et al., 2011). In the Malyi Karatau area, late Cryogenian strata comprise ~500 m thick volcano-sedimentary units of the Kurgan Formation (Eganov et al., 1986) which are dated to 766 ± 7 Ma (Levashova et al., 2011). Greenish Kurgan volcanics are overlain by ~0 - 150 m thick carbonate-siliciclastic strata of the Kyrshabakty Formation of Ediacaran to Cambrian age (Eganov et al., 1986; Popov et al., 2009; Weber et al., 2013). This estimate is based on the first occurrence of the Lower Cambrian small shelly fossil *Protohertzina anabarica* in the upper Kyrshabakty Formation (Popov et al., 2009; Weber et al., 2013). However, the exact position of the Pc-C boundary is unknown. The contact to the overlying dolomitic-phosphatic mixed Lower Cambrian Chulaktau Formation is characterized by the deposition of a black chert in the lowermost part. The Chulaktau Formation is followed by >2000 m dolo- and limestones of the Shabakty Formation (Eganov et al., 1984; Heubeck et al., 2013).

During field work in 2011, six sections near Zhanatas within the Malyi Karatau area were studied (Fig. 7; outcrop coordinates Appendix A4.1). The Kyrshabakty section was most suitable for isotope analyses because its well-preserved strata span nearly continuously from the basal Ediacaran into the early Cambrian.

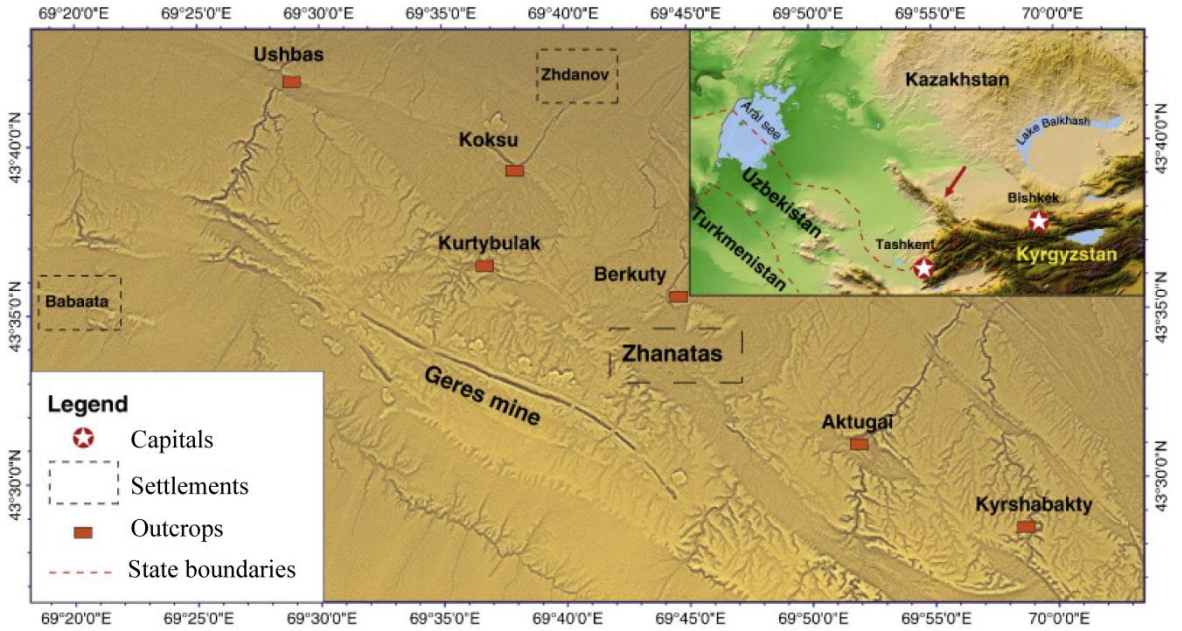

Figure 7: Topographic map of the study area in the vicinity of Zhanatas (Malyi Karatau) showing outcrops visited in 2011. The red arrow in the inlet map shows the location of the Karatau Range at a larger scale. For isotopic analyses, the Kyrshabakty and Berkuty sections were chosen. Map adapted from Weber et al. (2013).

Research in Malyi Karatau area focuses on the integration of Kazakh Pc-C strata into the global geochemical framework. $\delta^{13}C_{carb}$, $\delta^{13}C_{org}$ and $\delta^{15}N$ analyses give insights into Ediacaran biogeochemical cycling and allow comparisons to other microcontinents (chapter 7). A continuous $\delta^{15}N$ record from the basal Ediacaran to the early Cambrian is of interest because no such $\delta^{15}N$ record exists outside of South China. Additionally, the Kazakh $\delta^{15}N$ dataset is intended to clarify if a previous reported nitrogen isotopic anomaly in the lower Cambrian (Cremonese et al., 2014) can be confirmed and if thus nitrogen isotope geochemistry can serve as a reliable paleoenvironmental proxy for Pc-C sections of central Asia.

4.3 References

Alexeiev, D. V., Cook, H. E., Buvtyshkin, V. M., and Golub, L. Y., 2009, Structural evolution of the Ural-Tian Shan junction: A view from Karatau ridge, South Kazakhstan: Comptes Rendus Geoscience, v. 341, no. 2-3, p. 287-297.

Cai, Y., Hua, H., and Zhang, X., 2013, Tube construction and life mode of the late Ediacaran tubular fossil Gaojiashania cyclus from the Gaojiashan Lagerstätte: Precambrian Research, v. 224, no. 0, p. 255-267.

Cai, Y., Hua, H., Schiffbauer, J. D., Sun, B., and Yuan, X., 2014, Tube growth patterns and microbial mat-related lifestyles in the Ediacaran fossil Cloudina, Gaojiashan Lagerstätte, South China: Gondwana Research, v. 25, no. 3, p. 1008-1018.

Condon, D., Zhu, M., Bowring, S., Wang, W., Yang, A., and Jin, Y., 2005, U-Pb Ages from the Neoproterozoic Doushantuo Formation, China: Science, v. 308, no. 5718, p. 95-98.

Cremonese, L., Shields-Zhou, G., Struck, U., Ling, H.-F., Och, L., Chen, X., and Li, D., 2013, Marine biogeochemical cycling during the early Cambrian constrained by a nitrogen and organic carbon isotope study of the Xiaotan section, South China: Precambrian Research, v. 225, no. 0, p. 148-165.

Cremonese, L., Shields-Zhou, G. A., Struck, U., Ling, H.-F., and Och, L. M., 2014, Nitrogen and organic carbon isotope stratigraphy of the Yangtze Platform during the Ediacaran–Cambrian transition in South China: Palaeogeography, Palaeoclimatology, Palaeoecology, v. 398, no. 0, p. 165-186.

Eganov, E. A., Ergaliev, G. K., Ilyin, A. V., and Krasnov, A. A., 1984, Guidebook / International Geological Congress, XXVII Session Kazakhstan: Karatau Phosphorite Basin, Moskau, Nauka.

Eganov, E. A., Sovetov, Y. K., and Yanshin, A. L., 1986, Proterozoic and Cambrian phosphorites - deposits: Karatau, southern Kazakhstan, *in* Cook, P.J., Shergold, J.H., eds., Phosphate Deposits of the World: Volume 1 Proterozoic and Cambrian Phosphorites: Cambridge, Cambridge University Press, UK, p. 175-189.

Guo, Q., Strauss, H., Liu, C., Goldberg, T., Zhu, M., Pi, D., Heubeck, C., Vernhet, E., Yang, X., and Fu, P., 2007, Carbon isotopic evolution of the terminal Neoproterozoic and early Cambrian: Evidence from the Yangtze Platform, South China: Palaeogeography, Palaeoclimatology, Palaeoecology, v. 254, no. 1–2, p. 140-157.

Guo, Q., Deng, Y., and Yang, X., 2012, Carbon Isotopic Evolution of the Late Ediacaran Gaojiashan Biota on the Northern Yangtze Platform, South China: Acta Geologica Sinica-English Edition, v. 86, no. 6, p. 1447-1454.

Heubeck, C., 2001, Assembly of central Asia during the middle and late Paleozoic, *in* Davis, G., and M.S. Hendrix, eds., Paleozoic and Mesozoic tectonic evolution of central Asia: Geological Society of America Memoir 194, p. 1-22.

Heubeck, C., Ergaliev, G., and Evseev, S., 2013, Large-scale seismogenic deformation of a carbonate platform straddling the Precambrian-Cambrian boundary, Karatau Range, Kazakhstan: Journal of Sedimentary Research, v. 83, no. 11-12, p. 1005-1025.

Hoffman, P. F., Kaufman, A. J., Halverson, G. P., and Schrag, D. P., 1998, A Neoproterozoic snowball earth: Science, v. 281, no. 5381, p. 1342-1346.

Hua, H., Chen, Z., and Yuan, X., 2007, The advent of mineralized skeletons in Neoproterozoic Metazoa - new fossil evidence from the Gaojiashan Fauna: Geological Journal, v. 42, p. 263–279.

Ishikawa, T., Ueno, Y., Komiya, T., Sawaki, Y., Han, J., Shu, D., Li, Y., Maruyama, S., and Yoshida, N., 2008, Carbon isotope chemostratigraphy of a Precambrian/Cambrian boundary section in the Three Gorge area, South China: Prominent global-scale isotope excursions just before the Cambrian Explosion: Gondwana Research, v. 14, no. 1–2, p. 193-208.

Jenkins, R. J. F., Cooper, J. A., and Compston, W., 2002, Age and biostratigraphy of Early Cambrian tuffs from SE Australia and southern China: Journal of the Geological Society, v. 159, p. 645-658.

Jiang, G., Shi, X., Zhang, S., Wang, Y., and Xiao, S., 2011, Stratigraphy and paleogeography of the Ediacaran Doushantuo Formation (ca. 635–551 Ma) in South China: Gondwana Research, v. 19, p. 831-849.

Kikumoto, R., Tahata, M., Nishizawa, M., Sawaki, Y., Maruyama, S., Shu, D., Han, J., Komiya, T., Takai, K., and Ueno, Y., 2014, Nitrogen isotope chemostratigraphy of the Ediacaran and Early Cambrian platform sequence at Three Gorges, South China: Gondwana Research, v. 25, no. 3, p. 1057-1069.

Levashova, N. M., Meert, J. G., Gibsher, A. S., Grice, W. C., and Bazhenov, M. L., 2011, The origin of microcontinents in the Central Asian Orogenic Belt: Constraints from paleomagnetism and geochronology: Precambrian Research, v. 185, no. 1-2, p. 37-54.

Li, W.-X., Li, X.-H., and Li, Z.-X., 2005, Neoproterozoic bimodal magmatism in the Cathaysia Block of South China and its tectonic significance: Precambrian Research, v. 136, no. 1, p. 51-66.

Li, Z.-X., Evans, D. A. D., and Halverson, G. P., 2013, Neoproterozoic glaciations in a revised global palaeogeography from the breakup of Rodinia to the assembly of Gondwanaland: Sedimentary Geology, v. 294, no. 0, p. 219-232.

Li, Z. X., Bogdanova, S. V., Collins, A. S., Davidson, A., De Waele, B., Ernst, R. E., Fitzsimons, I. C. W., Fuck, R. A., Gladkochub, D. P., Jacobs, J., Karlstrom, K. E., Lu, S., Natapov, L. M., Pease, V., Pisarevsky, S. A., Thrane, K., and Vernikovsky, V., 2008, Assembly, configuration, and break-up history of Rodinia: A synthesis: Precambrian Research, v. 160, no. 1–2, p. 179-210.

Meert, J. G., Gibsher, A. S., Levashova, N. M., Grice, W. C., Kamenov, G. D., and Ryabinin, A. B., 2011, Glaciation and ~770 Ma Ediacara (?) Fossils from the Lesser Karatau Microcontinent, Kazakhstan: Gondwana Research, v. 19, p. 867-880.

Meyer, M., Schiffbauer, J. D., Xiao, S., Cai, Y., and Hua, H., 2012, Taphonomy of the upper Ediacaran enigmatic ribbonlike fossil Shaanxilithes: Palaios, v. 27, no. 5-6, p. 354-372

Popov, L. E., Bassett, M. G., Zhemchuzhnikov, V. G., Holmer, L. E., and Klishevich, I. A., 2009, Gondwanan faunal signatures from early Palaeozoic terranes of Kazakhstan and Central Asia: evidence and tectonic implications: Geological Society, London, Special Publications, v. 325, p. 23-64.

Pradhan, V. R., Meert, J. G., Levashova, N. M., and Gibsher, A. S., 2009, Preliminary paleomagnetic data on Late Cambrian to Ordovician carbonate beds of Tamdy Series from the Lesser Karatau microcontinent, South Kazakhstan: Geological Society of America *Abstracts with Programs*, v. 41, no. 7, p. 269.

Steiner, M., Li, G., Qian, Y., Zhu, M., and Erdtmann, B.-D., 2007, Neoproterozoic to Early Cambrian small shelly fossil assemblages and a revised biostratigraphic correlation of the Yangtze Platform (China): Palaeogeography, Palaeoclimatology, Palaeoecology, v. 254, no. 1–2, p. 67-99.

Vernhet, E., Heubeck, C., Zhu, M.-Y., and Zhang, J.-M., 2007, Stratigraphic reconstruction of the Ediacaran Yangtze Platform margin (Hunan Province, China) using a large olistolith: Palaeogeography, Palaeoclimatology, Palaeoecology, v. 254, p. 123-139.

Vernhet, E., and Reijmer, J. J. G., 2010, Sedimentary evolution of the Ediacaran Yangtze platform shelf (Hubei and Hunan provinces, Central China): Sedimentary Geology, v. 225, no. 3–4, p. 99-115.

Weber, B., Steiner, M., and Zhu, M.-Y., 2007, Precambrian–Cambrian trace fossils from the Yangtze Platform (South China) and the early evolution of bilaterian lifestyles: Palaeogeography, Palaeoclimatology, Palaeoecology, v. 254, no. 1-2, p. 328-349.

Weber, B., Steiner, M., Evseev, S., and Yergaliev, G., 2013, First report of a Meishucun-type early Cambrian (Stage 2) ichnofauna from the Malyi Karatau area (SE Kazakhstan): Palaeoichnological, palaeoecological and palaeogeographical implications: Palaeogeography Palaeoclimatology Palaeoecology, v. 392, p. 209-231.

Zhao, G., and Cawood, P. A., 2012, Precambrian geology of China: Precambrian Research, v. 222–223, no. 0, p. 13-54.

Zhu, M., Zhang, J., Steiner, M., Yang, A., Li, G., and Erdtmann, B. D., 2003, Sinian-Cambrian stratigraphic framework for shallow- to deep-water environments of the Yangtze Platform: an integrated approach: Progress in Natural Science, v. 13, no. 12, p. 951-960.

Zhu, M., Strauss, H., and Shields, G. A., 2007a, From snowball earth to the Cambrian bioradiation: Calibration of Ediacaran–Cambrian earth history in South China: Palaeogeography, Palaeoclimatology, Palaeoecology, v. 254, no. 1–2, p. 1-6.

Zhu, M., Zhang, J., and Yang, A., 2007b, Integrated Ediacaran (Sinian) chronostratigraphy of South China: Palaeogeography, palaeoclimatology, Palaeoecology, v. 254, p. 7-61.

Zhu, R. X., Li, X. H., Hou, X. G., Pan, Y. X., Wang, F., Deng, C. L., and He, H. Y., 2009, SIMS U-Pb zircon age of a tuff layer in the Meishucun section, Yunnan, southwest China: Constraint on the age of the Precambrian-Cambrian boundary: Science in China Series D-Earth Sciences, v. 52, no. 9, p. 1385-1392.

5. CHEMO- AND BIOSTRATIGRAPHY OF THE GAOJIASHAN SECTION (NORTHERN YANGTZE PLATFORM, SOUTH CHINA): A NEW PC-C BOUNDARY SECTION

5.1 Abstract

The widespread, terminal Ediacaran Dengying Formation (~551 - ~542 Ma) of South China hosts one of the most prominent negative carbonate carbon isotope excursions in Earth's history and thus bears on the correlation of Precambrian-Cambrian boundary events worldwide. The dominantly carbonate strata of the Dengying Formation are largely studied for its unique preservation of its terminal Ediacaran fauna but their geochemical context is poorly known. This study presents the first high-resolution stable isotope record ($\delta^{13}C$, $\delta^{18}O$) of calcareous siliciclastic shallow-water deposits of the Gaojiashan section (Shaanxi Province). The section includes (in ascending order) the Algal Dolomite Member, the Gaojiashan Member and the Beiwan Member of the Dengying Formation. Our data record a major $\delta^{13}C$ (carbonate carbon) negative excursion to -6‰ in the uppermost Gaojiashan Member which is comparable in shape and magnitude to the global Precambrian-Cambrian boundary negative $\delta^{13}C$ excursion. Our dataset is consistent with a "shallow-water anoxia" scenario which is thought to contribute to events at the "Cambrian explosion". The stratigraphic occurrence of *Cloudina* and the negative $\delta^{13}C$ excursion suggest the Precambrian-Cambrian boundary near the top of the Gaojiashan Member, and that consequently overlying carbonates and dolomites of the Beiwan Member are of lowermost Cambrian age. Thus the Gaojiashan section may represent a new shallow-water section spanning the Precambrian-Cambrian boundary. Although bio- and chemostratigraphic data support this novel interpretation we cannot exclude the possibility that the key excursions may represent a local perturbation indicating a restricted-basin environment.

Keywords: chemostratigraphy, $\delta^{13}C$ negative excursion, shallow-water anoxia, Shaanxi Province, Gaojiashan, Precambrian-Cambrian boundary

Highlights:

We present carbon and oxygen isotopic records of the Ediacaran Gaojiashan section, Shaanxi Province, South China.

$\delta^{13}C$ data define a negative excursion to as low as -6‰ in the uppermost Gaojiashan Member of the Dengying Formation.

Shape and magnitude of the $\delta^{13}C$ negative excursion suggest that it represents the Precambrian-Cambrian boundary.

The overlying Beiwan Member, formerly of late Ediacaran age, is suggested to be of Cambrian age.

The stratigraphic division in southern Shaanxi Province remains debated and requires reinvestigation and re-interpretation.

5.2 Introduction

The Ediacaran period (*ca.* 635 - 542 Ma) was a time of tectonic instability accompanied by a major global perturbation in biogeochemical cycles and the reorganization and evolution of metazoan life (Fike et al., 2006; Weber et al., 2007; Wang et al., 2012a). Following the end of the Marinoan glaciation, Ediacaran ocean chemistry and its ecosystems experienced dramatic changes, climaxing in the "Cambrian explosion". Major steps in the evolution of metazoan life during this time interval can be linked to global negative carbonate carbon isotope excursions ($\delta^{13}C$; Zhu et al., 2007; Shields-Zhou and Zhu, 2013). During the Ediacaran, ocean chemistry changed from anoxic, sulfate-rich bottom waters via one or several oxygenation events towards a fully oxygenated ocean dominating the Phanerozoic (e.g. Och et al., 2013). However, the explicit identification and documentation of stratigraphic sections recording events across the Precambrian-Cambrian (Pc-C) boundary with little or no hiatuses remains challenging. Because numerous lithostratigraphic studies worldwide have documented widespread terminal Ediacaran relative sea level fall, hiatuses or condensed sections are common; biostratigraphic positions and quality of index fossils are often controversial; and the validity of chemostratigraphic data is

negatively affected by weathering, early- and burial diagenetic overprint and alteration (Derry, 2010); in addition, the required age resolution of geochronological data is commonly insufficient. It is therefore widely accepted that only multi-disciplinary approaches can overcome the deficiencies of individual bio-, litho- or chemostratigraphic record studies. Traditionally, the global correlation of the Pc-C boundary interval is based on biostratigraphic analyses. Narbonne et al. (1987) proposed the first occurrence of the ichnotaxon *Treptichnus pedum* as the index fossil of the lowermost Cambrian. The earliest calcareous metazoans, e.g. *Cloudina*- and *Namacalathus* have been shown to be of latest Ediacaran age (Germs, 1972; Grotzinger et al., 2000; Kontorovich et al., 2008; Wood, 2011). Where trace fossils are missing or poorly preserved, chemostratigraphy has proven to be a powerful tool to complement biostratigraphy in Pc-C strata because terminal Ediacaran strata record one of the largest global isotopic excursions in Earth's history. Negative $\delta^{13}C$ excursions of up to -12‰ in magnitude (Li et al., 2013) can be correlated worldwide, e.g. in South China (Jiang et al., 2007; Li et al., 2009), Oman (Amthor et al., 2003), Mongolia (Brasier et al., 1996), Brazil (Boggiani et al., 2010), and Siberia (Brasier et al., 1994). Several of the best preserved and most continuous successions across the Pc-C boundary are found on the Yangtze platform in South China (Zhu et al., 2007).

In this study, we present an integrated interpretation of carbon isotopic and paleontological data from literature, combined with the first high-resolution $\delta^{13}C$ record from the Gaojiashan section (Fig. 8), Ningqiang county, southern Shaanxi Province (South China). We investigate the carbon ($\delta^{13}C$) and oxygen ($\delta^{18}O$) isotopic compositions as well as total organic carbon (TOC) contents of interbedded coastal carbonate-siliciclastic strata from the northern part of the Neoproterozoic-Devonian Yangtze platform.

5.3 Geological setting and regional stratigraphy

The Ediacaran period of the Yangtze platform is divided into the basal Doushantuo Formation (*ca.* 635 - 551 Ma) and the overlying Dengying Formation (*ca.* 551 - 542 Ma; Condon et al., 2005; Zhu et al., 2007). Strata of the Doushantuo Formation directly cover Cryogenian glacial deposits. In Shaanxi Province, the thick dolo- and limestones of the Dengying Formation, representing a prograding platform facies environment associated with a sea level regression, are unconformable overlain by the Cambrian Kuanchuanpu Formation (Zhu et al., 2003; Steiner et al., 2004). The Dengying Formation has received less attention than the underlying Doushantuo Formation which has yielded numerous paleontological, geochemical and stratigraphic insights. In part, this is because the Dengying Formation is up to 1000 m thick, consists nearly exclusively of variably dolomitized shallow-water platform carbonates dominated by monotonous shallow-marine and lagoonal-facies microbial boundstones, and lacks distinctive marker beds. It typically forms steep and subvertical cliffs and karsted surfaces. However, the middle to upper Dengying Formation at the northern margin of the Yangtze platform includes a siliciclastic interval, the Gaojiashan Member, which opens a rare preservational window into late Ediacaran evolution and has been investigated for its significant latest-Ediacaran metazoan fauna (Hua et al., 2001; Hua et al., 2003; Hua et al., 2005; Hua et al., 2007; Weber et al., 2007; Cai et al., 2010; Cai et al., 2011; Cai et al., 2012; Meyer et al., 2012; Cai et al., 2013).

The approximately 100 m thick Gaojiashan section (Fig. 8a) is located ~4 km south of Hujiaba town. It exposes (from base to top) the Algal Dolomite Member, the Gaojiashan Member, and the Beiwan Member of the Dengying Formation (Fig. 8b) which can be correlated to the Hamajing, Shibantan, and Baimatuo Members, respectively, of the same formation in the Yangtze Gorges type area (Zhu et al., 2003; Cai et al., 2010). The interbedded siliciclastic and carbonate units at the Gaojiashan section were deposited in a passive-margin setting in a dominating coastal to shallow-water carbonate environment affected by periodic siliciclastic sedimentation (Zhu et al., 2003; Weber et al., 2007). The Dengying Formation in Ningqiang county is thought to have been deposited between 551

and 541 Ma (Condon et al., 2005; Cai et al., 2010; Cai et al., 2011) and thus records the latest Ediacaran, immediately prior to the onset of the base-Cambrian radiation. The basal Algal Dolomite Member predominantly consists of algal-laminated dolostones with abundant dissolution features (Zhu et al., 2007; Cai et al., 2010). It is separated from interbedded fine-grained siliciclastics and carbonates of the overlying Gaojiashan Member by an erosional unconformity (Zhu et al., 2007). The Gaojiashan Member at the section of the same name reaches approximately 60 m thickness and can be subdivided in five mappable units. The basal unit, approximately 10 m thick, consists of dolomitic green-to-red shales. It is gradationally overlain by a shaly ~8 m thick dolomudstone which is glauconitic and phosphatic near its base and contains mass accumulations of *Shaanxilithes ningqiangensis*; it coarsens up into a dolograinstone of a tidal facies. This unit, in turn, is overlain by laminated, shale-clast-bearing green pyritic siltstone interbedded with some grey nodular dolomudstone approximately 18 m thick. Its upper part, about 5 - 8 m thick, contains the so-called Gaojiashan biota, comprising *Gaojiashania* and *Conotubus*. This unit coarsens upward into an impure biolaminated dolomitized calcarenite, ~8 m thick which displays oncoids, reworked microbial laminations and trace fossil horizons. A distinctive, medium- to coarse-grained, granule-bearing, well-sorted, channelized and cross-bedded dolomitic and quartz-rich arkose, coarsening-upward and approximately 9 m thick, marks the top of the Gaojiashan Member. Its top is gradationally overlain by silty dolomites and nodular limestones of the Beiwan Member. Overall, the lithologies, sedimentary structures and inferred facies successions are consistent with a regressive sub- to lower intertidal environment into which a delta prograded. Three important fossil taxa have been described from the Gaojiashan Member (Hua et al., 2005; Weber et al., 2007; Cai et al., 2010; Cai et al., 2012; Meyer et al., 2012; Cai et al., 2013): *Shaanxilithes ningqiangensis*, *Gaojiashania* and *Cloudina*. The latter is one of the earliest biomineralizing organisms and is used to correlate late Ediacaran (550 - 540 Ma) strata (Shields-Zhou and Zhu, 2013) in e.g. Namibia (Germs, 1972), Oman (Amthor et al., 2003), Canada (Hofmann and Mointjoy, 2001), and Paraguay (Warren et al., 2011). The Gaojiashan Member is capped by a distinct granuly arkose with carbonate-dolomite cement. Cai et al. (2010) refer to this lithology as

a "sandstone-conglomerate unit" which thins from west to east in the Gaojiashan outcrop belt, and thus implies a western provenance. The overlying Beiwan Member consists of thickbedded dolomitized limestone and varies widely in thickness (Cai et al., 2014). Cai et al. (2010) report *Cloudina* from this unit at this section, whereas more recent reports describe *Cloudina* only in the upper Gaojiashan Member (Guo et al., 2012; Meyer et al., 2012; Cai et al., 2014).

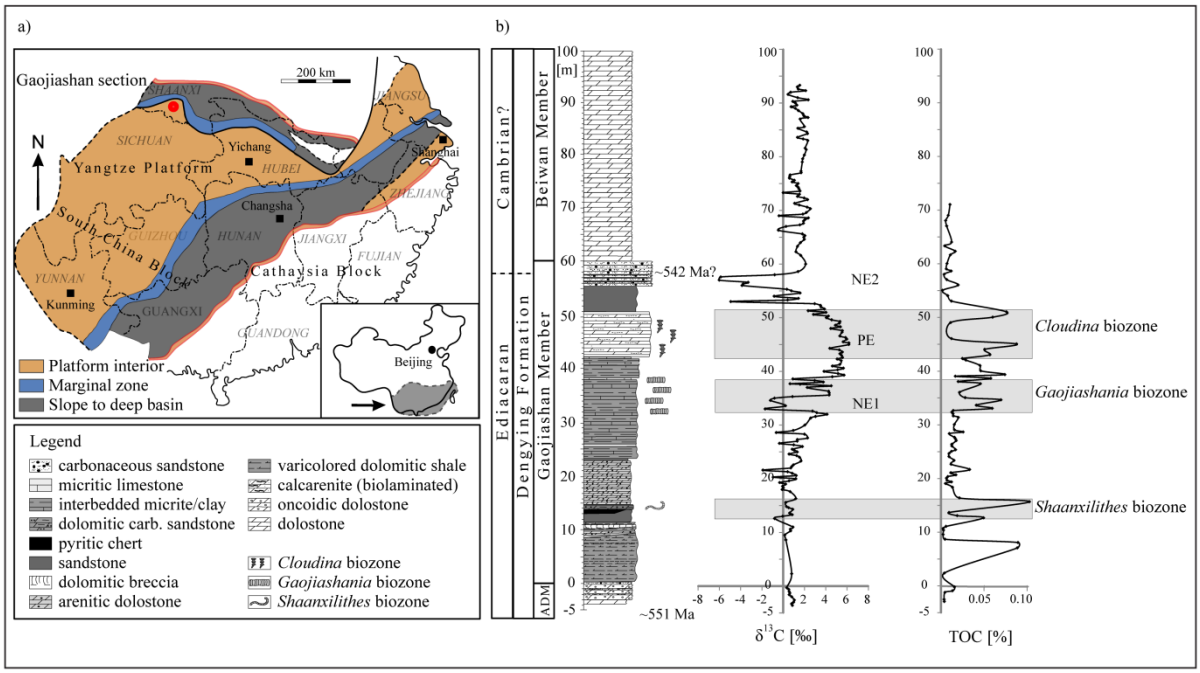

Figure 8: Paleoenvironmental reconstruction of the Ediacaran Yangtze platform (modified after Guo et al. (2007); Cremonese et al. (2013)) and the isotopic record of the Gaojiashan section. (a) Strata at the northern part of the platform display a coastal to shallow-shelf depositional environment. The Ediacaran slope faces south-east and grades into a deep-water basinal facies in Hubei, Hunan and Guizhou Provinces (Vernhet et al., 2007). The Gaojiashan section discussed here (red circle) is located in Ningqiang county of southern Shaanxi Province. (b) Isotopic records of δ¹³C and TOC data correlated to the stratigraphical column. Stratigraphic column and fossil assemblages are modified after Q. Scouflaire (pers. comm.). Note the two prominent δ¹³C excursions (PE, NE2) linked to changes in corresponding TOC content. Shaanxilithes ningqiangensis, Gaojiashania and Cloudina in the Gaojiashan section occupy distinct biozones which correlate with elevated TOC values. ADM: Algal Dolomite Member.

5.4 Analytical methods and materials

Approximately 200 samples spaced about 0.3 to 1 m apart were collected along a traverse *ca.* 100 m long from the "Gaojiashan section". To recognize and reduce the effects of a diagenetic overprint, we analyzed 23 petrographic thin sections, cathodoluminescent images and oxygen isotopic composition of selected samples. After removing weathered surfaces and macroscopically visible veins from samples, cleaned samples were ground to powder using an agate mill and analyzed for their bulk $\delta^{13}C$ and $\delta^{18}O$ isotope composition. Stable isotope ratio measurements were performed at the Museum für Naturkunde Berlin using a Thermo Finnigan Gasbench II coupled online with a Thermo Finnigan Delta V isotope ratio mass spectrometer. Approximately 100 - 400 µg of sample material was put into a clean 10 ml exetainer. After sealing the exetainer with a septum cap the remaining air was removed by flushing the exetainer with He for five minutes at a flow of 100 ml per minute. After flushing, approximately 30 microliters of anhydrous phosphoric acid were injected through the septum into the sealed exetainer by using a disposable syringe and allowed to react for approximately 1.5 h. Reference gas was pure CO_2 from a cylinder calibrated against the Vienna PeeDee Belemnite (VPDB) standard by using IAEA reference materials (NBS 18, NBS 19). Isotope values are shown in the conventional delta-notation ($\delta^{13}C$ and $\delta^{18}O$) in per mil (‰) versus VPDB. Reproducibility of replicate measurements of lab standards (Jurassic limestone) is generally better than 0.10‰ (one standard deviation).

After decalcifying the sample powder with 2 M HCl, total organic carbon content (TOC) was calculated by elemental analyzer - isotope ratio mass spectrometry (EA-IRMS) using a Thermo/Finnigan MAT V isotope ratio mass spectrometer coupled to a Thermo Flash EA 1112 elemental analyzer via a Thermo/Finnigan Conflo III-interface at the Museum für Naturkunde Berlin. The analytical error is within 3% of the material analyzed.

Rare Earth Element and Yttrium (REE+Y) concentrations were analyzed by the geochemistry group at Freie Universität Berlin. Following the method described in Hohl et al. (in prep.), 20 mg rock powder of three selected samples (Table 5)

were treated with 3 M acetic acid for at least 12 h; the supernatant was centrifuged and filtered. REE+Y analysis were performed in low-resolution mode on a Thermo Fisher Scientific Element XR sector-field ICP-MS using Scott type quartz spray chamber and 100 µl/min nebulizer. Sample time was 120 s with 20 samples/peak and 60 total scans. With this analytical setup tuning generally yielded low oxide rates of 2 - 5% CeO^+ and less than 1% BaO^+. Element concentrations were evaluated by external calibration method to the matrix-matching CAL-S carbonate standard (Yeghicheyan et al., 2003). We corrected for instrument drift using internal standard solutions containing In and Tl. Background corrections were performed by subtraction of the raw intensities of aspirated 0.28 M HNO_3. The analytical precisions were between 2 - 7% RSD for REE and Y. The detection limit of LREE was 100 - 620 pg/g and 16 - 240 pg/g of HREE. Procedural blanks of REE+Y were negligible (for further details, see Hohl et al., in prep.).

5.5 Results

Geochemical data are summarized in Table 4 and 5.

Table 4: Results of carbonate carbon ($\delta^{13}C$) and oxygen ($\delta^{18}O$) isotopic compositions as well as total organic carbon (TOC) concentration of samples from the Gaojiashan section (Gj).

Sample	Distance [m]	$\delta^{13}C$ [‰] vs. VPDB	$\delta^{18}O$ [‰] vs. VPDB	TOC [%]
Gj -3.6	-3.6	0.9	-2.5	
Gj -3.3	-3.3	0.8	-0.1	
Gj -3.0	-3.0	1.0	-0.8	0.003
Gj -2.6	-2.6	1.1	-1.8	0.003
Gj -2.0	-2.0	0.8	-2.7	
Gj -1.6	-1.6	0.6	-3.5	
Gj -1.3	-1.3	0.6	-1.4	0.004
Gj -1.0	-1.0	0.6	-3.1	0.013
Gj -0.6	-0.6	0.5	-1.6	
Gj -0.3	-0.3	0.3	-3.0	0.015
Gj 2.3	2.3	0.8	-2.0	0.004
Gj 7.0	7.0			0.089
Gj 8.0	8.0			0.089
Gj 8.6	8.6	0.3	-0.2	0.004
Gj 9.5	9.5	0.1	-0.4	0.002
Gj 10.3	10.3	0.7	-0.7	0.003
Gj 10.6	10.6	0.7	-0.9	0.002
Gj 11.0	11.0	0.9		0.006
Gj 12.6	12.6	-0.8	-3.7	0.049
Gj 13.0	13.0	-0.1	-5.3	0.019
Gj 13.3	13.3	0.8	-4.5	
Gj 13.6	13.6	0.6	-4.0	0.009
Gj 14.3	14.3	0.9		
Gj 14.6	14.6	0.5		
Gj 15.6	15.6	0.3		0.103
Gj 16.3	16.3	1.2	-4.8	0.021
Gj 17.6	17.6	0.7		
Gj 18.0	18.0	-0.1		
Gj 18.3	18.3	0.0		0.013
Gj 18.6	18.6	-0.1	-8.6	
Gj 19.0	19.0	0.2	-6.2	0.005
Gj 19.3	19.3	-0.3		0.012
Gj 19.6	19.6	0.6		0.007
Gj 20.0	20.0	1.2	-6.6	0.006
Gj 20.3	20.3	-0.9		0.008
Gj 20.6	20.6	1.2		0.017

Table 4 (continued)

Sample	Distance [m]	$\delta^{13}C$ [‰] vs. VPDB	$\delta^{18}O$ [‰] vs. VPDB	TOC [%]
Gj 21.0	21.0	0.9		0.011
Gj 21.3	21.3	0.4		
Gj 21.6	21.6	-1.9	-7.5	0.033
Gj 22.0	22.0	0.7	-6.0	
Gj 22.3	22.3	0.8		
Gj 22.6	22.6	1.0		0.011
Gj 23.3	23.3	1.7		0.015
Gj 24.0	24.0	1.5		0.009
Gj 24.3	24.3	1.3		
Gj 24.6	24.6	0.6		0.009
Gj 25.0	25.0	1.3		0.012
Gj 25.3	25.3	1.0	-6.6	0.017
Gj 25.5	25.5	0.8	-7.1	
Gj 26.0	26.0	1.8		0.012
Gj 26.3	26.3	1.0		0.012
Gj 26.6	26.6	-0.4	-7.5	
Gj 27.0	27.0	1.3	-6.5	0.017
Gj 27.3	27.3	1.3		0.017
Gj 27.6	27.6	2.3		0.015
Gj 28.3	28.3	2.0		0.009
Gj 28.6	28.6	-0.7		0.025
Gj 29.0	29.0	1.0	-6.6	0.015
Gj 30.0	30.0	2.0		0.015
Gj 31.3	31.3	2.6	-5.5	0.020
Gj 31.6	31.6	3.0	-5.7	0.014
Gj 32.0	32.0	4.1		0.014
Gj 32.3	32.3	3.2		0.012
Gj 32.6	32.6	2.7	-6.0	0.014
Gj 33.0	33.0	-1.7		0.059
Gj 33.6	33.6	0.2	-7.3	0.041
Gj 34.6	34.6	-1.2		0.070
Gj 35.0	35.0	-0.8	-7.8	0.028
Gj 35.3	35.3	0.9		
Gj 35.6	35.6	4.3	-4.9	
Gj 36.0	36.0	4.3	-5.8	0.021
Gj 36.3	36.3	4.3		
Gj 37.0	37.0	2.3		
Gj 37.3	37.3	4.5		
Gj 37.6	37.6	1.6	-7.3	0.046
Gj 37.7	37.7	0.6	-5.2	
Gj 38.0	38.0	3.8	-5.5	0.020
Gj 38.3	38.3	3.0	-7.6	

Table 4 (continued)

Sample	Distance [m]	$\delta^{13}C$ [‰] vs. VPDB	$\delta^{18}O$ [‰] vs. VPDB	TOC [%]
Gj 38.6	38.6	0.9	-7.8	0.058
Gj 39.0	39.0	4.6	-5.5	0.016
Gj 39.3	39.3	5.7	-5.6	0.074
Gj 39.6	39.6	5.2	-5.0	
Gj 40.0	40.0	3.8	-8.8	0.046
Gj 40.3	40.3	5.1	-5.3	
Gj 40.6	40.6	5.7	-6.5	
Gj 41.0	41.0	4.6		0.045
Gj 41.3	41.3	5.3	-5.6	
Gj 42.0	42.0	5.4	-5.3	0.029
Gj 42.3	42.3	5.1		0.025
Gj 42.6	42.6	5.6	-5.6	
Gj 43.0	43.0	5.5	-6.3	0.057
Gj 43.3	43.3	5.3	-7.0	
Gj 43.6	43.6	5.6	-6.0	
Gj 44.0	44.0	5.3		0.051
Gj 44.3	44.3	4.4	-6.1	
Gj 45.0	45.0	6.2		0.088
Gj 45.3	45.3	6.2	-6.1	
Gj 45.5	45.5	5.6	-6.0	
Gj 46.0	46.0	6.0	-5.7	0.012
Gj 46.3	46.3	5.9	-6.2	
Gj 46.6	46.6	5.3	-5.4	
Gj 47.3	47.3	5.5	-5.3	
Gj 47.6	47.6	5.6	-5.5	
Gj 48.0	48.0	4.5	-5.7	
Gj 48.3	48.3	5.4	-5.2	
Gj 48.6	48.6	4.9	-5.1	
Gj 49.0	49.0	5.3	-5.8	0.011
Gj 49.3	49.3	5.3	-5.5	
Gj 49.6	49.6	4.6	-5.5	
Gj 50.0	50.0	4.1		0.060
Gj 50.3	50.3	4.3	-4.6	
Gj 50.6	50.6	2.8	-6.9	
Gj 51.0	51.0	4.0	-5.8	0.076
Gj.51.3	51.3	2.4	-6.5	
Gj 51.6	51.6	3.9	-3.3	
Gj 52.0	52.0	3.6	-4.1	
Gj 52.3	52.3	3.5	-2.7	
Gj 52.6	52.6	3.0	-4.7	
Gj 53.0	53.0	-4.9	-6.8	0.012
Gj 53.3	53.3	0.4	-7.7	

Table 4 (continued)

Sample	Distance [m]	$\delta^{13}C$ [‰] vs. VPDB	$\delta^{18}O$ [‰] vs. VPDB	TOC [%]
Gj 53.6	53.6	1.4	-3.6	
Gj 54.0	54.0	-0.8	-6.1	0.008
Gj 54.6	54.6	1.6	-7.7	
Gj 55.0	55.0	0.8	-7.1	0.001
Gj 55.3	55.3	0.3	-7.0	
Gj 56.0	56.0	-3.9	-7.4	0.020
Gj 56.3	56.3	-3.8	-9.7	
Gj 56.6	56.6	-3.3	-8.9	
Gj 57.0	57.0	-6.0	-8.0	0.006
Gj 58.0	58.0	-0.8	-7.2	0.003
Gj 58.6	58.6	1.4	-5.1	0.012
Gj 59.0	59.0			0.006
Gj 60.0	60.0			0.007
Gj 61.6	61.6	1.7		0.010
Gj 62.3	62.3	1.2		0.016
Gj 63.3	63.3	1.3		0.004
Gj 64.0	64.0	1.6		0.012
Gj 64.6	64.6	2.0	-2.0	
Gj 65.0	65.0	1.9	-2.8	
Gj 65.3	65.3	2.0	-2.6	
Gj 65.6	65.6	1.8	-2.5	
Gj 66.3	66.3	-0.4	-2.6	
Gj 67.0	67.0	0.3	-2.3	0.006
Gj 67.3	67.3	1.6	-2.3	
Gj 67.6	67.6	1.9	-2.5	
Gj 68.0	68.0	1.9	-2.4	0.005
Gj 68.3	68.3	2.1	-2.1	
Gj 68.6	68.6	2.4	-1.6	
Gj 69.0	69.0	-0.4	-4.6	0.008
Gj 69.3	69.3	1.9	-2.1	
Gj 69.6	69.6	2.2	-2.5	
Gj 70.3	70.3	2.6	-2.1	
Gj 70.6	70.6	2.3	-2.4	
Gj 71.0	71.0	1.5		0.010
Gj 71.3	71.3	1.1	-2.9	
Gj 72.0	72.0	2.3	-4.4	
Gj 72.3	72.3	2.0	-4.0	
Gj 72.6	72.6	1.3	-4.0	
Gj 73.0	73.0	1.5	-3.2	
Gj 73.3	73.3	0.0	-4.1	
Gj 73.6	73.6	1.6	-3.4	
Gj 74.0	74.0	1.5	-3.2	

Table 4 (continued)

Sample	Distance [m]	$\delta^{13}C$ [‰] vs. VPDB	$\delta^{18}O$ [‰] vs. VPDB	TOC [%]
Gj 74.3	74.3	1.4	-3.1	
Gj 74.6	74.6	1.2	-3.3	
Gj 75.0	75.0	1.4	-2.7	
Gj 75.3	75.3	0.8	-4.4	
Gj 75.6	75.6	1.1	-2.8	
Gj 76.0	76.0	0.6	-8.0	
Gj 76.3	76.3	0.6	-8.7	
Gj 76.6	76.6	0.7	-7.8	
Gj 77.0	77.0	1.7	-7.7	
Gj 77.3	77.3	1.7	-3.7	
Gj 79.0	79.0	1.8	-1.5	
Gj 79.6	79.6	1.8	-5.7	
Gj 80.3	80.3	2.0	-2.6	
Gj 81.3	81.3	2.2	-5.5	
Gj 81.6	81.6	2.1	-5.7	
Gj 83.0	83.0	2.3	-4.4	
Gj 83.3	83.3	1.9		
Gj 83.6	83.6	1.3	-2.6	
Gj 84.3	84.3	2.3	-4.0	
Gj 84.6	84.6	2.2	-4.8	
Gj 85.3	85.3	1.4	-1.8	
Gj 85.6	85.6	2.0	-4.5	
Gj 87.0	87.0	1.6	-2.1	
Gj 87.3	87.3	2.3	-2.6	
Gj 87.6	87.6	2.0	-2.7	
Gj 88.0	88.0	1.8	-2.8	
Gj 88.6	88.6	1.4	-3.6	
Gj 89.0	89.0	1.1	-3.8	
Gj 89.3	89.3	0.8	-5.8	
Gj 89.6	89.6	1.3	-5.6	
Gj 90.0	90.0	1.1	-5.6	
Gj 90.3	90.3	0.9	-4.9	
Gj 90.6	90.6	2.4		
Gj 91.0	91.0	1.4	-2.4	
Gj 91.6	91.6	0.5	-3.2	
Gj 92.0	92.0	0.7	-1.6	
Gj 92.3	92.3	2.1	-6.0	
Gj 92.6	92.6	1.4		
Gj 93.0	93.0	1.3		
Gj 93.3	93.3	1.6	-6.2	

Table 5: REE+Y concentrations (µg/g) of acetic acid leachates from selected samples of the Gaojiashan Member at the Gaojiashan section analyzed by ICP-MS. Ce/Ce, Eu/Eu*, Y/Ho and Pr/Yb ratios are post-Archean Australian Shale (PAAS) normalized – for calculation of Ce and Eu anomalies see text.*

Sample	Y	La	Ce	Pr	Nd	Sm	Eu	Gd
Gj 56.3	6.358	2.133	6.207	0.638	3.193	0.644	0.196	0.649
Gj 56.6	5.425	2.351	6.018	0.630	3.189	0.606	0.182	0.599
Gj 57.0	3.242	1.558	3.459	0.352	1.748	0.343	0.119	0.343
Sample	**Tb**	**Dy**	**Ho**	**Er**	**Tm**	**Yb**	**Lu**	
Gj 56.3	0.109	0.720	0.161	0.526	0.080	0.578	0.096	
Gj 56.6	0.099	0.572	0.143	0.427	0.059	0.384	0.072	
Gj 57.0	0.057	0.387	0.086	0.286	0.041	0.296	0.059	
Sample	**Ce_N/Ce_N^***	**Eu_N/Eu_N^***	**Y_N/Ho_N**	**Pr_N/Yb_N**				
Gj 56.3	1.405	1.382	1.449	0.353				
Gj 56.6	1.398	1.395	1.397	0.524				
Gj 57.0	1.414	1.536	1.391	0.379				

5.5.1 Isotope and TOC data

The carbon isotope composition of the Gaojiashan section shows two negative excursions (NE1 and NE2) separated by one positive excursion (PE; Fig. 8b). The first negative excursion (NE1) is preceded by relatively uniform $\delta^{13}C$ values (~0.7‰) in the basal part of the section with corresponding $\delta^{18}O$ values ranging from -5.3 to 0‰ and TOC data below <0.01% (Fig. 8b). TOC concentrations reach highest values (~0.1%) within the *Shaanxilithes ningqiangensis* biozone. Isotopic values of overlying micritic limestones begin a positive $\delta^{13}C$ trend to 4‰ before they are truncated by the short but sharp negative excursion NE1 to values of ~-2‰. Concurrently, TOC increases to >0.01% along with *in situ* buried and pyritized *Gaojiashania*-group fossils reported from beds correlative with NE1 (Cai et al., 2010). In contrast to $\delta^{13}C$ data, $\delta^{18}O$ values do not correspond to the trend of NE1 but steadily decrease to -6‰ in overlying strata. Following NE1, biolaminated calcarenites of the middle Gaojiashan Member host a positive excursion (PE) to 6‰ associated with *Cloudina* and accompanied by increasing TOC content (~0.1%). A subsequent large $\delta^{13}C$ negative decrease to -6‰ (NE2; drop of ~10‰) and the last repeatedly documented occurrence of *Cloudina*, along with decreasing TOC values (~0.01%), mark the boundary interval from the Gaojiashan to the Beiwan Member. $\delta^{18}O$ values do not trace NE2 but show a decrease to -9‰ at the onset of NE2 and recover to ~-3.5‰ for the remaining section prior to the return of $\delta^{13}C$ compositions to ~0‰. Above NE2, $\delta^{13}C$ values stabilize around 2‰ in the uppermost coarse-grained sandstone beds and stay largely invariant throughout the overlying dolomites.

5.5.2 Rare Earth Element (REE+Y) data

Three samples (Gj 56.3, 56.6, 57.0) were analyzed for their REE+Y concentration. Data are normalized relative to post-Archean Australian Shale (PAAS; McLennan, 1989). Values for Ce/Ce* and Eu/Eu* were calculated following Lawrence and Kamber (2006): $Ce/Ce^* = Ce_N/(Pr_N * Pr_N/Nd_N)$ and $Eu/Eu^* = Eu_N/(Sm_N^2 * Tb_N)^{1/3}$. These equations avoid using La and Gd to distinguish real anomalies on Ce and Eu and not anomalies caused by an overabundance of the direct neighboring elements (Ling et al., 2013). However, it has been shown before that Eu anomalies can be misleading due to interference by BaO^+ molecules which cannot be completely resolved by ICP measurements (Dulski, 1994). Therefore Eu/Eu* anomalies are not discussed here.

The three analyzed sample leachates show typical seawater-like REE+Y patterns with relative enrichment of HREE over LREE (PrPAAS/YbPAAS between 0.35 and 0.52) and positive normalized Y/HoPAAS anomalies varying around 1.4 (Table 5; Fig. 9). Furthermore, all samples show positive Ce/Ce* anomalies near 1.4, indicating a relative enrichment of cerium to its neighboring LREE.

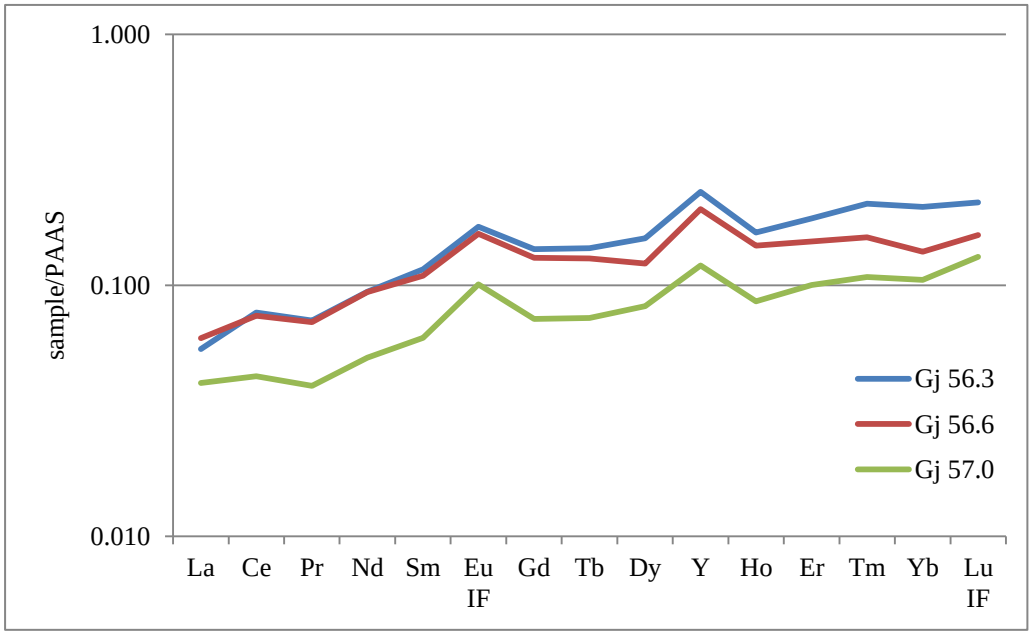

Figure 9: PAAS normalized REE+Y distribution patterns of samples Gj 56.3, 56.6 and 57.0 of the uppermost Gaojiashan Member at Gaojiashan section. Samples show a characteristic seawater-like signature with HREE over LREE enrichment and a distinct Y/Ho anomaly.

5.6 Discussion

5.6.1 Preservation of primary isotopic signatures

Carbon and oxygen isotopes of sediments are widely used as sensitive indicators of diagenetic overprint because their isotopic values change characteristically during progressive (burial) diagenesis (Knauth and Kennedy, 2009). Thereby $\delta^{18}O$ values < -10‰ and a positive correlation between $\delta^{13}C$ and $\delta^{18}O$ are usually interpreted as evidence for alteration (Derry, 2010; Li et al., 2013). Knauth and Kennedy (2009) proposed that numerous Neoproterozoic negative $\delta^{13}C$ anomalies were caused by meteoric alteration processes. However, Macouin et al. (2012) pointed out that a co-variation between the systems due to meteoric alteration had to involve terrestrial phytomass and organic-rich soils in which mineralization could occur. For this, no Neoproterozoic evidence exists.

We argue for the obtained isotopic dataset at Gaojiashan section to represent a primary marine isotope signature for the following reasons. $\delta^{18}O$ data range from -9 to 0‰ (average $\delta^{18}O$ = -5‰; Table 4) and therefore fail to fulfill the diagenetic criteria stated above. The $\delta^{18}O$ vs. $\delta^{13}C$ plot (Fig. 10) shows no correlation. Especially $\delta^{13}C$ and $\delta^{18}O$ data near the prominent negative $\delta^{13}C$ excursion (grey circles, Fig. 10) lack any correlation which would be expected if alteration had been a dominant post-depositional process during late open-system diagenesis. If fluid alteration had been present at all, it presumably was too weak to re-equilibrate the $\delta^{18}O$ isotopic composition of the mineral phases and thus too small to significantly alter the $\delta^{13}C$ composition of the rock (Kaufman and Knoll, 1995). Very early closed-system diagenesis could have occurred but did most likely not affect the isotope values.

Furthermore, strata comprising NE2 for which a diagenetic overprint could be suspected show a distinct marine seawater-like REE+Y pattern. There is no indication for post-depositional alteration effects like e.g. an increase in LREE or a decrease in the Y/Ho ratio (Ling et al., 2013). Instead obtained REE+Y values are consistent with open-ocean seawater-like REE signatures showing HREE enrichment over LREE and MREE and a characteristic positive Y/Ho anomaly

(Fig. 9; e.g. Bau and Dulski, 1996). If it is accepted that the REE+Y patterns record primary seawater signatures, it is most likely that the $\delta^{13}C$ and $\delta^{18}O$ values represent original marine signals too. Therefore, we argue for a primary oceanic signal of isotope data.

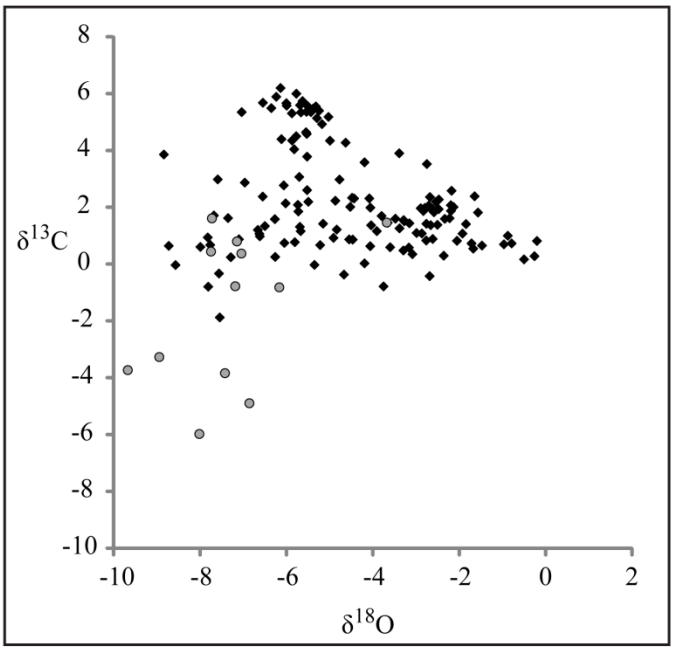

Figure 10: Cross-plot of $\delta^{18}O$ and $\delta^{13}C$ of samples from the Gaojiashan section to estimate alteration effects. Grey circles represent values within the range of the negative $\delta^{13}C$ excursion NE2. No significant correlation indicating diagenetic resetting is obvious.

5.6.2 Correlation of strata in the Ningqiang area

Lithostratigraphic correlation of late Ediacaran strata in southern Shaanxi Province remains debated due to large lateral thickness changes, limited outcrop and structural separation of the folded and faulted outcrop belts (Weber et al., 2007; Cai et al., 2010; Cai et al., 2014); in addition, chemostratigraphic work in Ningqiang county is poorly developed (Zhu et al., 2007; Guo et al., 2012).

Cai et al. (2010) correlate seven sections of the Dengying Formation across the Ningqiang area showing significant regional variations in the thickness of the Gaojiashan Member. Cai et al. (2010) based their correlation on the occurrence of *Shaanxilithes ningqiangensis* in the lower Gaojiashan Member and on the presence of a "sandstone-conglomerate unit" at its top. However, because the marker horizon is absent in three of these seven measured sections, its value is

less than perfect so that the regional correlation of the upper Gaojiashan Member remains ambiguous.

Large thickness variations in the Beiwan Member dolostones from >300 m (Hua et al., 2007; Weber et al., 2007; Zhu et al., 2007) to zero (Hua et al., 2003; Hua et al., 2005; Cai et al., 2014) also demonstrate the inadequacy of lithostratigraphy as a reliable correlation tool. Thick dolostones were variably and inconsistently assigned either to the Beiwan Member or to the Gaojiashan Member in literature (Hua et al., 2007; Weber et al., 2007; Cai et al., 2010; Guo et al., 2012; Cai et al., 2013; Cai et al., 2014). As a case in point, the Lijiaguo and the Gaojiashan sections (Fig. 11) graphically illustrate the stratigraphic uncertainties of the Precambrian-Cambrian boundary intervals in the Ningqiang area.

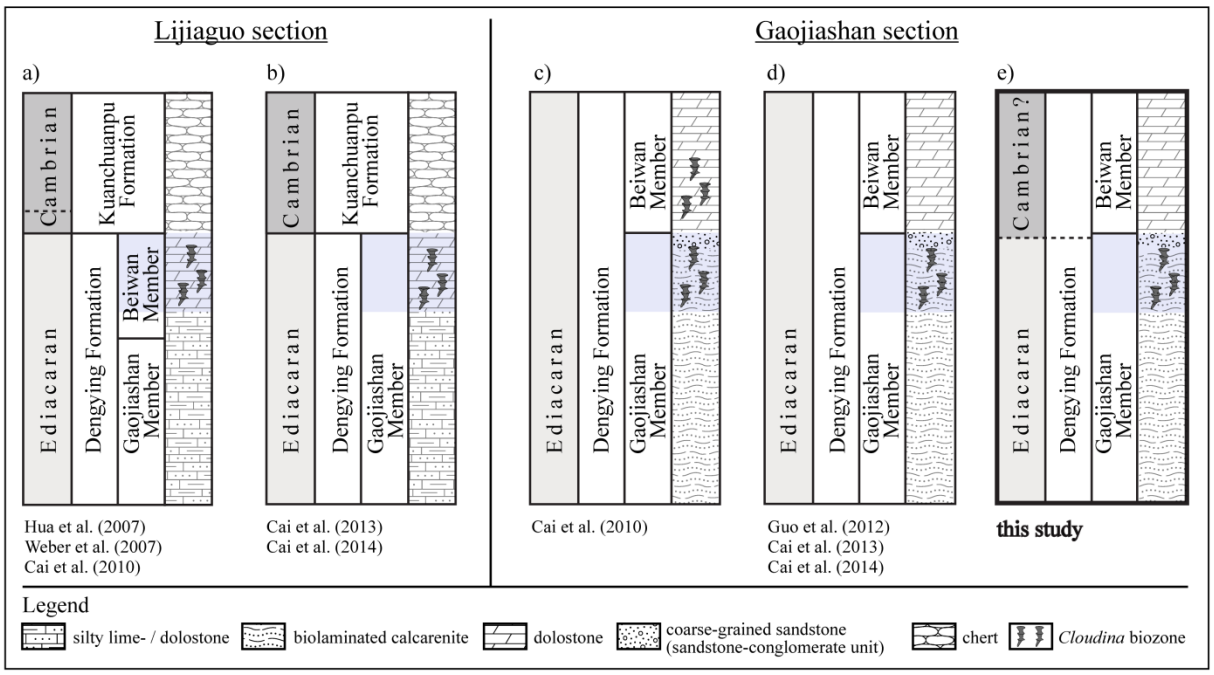

Figure 11: Comparison of simplified litho- and biostratigraphic columns of the Lijiaguo section (a,b) and the Gaojiashan section (c-e) in Ningqiang County. Stratigraphic columns reported in literature from both sections show significant stratigraphic uncertainties. Blue bars represent the occurrence of Cloudina used for correlation of columns shown. At Lijiaguo section (ca. 20 km NW of Gaojiashan section) the assignment of dolostones to either the Beiwan Member (a) or the Gaojiashan Member (b) is unresolved. Note that the marker horizon ("sandstone-conglomerate unit") of Cai et al. (2010) is absent at Lijiaguo section. At Gaojiashan section (c-e), the stratigraphical occurrence of Cloudina is probably limited to the upper Gaojiashan Member (d, e). Chemostratigraphic data (Fig. 12, this study) suggest that the Beiwan Member is of lower Cambrian age (e). Dashed lines represent assumed contacts.

At Lijiaguo section, the "sandstone-conglomerate unit" is absent (Cai et al., 2010) and the dolostone overlying the middle part of the Gaojiashan Member is assigned to either the Beiwan Member (Fig. 11a; Hua et al., 2007; Weber et al., 2007; Cai et al., 2010) or to the upper part of the Gaojiashan Member (Fig. 11b; Cai et al., 2013; Cai et al., 2014).

Discrepancies concerning the biostratigraphic occurrence of *Cloudina* complicate the stratigraphic framework at Gaojiashan section as well (Fig. 11c-e). While Cai et al. (2010) reported the occurrence of *Cloudina* in both the Gaojiashan and Beiwan Members (Fig. 11c), *Cloudina* is confirmed in more recent publications only for the Gaojiashan Member (Fig 11d; Guo et al., 2012; Cai et al., 2013; Cai et al., 2014); this is consistent with our own observations (Fig. 11e).

Lastly, the lithological nature of the contact between the Dengying Formation and the overlying Kuanchuanpu Formation is highly variable among sections. Whereas at the Lijiaguo section Dengying dolostones are overlain by cherts (Fig. 11a,b), Dengying dolostones at the Shizhonggou section are overlain by small-shelly-fossil-bearing limestones, both assigned to the Kuanchuanpu Formation (Steiner et al., 2004). Because of the lack of distinct lithological marker horizons, radiometric age data and detailed chemostratigraphical analyses, the age of Beiwan dolostones overlying the *Cloudina* biozone at Gaojiashan section and its uppermost unit, the "sandstone-conglomerate unit", is hence uncertain.

Thus, the highly variable stratigraphy between and within the outcrop belts demonstrates that biostratigraphic and lithological description alone are insufficient to reliably assign strata stratigraphically, and thus prerequisites for regional and supra-regional correlation require the integration of chemostratigraphy and geochronological data.

5.6.3 Chemostratigraphic correlation of the Gaojiashan section

Carbon isotope data of the Gaojiashan section show two prominent features. First, a positive $\delta^{13}C$ excursion (PE) associated with the appearance of *Cloudina* fossils in the upper Gaojiashan Member; second, a large negative $\delta^{13}C$ excursion (NE2) in the uppermost Gaojiashan Member. We suggest that the Gaojiashan section represents the Pc-C boundary interval and that NE2 correlates with the global negative $\delta^{13}C$ excursion associated with the approximate beginning of the lower Cambrian (Brasier et al., 1994; Narbonne et al., 1994; Brasier et al., 1996; Amthor et al., 2003; Kaufman et al., 2006; Ishikawa et al., 2013; Li et al., 2013).

This hypothesis is supported by the following arguments:

(1) $\delta^{13}C$ values of the lower Gaojiashan Member are in agreement with previously reported data from Guo et al. (2012) and other Dengying Formation shallow-water settings of South China (Jiang et al., 2007; Wang et al., 2012b). Additionally, $\delta^{18}O$ values near -5‰ match late Ediacaran $\delta^{18}O$ data from the Yangtze platform (Yang et al., 1999; Jiang et al., 2007).

(2) The presence of *Cloudina* fossils in the upper Gaojiashan Member is a global marker for terminal Ediacaran strata because *Cloudina* is known to become extinct just prior to the Pc-C boundary event (Amthor et al., 2003). Their association with a positive $\delta^{13}C$ interval preceding the prominent Pc-C negative $\delta^{13}C$ isotopic excursion is widely documented at late Ediacaran sections on the Yangtze platform (Zhu et al., 2003; Zhou and Xiao, 2007; Zhu et al., 2007) as well as in Oman (Amthor et al., 2003). Additionally, $^{87}Sr/^{86}Sr$ ratios between ~0.708 and ~0.709 reported from this part of the section (Ohnemueller et al., 2013) suggest open-ocean conditions and agree with global late Ediacaran sections (Halverson et al., 2007; Sawaki et al., 2014).

(3) The positive excursion PE is followed by a decrease in carbon isotope values with a minimum at -6‰ (NE2). Magnitude and shape of NE2 find remarkable equivalents in other Pc-C boundary sections (Fig. 12; e.g. Amthor et al., 2003; Zhu et al., 2007; Ishikawa et al., 2008; Li et al., 2013). Nevertheless, several small late Ediacaran carbon isotope excursions preceding the Pc-C boundary

excursion exist, e.g. in the Stirling Quartzite, SW Laurentia (Corsetti and Kaufman, 2003; Kaufman et al., 2007; Verdel et al., 2011) and the Krol D Formation of the Lesser Himalaya, northern India (Kaufman et al., 2006); however they are smaller in magnitude and maybe of local extent. No other negative $\delta^{13}C$ excursion of an offset of ~10‰ is known from the Dengying Formation; thus, NE2 at Gaojiashan section likely records global perturbations of the carbon cycle during the Pc-C boundary transition.

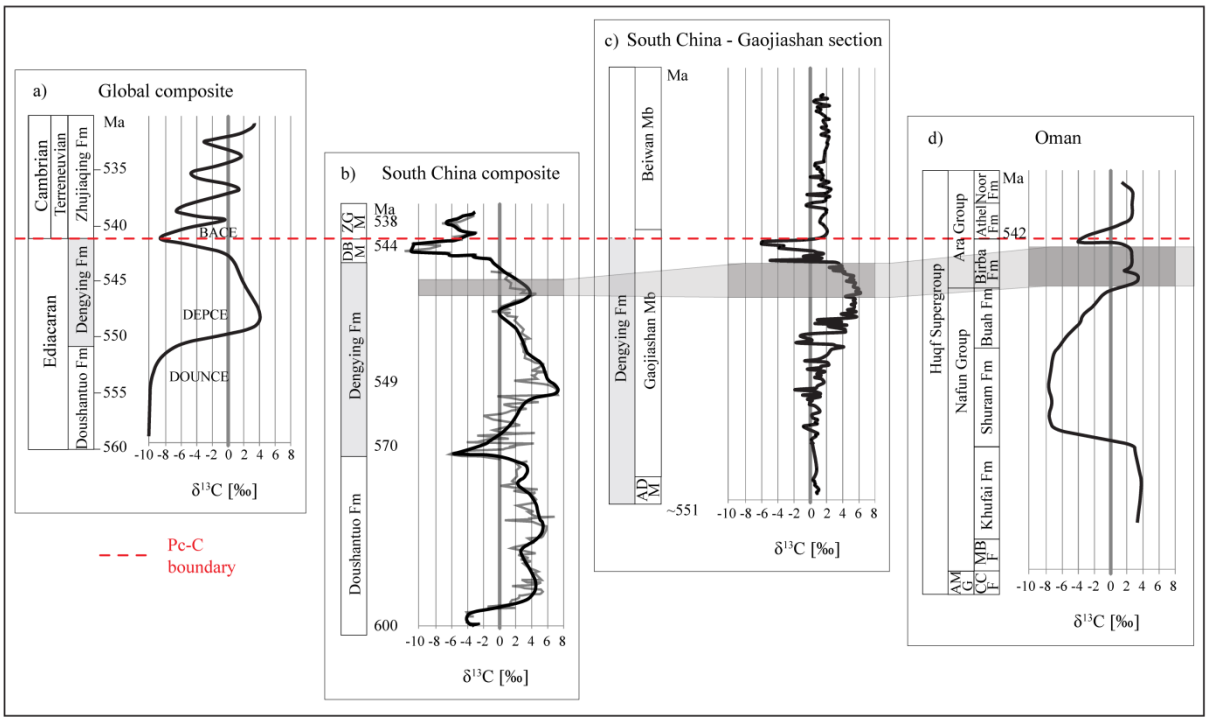

Figure 12: Proposed chemo- and biostratigraphical correlation of $\delta^{13}C$ profiles from Precambrian-Cambrian boundary intervals at different scales: (a) global scale composite (Shields-Zhou and Zhu, 2013), (b) South China composite - Yangtze platform (Zhu et al., 2003), (c) South China (Shaanxi Province), Gaojiashan section (this study), and (d) Oman - South Oman Salt Basin (Amthor et al., 2003). The stratigraphic occurrence of Cloudina below the negative $\delta^{13}C$ Pc-C boundary excursion and its association with a positive $\delta^{13}C$ interval (grey shaded bar) supports the correlation and indicates a high degree of similarity between the isotopic datasets. We suggest the prominent excursion NE2 at the Gaojiashan section to be a likely equivalent in shape and magnitude to the worldwide negative excursion in $\delta^{13}C$ at the Pc-C boundary. Following Zhu et al. (2003) and Amthor et al. (2003), we place the Precambrian-Cambrian boundary shortly above the negative $\delta^{13}C$ peak. Note that the scale at Gaojiashan section is not equal in all columns and strata thicknesses are not time-equivalent. Columns are graphically slightly modified. DBM: Daibu Member, ZGM: Zhangyicun Member, ADM: Algal Dolomite Member, AMG: Abu Mahara Group, CCF: Cap carbonate Formation, MBF: Masirah Bay Formation.

(4) The regression (Gaojiashan Member) - transgression (Beiwan Member) cycle related to the negative $\delta^{13}C$ excursion (NE2) at Gaojiashan section is in agreement with the globally observed major late Ediacaran regression - early Cambrian transgression character at the Pc-C boundary (Ishikawa et al., 2008).

Thus, we propose a correlation of the Gaojiashan section to worldwide Pc-C boundary sections. To illustrate our hypothesis, we compare the chemostratigraphy of the Gaojiashan section to global datasets (Amthor et al., 2003; Zhu et al., 2003; Shields-Zhou and Zhu, 2013) based on the two aforementioned $\delta^{13}C$ excursions (PE, NE2) and the known range of the *Cloudina* biozone (Fig. 12).

5.6.4 Causes of isotopic variations at Gaojiashan section and their paleoenvironmental implications

Two alternative scenarios may have caused isotopic variations at Gaojiashan section. The creation of a negative carbon isotopic trend to -6‰ (NE2) requires the formation of a strongly ^{13}C-depleted pool of dissolved inorganic carbon (DIC). High (surface-water) bioproductivity, suggested by two prominent developed biozones (*Gaojiashania* and *Cloudina*), contributed to the evolution of PE. Resulting increasing organic matter export to depth thus provoked high remineralization rates and oxygen depletion in bottom waters. Anoxic conditions in deep waters and in the sediment fuelled the oxidation of organic matter via e.g. sulfate-reducing bacteria which contributed to a ^{13}C-depleted deep-water DIC pool, a scenario similarly postulated for the Ediacaran Shuram-Wonoka anomaly (Jiang et al., 2007; McFadden et al., 2008). A subsequent shoaling of the chemocline and its chemical consequences likely strengthened water column stratification, led to vertical isotopic gradients (Jiang et al., 2007) and to a decrease in sedimentary $\delta^{13}C$ values. Subsequent rise of anoxic bottom waters to shallow-water depths provoked a decrease of $\delta^{13}C$ values to -6‰ (NE2) which is also indicated by a dramatic decrease from high TOC values during the uppermost occurrence of *Cloudina* to low TOC concentrations at the onset of NE2. The nutrient-driven eutrophication of surface waters (due to high

weathering rates) associated with an anoxic overturn is supported by $^{87}Sr/^{86}Sr$ analyses of other Neoproterozoic-Cambrian sections (Shields, 2007). Furthermore the positive Ce/Ce* anomaly indicative of suboxic to euxinic water conditions (German et al., 1991) is consistent with Pc-C REE data of India (Mazumdar et al., 1999) and strengthens an oceanic anoxia scenario. Upwelling of possibly euxinic water masses from greater depths near the platform margin to near-surface environments occurred at least episodically during the Pc-C boundary interval in transitional platform settings (Goldberg et al., 2007; Wille et al., 2008; Och et al., 2013), a situation which agrees well with the dataset at Gaojiashan.

A temporal and local change in the carbon turnover cycle proposed by Guo et al. (2012) causing the negative $\delta^{13}C$ excursion at the Gaojiashan section cannot entirely be excluded. The rapid shift of the negative $\delta^{13}C$ peak near a lithological contact may indicate a semi-restricted basin setting with intermittent water exchange for which the Black Sea and the Baltic Sea serve as modern analogues. Restricted access to the open ocean would have limited water circulation within the isolated basin. The consequent emerging stratification of water masses would have generated anoxic water masses similar to those described above and resulted in similar isotopic patterns. Nevertheless, the approximately simultaneous evolution, distribution and extinction of the global genus *Cloudina* argues against a restricted environment at least during the positive $\delta^{13}C$ excursion. Whether the negative $\delta^{13}C$ excursion documented in the arkose of the upper part of the Gaojiashan Member is associated with a terminal Ediacaran interval of increased erosion or even a glaciation (the so-called Baykonurian glaciation; Chumakov, 2009; Chumakov, 2011) is speculative. We consider the first theory (global anoxia model) most plausible.

The Gaojiashan section is the first section in Shaanxi Province to record high-resolution stable isotope analyses directly associated with well-documented terminal Ediacaran biozones. Pending confirmation, this is the first isotopic dataset reporting the Pc-C boundary interval in southern Shaanxi Province.

5.7 Conclusion

Chemostratigraphy is a powerful correlation tool to address the uncertain and highly variable litho- and biostratigraphical correlation of late Ediacaran strata at the northern margin of the South China platform. New high-resolution C- and O-isotopic data as well as TOC concentrations of shallow-water deposits at Gaojiashan section in combination with the detailed paleontological record (Weber et al., 2007; Guo et al., 2012; Meyer et al., 2012; Cai et al., 2013) allowed to correlate and reconstruct late Ediacaran paleoenvironmental conditions of the northern Yangtze platform. The identification of a large negative $\delta^{13}C$ excursion (NE2 to -6‰) in the upper Gaojiashan Member (Dengying Formation) together with the directly preceding extinction of *Cloudina* strongly argues for the Pc-C boundary near the top of the Gaojiashan Member. The overlying Beiwan Member of the Dengying Formation would thus be of lowermost Cambrian age. Gaojiashan data can be readily correlated to other Pc-C boundary sections on the Yangtze platform and also globally. Paleoenvironmental implications agree favorably with a global anoxia model suggesting upwelling of anoxic water masses to have dramatically affected the biosphere during the Pc-C transition interval (Cremonese et al., 2014). $^{87}Sr/^{86}Sr$ data (Ohnemueller et al., 2013) correlative with negative $\delta^{13}C$ excursion data could represent late Ediacaran local perturbations of the carbon cycle or be associated with a terminal Ediacaran glaciation.

5.8 Acknowledgments

We thank Quentin Scouflaire, Bernd Weber (Freie Universität Berlin), Simone Kasemann (Universität Bremen) and colleagues of the Forschergruppe 736 for valuable consultations and for providing the samples. We thank Ewgenjia Kuhl, Maria Diedrich, Yannik Steinmann and Hans-Rudolf Knöfler for aid with sample preparation (all Museum für Natkurkunde Berlin). The study was funded by the German Research Foundation (DFG-FOR 736). Field work was supported by the Natural Science Foundation of South China (NSFC).

5.9 References

Amthor, J. E., Grotzinger, J. P., Schröder, S., Bowring, S. A., Ramezani, J., Martin, M. W., and Matter, A., 2003, Extinction of Cloudina and Namacalathus at the Precambrian-Cambrian boundary in Oman: Geology, v. 31, p. 431-434.

Bau, M., and Dulski, P., 1996, Distribution of yttrium and rare-earth elements in the Penge and Kuruman iron-formations, Transvaal Supergroup, South Africa: Precambrian Research, v. 79, no. 1–2, p. 37-55.

Boggiani, P. C., Gaucher, C., Sial, A. N., Babinski, M., Simon, C. M., Riccomini, C., Ferreira, V. P., and Fairchild, T. R., 2010, Chemostratigraphy of the Tamengo Formation (Corumbá Group, Brazil): A contribution to the calibration of the Ediacaran carbon-isotope curve: Precambrian Research, v. 182, no. 4, p. 382-401.

Brasier, M. D., Rozanov, A. Y., Zhuravlev, A. Y., Corfield, R. M., and Derry, L. A., 1994, A carbon-isotope reference scale for the Lower Cambrian succession in Siberia - Report of IGCP project-303: Geological Magazine, v. 131, no. 6, p. 767-783.

Brasier, M. D., Shields, G., Kuleshov, V. N., and Zhegallo, E. A., 1996, Integrated chemo- and biostratigraphic calibration of early animal evolution: Neoproterozoic-early Cambrian of southwest Mongolia: Geological Magazine, v. 133, no. 4, p. 445-485.

Cai, Y., Hua, H., Schiffbauer, J. D., Sun, B., and Yuan, X., 2014, Tube growth patterns and microbial mat-related lifestyles in the Ediacaran fossil Cloudina, Gaojiashan Lagerstätte, South China: Gondwana Research, v. 25, no. 3, p. 1008-1018.

Cai, Y., Hua, H., Xiao, S., Schiffbauer, J. D., and Li, P., 2010, Biostratinomy of the late Ediacaran pyritized Gaojiashan Lagerstätte from Southern Shaanxi, South China: Importance of event deposits: Palaios, v. 25, no. 8, p. 487-506.

Cai, Y., Hua, H., and Zhang, X., 2013, Tube construction and life mode of the late Ediacaran tubular fossil Gaojiashania cyclus from the Gaojiashan Lagerstätte: Precambrian Research, v. 224, no. 0, p. 255-267.

Cai, Y., Schiffbauer, J. D., Hua, H., and Xiao, S., 2011, Morphology and paleoecology of the late Ediacaran tubular fossil Conotubus hemiannulatus from the Gaojiashan Lagerstätte of southern Shaanxi Province, South China: Precambrian Research, v. 191, no. 1–2, p. 46-57.

Cai, Y., Schiffbauer, J. D., Hua, H., and Xiao, S., 2012, Preservational modes in the Ediacaran Gaojiashan Lagerstatte: Pyritization, aluminosilicification, and carbonaceous compression: Palaeogeography Palaeoclimatology Palaeoecology, v. 326, p. 109-117.

Chumakov, N. M., 2009, The Baykonurian Glaciohorizon of the Late Vendian: Stratigraphy and Geological Correlation, v. 17, no. 4, p. 373-381.

Chumakov, N. M., 2011, Glacial deposits of the Baykonur Formation, Kazakhstan and Kyrgyzstan: Geological Society, London, Memoirs, v. 36, no. 1, p. 303-307.

Condon, D., Zhu, M., Bowring, S., Wang, W., Yang, A., and Jin, Y., 2005, U-Pb Ages from the Neoproterozoic Doushantuo Formation, China: Science, v. 308, no. 5718, p. 95-98.

Corsetti, F. A., and Kaufman, A. J., 2003, Stratigraphic investigations of carbon isotope anomalies and Neoproterozoic ice ages in Death Valley, California: Geological Society of America Bulletin, v. 115, no. 8, p. 916-932.

Cremonese, L., Shields-Zhou, G., Struck, U., Ling, H.-F., Och, L., Chen, X., and Li, D., 2013, Marine biogeochemical cycling during the early Cambrian constrained by a nitrogen and organic carbon isotope study of the Xiaotan section, South China: Precambrian Research, v. 225, no. 0, p. 148-165.

Cremonese, L., Shields-Zhou, G. A., Struck, U., Ling, H.-F., and Och, L. M., 2014, Nitrogen and organic carbon isotope stratigraphy of the Yangtze Platform during the Ediacaran–Cambrian transition in South China: Palaeogeography, Palaeoclimatology, Palaeoecology, v. 398, no. 0, p. 165-186.

Derry, L. A., 2010, A burial diagenesis origin for the Ediacaran Shuram–Wonoka carbon isotope anomaly: Earth and Planetary Science Letters, v. 294, no. 1–2, p. 152-162.

Dulski, P., 1994, Interferences of oxide, hydroxide and chloride analyte species in the determination of rare-earth elements in geological samples by inductively-coupled plasma-mass spectrometry: Fresenius Journal of Analytical Chemistry, v. 350, no. 4-5, p. 194-203.

Fike, D. A., Grotzinger, J. P., Pratt, L. M., and Summons, R. E., 2006, Oxidation of the Ediacaran Ocean: Nature, v. 444, no. 7120, p. 744-747.

German, C. R., Holliday, B. P., and Elderfield, H., 1991, Redox cycling of rare-earth elements in the suboxic zone of the black-sea: Geochimica et Cosmochimica Acta, v. 55, no. 12, p. 3553-3558.

Germs, G. J., 1972, New shelly fossils from the Nama Group, South-West Africa: American Journal of Science, v. 272, p. 752–761.

Goldberg, T., Strauss, H., Guo, Q., and Liu, C., 2007, Reconstructing marine redox conditions for the Early Cambrian Yangtze Platform: Evidence from biogenic sulphur and organic carbon isotopes: Palaeogeography, Palaeoclimatology, Palaeoecology, v. 254, no. 1–2, p. 175-193.

Grotzinger, J. P., Watters, W., and Knoll, A. H., 2000, Calcareous metazoans in thrombolitic bioherms of the terminal Proterozoic Nama Group, Namibia: Paleobiology, v. 26, p. 334–359.

Guo, Q., Deng, Y., and Yang, X., 2012, Carbon Isotopic Evolution of the Late Ediacaran Gaojiashan Biota on the Northern Yangtze Platform, South China: Acta Geologica Sinica-English Edition, v. 86, no. 6, p. 1447-1454.

Guo, Q., Strauss, H., Liu, C., Goldberg, T., Zhu, M., Pi, D., Heubeck, C., Vernhet, E., Yang, X., and Fu, P., 2007, Carbon isotopic evolution of the terminal Neoproterozoic and early Cambrian: Evidence from the Yangtze Platform, South China: Palaeogeography, Palaeoclimatology, Palaeoecology, v. 254, no. 1–2, p. 140-157.

Halverson, G. P., Dudas, F. O., Maloof, A. C., and Bowring, S. A., 2007, Evolution of the $^{87}Sr/^{86}Sr$ composition of Neoproterozoic seawater: Palaeogeography Palaeoclimatology Palaeoecology, v. 256, no. 3-4, p. 103-129.

Hofmann, H. J., and Mointjoy, E. W., 2001, Namacalathus-Cloudina assemblage in Neoproterozoic Miette Group (Byng Formation), British Columbia: Canada's oldest shelly fossils: Geology, v. 29, no. 12, p. 1091-1094.

Hohl, S., Becker, H., Herzlieb, S., and Guo, Q., in prep., Multiproxy constraints on alteration and primary compositions of Ediacaran deep-water carbonate rocks, Yangtze Platform, South China.

Hua, H., Chen, Z., and Yuan, X., 2007, The advent of mineralized skeletons in Neoproterozoic Metazoa - new fossil evidence from the Gaojiashan Fauna: Geological Journal, v. 42, p. 263–279.

Hua, H., Chen, Z., Yuan, X., Zhang, L., and Xiao, S., 2005, Skeletogenesis and asexual reproduction in the earliest biomineralizing animal Cloudina: Geology, v. 33, no. 4, p. 277-280.

Hua, H., Pratt, B. R., and Lu-Yi, Z., 2003, Borings in Cloudina Shells: Complex Predator-Prey Dynamics in the Terminal Neoproterozoic: Palaios, v. 18, p. 454-459.

Hua, H., Zhang, L.-Y., Zhang, Z.-F., and Wang, J.-P., 2001, Assemblage zones of Gaojiashan Biota and their characteristics: Journal of Stratigraphy, v. 25, no. 1, p. 13-17.

Ishikawa, T., Ueno, Y., Komiya, T., Sawaki, Y., Han, J., Shu, D., Li, Y., Maruyama, S., and Yoshida, N., 2008, Carbon isotope chemostratigraphy of a Precambrian/Cambrian boundary section in the Three Gorge area, South China: Prominent global-scale isotope excursions just before the Cambrian Explosion: Gondwana Research, v. 14, no. 1–2, p. 193-208.

Ishikawa, T., Ueno, Y., Shu, D., Li, Y., Han, J., Guo, J., Yoshida, N., and Komiya, T., 2013, Irreversible change of the oceanic carbon cycle in the earliest Cambrian: High-resolution organic and inorganic carbon chemostratigraphy in the Three Gorges area, South China: Precambrian Research, v. 225, no. 0, p. 190-208.

Jiang, G., Kaufmann, A. J., Christie-Blick, N., Zhang, S., and Wu, H., 2007, Carbon isotope variability across the Ediacaran Yangtze platform in South China: Implications for a large surface-to-deep ocean $\delta^{13}C$ gradient: Earth and Planetary Science Letters, v. 261, p. 303-320.

Kaufman, A. J., Corsetti, F. A., and Varni, M. A., 2007, The effect of rising atmospheric oxygen on carbon and sulfur isotope anomalies in the Neoproterozoic Johnnie Formation, Death Valley, USA: Chemical Geology, v. 237, no. 1-2, p. 47-63.

Kaufman, A. J., Jiang, G., Christie-Blick, N., Banerjee, D. M., and Rai, V., 2006, Stable isotope record of the terminal Neoproterozoic Krol platform in the Lesser Himalayas of northern India: Precambrian Research, v. 147, no. 1-2, p. 156-185.

Kaufman, A. J., and Knoll, A. H., 1995, Neoproterozoic variations in the C-isotopic composition of seawater: stratigraphic and biogeochemical implications: Precambrian Research, v. 73, no. 1–4, p. 27-49.

Knauth, L. P., and Kennedy, M. J., 2009, The late Precambrian greening of the Earth: Nature, v. 460, no. 7256, p. 728-732.

Kontorovich, A. E., Varlamov, A. I., Grazhdankin, D. V., Karlova, G. A., Klets, A. G., Kontorovich, V. A., Saraev, S. V., Terleev, A. A., Belyaev, S. Y., Varaksina, I. V., Efimov, A. S., Kochnev, B. B., Nagovitsin, K. E., Postnikov, A. A., and Filippov, Y. F., 2008, A section of Vendian in the east of West Siberian Plate (based on data from the Borehole Vostok 3): Russian Geology and Geophysics, v. 49, no. 12, p. 932-939.

Lawrence, M. G., and Kamber, B. S., 2006, The behaviour of the rare earth elements during estuarine mixing-revisited: Marine Chemistry, v. 100, no. 1–2, p. 147-161.

Li, D., Ling, H.-F., Jiang, S.-Y., Pan, J.-Y., Chen, Y.-Q., Cai, Y.-F., and Feng, H.-Z., 2009, New carbon isotope stratigraphy of the Ediacaran–Cambrian boundary interval from SW China: implications for global correlation: Geol. Mag., v. 146, no. 4, p. 465-484.

Li, D., Ling, H.-F., Shields-Zhou, G. A., Chen, X., Cremonese, L., Och, L., Thirlwall, M., and Manning, C. J., 2013, Carbon and strontium isotope evolution of seawater across the Ediacaran–Cambrian transition: Evidence from the Xiaotan section, NE Yunnan, South China: Precambrian Research, v. 225, no. 0, p. 128-147.

Ling, H.-F., Chen, X., Li, D., Wang, D., Shields-Zhou, G. A., and Zhu, M., 2013, Cerium anomaly variations in Ediacaran–earliest Cambrian carbonates from the Yangtze Gorges area, South China: Implications for oxygenation of coeval shallow seawater: Precambrian Research, v. 225, no. 0, p. 110-127.

Macouin, M., Ader, M., Moreau, M.-G., Poitou, C., Yang, Z., and Sun, Z., 2012, Deciphering the impact of diagenesis overprint on negative $\delta^{13}C$ excursions using rock magnetism: Case study of Ediacaran carbonates, Yangjiaping section, South China: Earth and Planetary Science Letters, v. 351–352, no. 0, p. 281-294.

Mazumdar, A., Banerjee, D. M., Schidlowski, M., and Balaram, V., 1999, Rare-earth elements and stable isotope geochemistry of early Cambrian chert-phosphorite assemblages from the Lower Tal formation of the Krol Belt (Lesser Himalaya, India): Chemical Geology, v. 156, no. 1-4, p. 275-297.

McFadden, K. A., Huang, J., Chu, X., Jiang, G., Kaufmann, A. J., Zhou, C., Yuan, X., and Xiao, S., 2008, Pulsed oxidation and biological evolution in the Ediacaran Doushantuo Formation: PNAS, v. 105, no. 9, p. 3197-3202.

McLennan, S. M., 1989, Rare earth elements in sedimentary rocks: Influence of provenance and sedimentary processes: Geochemistry and Mineralogy of Rare Earth Elements, v. 21, p. 169-200.

Meyer, M., Schiffbauer, J. D., Xiao, S., Cai, Y., and Hua, H., 2012, Taphonomy of the upper Ediacaran enigmatic ribbonlike fossil Shaanxilithes: Palaios, v. 27, no. 5-6, p. 354-372.

Narbonne, G. M., Kaufman, A. J., and Knoll, A. H., 1994, Integrated chemostratigraphy and biostratigraphy of the Windermere Supergroup, northwestern Canada - Implications for Neoproterozoic correlations and the early evolution of animals: Geological Society of America Bulletin, v. 106, no. 10, p. 1281-1292.

Narbonne, G. M., Myrow, P. M., Landing, E., and Anderson, M. M., 1987, A candidate Stratotype for the Precambrian-Cambrian boundary, Fortune Head, Burin Peninsula, southeastern Newfoundland: Journal of Earth Sciences, v. 24, p. 1277-1293.

Och, L. M., Shields-Zhou, G. A., Poulton, S. W., Manning, C., Thirlwall, M. F., Li, D., Chen, X., Ling, H., Osborn, T., and Cremonese, L., 2013, Redox changes in Early Cambrian black shales at Xiaotan section, Yunnan Province, South China: Precambrian Research, v. 225, no. 0, p. 166-189.

Ohnemueller, F., Meixner, A., Gamper, A., and Kasemann, S. A., 2013, Ocean-pH Evolution and Weathering Conditions during the Ediacaran: Insights from B, Sr & Li Isotopes at the Gaojiashan Section, South China: Mineralogical Magazine, v. 77, no. 5, p. 1881.

Sawaki, Y., Tahata, M., Ohno, T., Komiya, T., Hirata, T., Maruyama, S., Han, J., and Shu, D., 2014, The anomalous Ca cycle in the Ediacaran ocean: Evidence from Ca isotopes preserved in carbonates in the Three Gorges area, South China: Gondwana Research, v. 25, no. 3, p. 1070-1089.

Shields-Zhou, G., and Zhu, M., 2013, Biogeochemical changes across the Ediacaran–Cambrian transition in South China: Precambrian Research, v. 225, no. 0, p. 1-6.

Shields, G. A., 2007, A normalised seawater strontium isotope curve: possible implications for Neoproterozoic-Cambrian weathering rates and the further oxygenation of the Earth: eEarth, v. 2, no. 2, p. 35-42.

Steiner, M., Li, G., Qian, Y., and Zhu, M., 2004, Lower Cambrian Small Shelly Fossils of northern Sichuan and southern Shaanxi (China), and their biostratigraphic importance: Geobios, v. 37, no. 2, p. 259-275.

Verdel, C., Wernicke, B. P., and Bowring, S. A., 2011, The Shuram and subsequent Ediacaran carbon isotope excursions from southwest Laurentia, and implications for environmental stability during the metazoan radiation: Geological Society of America Bulletin, v. 123, no. 7-8, p. 1539-1559.

Vernhet, E., Heubeck, C., Zhu, M.-Y., and Zhang, J.-M., 2007, Stratigraphic reconstruction of the Ediacaran Yangtze Platform margin (Hunan Province, China) using a large olistolith: Palaeogeography, Palaeoclimatology, Palaeoecology, v. 254, p. 123-139.

Wang, J., Chen, D., Yan, D., Wei, H., and Xiang, L., 2012a, Evolution from an anoxic to oxic deep ocean during the Ediacaran–Cambrian transition and implications for bioradiation: Chemical Geology, v. 306–307, no. 0, p. 129-138.

Wang, W., Zhou, C., Yuan, X., Chen, Z., and Xiao, S., 2012b, A pronounced negative $\delta^{13}C$ excursion in an Ediacaran succession of western Yangtze Platform: A possible equivalent to the Shuram event and its implication for chemostratigraphic correlation in South China: Gondwana Research, v. 22, no. 3–4, p. 1091-1101.

Warren, L. V., Fairchild, T. R., Gaucher, C., Boggiani, P. C., Poiré, D. G., Anelli, L. E., and Inchausti, J. C. G., 2011, Corumbella and in situ Cloudina in association with thrombolites in the Ediacaran Itapucumi Group, Paraguay: Terra Nova, v. 23, no. 6, p. 382-389.

Weber, B., Steiner, M., and Zhu, M.-Y., 2007, Precambrian–Cambrian trace fossils from the Yangtze Platform (South China) and the early evolution of bilaterian lifestyles: Palaeogeography, Palaeoclimatology, Palaeoecology, v. 254, no. 1-2, p. 328-349.

Wille, M., Nagler, T. F., Lehmann, B., Schroder, S., and Kramers, J. D., 2008, Hydrogen sulphide release to surface waters at the Precambrian/Cambrian boundary: Nature, v. 453, no. 7196, p. 767-769.

Wood, R. A., 2011, Paleoecology of the earliest skeletal metazoan communities: Implications for early biomineralization: Earth-Science Reviews, v. 106, no. 1–2, p. 184-190.

Yang, J., Sun, W., Wang, Z., Xue, Y., and Tao, X., 1999, Variations in Sr and C isotopes and Ce anomalies in successions from China: evidence for the oxygenation of Neoproterozoic seawater?: Precambrian Research, v. 93, no. 2-3, p. 215-233.

Yeghicheyan, D., Carignan, J., Valladon, M., Bouhnik Le Coz, M., Samuel, J., BenBakkar, M., Bruguier, O., Keller, F., Pin, C., Pourtales, S., Hénin, O., Macé, J., Morin, N., Guilmette, C., and Marin, L., 2003, The new carbonate reference material Cal–S: preliminary results: Abs. Geoanal., p. 146.

Zhou, C., and Xiao, S., 2007, Ediacaran $\delta^{13}C$ chemostratigraphy of South China: Chemical Geology, v. 327, p. 89-108.

Zhu, M., Zhang, J., Steiner, M., Yang, A., Li, G., and Erdtmann, B. D., 2003, Sinian-Cambrian stratigraphic framework for shallow- to deep-water environments of the Yangtze Platform: an integrated approach: Progress in Natural Science, v. 13, no. 12, p. 951-960.

Zhu, M., Zhang, J., and Yang, A., 2007, Integrated Ediacaran (Sinian) chronostratigraphy of South China: Palaeogeography, palaeoclimatology, Palaeoecology, v. 254, p. 7-61.

6. CARBON AND NITROGEN ISOTOPE BIOGEOCHEMISTRY OF THE UPPER DENGYING FORMATION IN SOUTH CHINA: IMPLICATIONS FOR THE LATE EDIACARAN SHALLOW-MARINE ECOSPHERE AND OCEANIC REDOX CONDITIONS

6.1 Abstract

Late Neoproterozoic (Ediacaran) siliciclastic-calcareous shallow-water strata of southern Shaanxi Province (South China) at the northern margin of the South China platform contain three biozones: *Shaanxilithes ningqiangensis*, *Gaojiashania* and *Cloudina*. In order to constrain and support biostratigraphic data and to provide insights into the paleoenvironment of the late Dengying (latest Ediacaran) ecosystem, we studied nitrogen and organic carbon isotopic compositions of the Gaojiashan section. Our results suggest that biogeochemical cycles at the northern margin of the Ediacaran Yangtze platform were influenced by both local and global marine perturbations. A constant moderate nutrient supply from coastal regions to a deltaic depositional system may have triggered eutrophication of surface water and thus assisted in the creation of ecological niches (and possibly the evolution of new fauna elements) predating the Precambrian-Cambrian boundary. $\delta^{13}C_{org}$ data (~-30‰) associated with the occurrence of the global index fossil *Cloudina* indicate that the surface environment at the northern late Ediacaran Yangtze platform had a constant exchange with the open ocean. Continually rising $\delta^{15}N$ compositions (from 1 to ~5‰) may suggest a close association of biological innovations to changing nutrient conditions and indicate rising marine oxygen and nitrate concentrations during the evolution of late Ediacaran biota. Thereby, diazotrophic organisms were eventually outweighed by nitrate-assimilating primary producers in bio-productive surface layers hinting towards intensified nitrification-denitrification interactions during remineralization. Co-occurring with a global regression, the uprising of oxygen-depleted ^{12}C-enriched water masses to the surface is mirrored by a pronounced coupled $\delta^{13}C_{org}$ and $\delta^{13}C_{carb}$ negative excursion, most likely representing the Precambrian-Cambrian boundary event.

Keywords: Ediacaran, Pc-C boundary, Dengying Formation, South China, nitrogen isotopes, organic carbon isotopes, eutrophication, shallow-water anoxia

Highlights:

We present $\delta^{15}N$ and $\delta^{13}C_{org}$ data from late Ediacaran strata of South China.

Data suggest mildly oxygenated surface-water conditions during the middle and upper Gaojiashan Member.

A transition from N_2-fixation to NO_3^- based primary production adjusted in the upper Dengying Formation.

Eutrophication led to elevated remineralization, O_2-minimum zones and intense nitrification-denitrification interactions.

The uppermost Gaojiashan Member is associated with an oceanic anoxic overturn mirrored by a negative $\delta^{13}C_{carb}$ and $\delta^{13}C_{org}$ excursion.

6.2 Introduction

The late Neoproterozoic - Cambrian transitional period (~542 Ma) marks one of the most significant epochs in the evolution and radiation of skeletonized metazoans in Earth's history. It comprises the disappearance of the "Ediacaran biota" followed by the evolution of almost all precursors of today's animal phyla. The evolution of metazoans is accompanied by substantial reorganizations in marine biogeochemical cycles (e.g. Johnston et al., 2012b; Smith and Harper, 2013). Geochemical changes across the Precambrian-Cambrian (Pc-C) boundary event are expressed as systematical fluctuations of diverse isotopic proxies. The most prominent event displays a globally traceable carbonate carbon ($\delta^{13}C_{carb}$) anomaly used to correlate sections worldwide (Amthor et al., 2003; Jiang et al., 2007; Zhu et al., 2007; Ishikawa et al., 2008; Li et al., 2009; Ishikawa et al., 2013; Li et al., 2013). Scenarios affecting the simultaneous changes in biogeochemical cycles are of ongoing debate. One scenario triggering the $\delta^{13}C_{carb}$ excursion takes account of the release of methane hydrates from an anoxic, organic-carbon-rich ocean (Bjerrum and Canfield, 2011). Another widely applied theory involves a

water body stratification scenario with a deep-ocean anoxia and subsequent uprising of anoxic (and in part euxinic) water masses in the course of the global Pc-C transgression to have affected biogeochemical events (Kimura and Watanabe, 2001; Jiang et al., 2007; Wille et al., 2008; Wang et al., 2012). It has been shown that Rare Earth Element (REE+Y) signals in non-skeletal marine carbonates of modern and ancient seawater can preserve the composition of coeval seawater (Banner, 1988) and that cerium anomalies may be suitable as a proxy for paleo-oxygenation (Ling et al., 2013). Cerium is similar to other REEs trivalent (with exception to Eu which can be reduced to Eu^{2+}) but will be oxidized to a tetravalent state under oxic conditions in the water (e.g. Elderfield et al., 1988). Because of the preferential scavenging of $Ce^{4+}O_2$ onto Mn and Fe oxides and hydroxides, oxidized water bodies (and their precipitation products) will be depleted in Ce relative to post-Archean Australian Shale (PAAS) normalized REE abundances (Elderfield et al., 1988; Byrne and Kim, 1990; Alibo and Nozaki, 1999) and thus bear negative Ce/Ce* anomalies. In this regard, REE studies showed that carbonate leachates of late Ediacaran shallow-water strata and even deep-water strata of the Ediacaran Doushantuo Formation on the Yangtze platform reveal negative Ce/Ce* anomalies and most likely record sediment deposition under oxic conditions (Ling et al., 2013; Hohl et al., in prep.).

Furthermore, isotope analyses of biogenic elements like nitrogen ($\delta^{15}N$) and organic carbon ($\delta^{13}C_{org}$) are used as reliable paleoenvironmental indicators which complement further geochemical studies and contribute substantial information about the paleoecological framework (Kikumoto et al., 2014). Both isotopic systems document changes in nutrient availability as well as fluctuations in the oxygenation state of the seawater and provide information about the relative movement of the chemocline as well as the expansion of the oxygen minimum zone (Cremonese et al., 2013; Kikumoto et al., 2014). However, despite the reliability of nitrogen isotopes as a redox proxy (Robinson et al., 2012), $\delta^{15}N$ studies across the Pc-C boundary interval are rarely reported in literature; most available datasets are either of low resolution or predominantly comprise early Cambrian strata (Cremonese et al., 2013; Cremonese et al., 2014; Kikumoto et al., 2014; Spangenberg et al., 2014). Although the period immediately preceding

the "Cambrian explosion" records fundamental biogeochemical changes (e.g. strong perturbations of carbon cycling, evolution of bilaterian lifestyle; Shields-Zhou and Zhu, 2013) the Late Ediacaran remains geochemically poorly investigated especially in strata of southern Shaanxi Province (South China) where three excellently preserved biota were recorded. Therefore, we studied $\delta^{15}N$ and $\delta^{13}C_{org}$ isotope compositions of late Ediacaran carbonate-siliciclastic shallow-marine sediments from the northern part of the Yangtze platform (South China) at Gaojiashan section (Fig. 13) and support this dataset by REE analyses of three selected samples. Our study first combines high-resolution isotope data of biogenic elements with well-documented paleontological data for the first time (Hua et al., 2005; Hua et al., 2007; Weber et al., 2007; Cai et al., 2010; Cai et al., 2011; Cai et al., 2012; Guo et al., 2012; Meyer et al., 2012; Cai et al., 2013; Cai et al., 2014) and thus provides insights into the late Ediacaran shallow-marine ecosystem and its geochemical evolution.

6.3 Carbon and nitrogen isotopes as a paleoenvironmental proxy

Sedimentary organic carbon and nitrogen isotope compositions document profound changes of the marine biogeochemical cycle with nitrogen displaying a limiting factor for bioproductivity (Falkowski, 1997). It is widely acknowledged that both isotope proxies are largely resistant to post-depositional alteration effects and therefore find wide appliance in geochemistry (Farrell et al., 1995; Altabet, 2007; Ader et al., 2009; Cremonese et al., 2013; Ishikawa et al., 2013; Ader et al., 2014). $\delta^{13}C_{org}$ isotopic records document the rate of bioproductivity in surface waters, the effectiveness of the biological pump and the supply of inorganic carbon (Werne and Hollander, 2004). In turn, the nitrogen isotopic composition reflects shifts in the consumption of nutrient species among microorganisms and the composition of the assimilated nitrogen source (Altabet and Francois, 1994). In detail, the uptake of dissolved inorganic carbon (DIC) species by marine phytoplankton in modern oxygenated oceans typically results in $\delta^{13}C_{org}$ values ranging from in average -25 to -20‰ (Westerhausen et al., 1993) but can be up to ~-28‰ in redox-stratified marine environments depending on the isotopic composition of the used DIC source (Abrajano et al., 2002). In

contrast, the nitrogen cycle is far more complex. The dominant source of available nitrogen for the biosphere of modern oceans is nitrate (NO_3^-) which re-enters surface waters from deeper oceanic regions with initial $\delta^{15}N$ values of 5 to 6‰ (Sigman et al., 2000). Primary producers assimilate NO_3^- and therefore provide nitrogen compounds for the biological cycle. Subsequently, the particulate organic matter stored in the sediment is based on the $\delta^{15}N$ of the nitrogenous source and the isotopic fractionation during nitrogen uptake by phytoplankton (Farrell et al., 1995). $\delta^{15}N$ values of the sediment then mirror the relative NO_3^- consumption from near-surface water environments. The isotopic composition of dissolved deep-water NO_3^- is in turn controlled by water column denitrification working in a dys- to anoxic water body. Denitrifying bacteria enrich the remaining nitrate pool in ^{15}N leading to sedimentary $\delta^{15}N$ values of 8 to 12‰ (Cline and Kaplan, 1975; Struck, 2012). If NO_3^- is depleted, dinitrogen (N_2) can become a significant nitrogen source for cyanobacterial primary productivity. During the process called N_2-fixation diazotrophic organisms fix atmospheric N_2 ($\delta^{15}N_{air}$ = 0‰ per definition) initiating low $\delta^{15}N$ values around 0‰ of the respective organic sedimentary matter due to low isotopic fractionation (Carpenter et al., 1997; Montoya et al., 2002; Struck, 2012). Taken together, the sedimentary $\delta^{15}N$ value reproduces the fluctuating dominance of various processes within the nitrogen cycle and not the absence or exclusive occurrence of them (Struck, 2012). Therefore, nitrogen isotopes represent a trustful paleoenvironmental proxy documenting nutrient regimes and oxygenation states throughout the water column.

6.4 Geological setting - regional stratigraphy

Siliciclastic-calcareous strata of the upper Ediacaran Dengying Formation (551 - 542 Ma) crop out at the northern passive margin of the Neoproterozoic Yangtze platform in South China (Fig. 13). The studied Gaojiashan section is located in Ningqiang County, southern Shaanxi Province, and represents a marine shallow-water to coastal environment with significant siliciclastic input (Weber et al., 2007) which is unique for the thick, carbonate-dominated Dengying Formation. The stratigraphic record consists (in ascending order) of the Algal Dolomite Member, the Gaojiashan Member and the Beiwan Member of the Dengying Formation. Whereas the basal Algal Dolomite Member comprises mostly dolostones, the ~60 m thick Gaojiashan Member is dominated by interlayers of doloshales, dolomitic sandstones and biolaminated calcarenites which are in turn overlain by dolostones of the early Cambrian Beiwan Member. The litho- and chemostratigraphic framework at Gaojiashan section is reported and discussed in chapter 5.

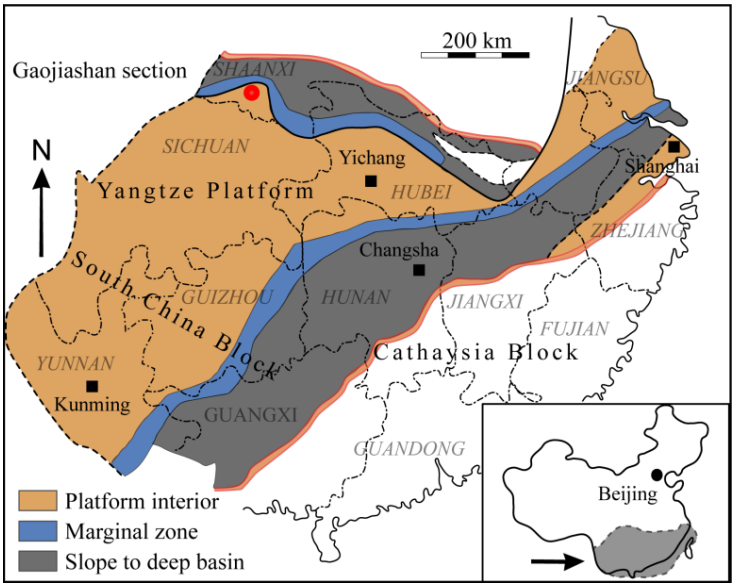

Figure 13: Sketch map of the Ediacaran Yangtze platform adapted from Guo et al. (2007) and Cremonese et al. (2013). The red circle marks the outcrop location of the Gaojiashan section in southern Shaanxi Province (Ningqiang area).

Three late Ediacaran fauna have been described at the Gaojiashan section and in close vicinity: *Shaanxilithes ningqiangensis*, *Gaojiashania* ("Gaojiashan biota") and *Cloudina* (e.g. Hua et al., 2007; Weber et al., 2007; Guo et al., 2012; Meyer et al., 2012; Cai et al., 2014). *Shaanxilithes ningqiangensis* was formerly interpreted as a collapsed trail or burrow of an epi- or infaunal living organism (Hua et al., 2001) and was recently reinterpreted to represent a cylindrical tube body fossil of a soft-bodied epibenthic organism (Meyer et al., 2012). The Gaojiashan biota represents slightly skeletonized organisms with an epibenthic lifestyle (Hua et al., 2005; Weber et al., 2007; Cai et al., 2012). The most prominent fossil assemblage of the late Ediacaran, *Cloudina*, represents the earliest biomineralizing organisms with a sessile epibenthic lifestyle attached to microbial-covered carbonate substrates in a shallow-water marine environment (Warren et al., 2011; Cai et al., 2014). Whereas the Gaojiashan biota is solely regionally distributed on the South China Yangtze platform (Hua et al., 2004; Weber et al., 2007; Cai et al., 2010; but see Zhuravlev et al., 2009 for disputed counter-example), *Shaanxilithes ningqiangensis* is also found on the North China block (Shen et al., 2007). In contrast, *Cloudina* serves as a global index fossil allowing a correlation of late Ediacaran strata of e.g. Oman (Amthor et al., 2003), Namibia (Germs, 1972), South China (Hua et al., 2005; Zhu et al., 2007; Shields-Zhou and Zhu, 2013) and Brazil (Boggiani et al., 2010; Spangenberg et al., 2014).

6.5 Analytical methods and materials

The sample suite of 123 samples from the Gaojiashan section (~96 m) comprises the middle to upper Dengying Formation (Ediacaran) and the lower Cambrian of Shaanxi Province, Ningqiang area, South China (Fig. 13). Investigated samples match with those reported in chapter 5.

Stable isotope ratios and concentration measurements of nitrogen ($^{15}N/^{14}N$) and organic carbon ($^{13}C_{org}/^{12}C_{org}$) by elemental analyzer - isotope ratio mass spectrometry (EA-IRMS) were determined using a Thermo/Finnigan MAT V isotope ratio mass spectrometer coupled to a Thermo Flash EA 1112 elemental analyzer via a Thermo/Finnigan Conflo III-interface at the Museum für

Naturkunde Berlin. $\delta^{15}N$ analyses were performed on the bulk rock sample powder, whereas for $\delta^{13}C_{org}$ measurements sample powders were decalcified using 2 M hydrochloric acid (HCl). Isotope ratios are expressed in the conventional delta notation ($\delta^{15}N$; $\delta^{13}C_{org}$) relative to AIR and VPDB (Vienna PeeDee Belemnite) standard, respectively. Standard deviation (σ) for repeated measurements of laboratory standard material (peptone) is generally better than 0.2‰. To avoid interferences between bulk rock nitrogen and carbon isotope signals, carbon dioxide (CO_2) was filtered out using a CO_2-trap after sample combustion but prior to isotopic measurement. We measured each sample (150 - 200 mg sample weight) with a detection length of 1000 s and two blank measurements after each sample to improve reproducibility of data. For $\delta^{13}C_{org}$ we applied a He dilution of 60 - 90%. To calculate the internal reproducibility, standard material (peptone) is measured after every fourth sample. $\delta^{15}N$ and $\delta^{13}C_{org}$ values of samples with a nitrogen and organic carbon content <0.01 mg are omitted from our interpretation due to low accuracy of signals.

Trace element analyses (phosphorus and sulfur) of 22 carbonate samples were conducted on an Agilent Technologies 700 Series ICP-OES at the inorganic geochemistry group of the Universität Bremen/MARUM, Germany. Prior to trace element concentration measurements, ~40 mg of sample material (powder) was dissolved in 2 ml 0.5 M HCl for 48 h inside a pre-cleaned Eppendorf Safe-Lock PTR vial and centrifuged afterwards. 1 ml of the solution was transferred into 5 ml centrifuge vials and diluted with additional 2 ml 0.5 M HCl. Subsequently, the solution was diluted again by a dilution factor of 3, 30 and 300 to get as accurate results as possible. The reference material was also diluted by a factor of 2, 10, and 20. This procedure allows for a very precise data evaluation. Three replicates of each dilution/concentration were measured and showed in general a relative standard deviation of better than 3%.

6.6 Results

Isotopic compositions of organic carbon and nitrogen as well as total nitrogen (TN) and trace element concentration are summarized in Table 6.

Table 6: Isotopic dataset ($\delta^{13}C_{org}$, $\delta^{15}N$), total nitrogen concentration (TN) and trace element concentration of phosphorus and sulfur of the upper Algal Dolomite Member, Gaojiashan Member and Beiwan Member at Gaojiashan section. $\delta^{13}C_{org}$ and $\delta^{15}N$ values of samples with concentrations below 0.01 mgC and 0.01 mgN have not been considered for interpretation due to insufficient data accuracy.

Sample	Distance [m]	$\delta^{13}C_{org}$ [‰] vs. VPDB	$\delta^{15}N$ [‰] vs. AIR	TN [%]	P [ppm]	S [ppm]
Gj -3.3	-3.3	-27.0	0.4	0.010	6720	306
Gj -3.0	-3.0	-26.0				
Gj -2.6	-2.6	-22.6				
Gj -2.0	-2.0	-24.8				
Gj -1.6	-1.6	-24.1				
Gj -1.3	-1.3	-27.6				
Gj -0.6	-0.6	-25.8				
Gj -0.3	-0.3	-28.0			46	26
Gj 2.3	2.3	-27.3			84	52
Gj 4.3	4.3		1.9	0.028		
Gj 6.0	6.0	-28.5	2.2	0.050		
Gj 6.5	6.5		1.8	0.025		
Gj 6.6	6.6		2.6	0.020		
Gj 7.0	7.0	-27.9	2.8	0.020		
Gj 7.3	7.3		2.6	0.023		
Gj 7.6	7.6		2.6	0.020		
Gj 8.0	8.0	-28.4	2.6	0.022		
Gj 8.3	8.3		2.2	0.021		
Gj 8.6	8.6	-23.9	1.7	0.007		
Gj 9.5	9.5	-24.2	2.4	0.006	137	180
Gj 10.3	10.3	-26.7	1.7	0.007		
Gj 10.6	10.6	-29.6			179	165
Gj 11.0	11.0	-25.7				
Gj 11.3	11.3		2.5	0.018		
Gj 12.0	12.0		2.8	0.007		
Gj 12.6	12.6	-30.5	2.4	0.011		
Gj 13.0	13.0	-33.9	3.1	0.008		
Gj 13.3	13.3	-32.8	3.3	0.006		
Gj 13.6	13.6	-31.4				
Gj 14.3	14.3	-33.5	3.1	0.011		
Gj 14.6	14.6		2.9	0.020		
Gj 15.0	15.0		3.0	0.011		

Table 6 (continued)

Sample	Distance [m]	$\delta^{13}C_{org}$ [‰] vs. VPDB	$\delta^{15}N$ [‰] vs. AIR	TN [%]	P [ppm]	S [ppm]
Gj 15.6	15.6	-32.1				
Gj 16.3	16.3	-33.7			8059	229
Gj 18.3	18.3	-28.0				
Gj 18.6	18.6	-32.9	1.4	0.005		
Gj 19.0	19.0	-30.6				
Gj 19.3	19.3	-30.7				
Gj 19.6	19.6	-32.2	1.9	0.007		
Gj 20.0	20.0	-27.8	3.0	0.006	433	169
Gj 20.3	20.3	-28.4				
Gj 20.6	20.6	-28.9				
Gj 21.0	21.0	-27.5				
Gj 21.3	21.3		3.0	0.006		
Gj 21.6	21.6	-32.3				
Gj 22.0	22.0	-28.4	3.6	0.007		
Gj 22.3	22.3	-28.9	3.2	0.006		
Gj 22.6	22.6	-26.8	2.7	0.006		
Gj 23 3	23.3	-28.8				
Gj 24.0	24.0	-30.5				
Gj 24.6	24.6	-28.1	3.0	0.007		
Gj 25.0	25.0	-27.6				
Gj 25.3	25.3	-29.8				
Gj 26.0	26.0	-29.4				
Gj 26.3	26.3	-30.3	3.8	0.005		
Gj 26.6	26.6	-32.0				
Gj 27.0	27.0	-30.5				
Gj 27.3	27.3	-31.2				
Gj 27.6	27.6	-27.2				
Gj 28.3	28.3	-29.1			690	168
Gj 28.6	28.6	-30.4				
Gj 29.0	29.0	-30.1	3.7	0.007		
Gj 30.0	30.0	-26.0				
Gj 31.3	31.3	-27.5	4.3	0.007		
Gj 31.6	31.6	-29.5		0.005		
Gj 32.0	32.0	-29.7	2.2	0.005	1517	303
Gj 32.3	32.3	-28.1				
Gj 32.6	32.6	-30.5	5.3	0.005	929	134
Gj 33.0	33.0	-26.0	4.5	0.017	1475	63
Gj 33.6	33.6	-29.3	4.1	0.019		
Gj 34.6	34.6	-25.4	4.2	0.018		
Gj 35.0	35.0	-28.8	4.6	0.017		
Gj 35.3	35.3		4.2	0.018		

Table 6 (continued)

Sample	Distance [m]	$\delta^{13}C_{org}$ [‰] vs. VPDB	$\delta^{15}N$ [‰] vs. AIR	TN [%]	P [ppm]	S [ppm]
Gj 36.0	36.0	-31.0			639	123
Gj 36.3	36.3	-25.9				
Gj 37.0	37.0	-28.5				
Gj 37.6	37.6	-28.3	4.4	0.013		
Gj 38.0	38.0	-29.1	4.2	0.012		
Gj 38.3	38.3		3.7	0.016		
Gj 38.6	38.6	-27.3	4.3	0.015		
Gj 39.0	39.0	-29.5	4.4	0.006		
Gj 39.3	39.3	-29.2	4.3	0.006		
Gj 40.0	40.0	-30.2	3.7	0.013		
Gj 41.0	41.0	-27.3				
Gj 42.0	42.0	-28.8			404	171
Gj 42.3	42.3	-30.1				
Gj 43.0	43.0	-25.2				
Gj 44.0	44.0	-27.0				
Gj 45.0	45.0	-27.3				
Gj 45.5	45.5		4.3	0.006		
Gj 46.3	46.3				545	189
Gj 46.0	46.0	-29.5				
Gj 46.6	46.6	-27.9				
Gj 47.6	47.6	-28.9				
Gj 49.0	49.0	-30.0			578	266
Gj 49.6	49.6	-25.9	4.6	0.005		
Gj 50.0	50.0	-26.7				
Gj 50.3	50.3		3.7	0.006		
Gj 50.6	50.6		4.3	0.006		
Gj 51.0	51.0	-25.5				
Gj 51.6	51.6	-28.2				
Gj 52.0	52.0	-30.1				
Gj 52.6	52.6	-29.9				
Gj 53.0	53.0	-33.5				
Gj 53.3	53.3				1332	375
Gj 54.0	54.0	-28.6				
Gj 55.0	55.0	-29.2				
Gj 55.6	55.6		3.8	0.007		
Gj 56.0	56.0	-33.0	4.9	0.006		
Gj 56.3	56.3				3340	1589
Gj 56.6	56.6	-33.8			3106	87
Gj 57.0	57.0	-33.5			2141	83
Gj 58.0	58.0	-25.6			205	137
Gj 58.6	58.6	-24.2				

Table 6 (continued)

Sample	Distance [m]	$\delta^{13}C_{org}$ [‰] vs. VPDB	$\delta^{15}N$ [‰] vs. AIR	TN [%]	P [ppm]	S [ppm]
Gj 59.0	59.0	-27.6				
Gj 60.0	60.0	-28.5				
Gj 61.6	61.6	-27.4				
Gj 62.3	62.3	-24.2			418	151
Gj 63.3	63.3	-27.8				
Gj 64.0	64.0	-24.7				
Gj 65.0	65.0	-26.6				
Gj 65.6	65.6				219	136
Gj 67.0	67.0	-27.9				
Gj 67.6	67.6	-26.3				
Gj 68.0	68.0	-27.1				
Gj 69.0	69.0	-26.3				
Gj 70.6	70.6	-26.3				
Gj 71.0	71.0	-27.1				
Gj 79.6	79.6	-17.6				
Gj 80.3	80.3	-21.5				
Gj 83.3	83.3	-18.0				
Gj 84.3	84.3	-21.5				
Gj 89.6	89.6	-23.0				
Gj 90.0	90.0	-23.8				
Gj 90.6	90.6	-21.2				
Gj 91.0	91.0	-23.1				
Gj 91.6	91.6	-20.6				
Gj 92.0	92.0	-20.5				
Gj 92.3	92.3	-21.2				
Gj 92.6	92.6	-22.3				
Gj 93.3	93.3	-22.3				

6.6.1 $\delta^{13}C_{org}$ and $\delta^{15}N$ isotopic profiles

Sedimentary $\delta^{13}C_{org}$ compositions express four significant trends. The Algal Dolomite Member is dominated by $\delta^{13}C_{org}$ values fluctuating around ~-25‰, merging into the lower and middle Gaojiashan Member with values down to ~-30‰ (Fig. 14). Most negative $\delta^{13}C_{org}$ values (-33.8‰) are documented during the uppermost Gaojiashan Member corresponding to the major $\delta^{13}C_{carb}$ negative excursion (NE2; chapter 5) $\delta^{13}C_{org}$ values return to ~-25‰ and eventually ~-20‰ in the overlying strata of the Beiwan Member (Fig.14).

$\delta^{15}N$ data demonstrate a smooth and gradual upward-increasing trend in the section by rising from ~2‰ in the lower part of the Gaojiashan Member to ~3‰ in its middle part (Fig. 14). Co-occurring with *Gaojiashania*-group fossils, $\delta^{15}N$ data stabilize around 4‰ in the upper Gaojiashan Member. Strata of the uppermost Gaojiashan Member and the overlying Beiwan Member do not contain nitrogen concentration above the detection limit.

6.6.2 Trace element concentration

Phosphorus (P) and sulfur (S) concentrations increase stepwise throughout the section, culminating in their highest values at the onset of NE2. Concentrations of ~100 ppm of both elements in the lower Gaojiashan Member increase to maxima of ~3000 ppm phosphorus and ~1500 ppm sulfur, respectively, in the upper Gaojiashan Member, followed by an abrupt decrease in concentrations to ~200 ppm phosphorus and ~80 ppm sulfur which correspond to the nadir of NE2 (Table 6).

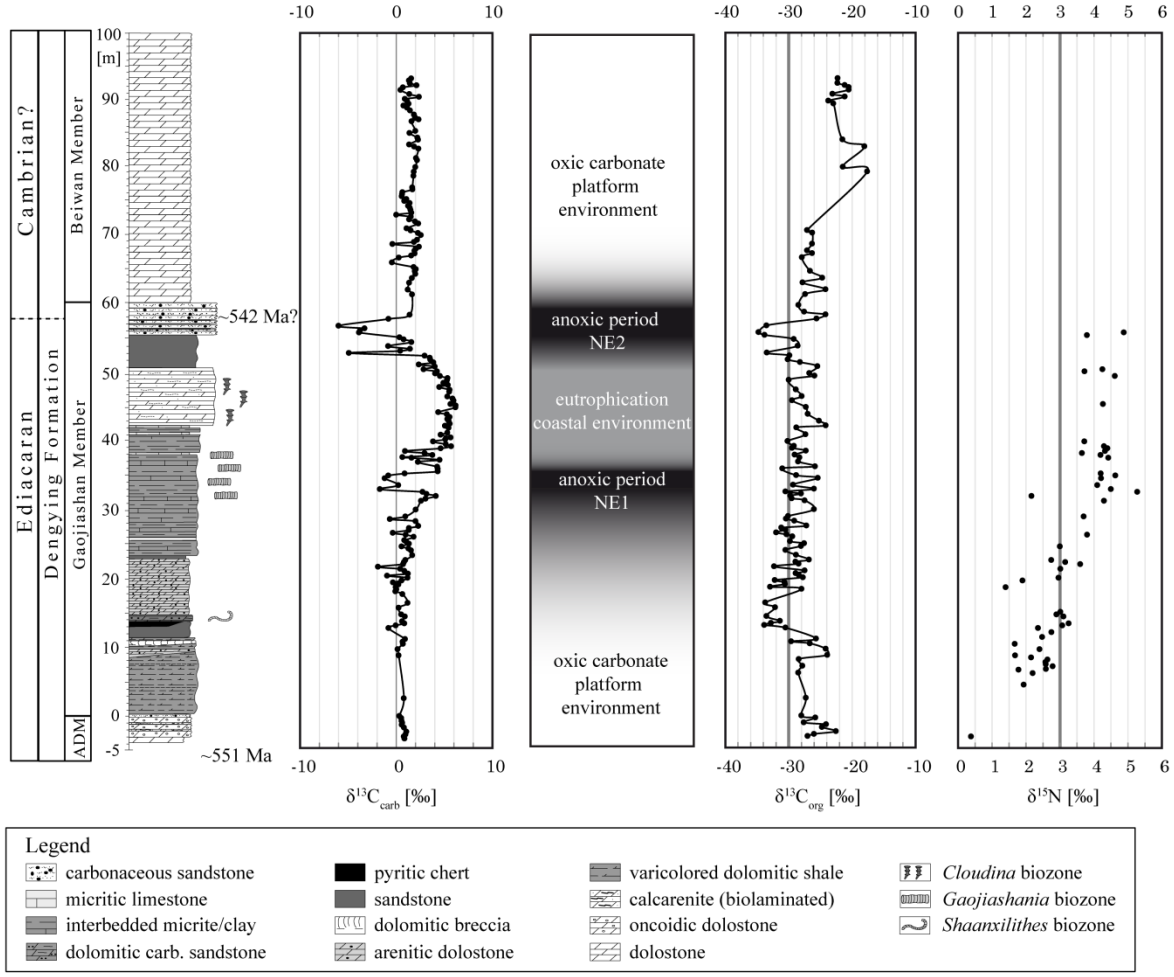

Figure 14: Isotopic profiles of $\delta^{13}C_{carb}$ (chapter 5), $\delta^{13}C_{org}$ and $\delta^{15}N$ and the stratigraphical column of the Gaojiashan section. A negative $\delta^{13}C_{carb}$ excursion of small magnitude (NE1) is documented in strata with pyritized Gaojiashania fossils. $\delta^{15}N$ values smoothly increase to ~4‰ in the middle Gaojiashan Member parallel to the occurrence of Gaojiashania and Cloudina fossils. Note that the second prominent $\delta^{13}C_{carb}$ excursion (NE2) is mirrored by the $\delta^{13}C_{org}$ signal and directly succeeds the last assumed occurrence of Cloudina. The middle rectangular column shows suggested geochemical changes during the deposition of the upper Algal Dolomite Member, the Gaojiashan Member and the Beiwan Member. Color gradations indicate postulated variations in shallow-water redox conditions.

6.7 Discussion

6.7.1 Evaluation of diagenetic alteration of organic C and N isotopic compositions

Post-depositional diagenetic processes may alter the sedimentary $\delta^{15}N$ and $\delta^{13}C_{org}$ signals (Ader et al., 2009; Thomazo and Papineau, 2013). During early diagenesis, bacterial degradation can cause a depletion of sedimentary $\delta^{13}C_{org}$ of 1 to 2‰ (Ader et al., 2009 and references therein). Because this effect does not exceed 2‰, bacterial degradation during early diagenesis in the sediments at Gaojiashan section is likely not responsible for the total range in $\delta^{13}C_{org}$ composition of ~10‰ during the Gaojiashan Member. The variance of $\delta^{13}C_{org}$ values mirrors the isotopic composition of the deposited biomass. The impact of early diagenesis and low-grade metamorphic reactions on the $\delta^{15}N$ signal is generally accepted to range between <1 and 3‰. Whereas heterotrophic degradation of organic matter during early diagenesis alters the $\delta^{15}N$ signal less than 1‰, other processes depending, e.g. on the water depth and the sinking flux of the organic material appear to affect the $\delta^{15}N$ composition more although their effects are still small (see for reviews, e.g. Robinson et al., 2012; Thomazo and Papineau, 2013).

Apparently, the variance of $\delta^{13}C_{org}$ and $\delta^{15}N$ values of Gaojiashan samples is independent from lithology, thus suggesting primary isotopic variations. Furthermore, the lack of co-variation of $\delta^{13}C_{carb}$ and $\delta^{18}O$ values reported in chapter 5 argues against a diagenetic overprint at Gaojiashan section. Moreover, analyses of the kerogen H/C ratio (an indicator for thermal maturity) of Gaojiashan sedimentary rocks indicate that the organic matter of samples was affected by thermal maturation effects only to a minor degree (Guo et al., 2012).

In Figure 15, $\delta^{15}N$, $\delta^{13}C_{org}$, TN and TOC data (reported in chapter 5) are plotted to evaluate a possible diagenetic overprint and the origin (source) of nitrogen species in the sediments. Figure 15a, b and c show no significant co-variation between the isotopic values and the TN and TOC concentrations which suggests that diagenetic processes did not affect isotopic signals (Cremonese et al., 2014).

The preferential loss of either nitrogen isotope during alteration and diagenetic processes can thus be minimized (Cremonese et al., 2013). A plot of TN vs. TOC (Fig. 15d) is used to identify the original source of nitrogen. In sedimentary rocks, nitrogen is present in two different forms: as organic-bound nitrogen or as ammonium-fixed nitrogen in clay minerals. Ammonium (NH_4^+) is known to substitute for potassium (K^+) in the exchange layers of clay minerals like illites (Schubert and Calvert, 2001). Schubert and Calvert (2001) showed that the inorganic-bound NH_4^+ lowers the $\delta^{15}N$ signal as nitrogen bound in clays represents a signal gained on land and therefore being close to the atmospheric $\delta^{15}N$ ratio. However, Figure 15d shows an intercept close to the origin which argues for a minor contribution of clay-bound nitrogen to the total nitrogen in the sediments and that most nitrogen is organically-bound (Cremonese et al., 2014).

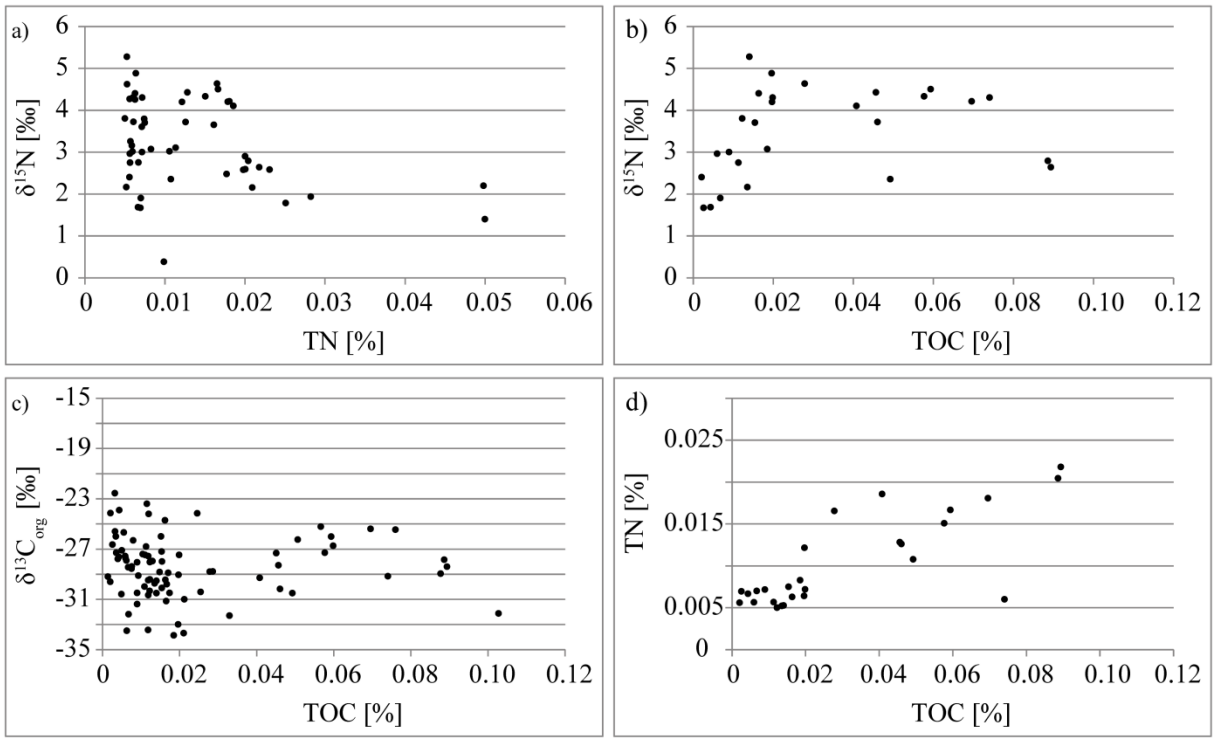

Figure 15: Cross-plots of (a) $\delta^{15}N$ vs. TN, (b) $\delta^{15}N$ vs. TOC, (c) $\delta^{13}C_{org}$ vs. TOC and (d) TN vs. TOC. TOC data are reported in chapter 5.

6.7.2 Eutrophication of surface waters and the evolution of Late Ediacaran biota in the upper Dengying Formation

The upper Algal Dolomite Member and lower Gaojiashan Member record $\delta^{13}C_{org}$ values of ~-26‰ which agrees with other organic carbon data from the middle Dengying Formation (Kikumoto et al., 2014) and are characteristic for marine phytoplankton. Low $\delta^{15}N$ values of ~2‰ describe a scenario where diazotrophic bacteria are responsible for the main input of bioavailable nitrogen to the ecosystem (Sachs and Repeta, 1999). Amongst light intensity, high amounts of phosphorus are known to fuel bioproductivity via N_2-fixation (Fu and Bell, 2003). This is supported by elevated, localized high phosphorus concentrations (Table 6) in host rocks embedding *Shaanxilithes ningqiangensis* (Meyer et al., 2012). Consequently, the availability of combined nitrogen species (e.g. NO_3^-) was limited because their presence is known to depress the N_2-fixation pathway (Fu and Bell, 2003). The source of phosphorus is mainly attributed to continental influx (Paytan and McLaughlin, 2007) sustained by nearby coastal regions (Weber et al., 2007). During the middle and upper Gaojiashan times, intensified continental weathering flux is recorded by $^{87}Sr/^{86}Sr$ data (Ohnemueller et al., 2013). The elevated nutrient influx most likely caused eutrophication and high bioproductivity in surface waters (Sawaki et al., 2010), marked by the occurrence of two biozones: *Gaojiashania* and *Cloudina*. Furthermore, $^{87}Sr/^{86}Sr$ ratios agree with global seawater Sr datasets (Halverson et al., 2007), however could also represent a local record (Ohnemueller et al., in prep.).

In the light of eutrophication, $\delta^{15}N$ data increase up to ~5‰ in strata co-occurring with the first appearance of *Gaojiashania* and are in general agreement with other reported late Ediacaran $\delta^{15}N$ datasets (Cremonese et al., 2013; Cremonese et al., 2014; Kikumoto et al., 2014). Apparently, NO_3^- became gradually the outweighing nutrient for primary producers (Cremonese et al., 2013) while N_2 partly remained unused in surface waters, possibly attributed to increased oxygen availability required for nitrification (Canfield et al., 2010). Thus elevated $\delta^{15}N$ values indicate that during late Ediacaran times (middle and upper Gaojiashan Member) intermediate waters on the shallow shelf must have been at least mildly oxygenated to allow remineralization of organic matter via

nitrification-denitrification interactions. Elevated $\delta^{15}N$ values further imply that degradation of organic matter via denitrification gained more influence because denitrifying bacteria are responsible for the $^{15}NO_3^-$ enrichment in the deep-water nutrient pool (Cline and Kaplan, 1975). Nitrogen values are in agreement with those reported from upper Dengying strata in Guizhou Province (Cremonese et al., 2014) arguing for slightly oxygenated shallow-water conditions on at least supra-regional scale, a scenario which might have existed already globally since early Ediacaran times (Ader et al., 2014).

The extinction of the Gaojiashan biota is followed by the first occurrence of *Cloudina*. *Cloudina*-bearing strata record the highest TOC and $\delta^{13}C_{carb}$ values of the section and thus demonstrate that enhanced bioproductivity is the main driver for $^{13}C_{carb}$-enrichment there (Ishikawa et al., 2013). During carbon uptake marine phytoplankton strongly discriminates against the ^{13}C-isotope, favoring the uptake of the isotopic "lighter" ^{12}C and thus enriching the residual dissolved inorganic carbon (DIC) pool in ^{13}C. In times of eutrophication and strong metabolic activities precipitated carbonates then mirror increased $\delta^{13}C_{carb}$ values, e.g. up to ~4‰ seen in the upper part of the section. However, large bioproductivity and dissolved organic carbon (DOC) export to depth stimulates a strong oxygen-consuming remineralization of the organic matter and establishes oxygen depletion in bottom waters (Fig. 16; Ishikawa et al., 2013) which further stabilizes nitrification-denitrification processes.

It remains speculative if the changing dominance among nitrogen species coupled to the proposed increasing availability of oxygen and nitrate influenced the evolution of certain Ediacaran biota like the Gaojiashan or *Cloudina* biota. The shifting nutrient regime could have either promoted or restricted the evolution of the Ediacaran fauna due to their ability/inability using specific nutrient-compounds for their metabolism. Another factor which could have affected the marine ecosphere is documented by the pyritization of non-mineralizing *Gaojiashania*, since this mechanism is associated with sulfidic water conditions and bacterial sulfate reduction in an anoxic environment (Xiao et al., 2010; Cai et al., 2012). Oceanic sulfate concentrations are suggested to have significantly increased at the onset of bioturbation at ~555 Ma (Canfield and Farquhar, 2009)

approximately matching with the occurrence of the Gaojiashan biota representing undermat miners which presumably shallow-bioturbated the sediment (Weber et al., 2007). Oxygen-depleted conditions and an increasing proportion of sulfur compounds may be supported by the negative $\delta^{13}C_{carb}$ excursion NE1 and elevated sulfur concentrations (up to 300 ppm) in strata prior to 32 m. However, due to the approximate short duration of NE1, the event most likely occurred on regional scale.

6.7.3 Shallow-marine redox condition across the Pc-C boundary interval and implications for the biosphere

In the upper Gaojiashan Member, $\delta^{13}C_{carb}$ data begin to decrease indicating a beginning overturn of a redox-stratified eutrophic basin (see chapter 5) which are also reported from late Ediacaran sections of Brazil (Spangenberg et al., 2014) and Uruguay (Frei et al., 2013). The strong negative $\delta^{13}C_{carb}$ and $\delta^{13}C_{org}$ data are consistent with a stratified ocean scenario during the late Neoproterozoic (Ishikawa et al., 2013) and are in agreement with the anoxic overturn model at the Pc-C boundary transition (Shen, 2002; Wang et al., 2012). This is supported by cerium data from strata comprising NE2 which show a clear positive Ce/Ce* anomaly (1.405; chapter 5) indicating a deposition under anoxic conditions and a release of cerium from settling oxides comparable to settings in modern stratified basins like the Black Sea or the Cariaco Basin. There, the settling and dissolution of oxides in deeper anoxic water masses will release excess cerium and thus cause positive Ce/Ce* anomalies (German et al., 1991). The REE dataset reported in chapter 5 therefore supports an earlier publication mentioning anoxic bottom waters at the Pc-C boundary inferred from a REE dataset from a profile in the southern Himalaya region (Mazumdar et al., 1999). Additionally, subsequent evolving sedimentary and water column anoxia would maintain elevated oceanic phosphate concentrations documented by maximal phosphorus values in respective sediments (Table 6) which further led to a positive response on surface bioproductivity (Struck et al., 2001; Higgins et al., 2010; Shimura et al., 2014). The preliminary last appearance of *Cloudina* in the upper Gaojiashan Member is associated with the negative $\delta^{13}C_{carb}$ anomaly NE2

likely representing the global anoxic Pc-C event (see chapter 5). Interestingly, $\delta^{13}C_{org}$ values show a concurrent negative peak down to -33.8‰ corresponding to NE2. The coupling of $\delta^{13}C_{carb}$ and $\delta^{13}C_{org}$ across the Pc-C transition has not been reported previously from Pc-C boundary sections which instead record clear decoupling until the early Cambrian (Ishikawa et al., 2013). However, the coupling of isotopic carbon-systems is a clear indicator for the lack of diagenetic alteration resetting isotopic signals (Johnston et al., 2012a).

The anoxia scenario finds support in several investigations of local and global equivalents, e.g. on the Yangtze platform (Goldberg et al., 2007; Och et al., 2013) and Iran (Kimura and Watanabe, 2001). Analyses of redox-sensitive elements like molybdenum in sections of South China (Wille et al., 2008; Och et al., 2013) support aforementioned REE analyses and suggest even intermittently euxinic (bottom) water conditions across the Pc-C boundary. A postulated enhanced seawater sulfate concentration is regarded to have enabled bacterial sulfate reduction (Och et al., 2013) operating as an effective process during remineralization of organic matter. Moreover sulfate reduction agrees with reported decreasing alkalinity as well as pH conditions of the seawater during the Pc-C transition interval at Gaojiashan section (Ohnemueller et al., 2013) and on global scale (Mazumdar et al., 1999; Tziperman et al., 2011). The subsequent remineralization of the deep-water DOC reservoir thus provided a ^{12}C-enriched carbon source for the formation of the negative carbon anomaly (Jiang et al., 2007). Upwelling of anoxic to euxinic ^{13}C-depleted bottom waters in the course of the global Pc-C transgression provoked the anoxic overturn (Fig. 16) and most likely reduced shallow-water bioproductivity due to H_2S poisoning (Wille et al., 2008) thus contributing to the extinction of certain Ediacaran biota across the Pc-C boundary interval (Kimura and Watanabe, 2001) and therefore significantly condensed the DOC pool (Ishikawa et al., 2013). Decreasing bioproductivity is supported by sharply decreasing TOC concentrations at the onset of NE2 (chapter 5) and the disappearance of *Cloudina* in respective strata.

Following the negative excursion NE2, biogeochemical circumstances return to an oxygenated ventilated oceanic environment with $\delta^{13}C_{carb}$ values (~2‰) and

$\delta^{13}C_{org}$ (~-20‰) representative of marine carbonate strata deposited during Phanerozoic times.

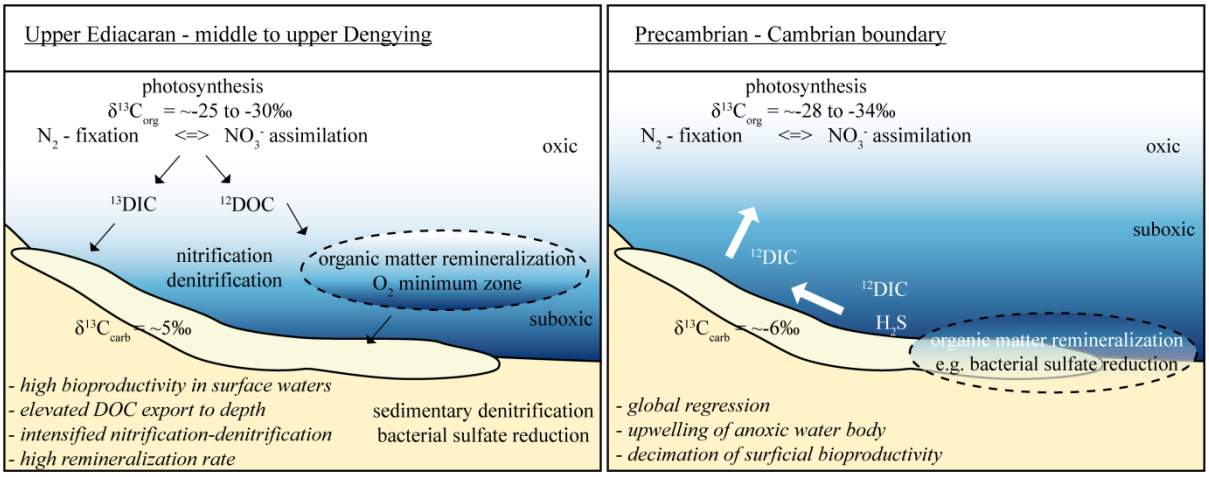

Figure 16: Paleobasin model for the shallow-water setting at Gaojiashan section during (a) lower to middle Dengying times and (b) across the Pc-C boundary. (a) Elevated bioproductivity during the deposition of the upper Dengying Formation led to a positive $\delta^{13}C_{carb}$ anomaly and enhanced DOC export to depth. N_2-fixation and NO_3^- assimilation both account for the supply of bioavailable nitrogen. (b) The Pc-C boundary interval is characterized by upwelling of H_2S and ^{12}C-DIC-enriched water due to elevated remineralization and associated evolving anoxic bottom-water conditions. NO_3^- displays the main nutrient for primary productivity until the oceanic anoxic overturn.

6.8 Conclusion

The Gaojiashan section (southern Shaanxi Province) provides valuable insights into evolutionary events of the late Ediacaran biota and the following "Cambrian explosion". Our data suggest that intensive continental weathering and nutrient influx during the lower and middle Gaojiashan Member promoted eutrophication of surface waters. Enhanced bioproductivity documented by the evolution of three distinct biozones (*Shaanxilithes ningqiangensis, Gaojiashania, Cloudina*) enriched the surficial DIC pool in ^{13}C causing a zenith of $\delta^{13}C_{carb}$ values (6.2‰) in concomitant strata. Progressively elevated $\delta^{15}N$ data (up to 4.9‰) indicate that nitrate became stable and available for bioproductivity in shallow waters. Hence, the late Neoproterozoic ocean on the Yangtze platform was presumably slightly oxygenated which fuelled nitrification-denitrification interactions and may have influenced the evolution of the Ediacaran biota. During the deposition of the upper Gaojiashan Member, massive mineralization of organic matter triggered oxygen depletion in bottom waters where bacterial denitrification and sulfate reduction dominated remineralization processes. In the course of the global Pc-C

boundary transgression uprising of anoxic to euxinic waters to the surface are proposed to have caused a decimation event of the biosphere (Kimura and Watanabe, 2001; Wille et al., 2008) which might have resulted in more responsive isotopic changes of carbon pools thus enabling coeval $\delta^{13}C_{carb}$ and $\delta^{13}C_{org}$ trends from that time on. The afterwards return to oxygenated, ventilated ocean waters possibly contributed to the Cambrian radiation of metazoan life.

6.9 Acknowledgements

We thank Quentin Scouflaire and Bernd Weber (Freie Universität Berlin) for sample collection as well as Christoph Heubeck (Friedrich-Schiller Universität Jena), Frank Ohnemueller and Simone Kasemann (Universität Bremen) for valuable consultations. We thank Ewgenjia Kuhl, Maria Diedrich, and Yannik Steinmann (all Museum für Naturkunde Berlin) for support during sample preparation and Silvana Pape (Universität Bremen) for ICP-OES trace element measurements. This work has benefited from discussions with colleagues of the Forschergruppe 736. The study was funded by the German Research Foundation (DFG-FOR 736). Field work was supported by the Natural Science Foundation of South China (NSFC).

6.10 References

Abrajano, T., Aksu, A. E., Hiscott, R. N., and Mudie, P. J., 2002, Aspects of carbon isotope biogeochemistry of late Quaternary sediments from the Marmara Sea and Black Sea: Marine Geology, v. 190, no. 1–2, p. 151-164.

Ader, M., Macouin, M., Trindade, R. I. F., Hadrien, M. H., Yang, Z., Sun, Z., and Besse, J., 2009, A multilayered water column in the Ediacaran Yangtze platform? Insights from carbonate and organic matter paired $\delta^{13}C$: Earth and Planetary Science Letters, v. 288, no. 1-2, p. 213-227.

Ader, M., Sansjofre, P., Halverson, G. P., Busigny, V., Trindade, R. I. F., Kunzmann, M., and Nogueira, A. C. R., 2014, Ocean redox structure across the Late Neoproterozoic Oxygenation Event: A nitrogen isotope perspective: Earth and Planetary Science Letters, v. 396, no. 0, p. 1-13.

Alibo, D. S., and Nozaki, Y., 1999, Rare earth elements in seawater: particle association, shale-normalization, and Ce oxidation: Geochimica et Cosmochimica Acta, v. 63, no. 3–4, p. 363-372.

Altabet, M. A., and Francois, R., 1994, Sedimentary nitrogen isotopic ratio as a recorder for surface ocean nitrate utilization: Global Biogeochemical Cycles, v. 8, p. 103-116.

Altabet, M. A., 2007, Constraints on oceanic N balance/imbalance from sedimentary ^{15}N records: Biogeosciences, v. 4, no. 1, p. 75-86.

Amthor, J. E., Grotzinger, J. P., Schröder, S., Bowring, S. A., Ramezani, J., Martin, M. W., and Matter, A., 2003, Extinction of Cloudina and Namacalathus at the Precambrian-Cambrian boundary in Oman: Geology, v. 31, p. 431-434.

Banner, J. L., 1988, Rare Earth Element and Nd Isotopic Variations in Regionally Extensive Dolomites From the Burlington-Keokuk Formation (Mississippian): Implications for Ree Mobility During Carbonate Diagenesis: Journal of Sedimentary Research, v. 58.

Bjerrum, C. J., and Canfield, D. E., 2011, Towards a quantitative understanding of the late Neoproterozoic carbon cycle: Proceedings of the National Academy of Sciences, v. 108, no. 14, p. 5542-5547.

Boggiani, P. C., Gaucher, C., Sial, A. N., Babinski, M., Simon, C. M., Riccomini, C., Ferreira, V. P., and Fairchild, T. R., 2010, Chemostratigraphy of the Tamengo Formation (Corumbá Group, Brazil): A contribution to the calibration of the Ediacaran carbon-isotope curve: Precambrian Research, v. 182, no. 4, p. 382-401.

Byrne, R. H., and Kim, K. H., 1990, Rare-earth element scavenging in seawater: Geochimica et Cosmochimica Acta, v. 54, no. 10, p. 2645-2656.

Cai, Y., Hua, H., Xiao, S., Schiffbauer, J. D., and Li, P., 2010, Biostratinomy of the late Ediacaran pyritized Gaojiashan Lagerstätte from Southern Shaanxi, South China: Importance of event deposits: Palaios, v. 25, no. 8, p. 487-506.

Cai, Y., Schiffbauer, J. D., Hua, H., and Xiao, S., 2011, Morphology and paleoecology of the late Ediacaran tubular fossil Conotubus hemiannulatus from the Gaojiashan Lagerstätte of southern Shaanxi Province, South China: Precambrian Research, v. 191, no. 1–2, p. 46-57.

Cai, Y., Schiffbauer, J. D., Hua, H., and Xiao, S., 2012, Preservational modes in the Ediacaran Gaojiashan Lagerstatte: Pyritization, aluminosilicification, and carbonaceous compression: Palaeogeography Palaeoclimatology Palaeoecology, v. 326, p. 109-117.

Cai, Y., Hua, H., and Zhang, X., 2013, Tube construction and life mode of the late Ediacaran tubular fossil Gaojiashania cyclus from the Gaojiashan Lagerstätte: Precambrian Research, v. 224, no. 0, p. 255-267.

Cai, Y., Hua, H., Schiffbauer, J. D., Sun, B., and Yuan, X., 2014, Tube growth patterns and microbial mat-related lifestyles in the Ediacaran fossil Cloudina, Gaojiashan Lagerstätte, South China: Gondwana Research, v. 25, no. 3, p. 1008-1018.

Canfield, D. E., and Farquhar, J., 2009, Animal evolution, bioturbation, and the sulfate concentration of the oceans: Proceedings of the National Academy of Sciences, v. 106, no. 20, p. 8123-8127.

Canfield, D. E., Glazer, A. N., and Falkowski, P. G., 2010, The Evolution and Future of Earth's Nitrogen Cycle: Science, v. 330, no. 6001, p. 192-196.

Carpenter, E. J., Harvey, H. R., Fry, B., and Capone, D. G., 1997, Biogeochemical tracers of the marine cyanobacterium Trichodesmium: Deep Sea Research Part I: Oceanographic Research Papers, v. 44, no. 1, p. 27-38.

Cline, J. D., and Kaplan, I. R., 1975, Isotopic fractionation of dissolved nitrate during denitrification in the eastern tropical north pacific ocean: Marine Chemistry, v. 3, no. 4, p. 271-299.

Cremonese, L., Shields-Zhou, G., Struck, U., Ling, H.-F., Och, L., Chen, X., and Li, D., 2013, Marine biogeochemical cycling during the early Cambrian constrained by a nitrogen and organic carbon isotope study of the Xiaotan section, South China: Precambrian Research, v. 225, no. 0, p. 148-165.

Cremonese, L., Shields-Zhou, G. A., Struck, U., Ling, H.-F., and Och, L. M., 2014, Nitrogen and organic carbon isotope stratigraphy of the Yangtze Platform during the Ediacaran–Cambrian transition in South China: Palaeogeography, Palaeoclimatology, Palaeoecology, v. 398, no. 0, p. 165-186.

Elderfield, H., Whitfield, M., Burton, J. D., Bacon, M. p., and Liss, P. S., 1988, The Oceanic Chemistry of the Rare-Earth Elements [and Discussion]: Philosophical Transactions of the Royal Society of London, v. 325, no. 1583, p. 105-126.

Falkowski, P. G., 1997, Evolution of the nitrogen cycle and its influence on the biological sequestration of CO_2 in the ocean: Nature, v. 387, no. 6630, p. 272-275.

Farrell, J. W., Pedersen, T. F., Calvert, S. E., and Nielsen, B., 1995, Glacial-interglacial changes in nutrient utilization in the equatorial Pacific Ocean: Nature, v. 377, no. 6549, p. 514-517.

Frei, R., Gaucher, C., Stolper, D., and Canfield, D. E., 2013, Fluctuations in late Neoproterozoic atmospheric oxidation - Cr isotope chemostratigraphy and iron speciation of the late Ediacaran lower Arroyo del Soldado Group (Uruguay): Gondwana Research, v. 23, no. 2, p. 797-811.

Fu, F.-X., and Bell, P. R. F., 2003, Factors affecting N_2 fixation by the cyanobacterium Trichodesmium sp. GBRTRLI101: FEMS Microbiology Ecology, v. 45, no. 2, p. 203-209.

German, C. R., Holliday, B. P., and Elderfield, H., 1991, Redox cycling of rare-earth elements in the suboxic zone of the black-sea: Geochimica et Cosmochimica Acta, v. 55, no. 12, p. 3553-3558.

Germs, G. J., 1972, New shelly fossils from the Nama Group, South-West Africa: American Journal of Science, v. 272, p. 752–761.

Goldberg, T., Strauss, H., Guo, Q., and Liu, C., 2007, Reconstructing marine redox conditions for the Early Cambrian Yangtze Platform: Evidence from biogenic sulphur and organic carbon isotopes: Palaeogeography, Palaeoclimatology, Palaeoecology, v. 254, no. 1–2, p. 175-193.

Guo, Q., Strauss, H., Liu, C., Goldberg, T., Zhu, M., Pi, D., Heubeck, C., Vernhet, E., Yang, X., and Fu, P., 2007, Carbon isotopic evolution of the terminal Neoproterozoic and early Cambrian: Evidence from the Yangtze Platform, South China: Palaeogeography, Palaeoclimatology, Palaeoecology, v. 254, no. 1–2, p. 140-157.

Guo, Q., Deng, Y., and Yang, X., 2012, Carbon Isotopic Evolution of the Late Ediacaran Gaojiashan Biota on the Northern Yangtze Platform, South China: Acta Geologica Sinica-English Edition, v. 86, no. 6, p. 1447-1454.

Halverson, G. P., Dudas, F. O., Maloof, A. C., and Bowring, S. A., 2007, Evolution of the $^{87}Sr/^{86}Sr$ composition of Neoproterozoic seawater: Palaeogeography Palaeoclimatology Palaeoecology, v. 256, no. 3-4, p. 103-129.

Higgins, M. B., Robinson, R. S., Carter, S. J., and Pearson, A., 2010, Evidence from chlorin nitrogen isotopes for alternating nutrient regimes in the Eastern Mediterranean Sea: Earth and Planetary Science Letters, v. 290, no. 1–2, p. 102-107.

Hohl, S., Becker, H., Herzlieb, S., and Guo, Q., in prep., Multiproxy constraints on alteration and primary compositions of Ediacaran deep-water carbonate rocks, Yangtze Platform, South China.

Hua, H., Zhang, L.-Y., Zhang, Z.-F., and Wang, J.-P., 2001, Assemblage zones of Gaojiashan Biota and their characteristics: Journal of Stratigraphy, v. 25, no. 1, p. 13-17.

Hua, H., Chen, Z., Yuan, X., Zhang, L., and Xiao, S., 2005, Skeletogenesis and asexual reproduction in the earliest biomineralizing animal Cloudina: Geology, v. 33, no. 4, p. 277-280.

Hua, H., Chen, Z., and Yuan, X., 2007, The advent of mineralized skeletons in Neoproterozoic Metazoa - new fossil evidence from the Gaojiashan Fauna: Geological Journal, v. 42, p. 263–279.

Ishikawa, T., Ueno, Y., Komiya, T., Sawaki, Y., Han, J., Shu, D., Li, Y., Maruyama, S., and Yoshida, N., 2008, Carbon isotope chemostratigraphy of a Precambrian/Cambrian boundary section in the Three Gorge area, South China: Prominent global-scale isotope excursions just before the Cambrian Explosion: Gondwana Research, v. 14, no. 1–2, p. 193-208.

Ishikawa, T., Ueno, Y., Shu, D., Li, Y., Han, J., Guo, J., Yoshida, N., and Komiya, T., 2013, Irreversible change of the oceanic carbon cycle in the earliest Cambrian: High-resolution organic and inorganic carbon chemostratigraphy in the Three Gorges area, South China: Precambrian Research, v. 225, no. 0, p. 190-208.

Jiang, G., Kaufmann, A. J., Christie-Blick, N., Zhang, S., and Wu, H., 2007, Carbon isotope variability across the Ediacaran Yangtze platform in South China: Implications for a large surface-to-deep ocean $\delta^{13}C$ gradient: Earth and Planetary Science Letters, v. 261, p. 303-320.

Johnston, D. T., Macdonald, F. A., Gill, B. C., Hoffman, P. F., and Schrag, D. P., 2012a, Uncovering the Neoproterozoic carbon cycle: Nature, v. 483, no. 7389, p. 320-323.

Johnston, D. T., Poulton, S. W., Goldberg, T., Sergeev, V. N., Podkovyrov, V., Vorob'eva, N. G., Bekker, A., and Knoll, A. H., 2012b, Late Ediacaran redox stability and metazoan evolution: Earth and Planetary Science Letters, v. 335, p. 25-35.

Kikumoto, R., Tahata, M., Nishizawa, M., Sawaki, Y., Maruyama, S., Shu, D., Han, J., Komiya, T., Takai, K., and Ueno, Y., 2014, Nitrogen isotope chemostratigraphy of the Ediacaran and Early Cambrian platform sequence at Three Gorges, South China: Gondwana Research, v. 25, no. 3, p. 1057-1069.

Kimura, H., and Watanabe, Y., 2001, Oceanic anoxia at the Precambrian-Cambrian boundary: Geology, v. 29, no. 11, p. 995-998.

Li, D., Ling, H.-F., Jiang, S.-Y., Pan, J.-Y., Chen, Y.-Q., Cai, Y.-F., and Feng, H.-Z., 2009, New carbon isotope stratigraphy of the Ediacaran–Cambrian boundary interval from SW China: implications for global correlation: Geol. Mag., v. 146, no. 4, p. 465-484.

Li, D., Ling, H.-F., Shields-Zhou, G. A., Chen, X., Cremonese, L., Och, L., Thirlwall, M., and Manning, C. J., 2013, Carbon and strontium isotope evolution of seawater across the Ediacaran–Cambrian transition: Evidence from the Xiaotan section, NE Yunnan, South China: Precambrian Research, v. 225, no. 0, p. 128-147.

Ling, H.-F., Chen, X., Li, D., Wang, D., Shields-Zhou, G. A., and Zhu, M., 2013, Cerium anomaly variations in Ediacaran–earliest Cambrian carbonates from the Yangtze Gorges area, South China: Implications for oxygenation of coeval shallow seawater: Precambrian Research, v. 225, no. 0, p. 110-127.

Mazumdar, A., Banerjee, D. M., Schidlowski, M., and Balaram, V., 1999, Rare-earth elements and stable isotope geochemistry of early Cambrian chert-phosphorite assemblages from the Lower Tal formation of the Krol Belt (Lesser Himalaya, India): Chemical Geology, v. 156, no. 1-4, p. 275-297.

Meyer, M., Schiffbauer, J. D., Xiao, S., Cai, Y., and Hua, H., 2012, Taphonomy of the upper Ediacaran enigmatic ribbonlike fossil Shaanxilithes: Palaios, v. 27, no. 5-6, p. 354-372.

Montoya, J. P., Carpenter, E. J., and Capone, D. G., 2002, Nitrogen fixation and nitrogen isotope abundances in zooplankton of the oligotrophic North Atlantic: Limnology Oceanography, v. 47, no. 6, p. 1617-1628.

Och, L. M., Shields-Zhou, G. A., Poulton, S. W., Manning, C., Thirlwall, M. F., Li, D., Chen, X., Ling, H., Osborn, T., and Cremonese, L., 2013, Redox changes in Early Cambrian black shales at Xiaotan section, Yunnan Province, South China: Precambrian Research, v. 225, no. 0, p. 166-189.

Ohnemueller, F., Meixner, A., Gamper, A., and Kasemann, S. A., 2013, Ocean-Ph Evolution and Weathering Conditions during the Ediacaran: Insights from B, Sr & Li Isotopes at the Gaojiashan Section, South China: Mineralogical Magazine, v. 77, no. 5, p. 1881.

Ohnemueller, F., Gamper, A., Meixner, A., Jiang, S.-Y., and Kasemann, S. A., in prep., Ocean pH and weathering conditions during the upper Ediacaran: Insights from the Chinese Gaojiashan Section.

Paytan, A., and McLaughlin, K., 2007, The oceanic phosphorus cycle: Chemical Reviews, v. 107, no. 2, p. 563-576.

Robinson, R. S., Kienast, M., Luiza Albuquerque, A., Altabet, M., Contreras, S., De Pol Holz, R., Dubois, N., Francois, R., Galbraith, E., Hsu, T.-C., Ivanochko, T., Jaccard, S., Kao, S.-J.,

Kiefer, T., Kienast, S., Lehmann, M., Martinez, P., McCarthy, M., Möbius, J., Pedersen, T., Quan, T. M., Ryabenko, E., Schmittner, A., Schneider, R., Schneider-Mor, A., Shigemitsu, M., Sinclair, D., Somes, C., Studer, A., Thunell, R., and Yang, J.-Y., 2012, A review of nitrogen isotopic alteration in marine sediments: Paleoceanography, v. 27, no. 4, p. PA4203.

Sachs, J. P., and Repeta, D. J., 1999, Oligotrophy and Nitrogen Fixation During Eastern Mediterranean Sapropel Events: Science, v. 286, no. 5449, p. 2485-2488.

Sawaki, Y., Ohno, T., Tahata, M., Komiya, T., Hirata, T., Maruyama, S., Windley, B. F., Han, J., Shu, D. G., and Li, Y., 2010, The Ediacaran radiogenic Sr isotope excursion in the Doushantuo Formation in the Three Gorges area, South China: Precambrian Research, v. 176, no. 1-4, p. 46-64.

Schubert, C. J., and Calvert, S. E., 2001, Nitrogen and carbon isotopic composition of marine and terrestrial organic matter in Arctic Ocean sediments: implications for nutrient utilization and organic matter composition: Deep Sea Research Part I: Oceanographic Research Papers, v. 48, no. 3, p. 789-810.

Shen, B., Xiao, S. H., Dong, L., Zhou, C. M., and Liu, J. B., 2007, Problematic macrofossils from Ediacaran successions in the North China and Chaidam blocks: Implications for their evolutionary roots and biostratigraphic significance: Journal of Paleontology, v. 81, no. 6, p. 1396-1411.

Shen, Y., 2002, C-isotope variations and paleoceanographic changes during the late Neoproterozoic on the Yangtze Platform, China: Precambrian Research, v. 113, no. 1–2, p. 121-133.

Shields-Zhou, G., and Zhu, M., 2013, Biogeochemical changes across the Ediacaran–Cambrian transition in South China: Precambrian Research, v. 225, no. 0, p. 1-6.

Shimura, T., Kon, Y., Sawaki, Y., Hirata, T., Han, J., Shu, D., and Komiya, T., 2014, In-situ analyses of phosphorus contents of carbonate minerals: Reconstruction of phosphorus contents of seawater from the Ediacaran to early Cambrian: Gondwana Research, v. 25, no. 3, p. 1090-1107.

Sigman, D. M., Altabet, M. A., McCorkle, D. C., Francois, R., and Fischer, G., 2000, The $\delta^{15}N$ of nitrate in the Southern Ocean: Nitrogen cycling and circulation in the ocean interior: Journal of Geophysical Research: Oceans, v. 105, no. C8, p. 19599-19614.

Smith, M. P., and Harper, D. A. T., 2013, Causes of the Cambrian Explosion: Science, v. 341, no. 6152, p. 1355-1356.

Spangenberg, J. E., Bagnoud-Velásquez, M., Boggiani, P. C., and Gaucher, C., 2014, Redox variations and bioproductivity in the Ediacaran: Evidence from inorganic and organic geochemistry of the Corumbá Group, Brazil: Gondwana Research, http://dx.doi.org/10.1016/j.gr.2013.08.014.

Struck, U., Emeis, K.-C., Voß, M., Krom, M. D., and Rau, G. H., 2001, Biological productivity during sapropel S5 formation in the Eastern Mediterranean Sea: Evidence from stable isotopes of nitrogen and carbon: Geochimica et Cosmochimica Acta, v. 65, no. 19, p. 3249-3266.

Struck, U., 2012, On The Use of Stable Nitrogen Isotopes in Present and Past Anoxic Environments, *in* Altenbach, A. V., Bernhard, J. M., and Seckbach, J., eds., Anoxia, Volume 21, Springer Netherlands, p. 497-513.

Thomazo, C., and Papineau, D., 2013, Biogeochemical Cycling of Nitrogen on the Early Earth: Elements, v. 9, no. 5, p. 345-351.

Tziperman, E., Halevy, I., Johnston, D. T., Knoll, A. H., and Schrag, D. P., 2011, Biologically induced initiation of Neoproterozoic snowball-Earth events: Proceedings of the National Academy of Sciences of the United States of America, v. 108, no. 37, p. 15091-15096.

Wang, J., Chen, D., Yan, D., Wei, H., and Xiang, L., 2012, Evolution from an anoxic to oxic deep ocean during the Ediacaran–Cambrian transition and implications for bioradiation: Chemical Geology, v. 306–307, no. 0, p. 129-138.

Warren, L. V., Fairchild, T. R., Gaucher, C., Boggiani, P. C., Poiré, D. G., Anelli, L. E., and Inchausti, J. C. G., 2011, Corumbella and in situ Cloudina in association with thrombolites in the Ediacaran Itapucumi Group, Paraguay: Terra Nova, v. 23, no. 6, p. 382-389.

Weber, B., Steiner, M., and Zhu, M.-Y., 2007, Precambrian–Cambrian trace fossils from the Yangtze Platform (South China) and the early evolution of bilaterian lifestyles: Palaeogeography, Palaeoclimatology, Palaeoecology, v. 254, no. 1-2, p. 328-349.

Werne, J. P., and Hollander, D. J., 2004, Balancing supply and demand: controls on carbon isotope fractionation in the Cariaco Basin (Venezuela) Younger Dryas to present: Marine Chemistry, v. 92, no. 1-4, p. 275-293.

Westerhausen, L., Poynter, J., Eglinton, G., Erlenkeuser, H., and Sarnthein, M., 1993, Marine and terrigenous origin of organic matter in modern sediments of the equatorial East Atlantic: the $\delta^{13}C$ and molecular record: Deep Sea Research Part I: Oceanographic Research Papers, v. 40, no. 5, p. 1087-1121.

Wille, M., Nagler, T. F., Lehmann, B., Schroder, S., and Kramers, J. D., 2008, Hydrogen sulphide release to surface waters at the Precambrian/Cambrian boundary: Nature, v. 453, no. 7196, p. 767-769.

Xiao, S., Schiffbauer, J. D., McFadden, K. A., and Hunter, J., 2010, Petrographic and SIMS pyrite sulfur isotope analyses of Ediacaran chert nodules: Implications for microbial processes in pyrite rim formation, silicification, and exceptional fossil preservation: Earth and Planetary Science Letters, v. 297, no. 3–4, p. 481-495.

Zhu, M., Zhang, J., and Yang, A., 2007, Integrated Ediacaran (Sinian) chronostratigraphy of South China: Palaeogeography, palaeoclimatology, Palaeoecology, v. 254, p. 7-61.

Zhuravlev, A. Y., Gámez Vintaned, J. A., and Ivantsov, A. Y., 2009, First finds of problematic Ediacaran fossil Gaojiashania in Siberia and its origin: Geological Magazine, v. 146, no. 5, p. 775–780.

7. EDIACARAN TO CAMBRIAN CHEMOSTRATIGRAPHY AND BIOGEOCHEMICAL CYCLING FROM CARBON AND NITROGEN ISOTOPES OF THE KYRSHABAKTY SECTION (SOUTHERN KAZAKHSTAN)

7.1 Abstract

The late Neoproterozoic and its transition to the Cambrian marks a time of drastic evolutionary and biogeochemical changes expressed in fluctuations of carbon and nitrogen isotope systems. However, to date high-resolution carbon and nitrogen isotope investigations have primarily concentrated on the Yangtze platform of South China; hitherto respective datasets from there thus lack global confirmation. To investigate the global significance and synchroneity of stable isotope records and their implications for oceanic biogeochemical perturbations, we present new isotope data ($\delta^{13}C_{carb}$, $\delta^{13}C_{org}$ and $\delta^{15}N$) from the ~200 m thick Kyrshabakty section of the Malyi Karatau Range, Kazakhstan. $\delta^{13}C_{carb}$ studies of the shallow-water section revealed three worldwide-correlative negative anomalies at (1) cap carbonate, (2) Shuram-Wonoka, and (3) Precambrian-Cambrian boundary level. They represent the first chemostratigraphic correlation of a Kazakh Ediacaran-Cambrian sequence to the global dataset. Low $\delta^{15}N$ data of Marinoan-age cap carbonates ($\delta^{15}N$ ~2‰) indicate a persistent N_2-fixing bacterial bloom in surface waters possibly initiated by rising pCO_2 in a beginning greenhouse climate. A negative $\delta^{13}C_{carb}$ interval down to -9.7‰ is consistent with an anoxic deep-ocean scenario proposed for the Shuram-Wonoka event. Decoupled $\delta^{13}C_{carb}$ and $\delta^{13}C_{org}$ systems agree with the stepwise oxygenation of a large DOC reservoir where active remineralization expands oxygen minimum zones and triggers nitrification-denitrification interactions. Elevated $\delta^{15}N$ data >3‰ reflect nitrate as the primary nutrient of planktonic organisms in surface and intermediate waters and thus argue for mildly oxygenated surface-water conditions. A pronounced negative $\delta^{13}C_{carb}$ and $\delta^{15}N$ excursion (down to -4.2 and -2.3‰, respectively) in the early Cambrian agrees with a widespread oceanic photic zone anoxia model and suggests a significant contribution of anoxygenic photosynthesis to the organic matter pool in intermittent euxinic photic zone

conditions. The negative $\delta^{15}N$ excursion confirms data of South China thus arguing for $\delta^{15}N$ signatures to represent a global signal.

Keywords: Precambrian-Cambrian, Malyi Karatau Range, carbon-nitrogen cycling, oceanic anoxia, photic zone euxinia, Kazakhstan

Highlights:

We present $\delta^{13}C_{carb}$, $\delta^{13}C_{org}$ and $\delta^{15}N$ data of the Kazakh sedimentary Kyrshabakty section.

We identify three negative $\delta^{13}C_{carb}$ excursions corresponding to the global cap carbonate, Shuram-Wonoka and Pc-C boundary anomalies.

Deposition of the cap carbonate is characterized by intensive nitrogen fixation in oxic surface waters potentially fuelled by elevated post-glacial pCO_2.

Low $\delta^{13}C_{carb}$ data, variable $\delta^{13}C_{org}$ and $\delta^{15}N$ values agree with a deep-ocean anoxia scenario including pulsed vertical fluctuations of the chemocline during the Shuram-Wonoka event.

Negative $\delta^{13}C_{carb}$ and $\delta^{15}N$ data in the lower Cambrian support an ocean anoxia setting and imply the presence of anoxygenic phototrophs in intermittent euxinic photic zone conditions.

7.2 Introduction

The Neoproterozoic advent of animals significantly changed the biogeochemical development of the Earth accompanied by glaciation events and numerous changes in the chemical composition of seawater (Halverson et al., 2005). The onset of metazoan life recorded in Ediacaran (*ca.* 635 - 542 Ma) strata is followed by a rapid metazoan diversification in the Cambrian (*ca.* 542 - 485 Ma) which is proposed to be likely a result of a complex interplay between abiotic and biotic processes (Johnston et al., 2012; Smith and Harper, 2013) in which an increased availability of oxygen in the Ediacaran ocean is thought to play a central role (e.g. Canfield et al., 2007). Recent carbonate carbon ($\delta^{13}C_{carb}$) and nitrogen ($\delta^{15}N$) isotope studies of Ediacaran to Cambrian successions revealed prominent negative $\delta^{13}C_{carb}$ and $\delta^{15}N$ anomalies likely due to strong compositional oceanographic perturbations (Jiang et al., 2007; Zhu et al., 2007; Kunimitsu et al., 2011; Cremonese et al., 2013; Li et al., 2013; Lu et al., 2013; Cremonese et al., 2014; Kikumoto et al., 2014) closely linked to biological evolutionary events (Fike et al., 2006; Wang et al., 2012a). Despite the ongoing debate, a stratified ocean model with anoxic bottom waters accompanied by a strong surface-to-deep-marine $\delta^{13}C_{carb}$ gradient during late Ediacaran times (Jiang et al., 2007; Li et al., 2010) and the subsequent migration of anoxic waters to shallow-marine environments represent probably major factors affecting biochemical cycles and the following "Cambrian radiation event" (Kimura and Watanabe, 2001; Ishikawa et al., 2008; Cremonese et al., 2013). Alternative scenarios intimately link biogeochemical perturbations and the co-occurring radiation of the Cambrian biosphere to the release of methane hydrates (Kirschvink and Raub, 2003; Bjerrum and Canfield, 2011) and the evolution of fecal pellet production by animals (Rothman et al., 2003).

Although subdivisions of the Ediacaran and Cambrian period are predominantly biostratigraphically defined, chemostratigraphic correlations adapted from three significant and global distributed negative $\delta^{13}C_{carb}$ isotope anomalies support biostratigraphical analyses: (1) The "cap carbonate" anomaly, (2) the "Shuram-Wonoka" anomaly and (3) the Precambrian-Cambrian boundary anomaly (e.g. Halverson et al., 2005; Le Guerroué et al., 2006; Zhu et al., 2007). Especially the

widespread $\delta^{13}C_{carb}$ negative excursion down to ~-10‰ (Maloof et al., 2005; Ishikawa et al., 2008; Halverson et al., 2010) across the Precambrian-Cambrian (Pc-C) boundary is a widely acknowledged chemostratigraphic marker because it follows the extinction of the late Ediacaran and earliest calcareous metazoan index fossil *Cloudina* (e.g. Amthor et al., 2003; Zhu et al., 2003) and predates the first occurrence of the lower Cambrian global GSSP index fossil *Treptichnus/Trichophycus pedum* (e.g. Brasier et al., 1994; Narbonne et al., 1994; Li et al., 2013).

Nevertheless, the correlation, synchroneity and primary origin of the Ediacaran-Cambrian isotopic anomalies are still discussed. Especially, strong Mid-Ediacaran $\delta^{13}C_{carb}$ isotope excursions are speculated to be of diagenetic origin (Knauth and Kennedy, 2009; Derry, 2010). To address this controversy, several high-resolution carbon isotopic records spanning Ediacaran to Cambrian strata have been published for sections in South China (Jiang et al., 2007; Zhu et al., 2007; Ishikawa et al., 2013) owing to the good preservation of deposits, low diagenetic overprint and a well-constrained biostratigraphic framework for global correlation there. Nitrogen isotope investigations, in contrast, are rare to date; high-resolution records only exist for the South China craton (Cremonese et al., 2013; Cremonese et al., 2014; Kikumoto et al., 2014).

Here, we add a new section to the growing framework of the Pc-C boundary interval, located on the Kazakh microcontinent which is suggested to have been closely associated to the South China craton and Paleo-Siberia (Pradhan et al., 2009; Weber et al., 2013). The geological record in the Malyi Karatau area of southern Kazakhstan records remarkably well-preserved rocks characterized by relatively unaltered sequences spanning from the late Cryogenian to the Cambrian. They offer ideal conditions for isotope studies (Meert et al., 2011). Yet, Ediacaran and Cambrian strata remained geochemically poorly investigated and have been predominantly studied for their fossil content (Weber et al., 2013). Here, we report the first integrated multi-proxy and high-resolution isotopic dataset ($\delta^{13}C_{carb}$, $\delta^{13}C_{org}$ and $\delta^{15}N$) from well-preserved sedimentary rocks at the Ediacaran to Cambrian Kyrshabakty section of the Malyi Karatau Range. We identify three significant $\delta^{13}C_{carb}$ negative excursions qualified for global

chemostratigraphic correlation and characterize biogeochemical conditions during each interval.

We apply the nitrogen isotopic proxy to the Kazakh Pc-C interval to test its application for global ocean redox conditions because nitrogen isotope compositions of sedimentary rocks illustrate specific biosignatures in the water column which are strongly dependent on the redox state of the ocean (Canfield et al., 2010; Thomazo and Papineau, 2013; Ader et al., 2014). Sedimentary nitrogen isotopes have shown to be a good indicator for biogeochemical and paleoenvironmental reconstruction (e.g. Peterson and Fry, 1987; Cremonese et al., 2013; Ader et al., 2014) because they show resiliance to secondary alteration effects by microbial processes during burial diagenesis and other diagenetic and low-grade metamorphic reactions (Robinson et al., 2012; Thomazo and Papineau, 2013). Because the marine biogeochemistry of nitrogen is strongly dependent on redox reactions predominantly mediated by microorganisms (Canfield et al., 2010), nitrogen isotope variability is closely linked to the oxygenation of the Earth's atmosphere and oceans and the microbial assemblages involved (Thomazo and Papineau, 2013). Dissolved nitrogen species (e.g. dinitrogen (N_2), nitrate (NO_3^-), ammonium (NH_4^+)) potentially experience several biological transformation processes (e.g. N_2-fixation, nitrification, denitrification, ammonification) with respective different isotopic fractionations and are finally transported as particles to the sediments where they are predominantly preserved as organic nitrogen but can as well be present as inorganic nitrogen bound to phyllosilicates (for detailed reviews see Canfield et al., 2010; Robinson et al., 2012; Cremonese et al., 2013). As a consequence, the biological-controlled nitrogen transformation process in the ocean imprints its specific isotope signature to the sediment.

NO_3^- assimilation by photoautotrophs is typically mirrored by sedimentary $\delta^{15}N$ values of 3 to 8‰ due to their uptake of ^{15}N-enriched deep-water NO_3^- with initial $\delta^{15}N$ ratios of ~5‰ (Cline and Kaplan, 1975; Sigman et al., 2000; Sigman et al., 2009; Struck, 2012). Once nitrate is consumed and depleted, nitrogen becomes bioavailable in the course of N_2-fixation, characterized by low $\delta^{15}N$ values (~0‰) due to the initial fixation of atmospheric N_2 ($\delta^{15}N$ = 0‰ per definition) by so-

called diazotrophic organisms and an associated low-isotopic fractionation effect (Carpenter et al., 1997; Montoya et al., 2002; Struck, 2012). In a reduced anaerobic environment, photoautotrophs are depleted in ^{15}N due to their assimilation of NH_4^+, a process which is associated with a large isotope effect resulting in strongly ^{15}N-depleted organic matter (Hoch et al., 1992; Sigman et al., 2009). High denitrification rates in the water column and at the sediment-water interface are recognized by elevated sedimentary $\delta^{15}N$ values from 8 to 12‰ (Struck, 2012). However, denitrification itself requires the presence of NO_3^- which in turn is strongly dependent on the availability of oxygen and NH_4^+ vital for nitrification and thus already implying the complexity of the nitrogen cycle (Canfield et al., 2010).

7.3 Geological setting

7.3.1 Stratigraphical framework

The Karatau Orogen is located in southern Kazakhstan building the northwestern branch of the Tien Shan Mountains of Central Asia; it forms part of the Central Asian Orogenic Belt (CAOB; Alexeiev et al., 2009; Levashova et al., 2011). The CAOB reaches from the Ural Mountains through Kazakhstan via the Tien Shan, the Altaids, and Mongolia to the Pacific and comprises several Precambrian microcontinental blocks which amalgamated during the Neoproterozoic and Paleozoic (Levashova et al., 2011). The deformation history of the CAOB is complex. Tectonic activity resulted in an Early to Late Paleozoic thrust-and-fold belt structure culminating in the formation of the Late Paleozoic Ural - Tien Shan junction (Fig. 17) which comprises the Karatau Ridge (Alexeiev et al., 2009). Today, microcontinents with Precambrian basement of the CAOB are mainly distributed in the area of central Kazakhstan and the Tien Shan (Meert et al., 2011). Kazakh microcontinents were suggested to be located in near-equatorial latitudes between Siberia and South China during the early Cambrian (Pradhan et al., 2009; Weber et al., 2013). A close association to South China is supported by similarities in ichnofacies and depositional regimes. While Paleo-Kazakhstan is suggested to have been an island arc, the South China

Yangtze platform, on the other hand, represents a continental shelf area which was separated by a narrow oceanic basin from Paleo-Kazakhstan (Weber et al., 2013).

The Karatau Range is separated into the Bolshoi (Greater) Karatau in the southwest and the Malyi (Lesser) Karatau in the northeast (Alexeiev et al., 2009), including the study area (Fig. 17). Tectonic deformation of the Karatau area mainly took place in three phases from the late Carboniferous through the early Mesozoic, leading to a complex thrust-and-fold architecture along the NW-SE trending Karatau fault. However, faulting and metamorphism dominantly affected the Bolshoi Karatau area whereas late Neoproterozoic - early Cambrian strata of the NE-vergent Malyi Karatau belt were affected to a lesser degree (Alexeiev et al., 2009; Weber et al., 2013).

7.3.2 Regional stratigraphy - the Kyrshabakty section

The Kyrshabakty section is located ~18 km E, the Berkuty section ~5 km N of Zhanatas, both within the Malyi Karatau Range (Fig. 17). The section comprises (in ascending order) the Kurgan Formation of the Malokaroy Series followed by the Kyrshabakty, Chulaktau and Shabakty Formations of the Tamdy Series (Eganov et al., 1986; Levashova et al., 2011).

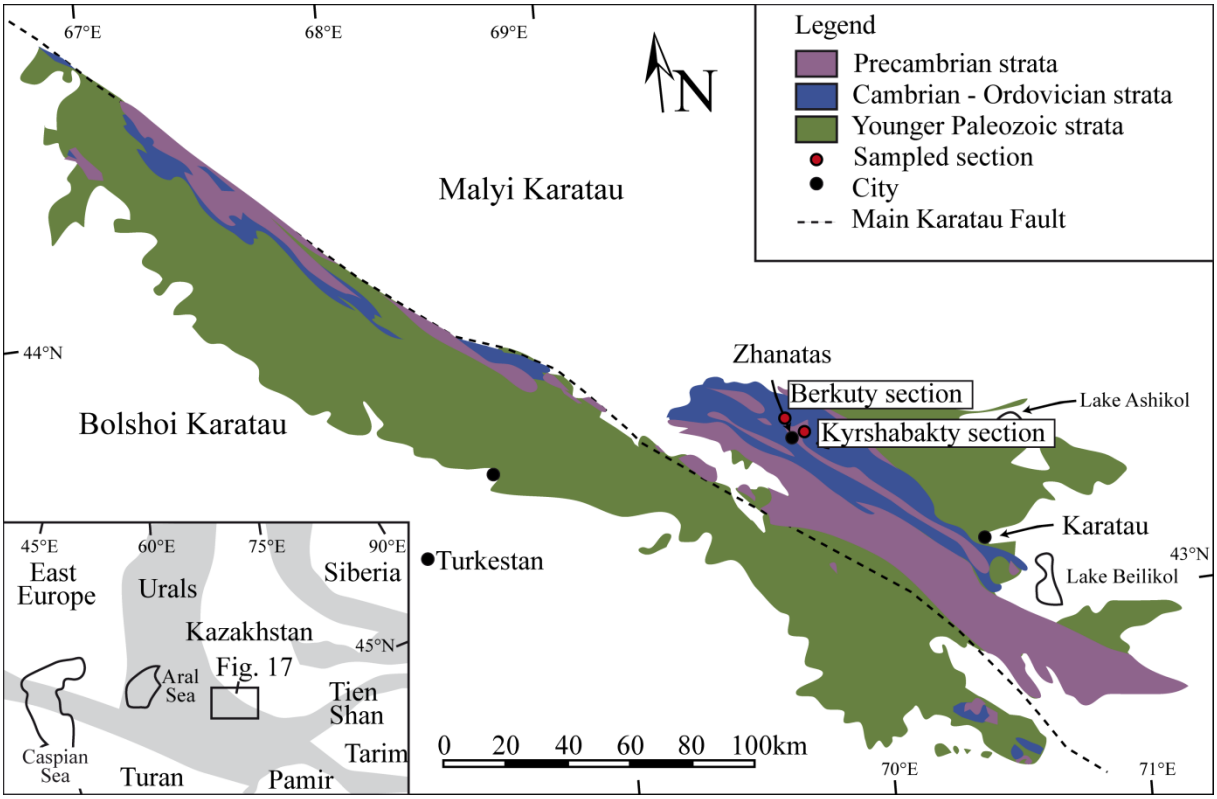

Figure 17: Geological map of the Karatau Range including a sketch map of the Ural - Tien Shan junction (grey color represents late Paleozoic to early Mesozoic thrust-and-fold belts); both adapted from Alexeiev et al. (2009). The NW-SE trending Karatau fault separates the Malyi Karatau from the Bolshoi Karatau. The study areas (red circles) are located close to the town of Zhanatas in the Malyi Karatau and comprises the Berkuty section in the north and the Kyrshabakty section to the east.

The basal section consists of volcano-sedimentary rocks of the Cryogenian Kurgan Formation (Meert et al., 2011) dated to 766 ± 7 Ma near the top of a nearby section (Levashova et al., 2011). Strata are overlain by Ediacaran to Cambrian siliciclastics and carbonates of the Tamdy Series representing a shallow-marine to coastal environment (Eganov et al., 1986; Popov et al., 2009; Weber et al., 2013). The Kyrshabakty Formation comprises at its base *ca.* 50 m of glacial deposits ("Aktas Tillite") which are unconformable overlain by a well exposed, finely-laminated, ~5 m thick pinkish "cap carbonate" of Marinoan age

(Meert et al., 2011) predominantly consisting of dolomite. Mixed siliciclastic-limestone sequences overlie the cap carbonate and are dominated by reddish dolomitic sandstones in the lower part followed by more common beige sandy limestone beds in the upper part. After ~20 m of unexposed strata, ~6 m thick, grey dolostones of the Berkuty Member represent the upper Kyrshabakty Formation. Heubeck et al. (2013) recently subdivided the Berkuty Member from nearby sections into three parts and interpreted the middle unit as a megabreccia resulting from seismic deformation. The Kyrshabakty section, however, shows no comparable sedimentological features (e.g. brittle and ductile structures). The upper part of the dolomitic Berkuty Member commonly shows phosphate and chert-lenses as well as SSFs of *Protohertzina anabarica* (ca. 0.7 m below the Aksai Member) which assign the horizon to the earliest Cambrian (C. Seidig, pers. comm.; Popov et al., 2009; Weber et al., 2013). Biostratigraphy in the Malyi Karatau is largely limited to well-preserved Cambrian fossil assemblages due to the wide lack of Ediacaran fossils. This, together with the paucity of radiometric data and of a profound chemostratigraphic record has made the accurate location of the Pc-C boundary in the Malyi Karatau uncertain. The Berkuty Member is overlain by intercalations of phosphate and (cherty) dolostone layers of the lower Cambrian Chulaktau Formation and comprises a variably colored ~1 m-thick chert horizon (Aksai Member) at the base. The Chulaktau Formation is followed by thick-bedded dolo- and limestone sequences of the Shabakty Formation. Biostratigraphic analyses of Weber et al. (2013) correlated the Chulaktau and Shabakty Formation to the upper Fortunian, Stage 2 and Stage 3. However, at Kyrshabakty section, strata of the lower Cambrian are condensed and not continuous exposed.

7.4 Analytical methods and materials

Samples for isotopic analyses were collected at two adjacent sections, the Kyrshabakty section and the Berkuty section (Fig. 17). The sample suite from the Kyrshabakty section comprises 62 samples (Ediacaran-Cambrian-age) collected every 0.2 to 1 m along a ~200 m long transect. The section was continuously sampled except for three intervals at 62 - 76 m, 93 - 107 m and 141 - 160 m (Fig. 18) where strata were not exposed.

At Berkuty section, 54 samples were collected from two units: The cap carbonate unit and the Berkuty Member. Both units correspond to the same unit at Kyrshabakty section. Therefore, the dataset of Berkuty section is readily integrated in the discussion and interpretation part of the isotopic dataset from Kyrshabakty section. Due to the different thicknesses of the respective units at the two sections, we present an approximate stratigraphic position for the Berkuty section data relative to the Kyrshabakty stratigraphic column and mark data points of Berkuty section by grey shaded circles in Figure 18.

Isotopic analyses were conducted at the Museum für Naturkunde Berlin, Germany. Prior to isotope measurements, rock samples were cleaned and cut into rock chips to minimize and eliminate sample contamination by secondary alteration marks or veining. Powdered samples were analyzed for their carbonate carbon ($\delta^{13}C_{carb}$) and oxygen ($\delta^{18}O$) isotopic composition using a Thermo Finnigan Gasbench II coupled online with a Thermo Finnigan Delta V isotope ratio mass spectrometer. 100 - 400 µg sample powder were filled in exetainers, sealed and flushed with helium for 5 min at a flow of 100 ml/min to remove the remaining air. Afterwards 30 µl of anhydrous phosphoric acid was added for 1.5 h to extract carbon dioxide (CO_2.). For carbon and oxygen elemental analyses pure CO_2 serves as reference gas calibrated against Vienna PeeDee Belemnite (VPDB) standard by using IAEA reference materials (NBS 18, NBS 19). Isotope values are presented in delta notation ($\delta^{13}C_{carb}$ and $\delta^{18}O$) in per mil (‰) relative to VPDB standard. The reproducibility of replicate measurements (one standard deviation) of the internal lab standard (limestone) is within 0.1‰.

For stable isotope measurement of organic carbon ($\delta^{13}C_{org}$) and nitrogen ($\delta^{15}N$) 2 to 14 g sample powder (depending on carbonate content) were decalcified using 2 M hydrochloric acid at room temperature until the carbonate fraction was removed. Acid residues were centrifuged and samples were rinsed with distilled water and afterwards dried at 40°C in glass tubes. Due to average low nitrogen contents in respective bulk samples (<0.1 mgN/sample) and resulting low data accuracy decalcified sample powder was analyzed instead of bulk sample powder to obtain representative $\delta^{15}N$ values due to enhanced concentration of organic matter after decalcification processes. This procedure is known for isotopic measurements of rocks containing low nitrogen content like Precambrian rocks (Thomazo et al., 2011) or Devonian samples (Sliwinski et al., 2011). The performance of $\delta^{15}N$ measurements on sedimentary samples with low nitrogen content has been shown to yield reliable isotope signatures (Bahlmann et al., 2010). Stable isotope ratio measurements were performed by elemental analyzer - isotope ratio mass spectrometry (EA-IRMS) using a Thermo Finnigan MAT V isotope ratio mass spectrometer coupled to a Thermo Flash EA 1112 elemental analyzer via a Thermo Finnigan Conflo III-interface. Isotope ratios are expressed in the conventional delta notation ($\delta^{15}N$, $\delta^{13}C_{org}$) in per mil (‰) relative to AIR and VPDB standard, respectively. 100 - 150 mg sample powder was packed in tin capsules and combusted at 1200°C in the EA for converting the nitrogen and organic carbon of the sample into N_2 and CO_2 and afterwards chromatographically separated in the EA. Helium is used as a carrier gas to transport the sample residue into the IRMS. We used a detection length of 1000 s with two blank measurements after each sample to ensure complete combustion of the material and minimizing an afterwards sample contamination. The internal reproducibility was obtained by measuring the internal standard material (peptone) after every fourth sample. Standard deviation for repeated measurements of laboratory standard material (peptone) is generally better than 0.2‰. For $\delta^{13}C_{org}$ measurements we applied a He dilution of 60%. Due to low accuracy of $\delta^{15}N$ and $\delta^{13}C_{org}$ signals in samples containing <0.010 mgN/sample and <0.010 mgC/sample respective isotopic values are not considered in the interpretation and are therefore not listed in Table 7 and 8. TOC contents of

samples were determined by EA-IRMS. The analytical error is within 3% of the material analyzed.

7.5 Results

Isotope data from Kyrshabakty section are summarized in Table 7; data from Berkuty section are listed in Table 8.

Table 7: Stable isotope ($\delta^{13}C_{carb}$*,* $\delta^{13}C_{org}$*,* $\delta^{15}N$*,* $\delta^{18}O$*) and TOC data of the Precambrian to Cambrian succession at Kyrshabakty section in the Malyi Karatau area. KY/KR: Kyrshabakty.*

Sample	Distance [m]	$\delta^{13}C_{carb}$ [‰] vs. VPDB	$\delta^{13}C_{org}$ [‰] vs. VPDB	$\delta^{15}N$ [‰] vs. AIR	$\delta^{18}O$ [‰] vs. VPDB	TOC [%]
KY 1	0.0		-34.1			0.016
KY 2	47.5					0.012
KY 3	58.4	-0.1	-23.0		-3.4	0.043
KY 4	58.6	-0.7	-31.0		-4.3	0.015
KY 5a	58.8	-1.4	-32.6	2.4	-4.5	0.014
KY 6b	59.3	-1.7	-28.1	1.8	-4.4	0.002
KY 7a	59.7	-2.4	-26.3	2.1	-5.0	0.005
KY 8	60.5	-1.3	-32.1	2.9		0.004
KY 9	61.6	-2.6	-28.4	0.5	-5.0	0.004
KY 10	61.9	-1.0	-30.6	1.9	-4.2	
KY 11	77.7	0.0	-34.2	3.2	-4.3	0.027
KY 13	87.9	1.3	-31.2	3.4	-7.3	0.012
KY 14	88.5	0.4	-33.3	3.1		0.012
KY 15	89.1	-0.6	-34.4	2.3		0.004
KY 16	89.2	-0.8	-29.7	3.9	-7.8	0.011
KY 17	92.5	0.0	-36.2	3.6		0.040
KY 18	107.2	-7.9	-30.1		-9.0	0.001
KY 19	107.7	-9.3	-30.8	3.1	-10.1	0.015
KY 20	114.2	-8.4	-30.0			
KY 21	115.3	-7.6	-24.1		-8.5	0.006
KY 22	117.7	-9.5	-24.2	1.6	-11.3	0.007
KY 23	118.9	-9.7	-30.4	3.2	-11.2	0.003
KY 24	120.4	-8.2	-30.7			0.003
KY 25	122.6	-7.7	-26.0		-8.8	0.004
KY 26	123.9	-7.7	-27.0			0.008
KY 27	125.5	-6.3	-26.1	1.6		0.003
KY 28	126.9	-6.3	-33.0	2.8	-7.7	0.005
KY 29	127.7	-7.7	-27.5	2.5		0.006
KY 30	128.7	-7.1	-30.1	3.7		0.015
KY 31	129.5	-5.8	-27.4	2.4		0.006
KY 33	135.6	-7.0	-30.9		-7.7	0.076
KY 34	136.1	-6.9	-30.9	1.9		0.049

Table 7 (continued)

Sample	Distance [m]	$\delta^{13}C_{carb}$ [‰] vs. VPDB	$\delta^{13}C_{org}$ [‰] vs. VPDB	$\delta^{15}N$ [‰] vs. AIR	$\delta^{18}O$ [‰] vs. VPDB	TOC [%]
KY 35	138.7	-6.9	-32.2	3.4	-7.2	0.033
KY 36	139.0	-4.6	-30.8	3.3	-4.6	0.041
KY 37	140.5	-4.9	-28.3	3.5	-5.5	0.026
KY 38	166.3	2.7	-30.4	1.8		0.008
KY 39	166.9	4.3	-32.4	1.2	-0.4	0.006
KY 41	168.2	3.3	-33.9	1.7	-2.3	0.009
KY 42	168.3	2.4	-30.2	2.1	-3.2	0.008
KY 43	168.5	2.1	-31.8	1.0	-3.5	0.004
KY 44	169.1	2.6	-31.2	0.9	-3.1	0.007
KY 45	169.3	0.5	-31.1	1.2	-4.1	0.005
KY 46	169.8	0.6	-31.0	2.2	-3.0	0.020
KY 47	169.9	-1.8	-32.7	0.8	-4.7	0.008
KR-11-02	170.9	-6.8	-34.7		-9.7	0.081
KY 48	170.9	1.5	-29.0	1.0		0.006
KY 49	172.2	-2.2			-5.8	
KY 50	172.6	-6.1	-37.5		-8.2	0.335
KY 51	173.5	-5.2	-32.1	1.1		0.454
KR-11-03	175.6	-5.9	-32.7	1.2	-8.1	0.105
KY 52	179.8	-3.8	-32.5		-6.9	0.080
KY 53	179.8	-1.4	-31.9	-0.8	-3.3	0.045
KR-11-07	181.1	-6.7	-33.2	3.8	-7.8	0.323
KY 54	183.0	-4.2	-25.7			0.036
KY 55	184.3	-2.4	-30.7	0.2	-6.9	0.132
KY 56	184.9	-1.1	-33.0	2.1		0.093
KY 57	185.4	0.7	-33.4	-0.9	-2.3	0.027
KR-11-12	187.7	-6.0	-35.2	0.1	-6.6	0.198
KY 58	188.3	-3.5	-32.1	-1.8	-7.5	0.001
KY 59	189.0	-0.9	-29.4	-1.3		0.087
KY 60	191.8	0.5			-3.2	
KY 61	192.8	-3.4	-32.0	-0.3	-7.2	0.048
KY 62a	193.9	-3.3	-31.6	-0.9	-7.8	0.071
KY 62c	193.9	0.8	-31.7	-2.3	-4.4	0.055
KY 63a	194.6	-0.6	-33.7	-1.5	-4.3	0.044
KY 63c	194.7	0.5	-31.7	-1.3	-3.7	0.055
KR-11-16	194.8	-6.9	-33.9	0.2	-12.1	0.118
KY 64	198.2	-0.9	-34.7	-1.4		0.003
KR-11-18	204.1	-3.2	-32.9		-4.2	0.099
KR-11-20	215.3	-4.8	-30.8	0.9	-9.0	0.086

Table 8: Stable isotope composition ($\delta^{13}C_{carb}$, $\delta^{13}C_{org}$, *$\delta^{15}N$,* $\delta^{18}O$*) and TOC data of strata from Berkuty section with corresponding transferred meters to the cap carbonate unit and Berkuty Member at Kyrshabakty section. BK: Berkuty.*

Sample	Distance [m]	$\delta^{13}C_{carb}$ [‰] vs. VPDB	$\delta^{13}C_{org}$ [‰] vs. VPDB	$\delta^{15}N$ [‰] vs. AIR	$\delta^{18}O$ [‰] vs. VPDB	TOC [%]
BK 1a	59.1	-2.2	-21.9		-5.3	0.011
BK 1b	59.1	-1.7			-4.8	
BK 1c	59.1	-1.5			-4.7	
BK 1d	59.2	-1.3			-4.6	
BK 2a	59.4	-1.5			-5.1	
BK 2b	59.4	-1.3			-5.1	
BK 2c	59.4	-1.3			-4.8	
BK 2d	59.5	-1.1			-4.4	
BK 3	59.7	-2.9	-29.0	1.6	-5.6	0.002
BK 4a	60.1	-1.1	-31.4			0.002
BK 4b	60.1	-3.0			-5.2	
BK 4c	60.1	-1.0				
BK 4d	60.2	-0.7				
BK 5	60.3	-3.3				
BK 5c	60.3	-2.9			-5.2	
BK 6a	60.4	-2.3	-28.7	0.8	-5.2	0.002
BK 6b	60.4	-2.2				
BK 6c	60.4	-1.8				
BK 6d	60.5	-2.0			-4.3	
BK 7	60.6	-2.7			-5.5	
BK 8a	60.8	-0.8	-24.6	2.6		0.005
BK 8b	60.9	-0.4				
BK 8c	60.9	0.0				
BK 8d	60.9	-0.9			-3.4	
BK 9	60.9	-2.2			-4.9	
BK 11a	59.1	-0.7				
BK 11c	59.1	-2.2			-4.8	
BK 11d	59.1	-1.5				
BK 13	59.3	-2.3			-5.0	
BK 14	59.9	-1.8	-29.8			0.002
BK 21	168.6	1.5	-28.8	2.9		0.002
BK 22	168.3	3.0	-30.4	0.4		0.004
BK 23	167.9	3.2				
BK 24	167.6	0.7	-26.4	0.2	-4.0	0.002
BK 25	167.3	2.3			-1.9	
BK 26	166.9	2.1	-27.0	1.4	0.2	0.003
BK 27	166.6	2.0			-0.8	
BK 28	166.3	1.1	-25.7	0.9	-1.0	0.003

We present isotopic data from the Berkuty section to verify the isotopic results of Kyrshabakty section on regional scale but do not separately discuss the Berkuty dataset because of similar isotopic trends. For convenience, we separated the section into three parts according to the occurrence of the $\delta^{13}C_{carb}$ negative intervals (C1 - C3): Part 1 (C1, 0 to 92.5 m), part 2 (C2, 107.2 to 140.5 m) and part 3 (C3, 166.3 to 215.3 m; Fig. 18).

7.5.1 Part 1

Cap carbonate strata show a gradually upwards decreasing trend in both $\delta^{13}C_{carb}$ and $\delta^{13}C_{org}$ data with a prominent negative $\delta^{13}C_{carb}$ excursion from ~0‰ down to -2.6‰ (C1; Fig. 18). $\delta^{13}C_{org}$ values of -23‰ at the base decrease to ~-32‰ at the upper cap carbonate unit with TOC values displaying a variable trend from 0.043% to 0.004%. $\delta^{15}N$ compositions span from 0.5‰ to 2.9‰ (Fig. 18); $\delta^{18}O$ is stable at ~-5‰ (Table 7). Throughout overlying red dolomitic sandstone strata $\delta^{13}C_{carb}$ values increase to 0‰ with $\delta^{13}C_{org}$ decreasing to -36.2‰ and $\delta^{18}O$ to -7.8‰. TOC values rise to 0.04% at the top of part 1 whereas $\delta^{15}N$ values steady at ~ 3.3‰.

7.5.2 Part 2

Persistent negative $\delta^{13}C_{carb}$ compositions (C2; Fig. 18) evolve in sandy limestones of part 2 beginning with -7.9‰ at the base, followed by a nadir at -9.7‰ and a gradual increase to -4.6‰ towards the top. $\delta^{13}C_{carb}$ data show a positive correlation with $\delta^{18}O$ (nadir -11.3‰; Table 7) and no correlation with $\delta^{13}C_{org}$ values which instead display fluctuations from -33.0‰ to -24.1‰. $\delta^{15}N$ data flexibly span from 1.6 to 3.7‰ (Fig. 18). TOC compositions show consistent low (~0.003%) concentrations which smoothly increase to 0.076% in the middle and decrease again to 0.026% in the upper part.

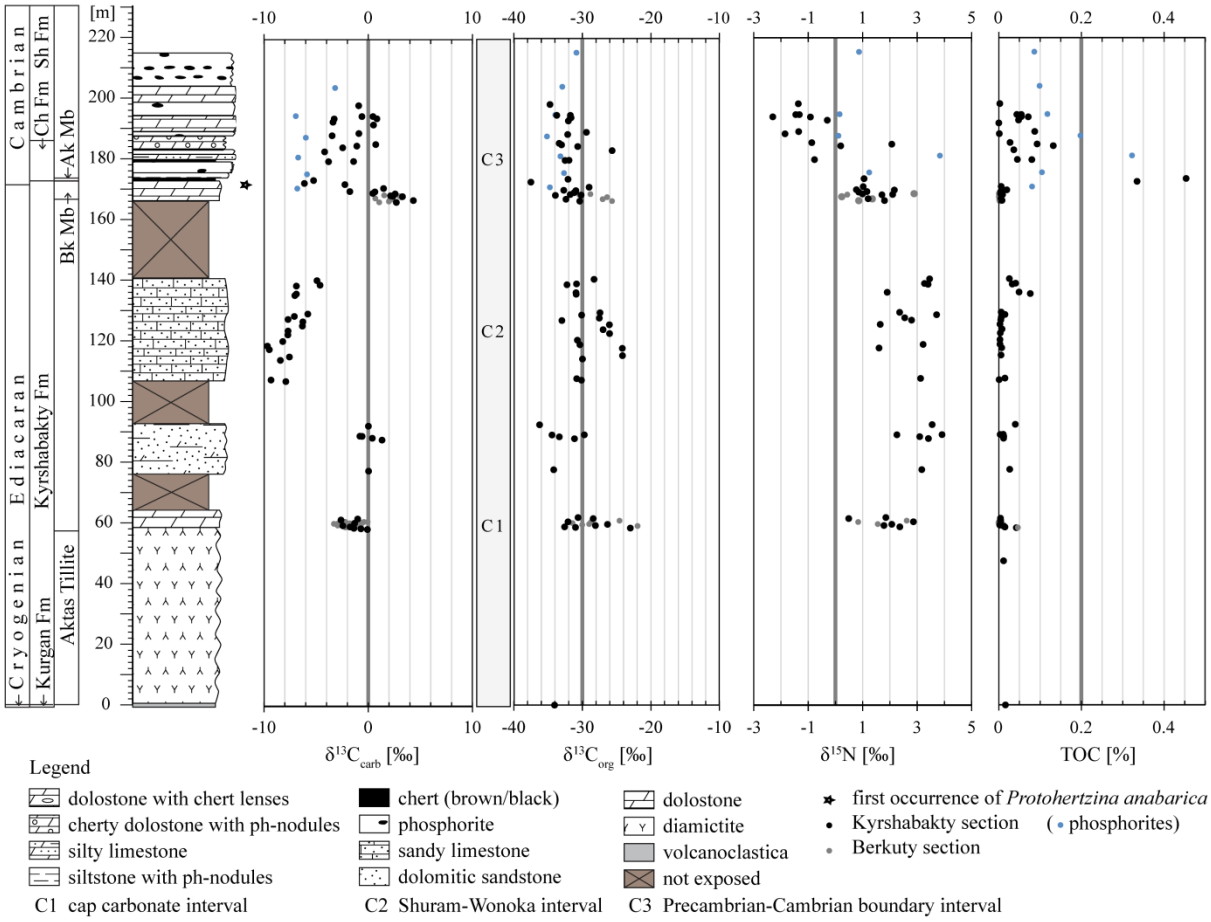

Figure 18: Lithostratigraphic column combined to carbonate carbon, organic carbon and nitrogen isotopic profiles as well as TOC concentration of the Ediacaran to Cambrian Kyrshabakty, Chulaktau and Shabakty Formation from the Kyrshabakty (black circles) and Berkuty (grey circles) sections (Malyi Karatau). Inferred age constraints for the cap carbonate unit are from Meert et al. (2011). The occurrence of SSFs is taken from C. Seidig (pers. comm.). Notice three prominent negative $\delta^{13}C_{carb}$ excursions (C1 - C3) evolving in strata comprising the cap carbonate (C1), the Shuram-Wonoka (C2) and the Precambrian-Cambrian boundary (C3) interval. Notice the lack of correlation between $\delta^{13}C_{carb}$ and $\delta^{13}C_{org}$ throughout C2. During the Pc-C boundary event a remarkable $\delta^{15}N$ negative excursion developed persisting through early Cambrian strata. Ch Fm: Chulaktau Formation, Sh Fm: Shabakty Formation, Bk Mb: Berkuty Member, Ak Mb: Aksai Member.

7.5.3 Part 3

Berkuty Member dolostones mark high $\delta^{13}C_{carb}$ and $\delta^{18}O$ values (up to 4.3‰ and -0.4‰, respectively) followed by an upwards smoothly decrease to -2.2‰ in $\delta^{13}C_{carb}$ and -5.8‰ in $\delta^{18}O$ (C3, Fig. 18; Table 7). $\delta^{13}C_{org}$ values fluctuate around -32‰ displaying in general lower values than in part 2 whereas $\delta^{15}N$ data are remarkably consistent from 0.8 to 2.2‰; TOC contents are low (~0.008%). Dolostones of the Chulaktau and Shabakty Formation display predominantly negative $\delta^{13}C_{carb}$ compositions (-4.2 to 0.5‰) with $\delta^{13}C_{org}$ data remaining variable

around -32‰ (Fig. 18) and fluctuating $\delta^{18}O$ data (Table 7). $\delta^{15}N$ data show a remarkable distinct negative trend down as low as -2.3‰. TOC concentrations of Cambrian strata are noticeable higher (average TOC concentration 0.110%). In contrast to dolomitic strata, intercalated phosphorite layers display strictly positive $\delta^{15}N$ values and low $\delta^{13}C_{carb}$ values (down to -6.9‰) whereas $\delta^{13}C_{org}$ data do not profoundly differ from dolomitic parts.

7.6 Discussion

7.6.1 Estimating a diagenetic overprint

Isotope data of rocks at Kyrshabakty section suggest that post-depositional alteration and substantial diagenetic or metamorphic overprint did not significantly change primary isotopic signals or caused the decoupling of biogeochemical cycles. Our opinion is based on the following arguments:

First, the majority of $\delta^{18}O$ values (Table 7, 8) does not exceed -10‰ which serves as the conventional criterion for a non-diagenetic origin for Pc-C isotope values (Li et al., 2013). Furthermore, $\delta^{18}O$ values are consistent with previous results from Kazakhstan (Meert et al., 2011) and other Pc-C records from South China (e.g. Jiang et al., 2007; Sawaki et al., 2014). Only two $\delta^{18}O$ values in part 2 (Shuram-Wonoka interval) fall below -10‰ (~-11‰; KY22, KY23; Table 7) and correlate with lowest $\delta^{13}C_{carb}$ data (~-9‰; Table 7) suggesting a possibly minor modification of isotope values by diagenesis in this part (Knauth and Kennedy, 2009; Derry, 2010). In general, there is good correlation of $\delta^{13}C_{carb}$ and $\delta^{18}O$ values in part 2 and 3. Post-depositional alteration can result in coupled oxygen and carbon ratios (Knauth and Kennedy, 2009; Derry, 2010); however, there also exist counter-examples (Kasemann et al., 2005; Halverson et al., 2007). If the $\delta^{13}C_{carb}$ signal is accepted to be pristine, obtained low $\delta^{18}O$ values seem to be of primary origin too, especially while considering the general long-term increase of $\delta^{18}O$ values from -8‰ to ~0‰ in the course of the Phanerozoic which suggests that the ocean water became progressively enriched in ^{18}O over time (Veizer et al., 1997; Veizer et al., 1999).

Second, the variation of $\delta^{13}C_{org}$ data (shift of ~14‰) largely exceeds the change biodegradation would cause (within 1 - 3‰) thus arguing for a primary origin of $\delta^{13}C_{org}$ isotopic signatures (Ader et al., 2009; Jiang et al., 2010). Additionally, there is no (negative) correlation between $\delta^{13}C_{org}$ and TOC observed which would be expected if diagenetic and metamorphic degradation had affected organic matter (Ishikawa et al., 2013).

Third, post-depositional alteration processes (e.g. bacterial degradation and low-metamorphic processes) shifting the $\delta^{15}N$ value about <1 to 3‰ (Robinson et al., 2012; Thomazo and Papineau, 2013) are too insignificant to explain the large $\delta^{15}N$ negative excursion in the upper part (Fig. 18). Furthermore, there is no significant correlation between $\delta^{15}N$ and TN content indicating the lack of nitrogen loss during burial diagenesis and metamorphism (Busigny et al., 2013). Additionally, a significant falsification of $\delta^{15}N$ values by nitrogen-bound clay can be excluded due to XRD analyses (semi-quantitative evaluation after Cook et al. (1975), performed at the Technische Universität Berlin, Germany) demonstrating a negligible fraction of clay (below <2%) present within samples.

7.6.2 Carbon isotope chemostratigraphy

Carbon isotope variations at Kyrshabakty section display three negative $\delta^{13}C_{carb}$ intervals (C1 - C3) qualified for chemostratigraphic correlation to further Ediacaran-Cambrian successions on global scale (Fig. 19).

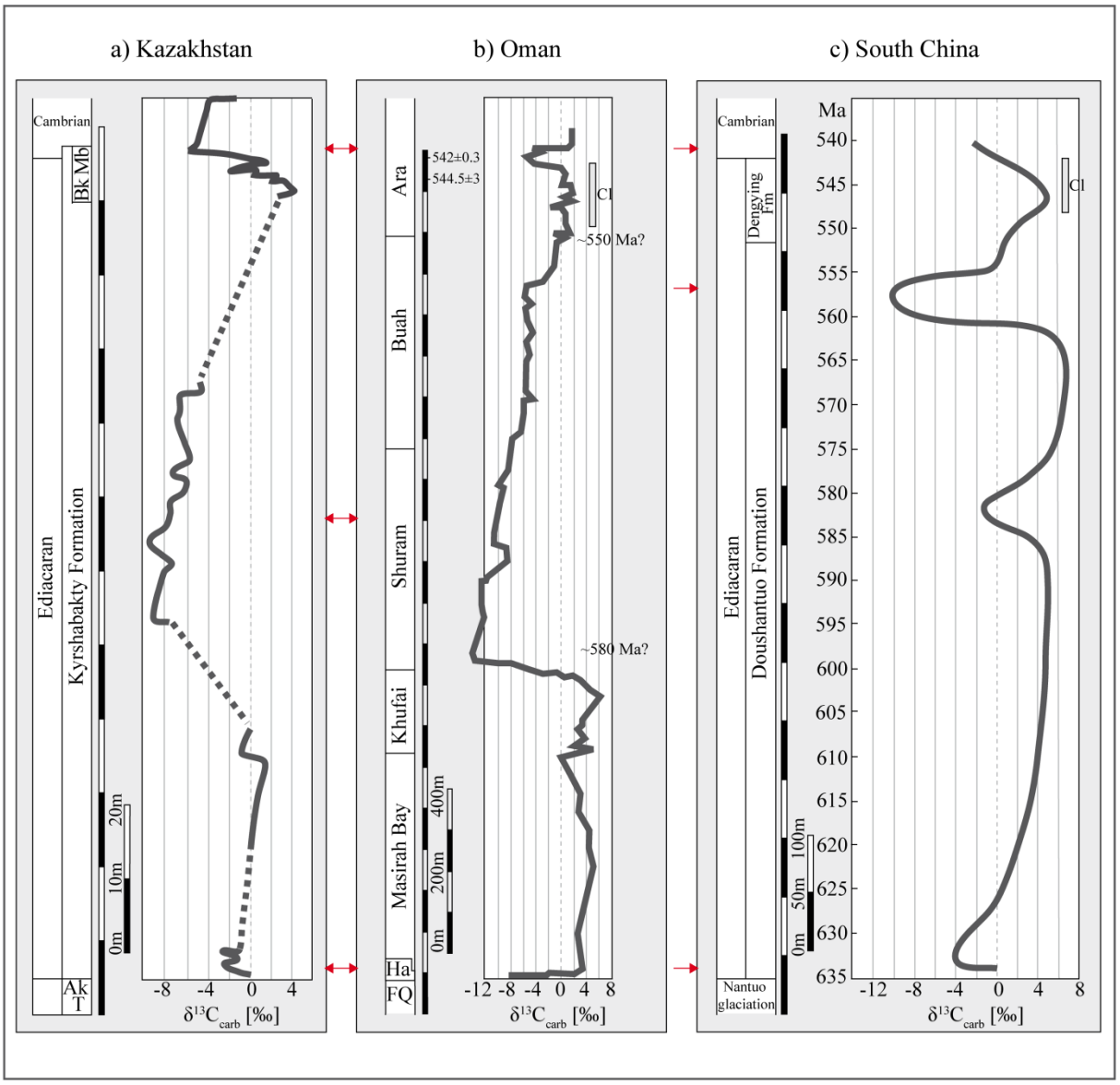

Figure 19: Proposed chemostratigraphy of Ediacaran-Cambrian successions from (a) Malyi Karatau, Kazakhstan (this study), (b) South Oman Salt Basin, Oman (Fike et al., 2006; Le Guerroué et al., 2006, from Jiang et al., 2007) and (c) Yangtze platform compilation, South China (Zhu et al., 2007). Each section reports characteristic $\delta^{13}C_{carb}$ negative anomalies indicated by red arrows expressing proposed correlation of isotopic excursions between sections. Ak T: Aktas Tillite, Bk Mb: Berkuty Member, FQ: Fiq Formation, Ha: Hadash Formation, Cl: Cloudina.

(1) Cap carbonate anomaly (C1)

The negative $\delta^{13}C_{carb}$ anomaly (C1) is conform with data reported by Meert et al. (2011) of the same section (termed in Meert et al., 2011 as "Aktas Cap Dolomite") who correlated the respective anomaly to the Maiberg cap anomaly of Namibia and concluded the underlying "Aktas Tillite" to be of late Cryogenian age. We agree with Meert et al. (2011) and propose a correlation of the Kyrshabakty cap carbonate to further worldwide Marinoan-age cap carbonates of e.g. Oman (Fike et al., 2006; Le Guerroué et al., 2006; Fig. 19b) and South China (e.g. Zhu et al., 2007; Fig. 19c). The global representativeness of obtained $\delta^{13}C_{carb}$ data is supported by $^{87}Sr/^{86}Sr$ ratios (~0.708 to ~0.709) and boron isotopes reported from cap carbonates of this section (Ohnemueller et al., in prep.; Ohnemueller et al., in review) which are in agreement with primary seawater values of further global early Ediacaran settings (Halverson et al., 2007; Kasemann et al., 2010; Romero et al., 2013).

(2) Shuram-Wonoka anomaly (C2)

The second prominent $\delta^{13}C_{carb}$ negative interval likely represents the Shuram-Wonoka anomaly (Meert et al., 2011) which is reported from several sections from Ediacaran continental fragments (e.g. Calver, 2000; Fike et al., 2006; Kaufman et al., 2006; Le Guerroué et al., 2006; Melezhik et al., 2008; Melezhik et al., 2009; Verdel et al., 2011; Lee et al., 2013; Lu et al., 2013; Macdonald et al., 2013). According to the magnitude (nadir -9.7‰), the characteristic expansion in limestone lithology and the long-lasting low $\delta^{13}C_{carb}$ trend through 33 m thickness, we propose a chemostratigraphic correlation of C2 to sections in Oman and South China (Fig. 19). The short-lived negative peak and the upwards recovery of the $\delta^{13}C_{carb}$ curve at Kyrshabakty section is remarkable similar to the isotopic trend recorded in the Shuram Formation in Oman (Fig. 19b). Moreover the nadir of C2 at ~-10‰ agrees with data from the Dounce anomaly in South China (Fig. 19c) which terminates in the upper Doushantuo Formation dated to ~551 Ma (Condon et al., 2005), displaying a widely acknowledged termination age of global "Dounce-Shuram-Wonoka" excursions (Bjerrum and Canfield, 2011; Lu et al., 2013).

The relation between the Shuram-Wonoka anomaly and a second Mid-Ediacaran $\delta^{13}C_{carb}$ negative excursion associated with the (regional) Gaskiers glaciation (~582 Ma; Bowring et al., 2003) is elusive (Hoffman and Li, 2009; Macdonald et al., 2013; Tahata et al., 2013). Isotope data from strata related to the Gaskiers glaciation in South China (Tahata et al., 2013) do not match isotopic values at Kyrshabakty section, therefore questioning a link of C2 to the aforementioned glaciation.

(3) The Pc-C boundary anomaly (C3)

We suggest that the $\delta^{13}C_{carb}$ isotopic excursion C3 resembles an equivalent of the global $\delta^{13}C_{carb}$ negative excursion associated with the beginning of the early Cambrian (e.g. Brasier et al., 1994; Narbonne et al., 1994; Brasier et al., 1996; Amthor et al., 2003; Boggiani et al., 2010; Ishikawa et al., 2013) and conclude that the upper Berkuty Member includes the Pc-C boundary. This hypothesis is based on the upwards gradually decreasing $\delta^{13}C_{carb}$ trend through the Berkuty Member (from ~4‰ down to ~-2‰) which is in shape and magnitude consistent with the characteristic Pc-C boundary $\delta^{13}C_{carb}$ negative anomaly in sections of, e.g. Oman and South China (Fig. 19). This is supported by the first occurrence of the key fossil for the Nemakit-Daldynian stage *Protohertzina anabarica* in the uppermost part of the Berkuty Member (~171 m) which confirms a lower Cambrian age for the respective depositional horizon (C. Seidig, pers. comm.). The association of *Protohertzina anabarica* with a $\delta^{13}C_{carb}$ negative excursion is documented from several sections, e.g. on the Yangtze platform (Goldberg et al., 2007; Ishikawa et al., 2008; Ishikawa et al., 2013) as well as in Canada (Narbonne et al., 1994) and Mongolia (Brasier et al., 1996). Additionally, $^{87}Sr/^{86}Sr$ seawater ratios of ~0.709 reported from this part (Ohnemueller et al., in prep.) agree with global Pc-C strontium patterns and argue for an open-ocean setting (Halverson et al., 2007; Sawaki et al., 2014). The association of C3 with the terminal Ediacaran Baykonurian glaciation (~550 - 540 Ma; Chumakov, 2009; Chumakov, 2011; Meert et al., 2011) cannot be excluded because of unexposed strata below the Berkuty Member. Nevertheless, the association of C3 to the occurrence of small shelly fossils convincingly argues for a Pc-C boundary setting.

7.6.3 Biogeochemical cycling across three significant Ediacaran to Cambrian intervals

7.6.3.1 The cap carbonate interval

The $\delta^{13}C_{carb}$ cap carbonate anomaly records major global biogeochemical changes in the aftermath of the Marinoan glaciation; however, mechanisms triggering the deposition of ^{13}C-depleted carbonates are still a matter of debate (e.g. Shields, 2005; Fairchild and Kennedy, 2007). Scenarios comprise the snowball Earth hypothesis (Hoffman et al., 1998), the methane hydrate destabilization hypothesis (Kennedy et al., 2001; Jiang et al., 2003; Jiang et al., 2006; Shields, 2008; Pokrovsky et al., 2010), the overturn of an anoxic deep ocean (Grotzinger and Knoll, 1995), the rise of atmospheric and aquatic carbon dioxide (CO_2) levels (Fairchild and Kennedy, 2007; Kasemann et al., 2010) and microbial mediated precipitation processes (Elie et al., 2007; Sergeev et al., 2013) including the "plumeworld" hypothesis (Shields, 2005). Yet, considering the magnitude of C1 (Fig. 18), each aforementioned hypothesis finds supporting evidence.

In contrast, the nitrogen isotope composition of cap carbonate strata yields unambiguous indication of strong N_2-fixation by diazotrophs. In the light of increasing post-glacial alkalinity supply to the oceans (Calver, 2000; Kasemann et al., 2005) and atmospheric CO_2 concentration (Hoffman et al., 1998; Kasemann et al., 2010), the elevated partial pressure of CO_2 (pCO_2) may have triggered a diazotrophic "bloom" supplying "new" nitrogen to the biological cycle. Consequently, bacterial CO_2 sequestration in the aftermath of the glaciation effectively draw down the pCO_2 (Shields, 2005) thus acting as a dynamic force in climate regulation (Falkowski, 1997). Additionally, elevated photosynthetic productivity would raise the aquatic oxygen content which is proposed to be closely linked to the following evolution of Ediacaran life (Hoffman and Schrag, 2002; Jiang et al., 2010). As a consequence, changes in carbon, nitrogen and oxygen fluxes possibly modified and re-strengthened the biological pump after a glacial "biological shutdown". Reinforced biological cycling could have affected the trophic structures of the ecological web (Hutchins et al., 2007) most likely

mirrored by decreasing $\delta^{13}C_{org}$ values towards the top of the cap carbonate displaying a multi-faceted biosphere with different contributions of autotrophic and heterotrophic organisms to the biomass (Spangenberg et al., 2014). Elevated $\delta^{15}N$ and $\delta^{13}C_{carb}$ data of overlying dolomitic sandstones indicate a transition to a more oxygenated marine environment where oxidized inorganic nitrogen species such as NO_3^- began to outcompete N_2 as the key nutrient and reduced N_2-fixation rates (Fu and Bell, 2003; Fig. 20a). The shift from predominantly diazotrophic to NO_3^- assimilating primary producers agrees with the radiation of multicellular eukaryotes (e.g. marine algae) in the aftermath of the Marinoan glaciation (Yuan et al., 2011).

7.6.3.2 The Shuram-Wonoka interval

Triggers for the pronounced $\delta^{13}C_{carb}$ negative excursion have been debated in various ways, with a number of competing interpretations (Calver, 2000; Rothman et al., 2003; Fike et al., 2006; Bristow and Kennedy, 2008; Knauth and Kennedy, 2009; Derry, 2010; Lu et al., 2013; Schrag et al., 2013; Wang et al., 2014). However, the prominent non-actualistic decoupling of $\delta^{13}C_{carb}$ and $\delta^{13}C_{org}$ isotopes during the Shuram-Wonoka interval is mainly attributed to strong differences in reservoir sizes between a large dissolved organic carbon (DOC) and a smaller DIC pool owing to low-oxygen bottom water conditions. In this regard, a stepwise remineralization/oxygenation of the former enormous DOC reservoir is suggested to have enabled isotope coupling seen in Phanerozoic times (Rothman et al., 2003; Fike et al., 2006; McFadden et al., 2008; Wang et al., 2012b).

At Kyrshabakty section, elevated organic matter remineralization in the light of variable oceanic redox conditions finds supportive evidence by nitrogen isotope compositions. Increasing availability of nitrate and thus the preferential assimilation of ^{15}N-depleted nitrate into biomass is postulated to be responsible for values above >2‰ during the Shuram-Wonoka event in South China (Kikumoto et al., 2014). Yet, we document as well low $\delta^{15}N$ values down to ~1.5‰ characteristic for the introduction of fixed nitrogen via N_2-fixation (Wada and Hattori, 1976). Therefore, we recommend that pulsed fluctuations of an anoxic

zone dependent on the degree of oxygen consumption during remineralization largely effected biogeochemical cycling on the late Neoproterozoic Kazakh microcontinent in terms of the stability of nitrate. Thereby, deepening of the redox boundary favors NO_3^- assimilation (due to strengthened nitrification) whereby the vertical expansion of the anoxic zone promotes diazotrophy to dominate primary production (Fig. 20b). In this sense, intensive remineralization would have consumed oxygen until the oxygen level became too low to sustain nitrate supply via nitrification, a situation comparable to sapropel formation in the modern Mediterranean Sea (Struck et al., 2001). In turn, a proposed "cyanobacterial" bloom would increase the ocean's oxygen inventory, thus setting nitrification-denitrification processes and therefore a nitrate-based primary productivity in motion.

However, whether $\delta^{15}N$ fluctuations record pulsed changes of the oxygen content within an oxygen minimum zone in a mildly oxygenated Neoproterozoic ocean (Ader et al., 2014) or represent global fluctuations of the chemocline in a highly stratified ocean (global signal) remains elusive. Nevertheless, $\delta^{15}N$ values explicitly show that nitrate was in some periods stable in the ocean during the Shuram-Wonoka event and thus assuming adequate marine oxygen levels for nitrification during respective times (Ader et al., 2014).

7.6.3.3 The Precambrian-Cambrian boundary interval and the early Cambrian

The onset of the $\delta^{13}C_{carb}$ and $\delta^{15}N$ negative excursion during the Pc-C transition through the early Cambrian can best be explained by elevated bioproductivity and extensive remineralization in a highly redox-stratified water column (Ishikawa et al., 2013) and is conform with records reported from Pc-C boundary platform settings in South China (Cremonese et al., 2013; Cremonese et al., 2014; Kikumoto et al., 2014), thus strongly arguing for a global paleooceanographic isotope signal.

Negative $\delta^{13}C_{carb}$ and $\delta^{15}N$ data of lower Cambrian dolomitic strata suggest a widespread oceanic anoxia scenario (Kimura and Watanabe, 2001; Ishikawa et

al., 2008) and intermittently euxinic conditions across the Pc-C boundary interval (Wille et al., 2008; Och et al., 2013; Cremonese et al., 2014). In turn, intercalated phosphoritic strata record periods of nutrient-rich deep-water upwelling after a time of circulation stagnation and widespread oceanic anoxia (Cook and Shergold, 1984).

Especially persistent negative $\delta^{15}N$ values indicative of (anoxygenic) NH_4^+ assimilating phototrophs suggest that anoxic water masses dominated surface-water environments. If the scenario of strong, episodically upwelling H_2S- and ^{13}C-DIC depleted bottom waters to shallow environments during the late Ediacaran and early Cambrian of South China (Goldberg et al., 2007; Cremonese et al., 2013; Och et al., 2013) can be applied in Kazakhstan, negative $\delta^{15}N$ values most likely indicate the presence of intermittent photic zone euxinia. Under the presence of H_2S instead of oxygen in the photic zone, anoxygenic phototrophic bacteria like e.g. purple sulfur bacteria (PSB) and green sulfur bacteria (GSB) are known to assimilate NH_4^+ but are also capable of N_2-fixation (Riederer-Henderson and Wilson, 1970; Ohkouchi et al., 2005). Because NH_4^+ uptake is associated with a large isotope fractionation effect, the biomass is strongly depleted in ^{15}N (Hoch et al., 1992) and thus bears negative $\delta^{15}N$ isotope compositions (Ohkouchi et al., 2005; Zerkle et al., 2011; Higgins et al., 2012). Anoxygenic nitrogen uptake is well supported by low sedimentary $\delta^{13}C_{org}$ data (~-35 to ~-29‰) reflecting $\delta^{13}C_{org}$ values of PSB and GSB cultures (Zyakun et al., 2009) and pigments from anoxygenic phototrophs and autotrophic and heterotrophic grown sulfate-reducing bacteria (Londry and Marais, 2003; Ohkouchi et al., 2005).

However, due to lithology-dependent (dolomitic vs. phosphoritic) scattering of $\delta^{13}C_{carb}$ and $\delta^{15}N$ values ($\delta^{15}N$ -2.3 to 2.1‰) during the lower Cambrian, we assume several redox shifts in the water column provoking a shifting dominance between NH_4^+ uptake and N_2-fixation among phototrophs depending on the availability of (upwelled) NH_4^+ for nitrogen uptake (Fig. 20c). Thereby, positive $\delta^{15}N$ and highly negative $\delta^{13}C_{carb}$ isotope compositions of phosphorites reflect strong N_2-fixation as the dominant biological response to excess of phosphorus and $^{12}CO_2$ availability during upwelling phases from oceanic anoxic parts

(Papineau et al., 2013; Cremonese et al., 2014), similar to recent coastal upwelling systems in the Atlantic and Pacific Ocean (e.g. Capone and Hutchins, 2013). In contrast, dolomitic strata represent times of circulation stagnation where massive oxygen depletion due to extensive remineralization decreases nitrification rates and leads to excess availability of reduced nitrogen species like NH_4^+ re-entering the photic zone (Higgins et al., 2012). Elevated remineralization rates are also suggested to provide an important reservoir for ^{13}C-depleted DIC triggering the negative Pc-C $\delta^{13}C_{carb}$ anomaly (Jiang et al., 2007).

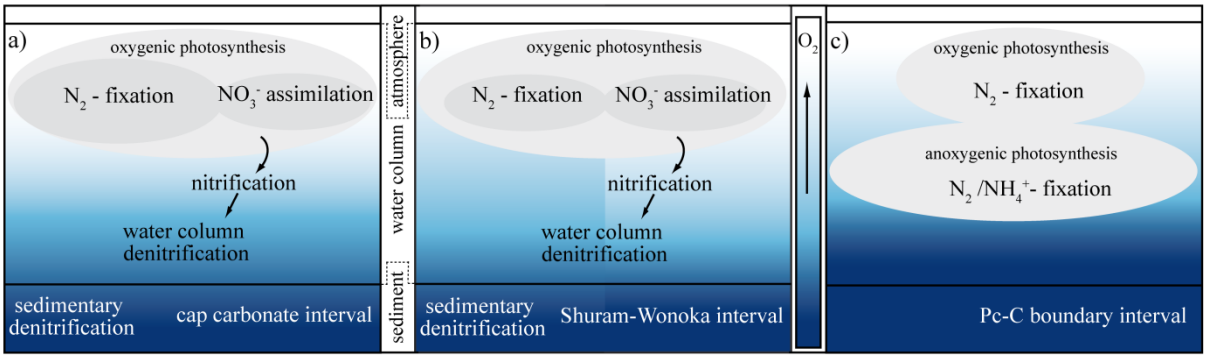

Figure 20: Sketch diagram of biological processes responsible for $\delta^{15}N$ values of strata at Kyrshabakty section during (a) cap carbonate interval, (b) Shuram-Wonoka interval and (c) Pc-C boundary interval. Only the dominant processes affecting the nitrogen cycle are shown; other biogeochemical nitrogen transformation reactions may have been present as well.

7.7 Conclusion

High-resolution isotopic records ($\delta^{13}C_{carb}$, $\delta^{13}C_{org}$, $\delta^{15}N$) from the Kyrshabakty section enable the first global chemostratigraphic correlation of Ediacaran to Cambrian strata of the Malyi Karatau area to global time-equivalent sections and offer the first comprehensive Ediacaran $\delta^{15}N$ record outside South China. Our results show that the Kyrshabakty section is a new representative of a global Pc-C section. Especially nitrogen isotopes are shown to represent a reliable marker for global marine biogeochemical perturbations which strongly argue for a severe global oceanic anoxia event in the early Cambrian.

Three major negative $\delta^{13}C_{carb}$ excursions can be correlated in shape and magnitude to the global cap carbonate anomaly, Shuram-Wonoka anomaly and Pc-C boundary anomaly, respectively. Our results indicate that biogeochemical cycling during the deposition of Kyrshabakty cap carbonates is influenced by extensive bacterial blooms of oxygenic N_2-fixing primary producers re-activating and intensifying the biological pump and thus promoting a shift towards a nitrate-dominated nutrient regime. Newly established biogeochemical conditions most likely contributed to the subsequent evolution of multicellular eukaryotes. Progressive oxidation of a large oceanic DOC pool during the Shuram-Wonoka event may explain decoupled $\delta^{13}C_{carb}$ and $\delta^{13}C_{org}$ values (e.g. McFadden et al., 2008) during times of pulsed expansion of an anoxic water body. Thereby, variable $\delta^{15}N$ compositions mirror a continuous shift in the nutrient mass balance between N_2 and NO_3^- depending on the oxygenation state of the ocean. Negative $\delta^{13}C_{carb}$ and $\delta^{15}N$ trends in the early Cambrian indicate a long-term deep oceanic anoxic setting with periodically intense photic zone anoxia to euxinia and confirm global datasets. Negative $\delta^{15}N$ values point to an intense contribution of anoxygenic phototrophs to the organic matter pool suggesting pronounced euxinic photic zone conditions. Thus, the obtained isotope dataset largely contributes to the understanding of biogeochemical processes across the pivotal Ediacaran-Cambrian transition and provide new information about carbon and nitrogen cycling of the paleomarine shallow-water environment on the Kazakh microcontinent.

7.8 Acknowledgements

We thank Christoph Heubeck (Friedrich-Schiller Universität Jena), Frank Ohnemueller (Universität Bremen), Michael Steiner and Bernd Weber (Freie Universität Berlin) for consultations, discussions and collaboration. We thank our Kazakh colleagues from the Kazakh Academy of Sciences, K. I. Satpaev Institute of Geological Sciences, Almaty, for logistical support during field work in Kazakhstan. We are grateful to Lisa Schlegelmilch, Maria Diedrich and Yannik Steinmann (all Museum für Naturkunde Berlin) for help with sample preparation, Christiane Behr (Freie Universität Berlin) for thin section preparation, and Dorothee Hippler and Ralf Oeser (Technische Universität Berlin) for XRD analyses and for providing phosphorite samples (KR-11). This study was funded by the German Research Foundation (DFG-FOR 736).

7.9 References

Ader, M., Macouin, M., Trindade, R. I. F., Hadrien, M. H., Yang, Z., Sun, Z., and Besse, J., 2009, A multilayered water column in the Ediacaran Yangtze platform? Insights from carbonate and organic matter paired $\delta^{13}C$: Earth and Planetary Science Letters, v. 288, no. 1-2, p. 213-227.

Ader, M., Sansjofre, P., Halverson, G. P., Busigny, V., Trindade, R. I. F., Kunzmann, M., and Nogueira, A. C. R., 2014, Ocean redox structure across the Late Neoproterozoic Oxygenation Event: A nitrogen isotope perspective: Earth and Planetary Science Letters, v. 396, no. 0, p. 1-13.

Alexeiev, D. V., Cook, H. E., Buvtyshkin, V. M., and Golub, L. Y., 2009, Structural evolution of the Ural-Tian Shan junction: A view from Karatau ridge, South Kazakhstan: Comptes Rendus Geoscience, v. 341, no. 2-3, p. 287-297.

Amthor, J. E., Grotzinger, J. P., Schröder, S., Bowring, S. A., Ramezani, J., Martin, M. W., and Matter, A., 2003, Extinction of Cloudina and Namacalathus at the Precambrian-Cambrian boundary in Oman: Geology, v. 31, p. 431-434.

Bahlmann, E., Bernasconi, S. M., Bouillon, S., Houtekamer, M., Korntheuer, M., Langenberg, F., Mayr, C., Metzke, M., Middelburg, J. J., Nagel, B., Struck, U., Voß, M., and Emeis, K.-C., 2010, Performance evaluation of nitrogen isotope ratio determination in marine and lacustrine sediments: An inter-laboratory comparison: Organic Geochemistry, v. 41, no. 1, p. 3-12.

Bjerrum, C. J., and Canfield, D. E., 2011, Towards a quantitative understanding of the late Neoproterozoic carbon cycle: Proceedings of the National Academy of Sciences, v. 108, no. 14, p. 5542-5547.

Bowring, S. A., Myrow, P., and Landing, E., 2003, Geochronological constraints on terminal Neoproterozoic events and the rise of Metazoan: Geophysical Research Abstracts, v. 5, p. 13219.

Brasier, M. D., Rozanov, A. Y., Zhuravlev, A. Y., Corfield, R. M., and Derry, L. A., 1994, A carbon-isotope reference scale for the Lower Cambrian succession in Siberia - Report of IGCP project-303: Geological Magazine, v. 131, no. 6, p. 767-783.

Brasier, M. D., Shields, G., Kuleshov, V. N., and Zhegallo, E. A., 1996, Integrated chemo- and biostratigraphic calibration of early animal evolution: Neoproterozoic-early Cambrian of southwest Mongolia: Geological Magazine, v. 133, no. 4, p. 445-485.

Bristow, T. F., and Kennedy, M. J., 2008, Carbon isotope excursions and the oxidant budget of the Ediacaran atmosphere and ocean: Geology, v. 36, no. 11, p. 863-866.

Busigny, V., Lebeau, O., Ader, M., Krapež, B., and Bekker, A., 2013, Nitrogen cycle in the Late Archean ferruginous ocean: Chemical Geology, v. 362, no. 0, p. 115-130.

Calver, C. R., 2000, Isotope stratigraphy of the Ediacarian (Neoproterozoic III) of the Adelaide Rift Complex, Australia, and the overprint of water column stratification: Precambrian Research, v. 100, no. 1–3, p. 121-150.

Canfield, D. E., Poulton, S. W., and Narbonne, G. M., 2007, Late-Neoproterozoic Deep-Ocean Oxygenation and the Rise of Animal Life: Science, v. 315, no. 5808, p. 92-95.

Canfield, D. E., Glazer, A. N., and Falkowski, P. G., 2010, The Evolution and Future of Earth's Nitrogen Cycle: Science, v. 330, no. 6001, p. 192-196.

Capone, D. G., and Hutchins, D. A., 2013, Microbial biogeochemistry of coastal upwelling regimes in a changing ocean: Nature Geoscience, v. 6, no. 9, p. 711-717.

Carpenter, E. J., Harvey, H. R., Fry, B., and Capone, D. G., 1997, Biogeochemical tracers of the marine cyanobacterium Trichodesmium: Deep Sea Research Part I: Oceanographic Research Papers, v. 44, no. 1, p. 27-38.

Chumakov, N. M., 2009, The Baykonurian Glaciohorizon of the Late Vendian: Stratigraphy and Geological Correlation, v. 17, no. 4, p. 373-381.

Chumakov, N. M., 2011, Glacial deposits of the Baykonur Formation, Kazakhstan and Kyrgyzstan: Geological Society, London, Memoirs, v. 36, no. 1, p. 303-307.

Cline, J. D., and Kaplan, I. R., 1975, Isotopic fractionation of dissolved nitrate during denitrification in the eastern tropical north pacific ocean: Marine Chemistry, v. 3, no. 4, p. 271-299.

Condon, D., Zhu, M., Bowring, S., Wang, W., Yang, A., and Jin, Y., 2005, U-Pb Ages from the Neoproterozoic Doushantuo Formation, China: Science, v. 308, no. 5718, p. 95-98.

Cook, H. E., Johnson, P. D., Matti, J. C., and Zemmels, I., 1975, Methods of sample preparation and X-ray diffraction data analysis, X-ray Mineralogy Laboratory, Deep Sea Drilling Project, University of California, Riverside: *in* Hayes, D.E., Frakes, L.A., et al., Init. Repts.

Cook, P. J., and Shergold, J. H., 1984, Phosphorus, phosphorites and skeletal evolution at the precambrian cambrian boundary: Nature, v. 308, no. 5956, p. 231-236.

Cremonese, L., Shields-Zhou, G., Struck, U., Ling, H.-F., Och, L., Chen, X., and Li, D., 2013, Marine biogeochemical cycling during the early Cambrian constrained by a nitrogen and organic carbon isotope study of the Xiaotan section, South China: Precambrian Research, v. 225, no. 0, p. 148-165.

Cremonese, L., Shields-Zhou, G. A., Struck, U., Ling, H.-F., and Och, L. M., 2014, Nitrogen and organic carbon isotope stratigraphy of the Yangtze Platform during the Ediacaran–Cambrian transition in South China: Palaeogeography, Palaeoclimatology, Palaeoecology, v. 398, no. 0, p. 165-186.

Derry, L. A., 2010, A burial diagenesis origin for the Ediacaran Shuram–Wonoka carbon isotope anomaly: Earth and Planetary Science Letters, v. 294, no. 1–2, p. 152-162.

Eganov, E. A., Sovetov, Y. K., and Yanshin, A. L., 1986, Proterozoic and Cambrian phosphorites - deposits: Karatau, southern Kazakhstanin, *in* Cook, P.J., Shergold, J.H., eds., Phosphate Deposits of the World: Volume 1 Proterozoic and Cambrian Phosphorites: Cambridge, Cambridge University Press, UK, p. 175-189.

Elie, M., Nogueira, A. C. R., Nédélec, A., Trindade, R. I. F., and Kenig, F., 2007, A red algal bloom in the aftermath of the Marinoan Snowball Earth: Terra Nova, v. 19, no. 5, p. 303-308.

Fairchild, I. J., and Kennedy, M. J., 2007, Neoproterozoic glaciation in the earth system: Journal of the Geological Society, v. 164, p. 895-921.

Falkowski, P. G., 1997, Evolution of the nitrogen cycle and its influence on the biological sequestration of CO_2 in the ocean: Nature, v. 387, no. 6630, p. 272-275.

Fike, D. A., Grotzinger, J. P., Pratt, L. M., and Summons, R. E., 2006, Oxidation of the Ediacaran Ocean: Nature, v. 444, no. 7120, p. 744-747.

Fu, F.-X., and Bell, P. R. F., 2003, Factors affecting N_2 fixation by the cyanobacterium Trichodesmium sp. GBRTRLI101: FEMS Microbiology Ecology, v. 45, no. 2, p. 203-209.

Goldberg, T., Strauss, H., Guo, Q., and Liu, C., 2007, Reconstructing marine redox conditions for the Early Cambrian Yangtze Platform: Evidence from biogenic sulphur and organic

carbon isotopes: Palaeogeography, Palaeoclimatology, Palaeoecology, v. 254, no. 1–2, p. 175-193.

Grotzinger, J. P., and Knoll, A. H., 1995, Anomalous Carbonate Precipitates: Is the Precambrian the Key to the Permian?: Palaios, v. 10, no. 6, p. 578-596.

Halverson, G. P., Hoffman, P. F., Schrag, D. P., Maloof, A. C., and Rice, A. H. N., 2005, Toward a Neoproterozoic composite carbon-isotope record: Geological Society of America Bulletin, v. 117, no. 9-10, p. 1181-1207.

Halverson, G. P., Dudas, F. O., Maloof, A. C., and Bowring, S. A., 2007, Evolution of the $^{87}Sr/^{86}Sr$ composition of Neoproterozoic seawater: Palaeogeography Palaeoclimatology Palaeoecology, v. 256, no. 3-4, p. 103-129.

Halverson, G. P., Wade, B. P., Hurtgen, M. T., and Barovich, K. M., 2010, Neoproterozoic chemostratigraphy: Precambrian Research, v. 182, no. 4, p. 337-350.

Heubeck, C., Ergaliev, G., and Evseev, S., 2013, Large-scale seismogenic deformation of a carbonate platform straddling the Precambrian-Cambrian boundary, Karatau Range, Kazakhstan: Journal of Sedimentary Research, v. 83, no. 11-12, p. 1005-1025.

Higgins, M. B., Robinson, R. S., Husson, J. M., Carter, S. J., and Pearson, A., 2012, Dominant eukaryotic export production during ocean anoxic events reflects the importance of recycled NH_4^+: Proceedings of the National Academy of Sciences, v. 109, no. 7, p. 2269-2274.

Hoch, M. P., Fogel, M. L., and Kirchman, D. L., 1992, Isotopic fractionation associated with ammonium uptake by a marine bacterium: Limnology and Oceanography, v. 37, no. 7, p. 1447-1459.

Hoffman, P. F., Kaufman, A. J., Halverson, G. P., and Schrag, D. P., 1998, A Neoproterozoic snowball earth: Science, v. 281, no. 5381, p. 1342-1346.

Hoffman, P. F., and Schrag, D. P., 2002, The snowball Earth hypothesis: testing the limits of global change: Terra Nova, v. 14, no. 3, p. 129-155.

Hoffman, P. F., and Li, Z.-X., 2009, A palaeogeographic context for Neoproterozoic glaciation: Palaeogeography, Palaeoclimatology, Palaeoecology, v. 277, no. 3–4, p. 158-172.

Hutchins, D. A., Fu, F. X., Zhang, Y., Warner, M. E., Feng, Y., Portune, K., Bernhardt, P. W., and Mulholland, M. R., 2007, CO_2 control of *Trichodesmium* N_2 fixation, photosynthesis, growth rates, and elemental ratios: Implications for past, present, and future ocean biogeochemistry: Limnology and Oceanography, v. 52, no. 4, p. 1293-1304.

Ishikawa, T., Ueno, Y., Komiya, T., Sawaki, Y., Han, J., Shu, D., Li, Y., Maruyama, S., and Yoshida, N., 2008, Carbon isotope chemostratigraphy of a Precambrian/Cambrian boundary section in the Three Gorge area, South China: Prominent global-scale isotope excursions just before the Cambrian Explosion: Gondwana Research, v. 14, no. 1–2, p. 193-208.

Ishikawa, T., Ueno, Y., Shu, D., Li, Y., Han, J., Guo, J., Yoshida, N., and Komiya, T., 2013, Irreversible change of the oceanic carbon cycle in the earliest Cambrian: High-resolution organic and inorganic carbon chemostratigraphy in the Three Gorges area, South China: Precambrian Research, v. 225, no. 0, p. 190-208.

Jiang, G., Kennedy, M. J., and Christie-Blick, N., 2003, Stable isotopic evidence for methane seeps in Neoproterozoic postglacial cap carbonates: Nature, v. 426, no. 6968, p. 822-826.

Jiang, G., Kennedy, M. J., Christie-Blick, N., Wu, H., and Zhang, S., 2006, Stratigraphy, sedimentary structures, and textures of the late Neoproterozoic Doushantuo cap carbonate in south China: Journal of Sedimentary Research, v. 76, no. 7-8, p. 978-995.

Jiang, G., Kaufmann, A. J., Christie-Blick, N., Zhang, S., and Wu, H., 2007, Carbon isotope variability across the Ediacaran Yangtze platform in South China: Implications for a large surface-to-deep ocean $\delta^{13}C$ gradient: Earth and Planetary Science Letters, v. 261, p. 303-320.

Jiang, G., Wang, X., Shi, X., Zhang, S., Xiao, S., and Dong, J., 2010, Organic carbon isotope constraints on the dissolved organic carbon (DOC) reservoir at the Cryogenian–Ediacaran transition: Earth and Planetary Science Letters, v. 299, p. 159-168.

Johnston, D. T., Poulton, S. W., Goldberg, T., Sergeev, V. N., Podkovyrov, V., Vorob'eva, N. G., Bekker, A., and Knoll, A. H., 2012, Late Ediacaran redox stability and metazoan evolution: Earth and Planetary Science Letters, v. 335, p. 25-35.

Kasemann, S. A., Hawkesworth, C. J., Prave, A. R., Fallick, A. E., and Pearson, P. N., 2005, Boron and calcium isotope composition in Neoproterozoic carbonate rocks from Namibia:

evidence for extreme environmental change: Earth and Planetary Science Letters, v. 231, no. 1-2, p. 73-86.

Kasemann, S. A., Prave, A. R., Fallick, A. E., Hawkesworth, C. J., and Hoffmann, K. H., 2010, Neoproterozoic ice ages, boron isotopes, and ocean acidification: Implications for a snowball Earth: Geology, v. 38, no. 9, p. 775-778.

Kaufman, A. J., Jiang, G., Christie-Blick, N., Banerjee, D. M., and Rai, V., 2006, Stable isotope record of the terminal Neoproterozoic Krol platform in the Lesser Himalayas of northern India: Precambrian Research, v. 147, no. 1-2, p. 156-185.

Kennedy, M. J., Christie-Blick, N., and Prave, A. R., 2001, Carbon isotopic composition of Neoproterozoic glacial carbonates as a test of paleoceanographic models for snowball Earth phenomena: Geology, v. 29, no. 12, p. 1135-1138.

Kikumoto, R., Tahata, M., Nishizawa, M., Sawaki, Y., Maruyama, S., Shu, D., Han, J., Komiya, T., Takai, K., and Ueno, Y., 2014, Nitrogen isotope chemostratigraphy of the Ediacaran and Early Cambrian platform sequence at Three Gorges, South China: Gondwana Research, v. 25, no. 3, p. 1057-1069.

Kimura, H., and Watanabe, Y., 2001, Oceanic anoxia at the Precambrian-Cambrian boundary: Geology, v. 29, no. 11, p. 995-998.

Kirschvink, J. L., and Raub, T. D., 2003, A methane fuse for the Cambrian explosion: carbon cycles and true polar wander: Comptes Rendus Geoscience, v. 335, no. 1, p. 65-78.

Knauth, L. P., and Kennedy, M. J., 2009, The late Precambrian greening of the Earth: Nature, v. 460, no. 7256, p. 728-732.

Kunimitsu, Y., Setsuda, Y., Furuyama, S., Wang, W., and Kano, A., 2011, Ediacaran chemostratigraphy and paleoceanography at a shallow marine setting in northwestern Hunan Province, South China: Precambrian Research, v. 191, no. 3–4, p. 194-208.

Le Guerroué, E., Allen, P. A., and Cozzi, A., 2006, Chemostratigraphic and sedimentological framework of the largest negative carbon isotopic excursion in Earth history: The Neoproterozoic Shuram Formation (Nafun Group, Oman): Precambrian Research, v. 146, no. 1–2, p. 68-92.

Lee, C., Fike, D. A., Love, G. D., Sessions, A. L., Grotzinger, J. P., Summons, R. E., and Fischer, W. W., 2013, Carbon isotopes and lipid biomarkers from organic-rich facies of the Shuram Formation, Sultanate of Oman: Geobiology, v. 11, no. 5, p. 406-419.

Levashova, N. M., Meert, J. G., Gibsher, A. S., Grice, W. C., and Bazhenov, M. L., 2011, The origin of microcontinents in the Central Asian Orogenic Belt: Constraints from paleomagnetism and geochronology: Precambrian Research, v. 185, no. 1-2, p. 37-54.

Li, C., Love, G. D., Lyons, T. W., Fike, D. A., Sessions, A. L., and Chu, X., 2010, A Stratified Redox Model for the Ediacaran Ocean: Science, v. 328, no. 5974, p. 80-83.

Li, D., Ling, H.-F., Shields-Zhou, G. A., Chen, X., Cremonese, L., Och, L., Thirlwall, M., and Manning, C. J., 2013, Carbon and strontium isotope evolution of seawater across the Ediacaran–Cambrian transition: Evidence from the Xiaotan section, NE Yunnan, South China: Precambrian Research, v. 225, no. 0, p. 128-147.

Londry, K. L., and Marais, D. J. D., 2003, Stable carbon isotope fractionation by sulfate-reducing bacteria: Applied and Environmental Microbiology, v. 69, no. 5, p. 2942-2949.

Lu, M., Zhu, M., Zhang, J., Shields-Zhou, G., Li, G., Zhao, F., Zhao, X., and Zhao, M., 2013, The DOUNCE event at the top of the Ediacaran Doushantuo Formation, South China: Broad stratigraphic occurrence and non-diagenetic origin: Precambrian Research, v. 225, no. 0, p. 86-109.

Macdonald, F. A., Strauss, J. V., Sperling, E. A., Halverson, G. P., Narbonne, G. M., Johnston, D. T., Kunzmann, M., Schrag, D. P., and Higgins, J. A., 2013, The stratigraphic relationship between the Shuram carbon isotope excursion, the oxygenation of Neoproterozoic oceans, and the first appearance of the Ediacara biota and bilaterian trace fossils in northwestern Canada: Chemical Geology, v. 362, no. 0, p. 250-272.

Maloof, A. C., Schrag, D. P., Crowley, J. L., and Bowring, S. A., 2005, An expanded record of Early Cambrian carbon cycling from the Anti-Atlas Margin, Morocco: Canadian Journal of Earth Sciences, v. 42, no. 12, p. 2195-2216.

McFadden, K. A., Huang, J., Chu, X., Jiang, G., Kaufmann, A. J., Zhou, C., Yuan, X., and Xiao, S., 2008, Pulsed oxidation and biological evolution in the Ediacaran Doushantuo Formation: PNAS, v. 105, no. 9, p. 3197-3202.

Meert, J. G., Gibsher, A. S., Levashova, N. M., Grice, W. C., Kamenov, G. D., and Ryabinin, A. B., 2011, Glaciation and ~770 Ma Ediacara (?) Fossils from the Lesser Karatau Microcontinent, Kazakhstan: Gondwana Research, v. 19, p. 867-880.

Melezhik, V. A., Roberts, D., Fallick, A. E., and Gorokhov, I. M., 2008, The Shuram-Wonoka event recorded in a high-grade metamorphic terrane: Insight from the Scandinavian Caledonides: Geological Magazine, v. 145, no. 2, p. 161-172.

Melezhik, V. A., Pokrovsky, B. G., Fallick, A. E., Kuznetsov, A. B., and Bujakaite, M. I., 2009, Constraints on $^{87}Sr/^{86}Sr$ of Late Ediacaran seawater: insight from Siberian high-Sr limestones: Journal of the Geological Society, v. 166, p. 183-191.

Montoya, J. P., Carpenter, E. J., and Capone, D. G., 2002, Nitrogen fixation and nitrogen isotope abundances in zooplankton of the oligotrophic North Atlantic: Limnology Oceanography, v. 47, no. 6, p. 1617-1628.

Narbonne, G. M., Kaufman, A. J., and Knoll, A. H., 1994, Integrated chemostratigraphy and biostratigraphy of the Windermere Supergroup, northwestern Canada - Implications for Neoproterozoic correlations and the early evolution of animals: Geological Society of America Bulletin, v. 106, no. 10, p. 1281-1292.

Och, L. M., Shields-Zhou, G. A., Poulton, S. W., Manning, C., Thirlwall, M. F., Li, D., Chen, X., Ling, H., Osborn, T., and Cremonese, L., 2013, Redox changes in Early Cambrian black shales at Xiaotan section, Yunnan Province, South China: Precambrian Research, v. 225, no. 0, p. 166-189.

Ohkouchi, N., Nakajima, Y., Okada, H., Ogawa, N. O., Suga, H., Oguri, K., and Kitazato, H., 2005, Biogeochemical processes in the saline meromictic Lake Kaiike, Japan: implications from molecular isotopic evidences of photosynthetic pigments: Environmental Microbiology, v. 7, no. 7, p. 1009-1016.

Ohnemueller, F., Ergaliev, G., and Kasemann, S. A., in prep., Ediacaran to Cambrian ocean-pH and continental weathering conditions: Implications from Southern Kazakhstan.

Ohnemueller, F., Prave, A. R., Fallick, A. E., and Kasemann, S. A., in review/subm., Ocean acidification in the aftermath of the Marinoan glaciation (Geology G35937).

Papineau, D., Purohit, R., Fogel, M. L., and Shields-Zhou, G. A., 2013, High phosphate availability as a possible cause for massive cyanobacterial production of oxygen in the Paleoproterozoic atmosphere: Earth and Planetary Science Letters, v. 362, p. 225-236.

Peterson, B. J., and Fry, B., 1987, Stable Isotopes in Ecosystem Studies: Annual Review of Ecology and Systematics, v. 18, no. 1, p. 293-320.

Pokrovsky, B. G., Chumakov, N. M., Melezhik, V. A., and Bujakaite, M. I., 2010, Geochemical properties of Neoproterozoic "cap dolomites" in the Patom paleobasin and problem of their genesis: Lithology and Mineral Resources, v. 45, no. 6, p. 577-592.

Popov, L. E., Bassett, M. G., Zhemchuzhnikov, V. G., Holmer, L. E., and Klishevich, I. A., 2009, Gondwanan faunal signatures from early Palaeozoic terranes of Kazakhstan and Central Asia: evidence and tectonic implications: Geological Society, London, Special Publications, v. 325, p. 23-64.

Pradhan, V. R., Meert, J. G., Levashova, N. M., and Gibsher, A. S., 2009, Preliminary paleomagnetic data on Late Cambrian to Ordovician carbonate beds of Tamdy Series from the Lesser Karatau microcontinent, South Kazakhstan: Geological Society of America *Abstracts with Programs*, v. 41, no. 7, p. 269.

Riederer-Henderson, M. A., and Wilson, P. W., 1970, Nitrogen Fixation by Sulphate-reducing Bacteria: Journal of General Microbiology, v. 61, no. Part 1, p. 27-31.

Robinson, R. S., Kienast, M., Luiza Albuquerque, A., Altabet, M., Contreras, S., De Pol Holz, R., Dubois, N., Francois, R., Galbraith, E., Hsu, T.-C., Ivanochko, T., Jaccard, S., Kao, S.-J., Kiefer, T., Kienast, S., Lehmann, M., Martinez, P., McCarthy, M., Möbius, J., Pedersen, T., Quan, T. M., Ryabenko, E., Schmittner, A., Schneider, R., Schneider-Mor, A., Shigemitsu, M., Sinclair, D., Somes, C., Studer, A., Thunell, R., and Yang, J.-Y., 2012, A review of nitrogen isotopic alteration in marine sediments: Paleoceanography, v. 27, no. 4, p. PA4203.

Romero, J. A. S., Lafon, J. M., Nogueira, A. C. R., and Soares, J. L., 2013, Sr isotope geochemistry and Pb-Pb geochronology of the Neoproterozoic cap carbonates, Tangara da Serra, Brazil: International Geology Review, v. 55, no. 2, p. 185-203.

Rothman, D. H., Hayes, J. M., and Summons, R. E., 2003, Dynamics of the Neoproterozoic carbon cycle: Proceedings of the National Academy of Sciences, v. 100, no. 14, p. 8124-8129.

Sawaki, Y., Tahata, M., Ohno, T., Komiya, T., Hirata, T., Maruyama, S., Han, J., and Shu, D., 2014, The anomalous Ca cycle in the Ediacaran ocean: Evidence from Ca isotopes preserved in carbonates in the Three Gorges area, South China: Gondwana Research, v. 25, no. 3, p. 1070-1089.

Schrag, D. P., Higgins, J. A., Macdonald, F. A., and Johnston, D. T., 2013, Authigenic Carbonate and the History of the Global Carbon Cycle: Science, v. 339, no. 6119, p. 540-543.

Sergeev, V. N., Chumakov, N. M., Semikhatov, M. A., and Vorob'eva, N. G., 2013, Microfossils from cap dolomites of the Lower Vendian Churochnaya Formation in the Polyudov Range (North Urals): Paleoecological approach to interpretation of Late Proterozoic glaciations: Stratigraphy and Geological Correlation, v. 21, no. 1, p. 1-7.

Shields, G., 2008, Palaeoclimate - Marinoan meltdown: Nature Geoscience, v. 1, no. 6, p. 351-353.

Shields, G. A., 2005, Neoproterozoic cap carbonates: a critical appraisal of existing models and the plumeworld hypothesis: Terra Nova, v. 17, no. 4, p. 299-310.

Sigman, D. M., Altabet, M. A., McCorkle, D. C., Francois, R., and Fischer, G., 2000, The $\delta^{15}N$ of nitrate in the Southern Ocean: Nitrogen cycling and circulation in the ocean interior: Journal of Geophysical Research: Oceans, v. 105, no. C8, p. 19599-19614.

Sigman, D. M., Karsh, K. L., and Casciotti, K. L., 2009, Nitrogen Isotopes in the Ocean, *in* Steele, J. H., ed., Encyclopedia of Ocean Sciences (2nd Edition): Oxford, Academic Press, p. 40-54.

Sliwinski, M. G., Whalen, M. T., Newberry, R. J., Payne, J. H., and Day, J. E., 2011, Stable isotope ($\delta^{13}C_{carb\ and\ org}$, $\delta^{15}N_{org}$) and trace element anomalies during the Late Devonian 'punctata Event' in the Western Canada Sedimentary Basin: Palaeogeography Palaeoclimatology Palaeoecology, v. 307, no. 1-4, p. 245-271.

Smith, M. P., and Harper, D. A. T., 2013, Causes of the Cambrian Explosion: Science, v. 341, no. 6152, p. 1355-1356.

Spangenberg, J. E., Bagnoud-Velásquez, M., Boggiani, P. C., and Gaucher, C., 2014, Redox variations and bioproductivity in the Ediacaran: Evidence from inorganic and organic geochemistry of the Corumbá Group, Brazil: Gondwana Research, http://dx.doi.org/10.1016/j.gr.2013.08.014.

Struck, U., Emeis, K.-C., Voß, M., Krom, M. D., and Rau, G. H., 2001, Biological productivity during sapropel S5 formation in the Eastern Mediterranean Sea: Evidence from stable isotopes of nitrogen and carbon: Geochimica et Cosmochimica Acta, v. 65, no. 19, p. 3249-3266.

Struck, U., 2012, On The Use of Stable Nitrogen Isotopes in Present and Past Anoxic Environments, *in* Altenbach, A. V., Bernhard, J. M., and Seckbach, J., eds., Anoxia, Volume 21, Springer Netherlands, p. 497-513.

Tahata, M., Ueno, Y., Ishikawa, T., Sawaki, Y., Murakami, K., Han, J., Shu, D., Li, Y., Guo, J., Yoshida, N., and Komiya, T., 2013, Carbon and oxygen isotope chemostratigraphies of the Yangtze platform, South China: Decoding temperature and environmental changes through the Ediacaran: Gondwana Research, v. 23, no. 1, p. 333-353.

Thomazo, C., Ader, M., and Philippot, P., 2011, Extreme ^{15}N-enrichments in 2.72-Gyr-old sediments: evidence for a turning point in the nitrogen cycle: Geobiology, v. 9, no. 2, p. 107-120.

Thomazo, C., and Papineau, D., 2013, Biogeochemical Cycling of Nitrogen on the Early Earth: Elements, v. 9, no. 5, p. 345-351.

Veizer, J., Bruckschen, P., Pawellek, F., Diener, A., Podlaha, O. G., Carden, G. A. F., Jasper, T., Korte, C., Strauss, H., Azmy, K., and Ala, D., 1997, Oxygen isotope evolution of Phanerozoic seawater: Palaeogeography, Palaeoclimatology, Palaeoecology, v. 132, no. 1–4, p. 159-172.

Veizer, J., Ala, D., Azmy, K., Bruckschen, P., Buhl, D., Bruhn, F., Carden, G. A. F., Diener, A., Ebneth, S., Godderis, Y., Jasper, T., Korte, C., Pawellek, F., Podlaha, O. G., and Strauss, H., 1999, $^{87}Sr/^{86}Sr$, $\delta^{13}C$ and $\delta^{18}O$ evolution of Phanerozoic seawater: Chemical Geology, v. 161, no. 1–3, p. 59-88.

Verdel, C., Wernicke, B. P., and Bowring, S. A., 2011, The Shuram and subsequent Ediacaran carbon isotope excursions from southwest Laurentia, and implications for environmental stability during the metazoan radiation: Geological Society of America Bulletin, v. 123, no. 7-8, p. 1539-1559.

Wada, E., and Hattori, A., 1976, Natural abundance of ^{15}N in particulate organic matter in the North Pacific Ocean: Geochimica et Cosmochimica Acta, v. 40, no. 2, p. 249-251.

Wang, J., Chen, D., Yan, D., Wei, H., and Xiang, L., 2012a, Evolution from an anoxic to oxic deep ocean during the Ediacaran–Cambrian transition and implications for bioradiation: Chemical Geology, v. 306–307, no. 0, p. 129-138.

Wang, W., Zhou, C., Yuan, X., Chen, Z., and Xiao, S., 2012b, A pronounced negative $\delta^{13}C$ excursion in an Ediacaran succession of western Yangtze Platform: A possible equivalent to the Shuram event and its implication for chemostratigraphic correlation in South China: Gondwana Research, v. 22, no. 3–4, p. 1091-1101.

Wang, W., Zhou, C., Guan, C., Yuan, X., Chen, Z., and Wan, B., 2014, An integrated carbon, oxygen, and strontium isotopic studies of the Lantian Formation in South China with implications for the Shuram anomaly: Chemical Geology, v. 373, no. 0, p. 10-26.

Weber, B., Steiner, M., Evseev, S., and Yergaliev, G., 2013, First report of a Meishucun-type early Cambrian (Stage 2) ichnofauna from the Malyi Karatau area (SE Kazakhstan): Palaeoichnological, palaeoecological and palaeogeographical implications: Palaeogeography Palaeoclimatology Palaeoecology, v. 392, p. 209-231.

Wille, M., Nagler, T. F., Lehmann, B., Schroder, S., and Kramers, J. D., 2008, Hydrogen sulphide release to surface waters at the Precambrian/Cambrian boundary: Nature, v. 453, no. 7196, p. 767-769.

Yuan, X., Chen, Z., Xiao, S., Zhou, C., and Hua, H., 2011, An early Ediacaran assemblage of macroscopic and morphologically differentiated eukaryotes: Nature, v. 470, no. 7334, p. 390-393.

Zerkle, A. L., Scheiderich, K., Maresca, J. A., Liermann, L. J., and Brantley, S. L., 2011, Molybdenum isotope fractionation by cyanobacterial assimilation during nitrate utilization and N_2 fixation: Geobiology, v. 9, no. 1, p. 94-106.

Zhu, M., Zhang, J., Steiner, M., Yang, A., Li, G., and Erdtmann, B. D., 2003, Sinian-Cambrian stratigraphic framework for shallow- to deep-water environments of the Yangtze Platform: an integrated approach: Progress in Natural Science, v. 13, no. 12, p. 951-960.

Zhu, M., Zhang, J., and Yang, A., 2007, Integrated Ediacaran (Sinian) chronostratigraphy of South China: Palaeogeography, palaeoclimatology, Palaeoecology, v. 254, p. 7-61.

Zyakun, A. M., Lunina, O. N., Prusakova, T. S., Pimenov, N. V., and Ivanov, M. V., 2009, Fractionation of stable carbon isotopes by photoautotrophically growing anoxygenic purple and green sulfur bacteria: Microbiology, v. 78, no. 6, p. 757-768.

8. CONCLUSION

8.1 Conclusion

We investigated carbon and nitrogen cycling on two Precambrian-Cambrian microcontinents linked to their global chemostratigraphic context including first, late Ediacaran Dengying strata of the South China Block (Yangtze platform; chapter 5 - 6), and second, Ediacaran to early Cambrian strata on the Kazakh microcontinent (Malyi Karatau Range; chapter 7). Corresponding rocks document oceanic compositional changes which are mirrored in large fluctuations in the carbon and nitrogen isotopic record. In this sense, nitrogen and carbon isotopes were used to investigate redox conditions, biogeochemistry and biological activity of an ancient marine ecosystem during a period where changes in the chemical composition of the ocean evolved together with new forms of multicellular life.

Obtained results reveal four major conclusions:

First, chemostratigraphic analyses document that the Gaojiashan and Kyrshabakty sections most likely span across the Pc-C boundary interval and thus serve as new representatives for global Pc-C boundary sections. Both isotope records show a prominent $\delta^{13}C_{carb}$ negative excursion down to ~-6‰ that correlates with the global negative $\delta^{13}C$ excursion associated with the approximate beginning of the lower Cambrian. Bio- and chemostratigraphic analyses of the Gaojiashan section imply the necessity for stratigraphic re-investigation in southern Shaanxi Province. In Kazakhstan, isotope results establish the first high-resolution global chemostratigraphic correlation based on three Ediacaran to Cambrian $\delta^{13}C_{carb}$ negative anomalies which demonstrate unambiguous similarities with isotopic records of South China and Oman. Furthermore, the obtained $\delta^{15}N$ dataset is the first broad nitrogen record across the Ediacaran into the early Cambrian outside South China.

Second, both $\delta^{15}N$ datasets point out that the Ediacaran nitrogen cycling did generally not differ from the modern nitrogen cycle. Elevated $\delta^{15}N$ values >3‰ show that nitrate was present in widespread oceanic parts (except for oxygen

minimum zones and anoxic water bodies) similar to today, thus suggesting at least mildly oxygenated surface and intermediate water conditions through most Ediacaran times. However, slightly fluctuating $\delta^{15}N$ values during the cap carbonate interval ($\delta^{15}N$ ~2‰) and across the Shuram-Wonoka event ($\delta^{15}N$ from 1.6 to 3.7‰) at the Kazakh Kyrshabakty section assume frequent variations in the water redox conditions. Because NO_3^- availability is strongly controlled by the depth of the redox transition zone, the variable presence of oxygen likely facilitated N_2-fixation to compensate for (weak) nitrate-limitation during the respective periods. In contrast, across the Pc-C boundary interval nitrogen cycling experienced significant changes indicated by a prominent $\delta^{15}N$ negative interval. Isotope values suggest a predominantly anoxic to euxinic photic zone which forced the nitrogen cycle towards strong nitrate-limitation and weak denitrification rates. In this scenario for which the Black Sea serves as a modern analogue, NH_4^+ assimilation and N_2-fixation are predominantly responsible for the introduction of new nitrogen via oxygenic and anoxygenic photosynthetic bacteria.

Third, the large-scale conformity of the $\delta^{15}N$ trend from the Ediacaran until the lower Cambrian obtained from Gaojiashan, Kyrshabakty and Berkuty sections as well as Longbizui and Xiaofenghe sections (Appendix A3.3, A3.4, respectively) with further datasets from South China (Cremonese et al., 2013; Ader et al., 2014; Cremonese et al., 2014; Kikumoto et al., 2014; Wang et al., in prep.) implies that obtained $\delta^{15}N$ data represent a global signal of perturbation in the past nitrogen cycle (Fig. 21). Small-scale fluctuations within the Ediacaran $\delta^{15}N$ record may result from regional environmental perturbations of the local nitrogen cycle causing temporal changes of the $\delta^{15}N$ in the local nitrate pool or are simply attributed to the different resolution of the datasets. In either way, data imply that the ocean periodically contained enough dissolved oxygen since the early Ediacaran and probably already since the later Neoproterozoic Era (Ader et al., 2014) to stabilize nitrate similar to the modern oceans.

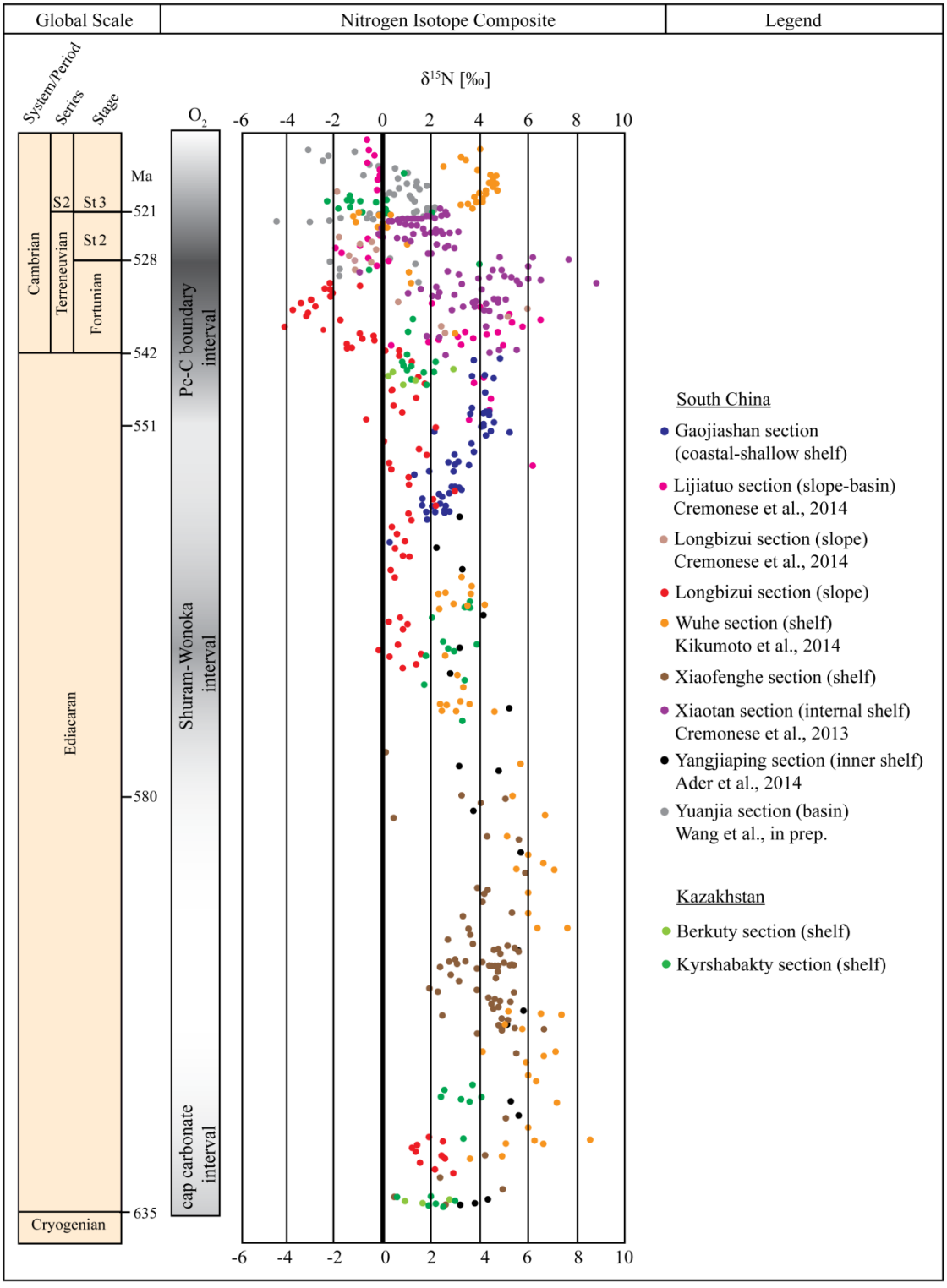

Figure 21: Schematic composite of Ediacaran to lower Cambrian $\delta^{15}N$ datasets of the following sections: Gaojiashan, Kyrshabakty, Berkuty, Longbizui, Xiaofenghe (all this study), Xiaotan (Cremonese et al., 2013), Longbizui, Lijiatuo (both Cremonese et al., 2014), Wuhe (drill core samples; Kikumoto et al., 2014), Yangjiaping (Ader et al., 2014) and Yuanjia (Wang et al., in prep.). Data show similar trends throughout the Ediacaran and lower Cambrian arguing for the $\delta^{15}N$ signature to represent global nitrogen cycle perturbation. Color gradations of the middle column indicate postulated variations in shallow-water redox conditions. S2: Series 2, St2: Stage 2, St3: Stage 3.

Fourth, obtained negative $\delta^{13}C_{carb}$ and $\delta^{15}N$ anomalies of Kazakhstan and South China manifest the scenario of a global "oceanic anoxic event" that was involved in the course of the Cambrian radiation. Negative $\delta^{15}N$ intervals during the lower Cambrian are documented on at least two different albeit closely associated Pc-C microcontinents arguing for widespread anoxic photic zone conditions. However, $\delta^{15}N$ chemostratigraphy finds its limits in organic-poor lithologies, as e.g. present across the Pc-C boundary interval at Gaojiashan section.

In conclusion, especially $\delta^{15}N$ isotope data of the Kyrshabakty section contributed to a deeper understanding of Ediacaran and Cambrian biogeochemical cycling as it is the first dataset spanning from the early Ediacaran into the lower Cambrian on a so far largely unstudied Pc-C microcontinent. Our data pave the way for further isotopic investigations in southern Kazakhstan associated with the Precambrian-Cambrian ecosphere (r)evolution.

8.2 References

Ader, M., Sansjofre, P., Halverson, G. P., Busigny, V., Trindade, R. I. F., Kunzmann, M., and Nogueira, A. C. R., 2014, Ocean redox structure across the Late Neoproterozoic Oxygenation Event: A nitrogen isotope perspective: Earth and Planetary Science Letters, v. 396, no. 0, p. 1-13.

Cremonese, L., Shields-Zhou, G., Struck, U., Ling, H.-F., Och, L., Chen, X., and Li, D., 2013, Marine biogeochemical cycling during the early Cambrian constrained by a nitrogen and organic carbon isotope study of the Xiaotan section, South China: Precambrian Research, v. 225, no. 0, p. 148-165.

Cremonese, L., Shields-Zhou, G. A., Struck, U., Ling, H.-F., and Och, L. M., 2014, Nitrogen and organic carbon isotope stratigraphy of the Yangtze Platform during the Ediacaran–Cambrian transition in South China: Palaeogeography, Palaeoclimatology, Palaeoecology, v. 398, no. 0, p. 165-186.

Kikumoto, R., Tahata, M., Nishizawa, M., Sawaki, Y., Maruyama, S., Shu, D., Han, J., Komiya, T., Takai, K., and Ueno, Y., 2014, Nitrogen isotope chemostratigraphy of the Ediacaran and Early Cambrian platform sequence at Three Gorges, South China: Gondwana Research, v. 25, no. 3, p. 1057-1069.

Wang, D., Struck, U., Ling, H., Guo, Q., Shields-Zhou, G., Zhu, M., and Yao, S., in prep., Nitrogen isotopes of black shales during Early Cambrian on Yangtze block, South China.

9. OUTLOOK AND FUTURE WORK

Despite the fact that our knowledge on the distribution of nitrogen isotopes in Precambrian-Cambrian strata is growing, it is still associated with a modest degree of uncertainty. The investigation of $\delta^{15}N$ records on further Pc-C microcontinents would be required to expand the application of $\delta^{15}N$ as a paleoenvironmental proxy. Thereby, Pc-C sections in Oman would offer great potential for nitrogen isotope investigation because of their well-studied bio-, litho-, and chemostratigraphic records and radiometric age dating of the Pc-C boundary. Furthermore, a reconnaissance trip in 2013 of several group members from the FOR 736 to Mongolia revealed that Mongolian Pc-C strata represent a promising study opportunity due to well-preserved, thick Pc-C boundary strata (M. Steiner and B. Weber, pers. comm.); however isotope investigations are sparse.

Furthermore, isotope analyses of the Ediacaran-Cambrian South China Longbizui section (Yangtze platform, Hunan Province; Appendix A3.3) yielded remarkable similarities regarding shape and magnitude of the Ediacaran and early Cambrian $\delta^{13}C_{carb}$ and $\delta^{15}N$ record with the Kazakh Kyrshabakty section. Figure 22 shows a preview of the chemostratigraphic correlation between both sections which is part of a fourth manuscript in preparation. This is the first chemostratigraphic correlation of high-resolution Ediacaran to early Cambrian $\delta^{15}N$ records of two sections located on two microcontinents linked to a comprehensive $\delta^{13}C_{carb}$ dataset.

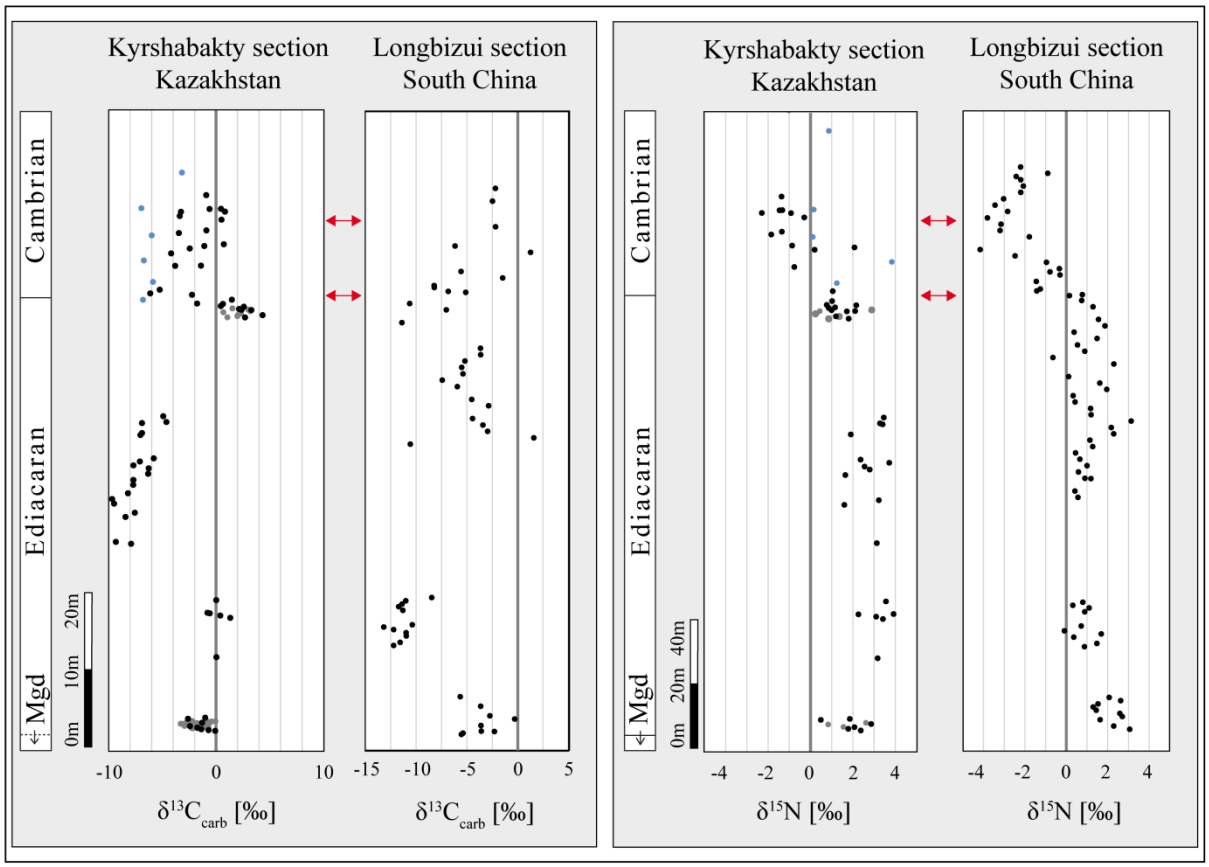

Figure 22: $\delta^{13}C_{carb}$ and $\delta^{15}N$ chemostratigraphic correlation of the South China Longbizui section and the Kazakh Kyrshabakty section (chapter 7; Fig. 18) spanning from the basal Ediacaran cap carbonate unit to the early Cambrian. Both sections show the prominent $\delta^{13}C_{carb}$ trend across the Pc-C boundary and a negative $\delta^{15}N$ interval during the lower Cambrian indicated by red arrows expressing proposed correlation of isotopic excursions between sections. The presence of the negative $\delta^{15}N$ period on both microcontinents strongly argues for the global representativeness of the nitrogen signal. Mgd: Marinoan-age glacial deposit.

Additionally, high-resolution nitrogen and carbon isotope measurements of the Ediacaran South China Doushantuo Formation at Xiaofenghe section (Yangtze platform, Hubei Province; Appendix A3.4) have been completed. Together with a REE dataset of the same samples conducted by Simon Hohl and Harry Becker (subproject 4, FOR 736), a manuscript examining a multi-proxy interpretation model to get insights into environmental changes during the early Ediacaran of South China is intended.

The investigation of sedimentary biomarkers can contribute greatly to paleoenvironmental studies and provide information about specific biological sources. Furthermore, the measurement of compound-specific $\delta^{15}N$ ratios of biomarkers like e.g. derivatives of chlorophyll (porphyrin) is an attractive opportunity to gain insights in surface-water processes because the photo-

pigments are used by all photosynthesizing organisms. Yet, these techniques require a specific amount of well-preserved organic material and it is hitherto ambiguous if the Pc-C rocks fulfill these criteria. For the purposes of biomarker extraction, samples spanning the Ediacaran and the Pc-C boundary from Kazakhstan (Kyrshabakty section) were sent to the laboratories of Prof. Richard Pancost (University of Bristol, School of Chemistry, Organic Geochemistry Unit, United Kingdom).

To address the question if oceanic anoxia and mass extinction events are coupled to periods of negative $\delta^{15}N$ data recorded in sediments through Earth's history, a section spanning the widespread Devonian mass extinction event called the "Kellwasser event" in the Harz Mountains, Germany was sampled. In the course of the Bachelor thesis of Yannik Steinmann (Freie Universität Berlin) nitrogen and carbon isotope datasets from two prominent Kellwasser horizons (black shales) were conducted which are proposed to be deposited during periods of widespread oceanic anoxia. Results showed that the Kellwasser horizons are characterized by a negative $\delta^{15}N$ excursion comparable to the early Cambrian (for further information, see Appendix A1). In this sense, it would be interesting to see if mass extinction events through Earth's history are in general associated to periods of widespread anoxic water conditions and negative $\delta^{15}N$ values.

APPENDIX

A1 Conference and Symposium contributions

Fermor Meeting of the Geological Society 2012, "The Neoproterozoic Era - Evolution, Glaciation, Oxygenation" (London, United Kingdom, Poster):

- **Gamper, A.**, Struck, U., Scouflaire, Q., Weber, B., Insights into causes of the Cambrian Explosion: A carbon and nitrogen isotope study

Centenary Meeting of the Paläontologische Gesellschaft 2012 (Berlin, Germany, Poster):

- **Gamper, A.**, Struck, U., Scouflaire, Q., Weber, B., Insights into causes of the Cambrian Explosion: A carbon and nitrogen isotope study
- abstract available at http://shop.strato.de/epages/61412926.sf/

Chinese-German Research Group Colloquium 2013 of the DFG-FOR 736 (Berlin, Germany, oral presentation):

- Insights into causes at the Precambrian-Cambrian transition interval: a nitrogen isotopic study

Goldschmidt Conference 2013 (Florence, Italy, Poster):

- **Gamper, A.**, Struck, U., Ergaliev, G., Tracking down the Ediacaran isotope anomalies in a sedimentary section from Kazakhstan
- abstract available at http://minmag.geoscienceworld.org/content/77/5/1239.full.pdf+html
- Hohl, S., Becker, H., Herzlieb, S., Guo, Q., **Gamper, A.**, Multi-proxy study of shallow- and deep-water Doushantuo carbonates, Yangtze Platform, South China
- abstract available at http://minmag.geoscienceworld.org/content/77/5/1239.full.pdf+html

- Ohnemueller, F., Meixner, A., **Gamper, A.**, Kasemann, S. A., Ocean-pH evolution and weathering conditions during the Ediacaran: Insights from B, Sr & Li isotopes at the Gaojiashan Section, South China
- abstract available at http://minmag.geoscienceworld.org/content/77/5/1869.full.pdf+html
- Steinmann, Y., Struck, U., **Gamper, A.**, Late Devonian "Kellwasser-Event" A global mass-extinction equivalent to the Precambrian-Cambrian boundary interval?
- abstract available at http://minmag.geoscienceworld.org/content/77/5/2018.full.pdf+html

GSA (The Geological Society of America) annual meeting 2014 (Vancouver, Canada, oral presentation, in prep.):

- **Gamper, A.**, Struck, U., Biogeochemistry and nitrogen isotope stratigraphy during the Ediacaran and early Cambrian of Central Asia

A2 Contribution to other Journal Articles

Manuscript in preparation for submission to *Earth and Planetary Science Letters*

- Ohnemueller, F., **Gamper, A.**, Meixner, A., Kasemann, S. A., Ocean pH and weathering conditions during the upper Ediacaran: Insights from the Chinese Gaojiashan Section

A3 Dataset South China

A3.1 Table I - Coordinates of visited sections

Section	Province	Coordinates	
Gaojiashan section	Shaanxi Province	32°57'29.48" N	106°27'33.80" E
Huajipo section	Hubei Province	30°46'52.00" N	111°01'58.00" E
Hushan-Wangji section	Hubei Province	31°24'29.58" N	112°17'43.14" E
Jijiawan (Maoping) section	Hubei Province	30°52'59.00" N	110°52'44.00" E
Jiulongwan section	Hubei Province	30°48'11.46" N	111°03'18.42" E
Lijiatuo section	Hunan Province	28°24'31.14" N	110°27'55.56" E
Longbizui section	Hunan Province	28°29'57.96" N	109°50'27.96" E
Sixi section	Hubei Province	30°45'22.50" N	110°55'24.00" E
Xiaofenghe section	Hubei Province	30°56'29.46" N	111°13'57.42" E
Xixi section	Hunan Province	no coordinates	

A3.2 Table II - Isotope dataset Gaojiashan section

Abbreviations: / = interbedded, w/ = with; samples with N values in bold/ italics (<0.01 mgN/sample) are only listed for data completeness (applicable for all listed datasets) and have not been considered for data interpretation

Sample		Distance [m]	Formation	Member	Lithology	$\delta^{13}C_{carb}$ [‰] vs. VPDB	$\delta^{18}O$ [‰] vs. VPDB	$\delta^{13}C_{org}$ [‰] vs. VPDB	mgC/ sample	C [%]	TOC [%]	$\delta^{15}N_{bulk}$ [‰] vs. AIR	mgN/ sample	N [%] (TN)
Gj	-3.6	-3.6	Dengying	Algal Dolomite	dolostone	0.9	-2.5							
Gj	-3.3	-3.3	Dengying	Algal Dolomite	dolostone	0.8	-0.1	-27.0	0.025	0.021		0.4	0.017	0.010
Gj	-3.0	-3.0	Dengying	Algal Dolomite	oncoidic dolostone	1.0	-0.8	-26.0	0.021	0.016	0.003			
Gj	-2.6	-2.6	Dengying	Algal Dolomite	oncoidic dolostone	1.1	-1.8	-22.6	0.030	0.024	0.003			
Gj	-2.0	-2.0	Dengying	Algal Dolomite	calcarenite (biolaminated)	0.8	-2.7	-24.8	0.133	0.109				
Gj	-1.6	-1.6	Dengying	Algal Dolomite	oncoidic dolostone	0.6	-3.5	-24.1	0.212	0.201				
Gj	-1.3	-1.3	Dengying	Algal Dolomite	oncoidic dolostone	0.6	-1.4	-27.6	0.036	0.033	0.004			
Gj	-1.0	-1.0	Dengying	Algal Dolomite	calcarenite (biolaminated)	0.6	-3.1		0.237	0.190	0.013			
Gj	-0.6	-0.6	Dengying	Algal Dolomite	oncoidic dolostone	0.5	-1.6	-25.8	0.068	0.055				
Gj	-0.3	-0.3	Dengying	Algal Dolomite	oncoidic dolostone	0.3	-3.0	-28.0	0.519	0.412	0.015			
Gj	2.3	2.3	Dengying	Gaojiashan	doloshale	0.8	-2.0	-27.3	0.035	0.029	0.004			
Gj	4.3	4.3	Dengying	Gaojiashan	doloshale							1.9	0.051	0.028
Gj	6.0	6.0	Dengying	Gaojiashan	doloshale			-28.5	0.131	0.120		2.2	0.085	0.050
Gj	6.3	6.3	Dengying	Gaojiashan	doloshale									
Gj	6.5	6.5	Dengying	Gaojiashan	doloshale							1.8	0.046	0.025
Gj	6.6	6.6	Dengying	Gaojiashan	doloshale							2.6	0.037	0.020
Gj	7.0	7.0	Dengying	Gaojiashan	doloshale			-27.9	0.096	0.090	0.089	2.8	0.036	0.020
Gj	7.3	7.3	Dengying	Gaojiashan	doloshale							2.6	0.040	0.023
Gj	7.6	7.6	Dengying	Gaojiashan	doloshale							2.6	0.035	0.020
Gj	8.0	8.0	Dengying	Gaojiashan	doloshale			-28.4	0.109	0.092	0.089	2.6	0.039	0.022
Gj	8.3	8.3	Dengying	Gaojiashan	doloshale							2.2	0.039	0.021
Gj	8.6	8.6	Dengying	Gaojiashan	arenitic dolostone	0.3	-0.2	-23.9	0.027	0.020	0.004	1.7	0.012	0.007
Gj	9.5	9.5	Dengying	Gaojiashan	arenitic dolostone	0.1	-0.4	-24.2	0.026	0.022	0.002	2.4	0.011	0.006
Gj	10.3	10.3	Dengying	Gaojiashan	doloshale	0.7	-0.7	-26.7	0.013	0.011	0.003	1.7	0.013	0.007

Sample	Distance [m]	Formation	Member	Lithology	$\delta^{13}C_{carb}$ [‰] vs. VPDB	$\delta^{18}O$ [‰] vs. VPDB	$\delta^{13}C_{org}$ [‰] vs. VPDB	mgC/ sample	C [%]	TOC [%]	$\delta^{15}N_{bulk}$ [‰] vs. AIR	mgN/ sample	N [%] (TN)
Gj 10.6	10.6	Dengying	Gaojiashan	dolomitic breccia	0.7	-0.9	-29.6	0.018	0.015	0.002		***0.008***	***0.005***
Gj 11.0	11.0	Dengying	Gaojiashan	dolomitic breccia	0.9	0.0	-25.7	0.028	0.023	0.006		***0.006***	***0.003***
Gj 11.3	11.3	Dengying	Gaojiashan	doloshale							2.5	0.032	0.018
Gj 12.0	12.0	Dengying	Gaojiashan	sandstone							2.8	0.012	0.007
Gj 12.3	12.3	Dengying	Gaojiashan	sandstone								***0.007***	***0.004***
Gj 12.6	12.6	Dengying	Gaojiashan	sandstone	-0.8	-3.7	-30.5	0.067	0.050	0.049	2.4	0.020	0.011
Gj 13.0	13.0	Dengying	Gaojiashan	sandstone	-0.1	-5.3	-33.9	0.040	0.032	0.019	3.1	0.015	0.008
Gj 13.3	13.3	Dengying	Gaojiashan	sandstone	0.8	-4.5	-32.8	0.032	0.027		3.3	0.010	0.006
Gj 13.6	13.6	Dengying	Gaojiashan	pyritic chert	0.6	-4.0	-31.4	0.026	0.022	0.009		***0.005***	***0.003***
Gj 14.3	14.3	Dengying	Gaojiashan	dolomitic carb. sandstone	0.9		-33.5	0.142	0.119		3.1	0.020	0.011
Gj 14.6	14.6	Dengying	Gaojiashan	dolomitic carb. sandstone							2.9	0.036	0.020
Gj 14.8	14.8	Dengying	Gaojiashan	dolomitic carb. sandstone	0.3								
Gj 15.0	15.0	Dengying	Gaojiashan	arenitic dolostone							3.0	0.020	0.011
Gj 15.6	15.6	Dengying	Gaojiashan	arenitic dolostone	0.3		-32.1	0.342	0.268	0.103			
Gj 16.3	16.3	Dengying	Gaojiashan	arenitic dolostone	1.2	-4.8	-33.7	0.054	0.051	0.021		***0.009***	***0.005***
Gj 17.6	17.6	Dengying	Gaojiashan	arenitic dolostone	0.7							***0.005***	***0.003***
Gj 18.0	18.0	Dengying	Gaojiashan	arenitic dolostone	-0.1							***0.006***	***0.003***
Gj 18.3	18.3	Dengying	Gaojiashan	arenitic dolostone	0.0		-28.0	0.014	0.013	0.013		***0.006***	***0.004***
Gj 18.6	18.6	Dengying	Gaojiashan	arenitic dolostone	-0.1	-8.6	-32.9	0.118	0.096		1.4	0.012	0.005
Gj 19.0	19.0	Dengying	Gaojiashan	arenitic dolostone	0.2	-6.2	-30.6	0.022	0.017	0.005		***0.006***	***0.003***
Gj 19.3	19.3	Dengying	Gaojiashan	arenitic dolostone	-0.3		-30.7	0.029	0.023	0.012			
Gj 19.6	19.6	Dengying	Gaojiashan	arenitic dolostone	0.6		-32.2	0.018	0.014	0.007	1.9	0.011	0.007
Gj 20.0	20.0	Dengying	Gaojiashan	arenitic dolostone	1.2	-6.6	-27.8	0.052	0.048	0.006	3.0	0.011	0.006
Gj 20.3	20.3	Dengying	Gaojiashan	arenitic dolostone	-0.9		-28.4	0.014	0.011	0.008			
Gj 20.6	20.6	Dengying	Gaojiashan	arenitic dolostone	1.2		-28.6	0.042	0.033	0.017		***0.007***	***0.004***
Gj 21.0	21.0	Dengying	Gaojiashan	arenitic dolostone	0.9		-27.5	0.047	0.041	0.011		***0.007***	***0.004***
Gj 21.3	21.3	Dengying	Gaojiashan	arenitic dolostone	0.4						3.0	0.011	0.006
Gj 21.6	21.6	Dengying	Gaojiashan	arenitic dolostone	-1.9	-7.5	-32.3	0.051	0.041	0.033			

Sample	Distance [m]	Formation	Member	Lithology	$\delta^{13}C_{carb}$ [‰] vs. VPDB	$\delta^{18}O$ [‰] vs. VPDB	$\delta^{13}C_{org}$ [‰] vs. VPDB	mgC/ sample	C [%]	TOC [%]	$\delta^{15}N_{bulk}$ [‰] vs. AIR	mgN/ sample	N [%] (TN)
Gj 22.0	22.0	Dengying	Gaojiashan	arenitic dolostone	0.7	-6.0	-28.4	0.019	0.016		3.6	0.013	0.007
Gj 22.3	22.3	Dengying	Gaojiashan	arenitic dolostone	0.8		-28.9				3.2	0.011	0.006
Gj 22.6	22.6	Dengying	Gaojiashan	arenitic dolostone	1.0		-26.8	0.051	0.042	0.011	2.7	0.010	0.006
Gj 23.3	23.3	Dengying	Gaojiashan	micrite/clay	1.7		-28.8	0.040	0.034	0.015			
Gj 24.0	24.0	Dengying	Gaojiashan	micrite/clay	1.5		-30.5	0.058	0.056	0.009		***0.005***	***0.003***
Gj 24.3	24.3	Dengying	Gaojiashan	micrite/clay	1.3							***0.007***	***0.004***
Gj 24.6	24.6	Dengying	Gaojiashan	micrite/clay	0.6		-28.1	0.030	0.028	0.009	3.0	0.013	0.007
Gj 25.0	25.0	Dengying	Gaojiashan	micrite/clay	1.3		-27.6	0.056	0.046	0.012		***0.008***	***0.004***
Gj 25.3	25.3	Dengying	Gaojiashan	micrite/clay	1.0	-6.6	-29.8	0.057	0.055	0.017		***0.009***	***0.005***
Gj 25.5	25.5	Dengying	Gaojiashan	micritic limestone	0.8	-7.1						***0.005***	***0.003***
Gj 26.0	26.0	Dengying	Gaojiashan	micrite/clay	1.8		-29.4	0.076	0.060	0.012		***0.008***	***0.005***
Gj 26.3	26.3	Dengying	Gaojiashan	micrite/clay	1.0		-30.3	0.087	0.078	0.012	3.8	0.011	0.005
Gj 26.6	26.6	Dengying	Gaojiashan	micrite/clay	-0.4	-7.5	-32.0	0.355	0.290				
Gj 27.0	27.0	Dengying	Gaojiashan	micrite/clay	1.3	-6.5	-30.5	0.106	0.078	0.017		***0.008***	***0.004***
Gj 27.3	27.3	Dengying	Gaojiashan	micrite/clay	1.3		-31.2	0.078	0.062	0.017			
Gj 27.6	27.6	Dengying	Gaojiashan	micrite/clay	2.3		-27.2	0.087	0.070	0.015		***0.009***	***0.005***
Gj 28.3	28.3	Dengying	Gaojiashan	micrite/clay	2.0		-29.1	0.078	0.067	0.009		***0.006***	***0.003***
Gj 28.6	28.6	Dengying	Gaojiashan	micrite/clay	-0.7		-30.4	0.113	0.106	0.025		***0.008***	***0.005***
Gj 29.0	29.0	Dengying	Gaojiashan	micrite/clay	1.0	-6.6	-30.1	0.029	0.025	0.015	3.7	0.018	0.007
Gj 30.0	30.0	Dengying	Gaojiashan	micrite/clay	2.0		-26.0	0.017	0.014	0.015		***0.007***	***0.004***
Gj 31.3	31.3	Dengying	Gaojiashan	micrite/clay	2.6	-5.5	-27.5	0.112	0.099	0.020	4.3	0.013	0.007
Gj 31.6	31.6	Dengying	Gaojiashan	micrite/clay	3.0	-5.7	-29.5	0.093	0.085	0.014		***0.009***	***0.005***
Gj 32.0	32.0	Dengying	Gaojiashan	micrite/clay	4.1		-29.7	0.060	0.051	0.014	2.2	0.010	0.005
Gj 32.3	32.3	Dengying	Gaojiashan	micrite/clay	3.2		-28.1	0.060	0.055	0.012		***0.007***	***0.004***
Gj 32.6	32.6	Dengying	Gaojiashan	micrite/clay	2.7	-6.0	-30.5	0.066	0.060	0.014	5.3	0.010	0.005
Gj 33.0	33.0	Dengying	Gaojiashan	micrite/clay	-1.7		-26.0	0.086	0.072	0.059	4.5	0.028	0.017
Gj 33.6	33.6	Dengying	Gaojiashan	micrite/clay	0.2	-7.3	-29.3	0.057	0.044	0.041	4.1	0.032	0.019
Gj 34.6	34.6	Dengying	Gaojiashan	micrite/clay	-1.2		-25.4	0.091	0.076	0.070	4.2	0.033	0.018

Sample	Distance [m]	Formation	Member	Lithology	$\delta^{13}C_{carb}$ [‰] vs. VPDB	$\delta^{18}O$ [‰] vs. VPDB	$\delta^{13}C_{org}$ [‰] vs. VPDB	mgC/ sample	C [%]	TOC [%]	$\delta^{15}N_{bulk}$ [‰] vs. AIR	mgN/ sample	N [%] (TN)
Gj 35.0	35.0	Dengying	Gaojiashan	micrite/clay	-0.8	-7.8	-28.8	0.042	0.034	0.028	4.6	0.029	0.017
Gj 35.3	35.3	Dengying	Gaojiashan	micrite/clay	0.9						4.2	0.033	0.018
Gj 35.6	35.6	Dengying	Gaojiashan	micrite/clay	4.3							***0.007***	***0.004***
Gj 36.0	36.0	Dengying	Gaojiashan	micrite/clay	4.3	-4.9	-31.0	0.118	0.098	0.021		***0.008***	***0.005***
Gj 36.3	36.3	Dengying	Gaojiashan	micrite/clay	4.3	-5.8	-25.9	0.353	0.344				
Gj 37.0	37.0	Dengying	Gaojiashan	micrite/clay	2.3		-28.5	0.414	0.324				
Gj 37.3	37.3	Dengying	Gaojiashan	micrite/clay	4.5	-5.6						***0.007***	***0.004***
Gj 37.6	37.6	Dengying	Gaojiashan	micrite/clay	1.6	-7.3	-28.3	0.077	0.060	0.046	4.4	0.021	0.013
Gj 37.7	37.7	Dengying	Gaojiashan	micrite/clay	0.6	-5.2							
Gj 38.0	38.0	Dengying	Gaojiashan	micritic limestone	3.8	-5.5	-29.1	0.092	0.083	0.020	4.2	0.020	0.012
Gj 38.3	38.3	Dengying	Gaojiashan	micrite/clay	3.0	-7.6					3.7	0.030	0.016
Gj 38.6	38.6	Dengying	Gaojiashan	micrite/clay	0.9	-7.8	-27.3	0.085	0.072	0.058	4.3	0.027	0.015
Gj 39.0	39.0	Dengying	Gaojiashan	micrite/clay	4.6	-5.5	-29.5	0.080	0.069	0.016	4.4	0.012	0.006
Gj 39.3	39.3	Dengying	Gaojiashan	micrite/clay	5.7		-29.2	0.940	0.768	0.074	4.3	0.011	0.006
Gj 39.6	39.6	Dengying	Gaojiashan	micrite/clay	5.2	-5.6						***0.009***	***0.005***
Gj 40.0	40.0	Dengying	Gaojiashan	micrite/clay	3.8	-8.8	-30.2	0.107	0.090	0.046	3.7	0.023	0.013
Gj 40.3	40.3	Dengying	Gaojiashan	micrite/clay	5.1	-5.3							
Gj 40.6	40.6	Dengying	Gaojiashan	micrite/clay	5.7	-6.5							
Gj 41.0	41.0	Dengying	Gaojiashan	micritic limestone	4.6	-5.4	-27.3	0.405	0.331	0.045			
Gj 41.3	41.3	Dengying	Gaojiashan	micrite/clay	5.3	-5.6						***0.009***	***0.005***
Gj 42.0	42.0	Dengying	Gaojiashan	micritic limestone	5.4	-5.3	-28.8	0.309	0.250	0.029		***0.009***	***0.005***
Gj 42.3	42.3	Dengying	Gaojiashan	calcarenite (biolaminated)	5.1		-30.1	0.076	0.070	0.025			
Gj 42.6	42.6	Dengying	Gaojiashan	calcarenite (biolaminated)	5.6	-5.6						***0.009***	***0.005***
Gj 43.0	43.0	Dengying	Gaojiashan	micritic limestone	5.5	-6.3	-25.2	0.505	0.401	0.057			
Gj 43.3	43.3	Dengying	Gaojiashan	calcarenite (biolaminated)	5.3	-7.0							
Gj 43.6	43.6	Dengying	Gaojiashan	calcarenite (biolaminated)	5.6	-6.0						***0.008***	***0.005***
Gj 44.0	44.0	Dengying	Gaojiashan	micritic limestone	5.3		-27.0	0.480	0.389	0.051			
Gj 44.3	44.3	Dengying	Gaojiashan	calcarenite (biolaminated)	4.4	-6.1						***0.008***	***0.005***

Sample	Distance [m]	Formation	Member	Lithology	$\delta^{13}C_{carb}$ [‰] vs. VPDB	$\delta^{18}O$ [‰] vs. VPDB	$\delta^{13}C_{org}$ [‰] vs. VPDB	mgC/ sample	C [%]	TOC [%]	$\delta^{15}N_{bulk}$ [‰] vs. AIR	mgN/ sample	N [%] (TN)
Gj 45.0	45.0	Dengying	Gaojiashan	calcarenite (biolaminated)	6.2		-27.3	1.161	0.926	0.088			
Gj 45.3	45.3	Dengying	Gaojiashan	calcarenite (biolaminated)	6.2	-6.1						***0.008***	***0.004***
Gj 45.5	45.5	Dengying	Gaojiashan	calcarenite (biolaminated)	5.6	-6.0					4.3	0.010	0.006
Gj 46.0	46.0	Dengying	Gaojiashan	micritic limestone	6.0	-5.7	-29.5	0.096	0.089	0.012		***0.008***	***0.004***
Gj 46.3	46.3	Dengying	Gaojiashan	calcarenite (biolaminated)	5.9	-6.2						***0.008***	***0.004***
Gj 46.6	46.6	Dengying	Gaojiashan	calcarenite (biolaminated)	5.3	-5.4	-27.9	1.486	1.219			***0.007***	***0.004***
Gj 47.3	47.3	Dengying	Gaojiashan	calcarenite (biolaminated)	5.5	-5.4						***0.006***	***0.004***
Gj 47.6	47.6	Dengying	Gaojiashan	calcarenite (biolaminated)	5.6	-5.8	-28.9	0.858	0.673			***0.005***	***0.003***
Gj 48.0	48.0	Dengying	Gaojiashan	calcarenite (biolaminated)	4.5	-5.9						***0.004***	***0.002***
Gj 48.3	48.3	Dengying	Gaojiashan	calcarenite (biolaminated)	5.4	-5.7						***0.008***	***0.005***
Gj 48.6	48.6	Dengying	Gaojiashan	calcarenite (biolaminated)	4.9	-5.4						***0.009***	***0.005***
Gj 49.0	49.0	Dengying	Gaojiashan	calcarenite (biolaminated)	5.3	-5.6	-30.0	0.115	0.101	0.011		***0.009***	***0.005***
Gj 49.3	49.3	Dengying	Gaojiashan	calcarenite (biolaminated)	5.3	-5.5						***0.007***	***0.004***
Gj 49.6	49.6	Dengying	Gaojiashan	calcarenite (biolaminated)	4.6	-5.3	-25.9	1.158	0.935		4.6	0.010	0.005
Gj 50.0	50.0	Dengying	Gaojiashan	calcarenite (biolaminated)	4.1		-26.7	1.125	0.909	0.060			
Gj 50.3	50.3	Dengying	Gaojiashan	calcarenite (biolaminated)	4.3	-4.7					3.7	0.011	0.006
Gj 50.6	50.6	Dengying	Gaojiashan	calcarenite (biolaminated)	2.8	-6.9					4.3	0.012	0.006
Gj 51.0	51.0	Dengying	Gaojiashan	sandstone	4.0	-5.9	-25.5	1.095	0.818	0.076		***0.008***	***0.005***
Gj 51.3	51.3	Dengying	Gaojiashan	sandstone	2.4	-6.3						***0.006***	***0.004***
Gj 51.6	51.6	Dengying	Gaojiashan	sandstone	3.9	-3.3	-28.2	0.479	0.381			***0.008***	***0.005***
Gj 52.0	52.0	Dengying	Gaojiashan	sandstone	3.6	-4.0	-30.1	0.018	0.016	0.003		***0.008***	***0.004***
Gj 52.3	52.3	Dengying	Gaojiashan	sandstone	3.5	-2.6						***0.009***	***0.005***
Gj 52.6	52.6	Dengying	Gaojiashan	sandstone	3.0	-5.1	-29.9	0.081	0.065			***0.007***	***0.004***
Gj 53.0	53.0	Dengying	Gaojiashan	sandstone	-4.9	-6.6	-33.5	0.147	0.113	0.012		***0.003***	***0.002***
Gj 53.3	53.3	Dengying	Gaojiashan	sandstone	0.4	-7.6						***0.004***	***0.036***
Gj 53.6	53.6	Dengying	Gaojiashan	sandstone	1.4	-3.5						***0.003***	***0.002***
Gj 54.0	54.0	Dengying	Gaojiashan	sandstone	-0.8	-6.1	-28.6	0.336	0.224	0.008			
Gj 54.6	54.6	Dengying	Gaojiashan	sandstone	1.6	-7.7							

Sample	Distance [m]	Formation	Member	Lithology	$\delta^{13}C_{carb}$ [‰] vs. VPDB	$\delta^{18}O$ [‰] vs. VPDB	$\delta^{13}C_{org}$ [‰] vs. VPDB	mgC/ sample	C [%]	TOC [%]	$\delta^{15}N_{bulk}$ [‰] vs. AIR	mgN/ sample	N [%] (TN)
Gj 55.0	55.0	Dengying	Gaojiashan	sandstone	0.8	-7.1	-29.2	0.059	0.045	0.001			
Gj 55.3	55.3	Dengying	Gaojiashan	carbonaceous sandstone	0.3	-6.9							
Gj 55.6	55.6	Dengying	Gaojiashan	carbonaceous sandstone							3.8	0.014	0.007
Gj 56.0	56.0	Dengying	Gaojiashan	sandstone	-3.9	-7.4	-33.0	0.237	0.122	0.020	4.9	0.011	0.006
Gj 56.3	56.3	Dengying	Gaojiashan	carbonaceous sandstone	-3.8	-9.7						***0.003***	***0.002***
Gj 56.6	56.6	Dengying	Gaojiashan	sandstone	-3.3	-8.9							
Gj 57.0	57.0	Dengying	Gaojiashan	carbonaceous sandstone	-6.0	-8.0	-33.5	0.031	0.026	0.006		***0.003***	***0.002***
Gj 57.6	57.6	Dengying	Gaojiashan	sandstone									
Gj 58.0	58.0	Dengying	Gaojiashan	carbonaceous sandstone	-0.8	-7.2	-25.6	0.008	0.006	0.003			
Gj 58.6	58.6	Dengying	Gaojiashan	carbonaceous sandstone	1.4	-6.0	-24.2	0.137	0.113	0.012		***0.002***	***0.001***
Gj 59.0	59.0	Dengying	Gaojiashan	carbonaceous sandstone			-27.6	0.008	0.006	0.006		***0.003***	***0.001***
Gj 60.0	60.0		Beiwan	dolostone			-28.5	0.093	0.085	0.007		***0.003***	***0.002***
Gj 61.6	61.6		Beiwan	dolostone	1.7		-27.4	0.106	0.085	0.010			
Gj 62.3	62.3		Beiwan	dolostone	1.2		-24.2	0.274	0.221	0.016			
Gj 63.3	63.3		Beiwan	dolostone	1.3	-2.4	-27.8	0.107	0.102	0.004			
Gj 64.0	64.0		Beiwan	dolostone	1.6		-24.7	0.174	0.141	0.012			
Gj 64.6	64.6		Beiwan	dolostone	2.0	-2.0						***0.003***	***0.002***
Gj 65.0	65.0		Beiwan	dolostone	1.9	-2.8	-26.6	0.090	0.081			***0.004***	***0.002***
Gj 65.3	65.3		Beiwan	dolostone	2.0	-2.6						***0.003***	***0.002***
Gj 65.6	65.6		Beiwan	dolostone	1.8	-2.5						***0.004***	***0.002***
Gj 66.3	66.3		Beiwan	dolostone	-0.4	-2.6						***0.005***	***0.003***
Gj 67.0	67.0		Beiwan	dolostone	0.3	-2.3	-27.9	0.052	0.042	0.006		***0.006***	***0.003***
Gj 67.3	67.3		Beiwan	dolostone	1.6	-2.3						***0.005***	***0.003***
Gj 67.6	67.6		Beiwan	dolostone	1.9	-2.5	-26.3	0.071	0.057			***0.004***	***0.002***
Gj 68.0	68.0		Beiwan	dolostone	1.9	-2.4	-27.1	0.069	0.056	0.005			
Gj 68.3	68.3		Beiwan	dolostone	2.1	-2.1						***0.007***	***0.004***
Gj 68.6	68.6		Beiwan	dolostone	2.4	-1.6						***0.003***	***0.002***
Gj 69.0	69.0		Beiwan	dolostone	-0.4	-4.6	-26.3	0.127	0.107			***0.004***	***0.002***

Sample	Distance [m]	Formation	Member	Lithology	$\delta^{13}C_{carb}$ [‰] vs. VPDB	$\delta^{18}O$ [‰] vs. VPDB	$\delta^{13}C_{org}$ [‰] vs. VPDB	mgC/ sample	C [%]	TOC [%]	$\delta^{15}N_{bulk}$ [‰] vs. AIR	mgN/ sample	N [%] (TN)
Gj 69.3	69.3		Beiwan	dolostone	1.9	-2.1						***0.004***	***0.002***
Gj 69.6	69.6		Beiwan	dolostone	2.2	-2.5						***0.003***	***0.002***
Gj 70.3	70.3		Beiwan	dolostone	2.6	-2.1						***0.003***	***0.002***
Gj 70.6	70.6		Beiwan	dolostone	2.3	-2.4	-26.3	0.147	0.117				
Gj 71.0	71.0		Beiwan	dolostone	1.5		-27.1	0.152	0.121				
Gj 71.3	71.3		Beiwan	dolostone	1.1	-2.9							
Gj 72.0	72.0		Beiwan	dolostone	2.3	-4.4						***0.005***	***0.003***
Gj 72.3	72.3		Beiwan	dolostone	2.0	-4.0						***0.005***	***0.003***
Gj 72.6	72.6		Beiwan	dolostone	1.3	-4.0						***0.006***	***0.003***
Gj 73.0	73.0		Beiwan	dolostone	1.5	-3.2						***0.005***	***0.003***
Gj 73.3	73.3		Beiwan	dolostone	0.0	-4.1						***0.004***	***0.002***
Gj 73.6	73.6		Beiwan	dolostone	1.6	-3.4						***0.003***	***0.002***
Gj 74.0	74.0		Beiwan	dolostone	1.5	-3.2						***0.004***	***0.002***
Gj 74.3	74.3		Beiwan	dolostone	1.4	-3.1						***0.003***	***0.002***
Gj 74.6	74.6		Beiwan	dolostone	1.2	-3.3						***0.004***	***0.002***
Gj 75.0	75.0		Beiwan	dolostone	1.4	-2.7						***0.004***	***0.002***
Gj 75.3	75.3		Beiwan	dolostone	0.8	-4.4						***0.003***	***0.002***
Gj 75.6	75.6		Beiwan	dolostone	1.1	-2.8						***0.004***	***0.002***
Gj 76.0	76.0		Beiwan	dolostone	0.6	-8.0							
Gj 76.3	76.3		Beiwan	dolostone	0.6	-8.7							
Gj 76.6	76.6		Beiwan	dolostone	0.7	-7.8							
Gj 77.0	77.0		Beiwan	dolostone	1.7	-7.7							
Gj 77.3	77.3		Beiwan	dolostone	1.7	-3.7							
Gj 79.0	79.0		Beiwan	dolostone	1.8	-1.5							
Gj 79.6	79.6		Beiwan	dolostone	1.8	-5.7	-17.6	0.812	0.660				
Gj 80.3	80.3		Beiwan	dolostone	2.0	-2.6	-21.5	0.561	0.660				
Gj 81.3	81.3		Beiwan	dolostone	2.2	-5.5							
Gj 81.6	81.6		Beiwan	dolostone	2.1	-5.7							

Sample	Distance [m]	Formation	Member	Lithology	$\delta^{13}C_{carb}$ [‰] vs. VPDB	$\delta^{18}O$ [‰] vs. VPDB	$\delta^{13}C_{org}$ [‰] vs. VPDB	mgC/ sample	C [%]	TOC [%]	$\delta^{15}N_{bulk}$ [‰] vs. AIR	mgN/ sample	N [%] (TN)
Gj 83.0	83.0		Beiwan	dolostone	2.3	-4.4							
Gj 83.3	83.3		Beiwan	dolostone	1.9		-18.0	1.603	1.432				
Gj 83.6	83.6		Beiwan	dolostone	1.3	-2.6							
Gj 84.3	84.3		Beiwan	dolostone	2.3	-4.0	-21.5	0.841	0.790				
Gj 84.6	84.6		Beiwan	dolostone	2.2	-4.8							
Gj 85.3	85.3		Beiwan	dolostone	1.4	-1.8							
Gj 85.6	85.6		Beiwan	dolostone	2.0	-4.5							
Gj 87.0	87.0		Beiwan	dolostone	1.6	-2.1							
Gj 87.3	87.3		Beiwan	dolostone	2.3	-2.6							
Gj 87.6	87.6		Beiwan	dolostone	2.0	-2.7							
Gj 88.0	88.0		Beiwan	dolostone	1.8	-2.8							
Gj 88.6	88.6		Beiwan	dolostone	1.4	-3.6							
Gj 89.0	89.0		Beiwan	dolostone	1.1	-3.8							
Gj 89.3	89.3		Beiwan	dolostone	0.8	-5.8							
Gj 89.6	89.6		Beiwan	dolostone	1.3	-5.6	-23.0	0.017	0.014				
Gj 90.0	90.0		Beiwan	dolostone	1.1	-5.6	-23.8	0.015	0.014				
Gj 90.3	90.3		Beiwan	dolostone	0.9	-4.9							
Gj 90.6	90.6		Beiwan	dolostone	2.4		-21.2	0.576	0.489				
Gj 91.0	91.0		Beiwan	dolostone	1.4	-2.4	-23.1	0.378	0.370				
Gj 91.6	91.6		Beiwan	dolostone	0.5	-3.2	-20.6	0.042	0.038				
Gj 92.0	92.0		Beiwan	dolostone	0.7	-1.6	-20.5	0.042	0.038				
Gj 92.3	92.3		Beiwan	dolostone	2.1	-6.0	-21.2	0.046	0.041				
Gj 92.6	92.6		Beiwan	dolostone	1.4		-22.3	0.015	0.014				
Gj 93.0	93.0		Beiwan	dolostone	1.3								
Gj 93.3	93.3		Beiwan	dolostone	1.6	-6.2	-22.3	0.514	0.414				

A3.3 Table III - Isotope dataset Longbizui section

Sample		Distance [m]	Formation	Lithology	$\delta^{13}C_{carb}$ [‰] vs. VPDB	$\delta^{13}C_{org}$ [‰] vs. VPDB	mgC/ sample	C [%]	TOC [%]	$\delta^{15}N_{bulk}$ [‰] vs. AIR	mgN/ sample	N [%] (TN)
LBZ	T1	0.0	Nantuo	glacial deposit								
LBZ	5.2	5.2	Doushantuo	limestone	-5.5						***0.006***	***0.003***
LBZ	5.6	5.6	Doushantuo	limestone	-5.4	-32.3	0.302	1.432	0.100		***0.007***	***0.003***
LBZ	6.1	6.1	Doushantuo	limestone	-2.3	-32.8	0.687	2.600	0.149		***0.009***	***0.003***
LBZ	6.2	6.2	Doushantuo	limestone	-3.6	-33.0	0.978	4.581	0.156		***0.008***	***0.003***
LBZ	7.0	7.0	Doushantuo	tuff		-27.5	0.258	0.435	0.425	3.1	0.059	0.046
LBZ	8.0	8.0	Doushantuo	mudstone	-3.6	-33.4	0.155	0.074	0.047	2.3	0.036	0.024
LBZ	10.0	10.0	Doushantuo	mudstone	-0.3	-31.5	0.082	0.078	0.070	1.6	0.046	0.035
LBZ	11.0	11.0	Doushantuo	mudstone	-2.7	-30.7	0.075	0.071	0.058	2.7	0.046	0.033
LBZ	12.0	12.0	Doushantuo	mudstone						2.6	0.049	0.037
LBZ	13.0	13.0	Doushantuo	mudstone		-31.0	0.073	0.186	0.181	1.4	0.047	0.037
LBZ	14.0	14.0	Doushantuo	mudstone	-3.6	-25.8	0.198	0.976	0.927	1.3	0.040	0.026
LBZ	15.0	15.0	Doushantuo	mudstone		-31.7	0.827	1.688	1.621	1.5	0.042	0.040
LBZ	16.0	16.0	Doushantuo	mudstone		-30.6	0.077	0.083	0.073	2.6	0.048	0.037
LBZ	17.0	17.0	Doushantuo	mudstone	-5.6	-31.1	0.082	0.091	0.084	2.1	0.027	0.020
LBZ	33.0	33.0	Doushantuo	black mudstone	-12.2	-30.9	0.064	0.098	0.058	0.9	0.085	0.044
LBZ	34.0	34.0	Doushantuo	black mudstone	-11.6	-31.7	0.063	0.199	0.102	1.5	0.044	0.040
LBZ	36.0	36.0	Doushantuo	black mudstone	-11.0	-32.4	0.053	0.110	0.085	0.4	0.087	0.062
LBZ	37.0	37.0	Doushantuo	black mudstone	-11.0	-32.5	0.071	0.071	0.052	1.7	0.069	0.056
LBZ	38.0	38.0	Doushantuo	black mudstone	-12.2	-31.6	0.060	0.062	0.024	-0.1	0.031	0.014
LBZ	38.8	38.8	Doushantuo	black mudstone	-13.2	-26.0	0.029	0.026	0.005			
LBZ	39.5	39.5	Doushantuo	black mudstone	-10.4	-32.7	0.048	0.049	0.037	0.7	0.056	0.039
LBZ	44.0	44.0	Doushantuo	dolostone/limestone	-11.3	-31.3	0.061	0.031	0.022	0.9	0.048	0.040
LBZ	45.2	45.2	Doushantuo	dolostone/limestone	-11.7	-30.4	0.026	0.018	0.010	1.1	0.041	0.031
LBZ	46.0	46.0	Doushantuo	dolostone/limestone	-11.4	-30.3	0.060	0.031	0.021	0.3	0.047	0.038

Sample		Distance [m]	Formation	Lithology	$\delta^{13}C_{carb}$ [‰] vs. VPDB	$\delta^{13}C_{org}$ [‰] vs. VPDB	mgC/ sample	C [%]	TOC [%]	$\delta^{15}N_{bulk}$ [‰] vs. AIR	mgN/ sample	N [%] (TN)
LBZ	47.0	47.0	Doushantuo	dolostone/limestone	-11.0	-30.8	0.047	0.021	0.016	0.8	0.082	0.061
LBZ	48.0	48.0	Doushantuo	dolostone/limestone	-8.5	-31.4	0.051	0.021				
LBZ	80.0	80.0	Liuchapo	siliceous mudstone		-34.7	0.249	1.097	1.080	0.6	0.030	0.025
LBZ	82.0	82.0	Liuchapo	siliceous mudstone		-33.6	0.153	0.441	0.434	0.4	0.047	0.042
LBZ	85.9	85.9	Liuchapo	chert		-35.2	0.120	0.311	0.314	1.2	0.065	0.047
LBZ	86.0	86.0	Liuchapo	chert		-35.2	0.360	0.798	0.794	0.9	0.077	0.077
LBZ	88.0	88.0	Liuchapo	chert		-34.4	0.139	0.421	0.414	0.6	0.047	0.019
LBZ	90.0	90.0	Liuchapo	chert		-33.6	0.093	0.125	0.124	1.0	0.061	0.045
LBZ	92.0	92.0	Liuchapo	chert		-33.8	0.090	0.154	0.152	0.7	0.064	0.050
LBZ	94.0	94.0	Liuchapo	chert		-35.2	0.127	0.209	0.207	0.5	0.062	0.051
LBZ	96.0	96.0	Liuchapo	chert	-10.6	-34.7	0.166	0.263	0.261	1.3	0.042	0.040
LBZ	98.0	98.0	Liuchapo	chert	1.6	-34.8	0.636	1.145	1.123	1.1	0.018	0.010
LBZ	100.0	100.0	Liuchapo	chert	-3.0	-36.1	0.255	1.638	1.468	2.3	0.199	0.095
LBZ	102.0	102.0	Liuchapo	chert	-3.4	-35.6	0.784	2.086	1.882	2.2	0.138	0.067
LBZ	104.0	104.0	Liuchapo	chert	-4.4	-34.0	0.488	0.505	0.490	3.1	0.038	0.018
LBZ	106.0	106.0	Liuchapo	chert		-35.3	0.595	1.174	1.162	1.2	0.048	0.021
LBZ	108.0	108.0	Liuchapo	chert	-2.9	-30.0	0.170	0.088	0.086	1.2	0.015	0.006
LBZ	110.0	110.0	Liuchapo	chert	-4.5	-32.8	0.334	0.172	0.169	0.4	0.035	0.014
LBZ	112.0	112.0	Liuchapo	chert		-34.2	0.166	0.217	0.215	0.3	0.083	0.041
LBZ	114.0	114.0	Liuchapo	chert	-5.9	-35.1	0.298	0.412	0.406	2.0	0.055	0.028
LBZ	116.0	116.0	Liuchapo	chert	-7.4	-33.9	0.056	0.400	0.398	1.6	0.032	0.016
LBZ	118.0	118.0	Liuchapo	chert	-5.4	-36.1	0.239	0.964	0.951	0.1	0.034	0.015
LBZ	120.0	120.0	Liuchapo	chert	-5.5	-34.2	0.583	0.651	0.632			
LBZ	122.0	122.0	Liuchapo	chert	-5.2	-35.9	0.160	1.004	0.977	2.3	0.037	0.016
LBZ	124.0	124.0	Liuchapo	chert	-3.6	-32.4	0.546	0.285	0.280	-0.6	0.124	0.081
LBZ	126.0	126.0	Liuchapo	chert	-3.7	-31.0	0.140	0.141	0.138	0.9	0.054	0.032
LBZ	128.0	128.0	Liuchapo	chert		-35.6	0.101	0.585	0.588	0.5	0.334	0.139

Sample		Distance [m]	Formation	Lithology	$\delta^{13}C_{carb}$ [‰] vs. VPDB	$\delta^{13}C_{org}$ [‰] vs. VPDB	mgC/ sample	C [%]	TOC [%]	$\delta^{15}N_{bulk}$ [‰] vs. AIR	mgN/ sample	N [%] (TN)
LBZ	130.0	130.0	Liuchapo	chert		-36.0	0.083	0.331	0.328	1.5	0.151	0.066
LBZ	132.0	132.0	Liuchapo	chert		-37.0	0.158	0.984	0.955	0.4	0.060	0.027
LBZ	134.0	134.0	Liuchapo	chert	-11.4	-35.4	0.417	0.462	0.453	1.9	0.041	0.019
LBZ	136.0	136.0	Liuchapo	chert		-34.9	0.133	0.147	0.142	1.6	0.145	0.114
LBZ	138.0	138.0	Liuchapo	chert	-7.0	-36.8	0.090	0.324	0.319			
LBZ	140.0	140.0	Liuchapo	chert	-10.6	-36.1	0.075	0.497	0.485	1.3	0.037	0.019
LBZ	142.0	142.0	Liuchapo	nodulare chert		-31.3	0.313	0.352	0.340	0.7	0.025	0.013
LBZ	143.0	143.0	Liuchapo	nodulare chert		-37.0	0.156	0.561				
LBZ	143.5	143.5	Liuchapo	nodulare chert	-5.1	-34.2	0.447	0.476	0.469	0.2	0.026	0.012
LBZ	143.8	143.8	Liuchapo	nodulare chert	-6.8	-34.8	0.230	1.028	0.641	0.8	0.069	0.035
LBZ	145.0	145.0	Niutitang	nodulare chert/phosphorite	-8.2	-31.3	0.297	1.764	1.400	-1.4	0.028	0.015
LBZ	145.6	145.6	Niutitang	nodulare chert/phosphorite	-8.2	-24.5	1.307	6.222	4.415	-1.3	0.092	0.047
LBZ	148.0	148.0	Niutitang	nodulare chert/phosphorite	-1.5	-32.5	0.149	0.721	0.699	-1.5	0.025	0.013
LBZ	150.0	150.0	Niutitang	cherty phosphorite	-5.6	-31.5	0.677	2.866	2.764	-0.3	0.031	0.048
LBZ	151.0	151.0	Niutitang	cherty phosphorite		-32.4	0.705	4.515	4.448	-0.8	0.131	0.200
LBZ	152.0	152.0	Niutitang	black mudstone		-34.2	0.354	3.090	3.038	-0.3	0.203	0.294
LBZ	154.0	154.0	Niutitang	black mudstone		-33.2	0.599	4.536	4.491	-1.0	0.250	0.375
LBZ	156.0	156.0	Niutitang	black mudstone	1.3	-36.9	0.652	4.743	4.515	-2.5	0.249	0.305
LBZ	158.0	158.0	Niutitang	black mudstone	-6.2	-34.1	1.280	8.321	1.138	-4.2	0.022	0.021
LBZ	162.0	162.0	Niutitang	black mudstone		-33.1	0.924	5.876	5.693	-1.8	0.243	0.348
LBZ	164.0	164.0	Niutitang	black mudstone	-2.2	-29.6	0.582	4.095	3.762	-3.2	0.156	0.235
LBZ	166.0	166.0	Niutitang	black mudstone		-32.4	0.703	4.222	3.997	-3.2	0.133	0.198
LBZ	168.0	168.0	Niutitang	black mudstone		-33.1	0.775	4.854	4.729	-3.8	0.026	0.066
LBZ	170.0	170.0	Niutitang	black mudstone		-36.1	0.697	4.638	4.450	-2.8	0.092	0.168
LBZ	172.0	172.0	Niutitang	black mudstone	-2.5	-31.4	0.642	4.195	3.935	-3.4	0.081	0.136
LBZ	174.0	174.0	Niutitang	black mudstone		-36.0	0.656	3.930	3.760	-3.0	0.071	0.123
LBZ	176.0	176.0	Niutitang	black mudstone	-2.2	-25.1	0.890	6.039	5.517	-2.2	0.058	0.104

Sample		Distance [m]	Formation	Lithology	$\delta^{13}C_{carb}$ [‰] vs. VPDB	$\delta^{13}C_{org}$ [‰] vs. VPDB	mgC/ sample	C [%]	TOC [%]	$\delta^{15}N_{bulk}$ [‰] vs. AIR	mgN/ sample	N [%] (TN)
LBZ	178.0	178.0	Niutitang	black mudstone		-31.4	0.969	4.365	4.320	-2.1	0.063	0.115
LBZ	180.0	180.0	Niutitang	black mudstone		-30.9	1.031	2.932	2.902	-2.2	0.051	0.086
LBZ	181.0	181.0	Niutitang	black mudstone		-33.3	0.945	9.503	2.149	-2.4	0.034	0.034
LBZ	182.0	182.0	Niutitang	black mudstone		-30.4	0.566	3.999	3.899	-0.9	0.077	0.137
LBZ	184.0	184.0	Niutitang	black mudstone		-29.3	0.430	3.120	3.073	-2.2	0.131	0.235

A3.4 Table IV - Isotope dataset Xiaofenghe section

Sample		Distance [m]	Formation	Lithology	$\delta^{13}C_{carb}$ [‰] vs. VPDB	$\delta^{13}C_{org}$ [‰] vs. VPDB	mgC/ sample	C [%]	TOC [%]	$\delta^{15}N_{bulk}$ [‰] vs. AIR	mgN/ sample	N [%] (TN)
NXF	-0.10	-0.1	Nantuo	gacial deposit		-28.9	0.271	0.000				
NXF	0.20	0.2	Doushantuo	dolostone	-3.6	-28.0	0.217	0.171	0.008		***0.006***	***0.003***
NXF	0.75	0.8	Doushantuo	miciritic dolostone	-3.5	-26.7	0.813	0.677	0.107		***0.005***	***0.003***
NXF	1.60	1.6	Doushantuo	miciritic dolostone	-3.7					2.6	0.013	0.006
NXF	2,35	2.3	Doushantuo	miciritic dolostone	-3.8	-26.7	0.986	0.001			***0.009***	***0.005***
NXF	3.85	3.9	Doushantuo	miciritic dolostone	-2.8					0.5	0.016	0.011
NXF	4.80	4.8	Doushantuo	miciritic dolostone	-2.0	-28.4	0.582	0.552	0.060		***0.009***	***0.004***
NXF	6.70	6.7	Doushantuo	black limestone w/ chert nodules	-0.2	-25.4	0.083	0.050	0.016	4.9	0.118	0.066
NXF	12.10	12.1	Doushantuo	black limestone w/ chert nodules	7.5	-28.1	0.737	0.775	0.252	2.4	0.014	0.008
NXF	37.50	37.5	Doushantuo	black limestone w/ chert nodules	0.9	-28.3	0.617	0.607	0.211	5.1	0.024	0.014
NXF	65.00	65.0	Doushantuo	black limestone w/ chert nodules	6.7	-29.0	0.269	0.194	0.122	5.5	0.036	0.028
NXF	73.3	73.7	Doushantuo	black limestone w/ chert nodules	5.9	-25.5	1.482	0.001		3.9	0.027	0.017
NXF	75.60	75.6	Doushantuo	silty-muddy dolostone	5.7	-26.8	1.198	1.207	0.612	6.6	0.210	0.130
NXF	76.00	76.0	Doushantuo	silty-muddy dolostone	3.7	-28.1	0.422	0.483	0.223	5.4	0.060	0.034
SXF	-25.50	76.5	Doushantuo	limestone	6.6					4.8	0.036	0.023
NXF	77.5 II	77.5	Doushantuo	silty-muddy dolostone	5.5	-29.4	2.354	2.068	0.422	5.0	0.053	0.032
SXF	-22.50	79.5	Doushantuo	silty-muddy dolostone	4.9	-27.0	1.158	1.093	0.412	5.2	0.079	0.044
SXF	-21.50	80.5	Doushantuo	limestone	4.0	-28.8	1.381	1.313	0.375	4.9	0.090	0.049
SXF	-20.50	81.5	Doushantuo	limestone	4.5	-27.9	0.011	0.010	0.006	2.5	0.152	0.092
SXF	-17.50	84.5	Doushantuo	limestone	5.8	-28.3	1.546	1.450	0.446	4.6	0.055	0.031
SXF	-17.00	85.0	Doushantuo	limestone	5.6	-28.8	0.966	0.914	0.483	4.8	0.057	0.034
SXF	-16.00	86.0	Doushantuo	oolitic dolostone w/ chert nodules	4.0	-28.6	2.412	2.446	0.920	4.5	0.125	0.067
SXF	-14.80	87.2	Doushantuo	oolitic dolostone w/ chert nodules	5.3	-26.5	1.779	1.712	0.708	5.3	0.081	0.044
SXF	-14.00	88.0	Doushantuo	oolitic dolostone w/ chert nodules	3.7	-30.1	1.800	1.702	0.357	4.8	0.062	0.037
SXF	-13.30	88.7	Doushantuo	oolitic dolostone w/ chert nodules	5.0	-27.2	1.635	1.866	0.711	4.6	0.077	0.048
SXF	-13.00	89.0	Doushantuo	oolitic dolostone w/ chert nodules	5.2	-27.0	1.024	0.001		4.4	0.082	0.044

Sample		Distance [m]	Formation	Lithology	$\delta^{13}C_{carb}$ [‰] vs. VPDB	$\delta^{13}C_{org}$ [‰] vs. VPDB	mgC/ sample	C [%]	TOC [%]	$\delta^{15}N_{bulk}$ [‰] vs. AIR	mgN/ sample	N [%] (TN)
SXF	-12.00	90.0	Doushantuo	oolitic dolostone w/ chert nodules	5.8	-28.8	1.970	2.001	0.937		***0.004***	***0.002***
SXF	-10.80	91.2	Doushantuo	oolitic dolostone w/ chert nodules	4.5	-27.7	1.811	1.817	0.287	2.3	0.035	0.017
SXF	-10.30	91.7	Doushantuo	oolitic dolostone w/ chert nodules	5.8	-27.6	2.479	2.423	0.771	5.4	0.169	0.087
SXF	-9.50	92.5	Doushantuo	oolitic dolostone w/ chert nodules	4.4					3.9	0.040	0.020
SXF	-9.00	93.0	Doushantuo	oolitic dolostone w/ chert nodules	4.5	-27.3	0.911	0.857	0.258	1.9	0.021	0.011
SXF	-5.80	96.2	Doushantuo	oolitic dolostone w/ chert nodules	4.5	-28.6	0.773	0.765	0.351	3.2	0.028	0.014
SXF	-4.00	98.0	Doushantuo	oolitic dolostone w/ chert nodules	3.3	-27.9	1.094	1.089	0.348	4.7	0.068	0.040
SXF	-3.00	99.0	Doushantuo	oolitic dolostone w/ chert nodules	5.0	-27.9	0.287	0.294	0.146	2.8	0.019	0.011
SXF	-2.15	99.9	Doushantuo	oolitic dolostone w/ chert nodules	4.6	-29.2	0.973	0.958	0.316	4.8	0.120	0.060
NXF	101.50	101.5	Doushantuo	oolitic dolostone w/ chert nodules	5.6	-28.7	1.453	1.265	0.649	3.9	0.035	0.019
SXF	-0.15	101.9	Doushantuo	oolitic dolostone w/ chert nodules	5.7	-28.6	1.206	1.160	0.277	2.4	0.031	0.017
SXF	0.10	102.4	Doushantuo	black shale	5.0					4.8	0.163	0.094
SXF	0.40	102.6	Doushantuo	black shale	6.3	-29.0	1.920	2.467	0.950	4.5	0.142	0.097
NXF	102.60	102.7	Doushantuo	black shale	2.0	-28.8	1.082	1.105	0.400	4.4	0.137	0.085
NXF	102.70	102.7	Doushantuo	black shale	5.4	-32.0	3.424	2.951	1.035	4.6	0.105	0.051
SXF	0.70	103.0	Doushantuo	black shale	5.4	-27.2	0.802	0.790	0.207	5.3	0.246	0.137
NXF	103.00	103.0	Doushantuo	black shale	5.7	-33.8	1.620	1.661	0.968	5.4	0.215	0.126
SXF	1.00	103.0	Doushantuo	black shale	7.8	-28.1	2.081	1.943	0.894	5.3	0.172	0.104
NXF	103.50	103.5	Doushantuo	muddy dolostone	4.9	-31.2	1.445	1.182	0.587	3.1	0.027	0.015
NXF	104.00	104.0	Doushantuo	muddy dolostone	7.0	-29.2	0.552	0.556	0.114	5.0	0.051	0.029
NXF	104.25	104.3	Doushantuo	muddy dolostone w/ chert nodules	3.8	-27.8	1.126	1.186	0.168	3.4	0.029	0.015
NXF	104.50	104.5	Doushantuo	muddy dolostone w/ chert nodules	3.4	-27.3	0.718	0.783	0.147	4.1	0.022	0.012
SXF	2.50	104.5	Doushantuo	muddy dolostone w/ chert nodules	5.2	-28.3	1.117	1.090	0.225	2.7	0.029	0.018
NXF	105.50	105.5	Doushantuo	muddy dolostone w/ chert nodules	4.5	-25.8	0.643	0.704	0.434	3.0	0.014	0.009
NXF	108.15	108.2	Doushantuo	limestone	2.5	-31.9	0.838	0.830	0.214	4.9	0.061	0.039
NXF	108.70	108.7	Doushantuo	shaly mudstone	3.8	-27.3	1.279	1.340	0.560	5.6	0.161	0.126
NXF	109.50	109.5	Doushantuo	limestone	4.4	-27.8	0.624	0.669	0.134	4.6	0.022	0.013
NXF	110.00	110.0	Doushantuo	limestone	3.4	-28.6	0.820	0.814	0.096	4.8	0.016	0.010

Sample	Distance [m]	Formation	Lithology	$\delta^{13}C_{carb}$ [‰] vs. VPDB	$\delta^{13}C_{org}$ [‰] vs. VPDB	mgC/ sample	C [%]	TOC [%]	$\delta^{15}N_{bulk}$ [‰] vs. AIR	mgN/ sample	N [%] (TN)
NXF 110.50	110.5	Doushantuo	limestone	3.9	-28.4	0.700	0.722	0.087	5.5	0.016	0.010
NXF 111.10	111.1	Doushantuo	limestone	3.2	-29.6	0.886	0.813	0.140	5.2	0.023	0.015
NXF 112.20	112.2	Doushantuo	limestone	2.8					3.7	0.012	0.008
NXF 113.90	113.9	Doushantuo	limestone	6.8					2.7	0.012	0.007
NXF 116.00	116.0	Doushantuo	limestone	6.9					3.6	0.016	0.010
NXF 118.50	118.5	Doushantuo	limestone	5.9	-27.2	0.607	0.692	0.072	3.6	0.016	0.009
NXF 123.80	123.8	Doushantuo	limestone	6.6	-28.6	0.536	0.626	0.174	3.3	0.020	0.012
NXF 125.00	125.0	Doushantuo	limestone	5.7	-31.0	0.968	1.244	0.236	5.3	0.028	0.018
NXF 130.00	130.0	Doushantuo	limestone w/ chert nodules	5.7					4.1	0.014	0.009
NXF 133.50	133.5	Doushantuo	limestone	5.0	-30.1	1.618	1.781	0.157	4.2	0.011	0.008
SXF 51.00	135.0	Doushantuo	dolostone	2.7	-29.2	0.825	0.657	0.308	4.4	0.012	0.007
NXF 136.00	136.0	Doushantuo	limestone	5.3	-27.8	1.314	1.854	0.126	3.9	0.060	0.034
SXF 58.40	142.4	Doushantuo	shale	-1.5	-29.2	2.813	2.789	1.612	5.9	0.069	0.048
SXF 68.00	152.0	Doushantuo	shale	2.0							
SXF 70.00	154.0	Doushantuo	shale	9.1	-25.9	0.910	0.672	0.043		***0.007***	***0.004***
SXF 72.50	156.5	Doushantuo	shaly dolostone	-0.6	-28.1	0.320	0.339	0.126	5.6	0.038	0.023
SXF 74.00	158.0	Doushantuo	dolostone	1.2	-28.5	0.204	0.186	0.065	4.3	0.013	0.008
SXF 82.00	166.0	Doushantuo	dolostone	0.3	-23.3	0.965	2.376	0.044	0.4	0.013	0.008
SXF 83.00	167.0	Doushantuo	dolostone/chert	0.4	-26.1	0.032	0.034	0.022		***0.003***	***0.002***
SXF 84.50	168.5	Doushantuo	dolostone	-0.5	-27.8	0.067	0.060	0.032		***0.005***	***0.003***
SXF 84.60	168.6	Doushantuo	dolostone w/ chert nodules	-2.5	-26.5	0.068	0.065	0.035		***0.004***	***0.003***
SXF 88.20	172.2	Doushantuo	dolostone	3.6	-28.5	0.612	0.646	0.180	4.1	0.017	0.010
SXF 90.00	174.0	Doushantuo	dolostone	3.5	-27.1	0.352	0.384	0.089	5.1	0.041	0.022
SXF 91.50	175.5	Doushantuo	dolostone	4.1	-28.0	0.102	0.100	0.026	3.3	0.012	0.008
SXF 93.30	177.3	Doushantuo	dolostone	6.0	-26.5	0.510	0.718	0.094			
SXF 95.80	179.8	Doushantuo	dolostone	5.2	-27.0	0.454	0.495	0.143		**0.008**	**0.005**
SXF 96.00	180.0	Doushantuo	dolostone	4.6	-25.6	0.406	0.670	0.086		***0.006***	***0.003***
SXF 98.00	182.0	Doushantuo	dolostone	5.8	-26.3	0.601	0.588	0.078			
SXF 110.00	194.0	Doushantuo	dolostone	1.8	-27.9	0.856	0.700	0.092	0.2	0.013	0.008

A4 Dataset Kazakhstan

A4.1 Table V - Coordinates of visited sections

Section	Region	Coordinates	
Kyrshabakty section	Malyi Karatau	43°32'03.10" N	69°57'11.90" E
Berkuty section	Malyi Karatau	43°37'29.00" N	69°45'17.60" E
Aktugai section	Malyi Karatau	43°28'31.10" N	69°51'45.20" E
Koksu section	Malyi Karatau	43°38'02.40" N	69°39'45.80" E
Ushbas section	Malyi Karatau	43°37'13.40" N	69°27'15.00" E
Kurtybulak section	Malyi Karatau	43°35'51.80" N	69°38'21.50" E
Unnamed section	Bolshoi Karatau	44°18'45.10" N	67°34'14.80" E

A4.2 Table VI - Isotope dataset Kyrshabakty section

Sample		Distance [m]	Formation	Member	Lithology	$\delta^{13}C_{carb}$ [‰] vs. VPDB	$\delta^{18}O$ [‰] vs. VPDB	$\delta^{13}C_{org}$ [‰] vs. VPDB	mgC/ sample	C [%]	TOC [%]	$\delta^{15}N_{dec}$ [‰] vs. AIR	mgN/ sample	N [%] (TN)
KY	1	0.0	Kurgan		volcanoclastica			-34.1	0.033	0.016	0.016		***0.008***	***0.004***
KY	2	47.5	Kyrshabakty	Aktas	glacial deposit				0.024	0.012	0.012		***0.006***	***0.003***
KY	3	58.4	Kyrshabakty		dolostone	-0.1	-3.38	-23.0	0.101	0.077	0.043		***0.003***	***0.003***
KY	4	58.6	Kyrshabakty		dolostone	-0.7	-4.34	-31.0	0.092	0.073	0.015		***0.004***	***0.003***
KY	5a	58.8	Kyrshabakty		dolostone	-1.4	-4.51	-32.6	0.173	0.140	0.014	2.4	0.010	0.006
KY	6b	59.3	Kyrshabakty		dolostone	-1.7	-4.41	-28.1	0.052	0.045	0.002	1.8	0.033	0.028
KY	7a	59.7	Kyrshabakty		dolostone	-2.4	-4.98	-26.3	0.079	0.064	0.005	2.1	0.035	0.029
KY	8	60.5	Kyrshabakty		dolostone	-1.3		-32.1	0.052	0.042	0.004	2.9	0.019	0.015
KY	9	61.6	Kyrshabakty		dolostone	-2.6	-5.03	-28.4	0.091	0.077	0.004	0.5	0.045	0.038
KY	10	61.9	Kyrshabakty		dolostone	-1.0	-4.24	-30.6	0.143	0.109		1.9	0.043	0.033
KY	11	77.7	Kyrshabakty		dolomitic sandstone	0.0	-4.28	-34.2	2.128	1.810	0.027	3.2	0.033	0.028
KY	13	87.9	Kyrshabakty		dolomitic sandstone	1.3	-7.29	-31.2	0.083	0.071	0.012	3.4	0.020	0.017
KY	14	88.5	Kyrshabakty		dolomitic sandstone	0.4		-33.3	0.064	0.059	0.012	3.1	0.012	0.011
KY	15	89.1	Kyrshabakty		dolomitic sandstone	-0.6		-34.4	0.044	0.028	0.004	2.3	0.011	0.007
KY	16	89.2	Kyrshabakty		dolomitic sandstone	-0.8	-7.82	-29.7	0.035	0.028	0.011	3.9	0.013	0.011
KY	17	92.5	Kyrshabakty		dolomitic sandstone	0.0		-36.2	0.081	0.072	0.040	3.6	0.021	0.019
KY	18	107.2	Kyrshabakty		sandy limestone	-7.9	-9.04	-30.1	0.200	0.157	0.001		***0.006***	***0.005***
KY	19	107.7	Kyrshabakty		sandy limestone	-9.3	-10.10	-30.8	0.081	0.068	0.015	3.1	0.011	0.007
KY	20	114.2	Kyrshabakty		sandy limestone	-8.4		-30.0	0.084	0.065			***0.008***	***0.006***
KY	21	115.3	Kyrshabakty		sandy limestone	-7.6	-8.51	-24.1	0.035	0.027	0.006		***0.009***	***0.007***
KY	22	117.7	Kyrshabakty		sandy limestone	-9.5	-11.27	-24.2	0.029	0.024	0.007	1.6	0.010	0.008
KY	23	118.9	Kyrshabakty		sandy limestone	-9.7	-11.20	-30.4	0.018	0.015	0.003	3.2	0.010	0.007
KY	24	120.4	Kyrshabakty		sandy limestone	-8.2		-30.7	0.018	0.015	0.003		***0.006***	***0.005***
KY	25	122.6	Kyrshabakty		sandy limestone	-7.7	-8.84	-26.0	0.032	0.025	0.004		***0.008***	***0.006***
KY	26	123.9	Kyrshabakty		sandy limestone	-7.7		-27.0	0.031	0.023	0.008		***0.008***	***0.006***

Sample		Distance [m]	Formation	Member	Lithology	$\delta^{13}C_{carb}$ [‰] vs. VPDB	$\delta^{18}O$ [‰] vs. VPDB	$\delta^{13}C_{org}$ [‰] vs. VPDB	mgC/ sample	C [%]	TOC [%]	$\delta^{15}N_{dec}$ [‰] vs. AIR	mgN/ sample	N [%] (TN)
KY	27	125.5	Kyrshabakty		sandy limestone	-6.3		-26.1	0.022	0.017	0.003	1.6	0.010	0.008
KY	28	126.9	Kyrshabakty		sandy limestone	-6.3	-7.68	-33.0	0.029	0.022	0.005	2.8	0.011	0.008
KY	29	127.7	Kyrshabakty		sandy limestone	-7.7		-27.5	0.029	0.025	0.006	2.5	0.010	0.007
KY	30	128.7	Kyrshabakty		sandy limestone	-7.1		-30.1	0.060	0.051	0.015	3.7	0.010	0.009
KY	31	129.5	Kyrshabakty		sandy limestone	-5.8		-27.4	0.030	0.024	0.006	2.4	0.010	0.008
KY	33	135.6	Kyrshabakty		sandy limestone	-7.0	-7.73	-30.9	0.211	0.172	0.076		***0.008***	***0.007***
KY	34	136.1	Kyrshabakty		sandy limestone	-6.9		-30.9	0.144	0.096	0.049	1.9	0.012	0.008
KY	35	138.7	Kyrshabakty		sandy limestone	-6.9	-7.20	-32.2	0.108	0.081	0.033	3.4	0.010	0.008
KY	36	139.0	Kyrshabakty		sandy limestone	-4.6	-4.60	-30.8	0.108	0.075	0.041	3.3	0.012	0.009
KY	37	140.5	Kyrshabakty		sandy limestone	-4.9	-5.46	-28.3	0.082	0.054	0.026	3.5	0.010	0.007
KY	38	166.3	Kyrshabakty	Berkuty	dolostone	2.7		-30.4	0.146	0.108	0.008	1.8	0.050	0.013
KY	39	166.9	Kyrshabakty	Berkuty	dolostone	4.3	-0.36	-32.4	0.145	0.115	0.006	1.2	0.048	0.038
KY	41	168.2	Kyrshabakty	Berkuty	dolostone	3.3	-2.35	-33.9	0.347	0.319	0.009	1.7	0.040	0.037
KY	42	168.3	Kyrshabakty	Berkuty	dolostone	2.4	-3.17	-30.2	0.288	0.233	0.008	2.1	0.041	0.033
KY	43	168.5	Kyrshabakty	Berkuty	dolostone	2.1	-3.52	-31.8	0.183	0.163	0.004	1.0	0.030	0.027
KY	44	169.1	Kyrshabakty	Berkuty	dolostone	2.6	-3.09	-31.2	0.235	0.176	0.007	0.9	0.037	0.027
KY	45	169.3	Kyrshabakty	Berkuty	dolostone	0.5	-4.11	-31.1	0.260	0.223	0.005	1.2	0.040	0.034
KY	46	169.8	Kyrshabakty	Berkuty	dolostone	0.6	-3.03	-31.0	0.298	0.267	0.020	2.2	0.026	0.023
KY	47	169.9	Kyrshabakty	Berkuty	dolostone	-1.8	-4.72	-32.7	0.224	0.176	0.008	0.8	0.015	0.011
KY	11-02	170.9	Kyrshabakty	Berkuty	phosphorite	-6.8	-9.69	-34.7	0.726	0.621	0.081		***0.007***	***0.006***
KY	48	170.9	Kyrshabakty	Berkuty	dolostone	1.5		-29.0	0.112	0.114	0.006	1.0	0.037	0.031
KY	49	172.2	Kyrshabakty	Berkuty	dolostone	-2.2	-5.84						***0.003***	***0.002***
KY	50	172.6	Chulaktau	Aksai	chert	-6.1	-8.16	-37.5	0.517	0.432	0.335			
KY	51	173.5	Chulaktau		siltstone	-5.2		-32.1	0.590	0.518	0.454	1.1	0.040	0.036
KY	11-03	175.6	Chulaktau	Karatau	phosphorite	-5.9	-8.07	-32.7	0.512	0.487	0.105	1.2	0.010	0.010
KY	52	179.8	Chulaktau	Ushbas	chert	-3.8	-6.87	-32.5	0.122	0.082	0.080			
KY	53	179.8	Chulaktau	Ushbas	silty limestone	-1.4	-3.31	-31.9	0.865	0.733	0.045	-0.8	0.034	0.029
KY	11-07	181.1	Chulaktau	Ushbas	phosphorite	-6.7	-7.84	-33.2	1.052	0.864	0.323	3.8	0.017	0.014

Sample		Distance [m]	Formation	Member	Lithology	$\delta^{13}C_{carb}$ [‰] vs. VPDB	$\delta^{18}O$ [‰] vs. VPDB	$\delta^{13}C_{org}$ [‰] vs. VPDB	mgC/ sample	C [%]	TOC [%]	$\delta^{15}N_{dec}$ [‰] vs. AIR	mgN/ sample	N [%] (TN)
KY	54	183.0	Shabakty		cherty dolostone	-4.2		-25.7	0.053	0.041	0.036		***0.005***	***0.004***
KY	55	184.3	Shabakty		cherty dolostone	-2.4	-6.90	-30.7	0.199	0.136	0.132	0.2	0.010	0.006
KY	56	184.9	Shabakty		cherty dolostone	-1.1		-33.0	0.237	0.122	0.093	2.1	0.013	0.007
KY	57	185.4	Shabakty		cherty dolostone	0.7	-2.28	-33.4	0.141	0.113	0.027	-0.9	0.049	0.038
KY	11-12	187.7	Shabakty		phosphorite	-6.0	-6.65	-35.2	0.635	0.536	0.198	0.1	0.015	0.013
KY	58	188.3	Shabakty		dolostone	-3.5	-7.47	-32.1	0.125	0.104	0.001	-1.8	0.125	0.104
KY	59	189.0	Shabakty		dolostone	-0.9		-29.4	1.332	1.158	0.087	-1.3	0.034	0.030
KY	60	191.8	Shabakty		dolostone	0.5	-3.20							
KY	61	192.8	Shabakty		dolostone	-3.4	-7.15	-32.0	3.709	2.534	0.048	-0.3	0.070	0.048
KY	62a	193.9	Shabakty		dolostone	-3.3	-7.75	-31.6	4.157	3.799	0.071	-0.9	0.073	0.066
KY	62c	193.9	Shabakty		dolostone	0.8	-4.39	-31.7	1.855	1.466	0.055	-2.3	0.100	0.073
KY	63a	194.6	Shabakty		dolostone	-0.6	-4.32	-33.7	1.740	1.521	0.044	-1.5	0.047	0.041
KY	63c	194.7	Shabakty		dolostone	0.5	-3.71	-31.7	1.855	1.466	0.055	-1.3	0.053	0.042
KY	11-16	194.8	Shabakty		phosphorite	-6.9	-12.14	-33.9	0.891	0.684	0.118	0.2	0.017	0.013
KY	64	198.2	Shabakty		dolostone	-0.9		-34.7	0.100	0.071	0.003	-1.4	0.025	0.018
KY	11-18	204.1	Shabakty		phosphorite	-3.2	-4.23	-32.9	0.151	0.104	0.099		***0.005***	***0.004***
KY	11-20	215.3	Shabakty		phosphorite	-4.8	-8.98	-30.8	0.360	0.242	0.086	0.9	0.019	0.013

A4.3 Table VII - Isotope dataset Berkuty section

Sample		Distance [m]	Formation	Member	Lithology	$\delta^{13}C_{carb}$ [‰] vs. VPDB	$\delta^{18}O$ [‰] vs. VPDB	$\delta^{13}C_{org}$ [‰] vs. VPDB	mgC/ sample	C [%]	TOC [%]	$\delta^{15}N_{dec}$ [‰] vs. AIR	mgN/ sample	N [%] (TN)
BK	1a	59.05	Kyrshabakty		dolostone	-2.2	-5.3	-21.9	0.050	0.040	0.011		***0.006***	***0.005***
BK	1b	59.07	Kyrshabakty		dolostone	-1.7	-4.8							
BK	1c	59.10	Kyrshabakty		dolostone	-1.5	-4.7							
BK	1d	59.15	Kyrshabakty		dolostone	-1.3	-4.6							
BK	2a	59.35	Kyrshabakty		dolostone	-1.5	-5.1							
BK	2b	59.37	Kyrshabakty		dolostone	-1.3	-5.1							
BK	2c	59.40	Kyrshabakty		dolostone	-1.3	-4.8							
BK	2d	59.45	Kyrshabakty		dolostone	-1.1	-4.4							
BK	3	59.70	Kyrshabakty		dolostone	-2.9	-5.6	-29.0	0.044	0.035	0.002	1.6	0.017	0.013
BK	4a	60.05	Kyrshabakty		dolostone	-1.1		-31.4	0.034	0.025	0.002		***0.004***	***0.003***
BK	4b	60.07	Kyrshabakty		dolostone	-3.0	-5.2							
BK	4c	60.10	Kyrshabakty		dolostone	-1.0								
BK	4d	60.15	Kyrshabakty		dolostone	-0.7								
BK	5	60.25	Kyrshabakty		dolostone	-3.3								
BK	5c	60.30	Kyrshabakty		dolostone	-2.9	-5.2							
BK	6a	60.35	Kyrshabakty		dolostone	-2.3	-5.2	-28.7	0.045	0.035	0.002	0.8	0.025	0.020
BK	6b	60.37	Kyrshabakty		dolostone	-2.2								
BK	6c	60.40	Kyrshabakty		dolostone	-1.8								
BK	6d	60.45	Kyrshabakty		dolostone	-2.0	-4.3							
BK	7	60.55	Kyrshabakty		dolostone	-2.7	-5.5							
BK	8a	60.80	Kyrshabakty		dolostone	-0.8		-24.6	0.067	0.057	0.005	2.6	0.033	0.028
BK	8b	60.85	Kyrshabakty		dolostone	-0.4								
BK	8c	60.87	Kyrshabakty		dolostone	0.0								
BK	8d	60.88	Kyrshabakty		dolostone	-0.9	-3.4							
BK	9	60.90	Kyrshabakty		dolostone	-2.2	-4.9							
BK	11a	59.05	Kyrshabakty		dolostone	-0.7								
BK	11b	59.07	Kyrshabakty		dolostone									

Sample	Distance [m]	Formation	Member	Lithology	$\delta^{13}C_{carb}$ [‰] vs. VPDB	$\delta^{18}O$ [‰] vs. VPDB	$\delta^{13}C_{org}$ [‰] vs. VPDB	mgC/ sample	C [%]	TOC [%]	$\delta^{15}N_{dec}$ [‰] vs. AIR	mgN/ sample	N [%] (TN)
BK 11c	59.10	Kyrshabakty		dolostone	-2.2	-32.11							
BK 11d	59.13	Kyrshabakty		dolostone	-1.5								
BK 12a	59.15	Kyrshabakty		dolostone									
BK 12b	59.17	Kyrshabakty		dolostone									
BK 12c	59.20	Kyrshabakty		dolostone									
BK 12d	59.23	Kyrshabakty		dolostone									
BK 13	59.25	Kyrshabakty		dolostone	-2.3	-32.13							
BK 14	59.90	Kyrshabakty		dolostone	-1.8		-29.8	0.043	0.033	0.002		***0.003***	***0.003***
BK 21	168.60	Kyrshabakty	Berkuty	dolostone	1.5		-28.8	0.038	0.031	0.002	2.9	0.014	0.011
BK 22	168.30	Kyrshabakty	Berkuty	dolostone	3.0		-30.4	0.065	0.054	0.004	0.4	0.034	0.028
BK 23	167.90	Kyrshabakty	Berkuty	dolostone	3.2								
BK 24	167.60	Kyrshabakty	Berkuty	dolostone	0.7	-4.0	-26.4	0.054	0.046	0.002	0.2	0.029	0.025
BK 25	167.30	Kyrshabakty	Berkuty	dolostone	2.3	-1.9							
BK 26	166.90	Kyrshabakty	Berkuty	dolostone	2.1	0.2	-27.0	0.046	0.038	0.003	1.4	0.023	0.019
BK 27	166.60	Kyrshabakty	Berkuty	dolostone	2.0	-0.8							
BK 28	166.30	Kyrshabakty	Berkuty	dolostone	1.1	-1.0	-25.7	0.063	0.049	0.003	0.9	0.018	0.014